Distribution Agreement

In presenting this thesis or dissertation as a partial fulfillment of the requirements for an advanced degree from Emory University, I hereby grant to Emory University and its agents the non-exclusive license to archive, make accessible, and display my thesis or dissertation in whole or in part in all forms of media, now or hereafter known, including display on the world wide web. I understand that I may select some access restrictions as part of the online submission of this thesis or dissertation. I retain all ownership rights to the copyright of the thesis or dissertation. I also retain the right to use in future works (such as articles or books) all or part of this thesis or dissertation.

Signature:

_____	08/07/2017
James Ya Zhang	Date

Optogenetic Stimulation of Transplanted Stem Cells to Enhance Regeneration and Repair After Traumatic Brain Injury

By

James Zhang
Doctor of Philosophy

Graduate Division of Biological and Biomedical Science
Neuroscience Program

_____

Dr. Ling Wei, M.D.
Advisor

_____

Dr. Robert Gross, M.D., Ph.D.
Committee Member

_____

Dr. Dieter Jaeger, Ph.D.
Committee Member

_____

Dr. Shan Ping Yu, M.D., Ph.D.
Committee Member

_____

Dr. Yimin Zou, Ph.D.
Committee Member

Accepted:

_____

Lisa A. Tedesco, Ph.D.
Dean of the James T. Laney School of Graduate Studies

_____

Date

Optogenetic Stimulation of Transplanted Stem Cells to Enhance Regeneration and Repair After Traumatic Brain Injury

By

James Zhang
B.S.E., Biomedical Engineering, Duke University, May 2010

Advisor: Dr. Ling Wei, M.D.

An abstract of a dissertation submitted to the Faculty of the
James T. Laney School of Graduate Studies of Emory University
in partial fulfillment of the requirements for the degree of
Doctor of Philosophy in
Graduate Division of Biological and Biomedical Science (GDBBS)
Neuroscience Program
2017

Abstract

Optogenetic Stimulation of Transplanted Stem Cells to Enhance Regeneration and Repair After Traumatic Brain Injury
By James Zhang

Stem cells provide the unique opportunity to address the treatment gap for many intractable disorders, including traumatic brain injury (TBI). TBI is the leading cause of morbidity and mortality amongst children and young adults. Despite its being such a prevalent healthcare burden, there are currently no effective treatment options for TBI. While stem cell therapy has emerged as a promising candidate for treatment, it remains suboptimal. One of the primary challenges with cell therapy is the hostile transplantation environment and the glial scar, which prohibit neuritogenesis and plasticity in the peri-contusion region. To bridge this treatment gap, I genetically engineered a stable induced pluripotent stem cell (iPSC) line that expresses the fusion protein luminopsin (LMO), which is comprised of a light-emitting luciferase with a light-sensitive excitatory channelrhodopsin, to allow for control of neural activity by intranasal delivery of the luciferase substrate, coelenterazine (CTZ). I first demonstrated that photostimulation of iPS-neurons by either CTZ or laser both resulted in upregulation of activity-dependent factors BDNF and NGF within in vitro models of iPS-derived neurons, as well as enhancement of axon outgrowth and plasticity, even beyond regions of axonal inhibition, such as into CSPG droplets. Next, the neurotrophic upregulation with intranasal CTZ stimulation was corroborated in the controlled cortical impact (CCI) mouse model of TBI. Furthermore, stimulation resulted in greater axonal outgrowth and reorganization with enhanced parallelism of axon bundles. CTZ stimulation also improved endogenous neurovascular repair by promoting neovascularization and restoring local cerebral blood flow (LCBF), which counters ischemic cytotoxic edema, a key secondary effect of TBI. As a result, stimulation enhanced the neuroprotective effect of stem cell transplantation, which led to decreased contusion volumes and improved functional outcomes. Overall, I have established and characterized a next-generation stem cell strategy to augment the function and efficacy of cell therapy after transplantation by driving grafted cell activity. While this dissertation has focused on the efficacy of this combination therapy for TBI, this novel non-invasive approach provides great translational potential and sets the precedence for diverse stem cell applications and treatments.

Optogenetic Stimulation of Transplanted Stem Cells to Enhance Regeneration and Repair After Traumatic Brain Injury

By

James Zhang
B.S.E., Biomedical Engineering, Duke University, May 2010

Advisor: Dr. Ling Wei, M.D.

A dissertation submitted to the Faculty of the
James T. Laney School of Graduate Studies of Emory University
in partial fulfillment of the requirements for the degree of
Doctor of Philosophy in
Graduate Division of Biological and Biomedical Science (GDBBS)
Neuroscience Program
2017

Acknowledgements

Firstly, I would like to extend my sincerest gratitude towards my primary advisor, Dr. Ling Wei. Without her, none of this would've been possible. Throughout the four years, she has always put my interests and benefits first and ensured that I received the best graduate training possible. From experiment design to technical knowledge to scientific writing to grant applications, Dr. Wei has always been willing to dedicate her time and energy towards our development, even if it meant providing time-consuming hands-on support. She was also a great role model and stalwart of emotional support. She always believed in me, even at times when I doubted myself, and gave me the motivation that I might not have wanted, but needed to move forward with my project, my career, and sometimes my life decisions. Next, I would like to thank the other members of my committee. Dr. Shan Ping Yu has been a reliable source for me to turn to for both experimental advice and for helping me revise manuscripts and review papers. He has helped teach me the art of scientific writing and develop into a much more polished research scientist. Dr. Robert Gross has been a wonderful liaison for me with the MD/PhD program and has provided invaluable advice for when I struggled through the sometimes grueling graduate phase of training, as well as the development towards becoming a clinician scientist. Dr. Dieter Jaeger has served as a terrifically dependent member of my thesis committee and I have enjoyed our conversations both related and unrelated to research, and having him on my committee was a wonderful experience. Finally, while Dr. Yimin Zou had the disadvantage of being located across the country in sunny San Diego, I am very gracious for his dedication and advice as a committee member. I would also like to acknowledge all the members of my lab, both present and past. For the past members, I want to thank Todd Deveau, Monica Chau, Dongdong Chen, Mallory Harris, Cody Wenyuan Cao, and Jenny Zhen, who have all played a role, big or small, in my completing of my thesis. As for the present members, I have to thank Michael Jiang for his unwavering friendship both in and out of lab. We joined the lab at around the same time and have gone through the crucible of the PhD journey together. The journey was made much more pleasant having the support of such a wonderful friend and labmate. I would also like to thank Xiaohuan "Hannah" Gu for also being such a terrific friend and coworker. During my time in grad school, she has taught me so much related to animal work and surgeries, as well as pro-tips in lab, and it was very uplifting having someone to joke around with. I also want to thank Myles McCrary for his friendship and help over the past year. Through the projects we've worked on together and through our shared love of Indian buffets, we've grown to be great friends, and I know the lab will be in good hands with him after I leave. There are so many other lab members too, and I want to acknowledge all of them, including Zheng "Zachory" Wei, Xin Huang, and all of our awesome undergrads, Sam Kim, Kaleena Jesson, Ryan Chin, Ameya Gangal, Solana Liu, Gemy Sethaputra, and Enakshi Das. Collaboration is of utmost importance in research, and throughout the years, I've developed great relationships with members of others labs, especially Dr. Gross's lab. Importantly, I would like to thank Jack Tung for his countless advice and assistance throughout the past few years, from grant applications to carrying out experiments to professional development. As a fellow MD/PhD student who is a year above me, he provided many pearls of wisdom for me along the way. I am also grateful to Ken Berglund for his contributions to my project, especially related to electrophysiology and the creation and characterization of the eLMO3 variant. I also want to thank Claire-Anne Gutekunst for her advice with experimental design and execution, especially the CSPG droplet assay, as well as Thomas Shiu for his help with the Arduino microcontroller for laser stimulation. I also must acknowledge my social and emotional support group, including my parents, my friends here, and the great administration and faculty at Emory. Last but certainly not least, I have to extend the greatest gratitude and appreciation towards my loving wife, Yuan Chang, for her unconditional support and patience with me during the rough and tumble of the PhD. She deserves a badge of honor for bearing with me through all this, all while completing a PhD of her own. Amongst her many roles that she has contributed for me, she has been an amazing caretaker, support base, friend, counselor, and Adobe Illustrator graphic designer. Thank you all for your support in my journey!

Table of Contents

List of Figures

List of Tables

List of Initialisms

TBI	Traumatic brain injury
GCS	Glasgow coma scale
GOS	Glasgow outcome scale
DTI	Diffusion tensor imaging
ADC	Apparent diffusion coefficient
CCI	Controlled cortical impact
FPI	Fluid percussion injury
CHI	Closed head injuries
DAI	Diffuse axonal injury
NSC	Neural stem cells
SGZ	Subgranular zone
SCZ	Subcallosal zone
SVZ	Subventricular zone
GABA	gamma-aminobutyric acid
NPC	Neural progenitor cell
RMS	Rostral migratory stream
SDF1	Stromal-derived fator 1
ESC	Embryonic stem cell
iPSC	Induced pluripotent stem cell
CNS	Central nervous system
PD	Parkinson’s disease
HD	Huntington’s disease
FD	Familial dysautonomia
RTT	Rett syndrome
ALS	Amyotropic lateral sclerosis
NIH	National Institutes of Health
MSC	Mesenchymal stem cell
CD	Cluster of differentiation

HLA-DR	Human leukocyte antigen D related
BMSC	Bone marrow stem cells
FGF	Fibroblast growth factor
SHH	Sonic hedgehog
BDNF	Brain-derived neurotrophic factor
RA	Retinoic acid
EB	Embryoid body
LIF	Leukemia inhibitory factor
bFGF	Basic fibroblast growth factor
IC	Intracranial
CSF	Cerebrospinal fluid
IV	Intravenous
IN	Intranasal
NGF	Nerve growth factor
NT	Neurotrophin
VEGF	Vascular endothelial growth factor
IL	Interleukin
TNF-α	Tumor necrosis factor-α
PBMC	Peripheral blood mononuclear cell
IFN-γ	Interferon-γ
HUVEC	Human umbilical vein endothelial cells
BrdU	5-bromo-2-deoxyuridine
NeuN	Neuronal nuclear antigen
MAP2	Microtubule-associated protein 2
GDNF	Glial derived neurotrophic factor
CNTF	Ciliary neurotrophic factor
NSS	Neurological Severity Score
BCL	B-cell lymphoma

CXCR	C-X-C chemokine receptor
HP	Hypoxic preconditioning
OGD	Oxygen-glucose deprivation
EPO	Erythropoietin
ECM	Extracellular matrix
CREB	cAMP response element-binding protein
DBS	Deep brain stimulating
TDCS	Transcranial direct current stimulation
TMS	Transcranial magnetic stimulation
DREADD	Designer receptors exclusively activated by designer drugs
CNO	Clozapine-N-oxide
ChR	Channelrhodopsin
NpHR	Halorhodopsin
SFO	Step-function opsins
TS	Trafficking sequences
ER	Endoplasmic reticulum
AAV	Adeno-associated virus
HSV	Herpes simplex virus
EF1α	Elongation factor 1-α
CMV	Cytomegalovirus immediate-early enhancer
CAG	CMV - β-actin promoter – splice acceptor of β-globin
CAMKIIα	α-Calcium/calmodulin-dependent protein kinase II
LED	Light-emitting diode
NA	Numerical aperture
RF	Radio-frequency
CTZ	Coelenterazine
LMO	Luminopsin
EYFP	Enhanced yellow fluorescent protein

DIV	Days in vitro
RT-PCR	Reverse transcriptase polymerase chain reaction
BLAST	Basic local alignment search tool
RE	Restriction enzymes
iPS-NPC	iPS-derived neural progenitor cell
CyD	(2-Hydroxypropyl)-β-cyclodextrin
BSA	Bovine serum albumin
Tuj1	β-III tubulin
VGLUT	Vesicular glutamate transporter
TUNEL	Terminal deoxynucleotidyl transferase dUTP nick end labeling
IHC	Immunohistochemistry
GLUT1	Glucose transporter 1
GFAP	Glial fibrillary acidic protein
MBP	Myelin basic protein
LI	Laterality index
SMA	Smooth muscle actin
LCBF	Local cerebral blood flow
HEK	Human embryonic kidney
SSEA1	Stage-specific embryonic antigen 1
NF	Neurofilament
CREB	cAMP responsive element binding protein
PSD	Post-synaptic density protein
AXIS	Axon investigation system
GAP-43	Growth-associated protein 43
HIF1α	Hypoxia-inducible factor 1α
BC	Barrel cortex
VPM	Ventroposteromedial

Chapter 1: Traumatic Brain Injury

1.1 Introduction: Epidemiology, subtypes, and stratification

Traumatic brain injury (TBI) is a leading cause of death and disability in the United States, causing 50,000 deaths per year and long-term disability in another 124,000 people discharged with TBI [1, 2]. Although TBI is caused by and manifests in a myriad of ways in the clinical setting, TBI can be categorized as either closed TBI or penetrating TBI. Closed TBIs are associated with static and dynamic loading of mechanical insult. Static loading entails gradual forces being applied to the head, such as a head being trapped under a car, while dynamic loading involves rapid acceleration and deceleration of the brain [3]. Additionally, dynamic loading can be caused by both contact and inertial when being struck by an object, or only inertial forces in the case of rapid stops. Tissue strain and deformation are evident in both types of TBI, and lead to the primary and secondary pathologies listed below. Penetrating brain injuries are caused by high velocity projectiles or low velocity sharp objects, and are most commonly associated with armed combat [4]**.** In the clinical setting, the Glasgow coma scale (GCS) and Glasgow outcome scale (GOS) remain the primary means of assessing levels of consciousness and the severity of TBI by measuring levels of eye, motor, and verbal responses [5, 6]. The GCS is recognized as a reliable tool for monitoring the status of TBI patients, with TBIs being classified as Mild (13-15), Moderate (9-12), or Severe (3-8) [7].

1.2 Pathophysiology

TBI is characterized by primary and secondary injury. Primary injury, usually caused by contact injuries or inertial forces, occurs at the moment of impact [8]. These frequently result in focal injuries, such as contusions and hematomas, and diffuse injury, such as axonal shearing [9]. Secondary injury manifests minutes or months after initial impact and is characterized by progressive degeneration of neurons, glial cells, and axons [10, 11]**.** These degenerative processes, in part mediated by glutamate toxicity [12] and the production of free radicals [13], are associated with a myriad of detrimental conditions such as BBB leakage**,** hypoxia**,** and increased intracranial pressure [14-16]. These secondary effects are especially susceptible to delayed degeneration and cell death, similar to a stroke penumbra. More recently, diffusion tensor imaging (DTI) has further stratified these traumatic penumbras, with the core zone identified in DTI as an area of restricted diffusion, and the surrounding penumbra is characterized by elevated apparent diffusion coefficient (ADC), bordered by another even thinner rim of lowered ADC [17]. The ADC is used to describe whether the water diffusion in the region of interest is directionally uniform, and a low intensity ADC corresponds to ischemic cytotoxic edema, while high intensity ADC corresponds to vasogenic edema. As the contusion enlarged over time (days-weeks), the rim of ADC hypointensity would subsume into area of hyperintensity, reflecting the expansion of the injury, possibly due to a combination of hypoperfusion and vasogenic edema from hemorrhagic progression after BBB breakdown [17-19].

The neural network is closely coupled to the vasculature, forming a neurovascular niche [20]. Thus, injury to neurons and secondary cell death leads to further aberrations of surrounding vessels. Both the acute phase and the more delayed chronic phases of TBI present opportunities for therapy given the continuously elevated levels of cell death.

1.3 Current Status of Treatments

Current treatments for TBI aim to ameliorate primary injury and prevent further secondary injury through techniques such as oxygenation, decompressive craniectomy, and hypothermic therapy [21-23]**.** However, almost no treatments exist that improve neurological outcomes in TBI patients, with almost all Phase II and III clinical trials for neuroprotective agents failing [24, 25]. One specific example is progesterone treatment, which has been beneficial in pre-clinical studies of TBI recovery [26, 27]. Stein suggests that this is in part due to the role progesterone plays in reducing excitotoxicity and inflammation, as well as regulating normal levels of cell proliferation and apoptosis [28, 29]**.** However, trials to treat adult TBI, including recent Phase III clinical trials, produced no significant beneficial effects [30-32]. Consequently, the identification and implementation of regenerative approaches for TBI treatment remains an unmet clinical need. For this reason, continued and renewed effort towards translational research involving TBI by using effective animal models are necessary for the development of novel therapeutic interventions.

1.4 Animal Models of TBI

There are multiple models for inducing reproducible TBI in animal models that vary based on whether they are open head or closed head, or whether they are penetrating or non-penetrating injuries. The controlled cortical impact (CCI), fluid percussion injury (FPI), weight drop injury, and blast injury are the most widely used models to study TBI in rodents [33].

1.4.1 Controlled cortical impact

In the CCI model, a craniotomy is performed, and a pneumatic or electromagnetic impactor is used to strike the exposed dura matter [34, 35]. CCI produces many features characteristic of

TBI, such as cortical contusion, intraparenchymal and subarachnoid hemorrhages, brain atrophy, decreased cerebral blood flow, and axonal injury [34, 36, 37]**.** These pathological effects and anatomical deformities also increase in severity along with increases in depth and velocity of impact [38, 39]. Consequently, the graded effects, ease of adjusting various impact parameters, and the consistency and precision of injury make CCI an attractive model to investigate varying pathological features of TBI.

1.4.2 Fluid percussion injury

The FPI model consists of a pendulum that strikes a saline-filled reservoir, which causes pressurized fluid to impact the cranial cavity [40, 41]. The severity of impact can be controlled by adjusting the height of the pendulum drop. It is important to note that FPI models cannot replicate skull fractures, though other clinical characteristics of TBI pathology, such as hemorrhage and brain atrophy, and cognitive impairments are observed in a graded manner in relation to impact severity [42, 43].

1.4.3 Weight drop

Weight drop models involve dropping a free falling weight through tubing onto the exposed skull of the rat or mouse [44, 45]. Severity of injury is adjusted by controlling the mass of the weight and the height of its drop. Conditions of the weight drop model can be altered to mimic various types of TBI, such as closed head injuries (CHI) and diffuse TBI, and consistently produces clinical features of TBI, such as cortical cell loss, contusion and hemorrhage formation, and motor and cognitive deficits [46-48]. The relative speed and ease of use of the weight drop model make

it an attractive model for studying TBI, although it also presents the possibility of rebound injuries, inaccurate impact position, and skull fractures at high magnitudes of injury severity [3].

1.4.4 Blast model

In order to study the effects of non-impact blast TBIs typically seen in military personnel, the blast injury model exposes rodent heads to blasts created by compression-driven shock tubes, such as the McMillan blast device [49-51]. Blasts produce effects such as neurological dysfunction and diffuse axonal injury (DAI), as well as pathology unique to blast injuries, such as phosphorylated tauopathy [52-54]. Consequently, the blast injury model is effective in reproducing the highly specific conditions and pathologies commonly seen in blast injuries.

There has been a growing revelation of the insidious comorbidities that presents even many years after the initial trauma, even if the initial trauma is not classified as severe or symptomatic [55, 56], such as concussions that occur in athletics or blast-associated injuries in combat, which make up the majority of TBI subtypes [57]. Thus, there may need to be a greater adoption of animal models that better emulate these injuries, such as using non-penetrating impacts like the blast model. Furthermore, while most of the behavioral outcome metrics have focused on motor and cognitive recovery, mild TBI is also highly associated with concomitant mental health conditions. 89% of veterans have also been diagnosied with psychiatric comorbidities, which is 4-fold greater than that of veterans who have not suffered a TBI [58].

1.5 Endogenous response and extent for brain repair

Brain injury recovery is characterized by neural network remodeling and neural plasticity. These changes are associated with processes such as neurogenesis, axonal sprouting and regeneration, and angiogenesis [59]. Within mammalian brains, postnatal and adult neural stem cells (NSCs) have been found to reside within the subgranular zone (SGZ) of the hippocampal dentate gyrus, the subcallosal zone (SCZ) between the hippocampus and the corpus callosum [60], and the subventricular zone (SVZ) flanking the lateral ventricles, with SVZ progenitor cells also migrating to injury sites [61-63]. Likewise, neurogenesis occurs within the SVZ in humans, and given the central location of the SVZ with respect to potential focal injuries, this suggests that SVZ NSCs and progenitors could contribute to endogenous repair in the case of brain injury [64, 65]**.**

NSCs are defined as multipotent cells that are capable of self-renewal and differentiating into any neuronal or glial subtype throughout the neuraxis [66-68]. While they are mostly predominant during development, they have been shown to populate the CNS after degeneration or injury as well [69]. NSCs were first isolated and described as a self-renewing, multipotent progenitor and stem cell line from the developing rat forebrain in 1989 [70]. Next, Reynolds and Weiss demonstrated that NSCs could be dissected from adult striatal tissue, including the SVZ, which was determined to be a niche for self-renewing cells in adults [71]. The NSCs in the SVZ typically follow a fixed asymmetric division cycle to replenish γ-aminobutyric acid (GABA)-ergic interneurons of the olfactory bulb [68]. The NSC niche renews as transient amplifying cells that divide into NPCs, which begin to travel as migratory neuroblasts along the rostral migratory stream (RMS) along specialized astrocytes [72] towards the olfactory bulb, where they finally differentiate into GABAergic cells [73]. In the normal CNS, these NSCs will only give rise to their committed lineages, but during pathological conditions, the NSCs are induced to alter fates to

partially restore lost neurons instead, and new neurons appear in areas where neurogenesis does not normally happen, such as the generation of new corticothalamic neurons with repaired connectivity [74]. New neurons are able to home towards the injury region because of chemoattractants, such as stromal-derived factor 1 (SDF1, AKA CXCL12), which is upregulated and released by reactive astrocytes and local endothelium, which gives rise to a chemo-gradient [75]. There is new evidence that suggests that endogenous neurogenesis not only contributes towards cell replacement after injuries, but also towards global plasticity as well [76]. This was corroborated by our recent study involving a focal cortical stroke [77]. Despite the stroke being localized to the barrel cortex, we observed increased levels of hippocampal neurogenesis, and this plasticity was suppressed when we partially blocked endogenous neurogenesis by inhibition of the canonical Wnt signaling pathway [77].

In the case of endogenous repair, only a small number of dead neurons are replaced, and the number of migrating neuroblasts decreases with age , further decreasing healing potential in aging populations [78, 79]. Thus, extensive focus has been placed on both leveraging the mechanisms of endogenous regeneration and supplying exogenous stem cells for facilitating brain repair after injury.

1.6 Summary

Traumatic brain injury (TBI) is a leading cause of death and disability in the United States [1]. TBI, which involves mechanical and inertial insult to the head and brain, can manifest many different ways in the clinical setting [3, 7]. Additionally, TBI is understood to follow a pathophysiology characterized by the primary injury, caused by inertia or direct contact, and the

secondary injury, which involves degenerative processes such as glutamate toxicity and blood brain barrier (BBB) leakage [8, 12, 14]. Despite the obvious health and economic burden of TBI, treatments are extremely limited, with almost no treatments improving neurological outcome in TBI patients [25]. However, much exciting and progressive research is currently being done, due in part to various animal TBI models that have been developed, as well as the relatively recent interest in endogenous and exogenous brain repair [63, 65, 80].

Chapter 2: Stem Cell Therapy

2.1 Introduction

Over the past several decades, stem cells have emerged as a promising breakthrough of basic and clinical science. Because of their pluripotency and proliferative capacity, this unique population of cells have provided the tremendous versatility for in vitro modeling or tissue engineering of nearly any organ system, as well as the regenerative potential for delayed treatment of pathologies, especially those that are currently intractable, such as injuries and diseases of the brain. While the origin of stem cells dates back to 1978 with the discovery of stem cells in cord blood by Gregor Prindull [81], the true inception of modern stem cell therapy was inaugurated with the isolation and maintenance of embryonic stem cells (ESCs) in 1988 [82, 83]. The next breakthrough was marked by the creation of induced pluripotent stem cells (iPSCs) through reprogramming fibroblasts in 2006 with “Yamanaka factors” [84]. With the advent of ESCs and iPSCs, scientists finally possessed the latitude to differentiate cells into any subpopulation of cells, ushering in a new era of excitement and possibility in biology and medicine. Since those seminal

discoveries, many incremental advancements have been made in the field of stem cells, including creation of more relevant and translational human cell lines, improvements in survival and differentiation, and importantly, stem cell therapy. In fact, the once lofty aspiration of stem cell transplantation in humans has now become a reality, with clinical trials under way and completed, and some demonstrating promising results.

Cellular therapy serves as an attractive treatment option for brain injuries due to its ability to target and modulate endogenous neurogenesis activities and replace damaged and dying cells [80]. Stem cells, which are defined by their propensity for self-renewal and differentiation into multiple cell types, can directly replace damaged cells and contribute to environmental enrichment by secreting cytokines, growth factors, and other trophic factors [85, 86]. However, primary and secondary injuries after a focal brain lesion create a hostile environment for the survival and integration of transplanted cells, thus the stem cell type, mode of administration, and timing of transplantation should be carefully considered [87].

2.2 Stem Cell Types

2.2.1 Embryonic stem cells

Embryonic stem cells (ESCs) are derived from the inner cell mass of mammalian blastocysts [88, 89]. ESCs hold great potential for TBI treatment due to their pluripotency and ability to differentiate into derivatives of all three cellular germ layers [90, 91]. Transplantation of ESCs has demonstrated various therapeutic effects such as increases in angiogenesis and neuronal survival, reduction of lesion volumes, and improved motor and cognitive function [85]. However,

many ethical and political concerns surround the development and implementation of ESCs, mainly due to the fact that isolation of ESCs results in destruction of the blastocyst, which is an early stage embryo [92, 93].

So far, following precisely choreographed programs, human ESCs have been effectively differentiated to various transplantable neuronal and glial types and NPCs, including cerebral glutamatergic, striatal GABAergic, forebrain cholinergic, midbrain dopaminergic, serotoninergic and spinal motor neurons, as well as astrocytes and oligodendrocytes [94-106]. Furthermore, the differentiated products, including neurons, astrocytes, and oligodendrocytes can be used to treat the CNS diseases involving focal regions or cell types by exogenous transplantation. This has been evaluated extensively in animal models, but the work has gradually transitioned into clinical trials involving cell therapy for a variety of neurological disorders, including: 1) Parkinson's disease (PD), in which nigro striatal neurons are lost before other neurons, 2) Huntington's disease (HD), in which medium spiny neurons are lost, resulting in striatal atrophy, and 3) glial and myelin disorders [107-110]

2.2.2 Induced pluripotent stem cells

Induced pluripotent stem cells (iPSCs) are adult human fibroblasts that are reprogrammed to pluripotent embryonic stem cells through the introduction of transcription factors Oct4, Sox2, c-Myc, and Klf4 [84]. The benefit of iPSCs is evident through solving the ethical concerns of ESCs. Additionally, iPSCs eliminate the possibility of immunological rejection because the cells are generated from the subject or patient themselves [111]. This is because the autologous nature of iPSCs minimizes the risk of immune rejection, although a recent finding shows that unusual gene expression in some cells derived from iPSCs can trigger an immune response [121].

However, the risk of tumor formation, as well as the low efficiency of reprogramming during iPSC production, warrant further evaluation before iPSC therapy can attain significant clinical relevance [91, 112].

There are also other epigenetic differences between iPSCs and ESCs in many aspects, such as the expression of a unique stem cell genetic signatures, the capacity for teratoma formation, and differentiation potency and flexibility, including the potential for differentiation into various transplantable neural cells [113, 114]. Meanwhile, iPSCs have some advantages compared to ESCs, which together make them more amenable as donor cells for cell replacement therapy, in vitro disease models, and drug screening [115-120]. Firstly, iPSCs are derived from adult somatic cells, which can easily be obtained from patients and be banked and stored. Secondly, working with iPSCs carry similar technical difficulties as human ESCs, but the generation of iPSCs harbors much less ethical concern and opposition. Thirdly, iPSCs minimize immunoreactivity.

Mouse and human iPSCs provide a powerful tool for both research involving developmental biology and translational medicine. In developing improved pharmaceutical agents, the combination of iPSCs with microfluidic technology have provided high-throughput preclinical drug screening platforms. This process can lead to the rapid identification and optimization of molecules/drugs and thus move forward new pharmacological therapies for a wide range of neurological disorders [120]. Furthermore, iPSCs allow for greater experimental interrogation and convenience than transgenic animal models for determining clinically relevant doses, as well as short-term and long-term adverse effects.

One of the more exciting features of iPSCs is the potential to establish disease-relevant phenotypes in vitro to simulate and recapitulate the earliest molecular signatures of pathogenesis. This has been implemented in a wide variety of neurological disorders, including familial

dysautonomia (FD), Rett syndrome (RTT), HD, AD, ALS, PD, and schizophrenia [122], [123-129]. To fulfill the need for better systematic safety and reliability standards, The US National Institutes of Health (NIH) has established relevant ethical guidelines and standards. The human iPSC repositories of personalized cell lines from patients are being developed and banked, which will enable the use of iPSC technology to model disease and screen drugs [130]. In addition to mimicking disease development to better understand their etiology and pathogenesis, another future goal centers around the genetic modifications and enhancements of patient iPSCs for reinfusion, especially for the patients with sporadic disease. Together, iPSC and genome editing techniques will enable researchers to better understand and ultimately resolve the complex genetic etiologies underlying the diverse spectrum of neurological disorders.

2.2.3 Adult neural stem cells

Adult neural stem cells (NSCs) are multipotent stem cells that reside in regions of the brain such as the SVZ, SGZ, and SCZ [60, 131-133]. They easily differentiate into astrocytes, neurons, and oligodendrocytes [134]**,** and can successfully integrate into brain circuitry when added to the injured brain [135], making them an attractive option for stem cell treatment. Additionally, NSC activity can be modulated by various intrinsic and extrinsic factors, such as proliferation and differentiation regulation by transcription factors, hypoxia, and growth factors [136-139]. NSCs are usually cultured as neurospheres *in vitro*, and also self-renew and differentiate into different cell types easily [140]. However, NSCs must be isolated from deep within embryonic, fetal, or adult mammalian brains, highly limiting the accessibility of retrieving this stem cell type [86].

2.2.4 Mesenchymal stem cells

Mesenchymal stem cells (MSCs) are multipotent adult stem cells found within bone marrow and other tissues, such as the umbilical cord and adipose tissue [141]. MSCs adhere to plastic during culture, express certain hematopoietic markers such as CD34 and HLA-DR, and can differentiate into adipocytes, osteocytes, and chondrocytes *in vitro* [142, 143]. These properties, which contribute to the high plasticity, proliferation, and differentiation of MSCs, along with the various neuroprotective and functional improvements exhibited in injured models transplanted with MSCs, make MSCs one of the most promising treatments for TBI [85, 141, 144, 145].

2.3 Neuronal Induction of Pluripotent Stem Cells

Pluripotent stem cells, including ESCs and iPSCs and to a limited extent, BMSCs as well, have the versatility to differentiate into multiple lineages depending on the inducible factors they are exposed to during a critical window. There are varying inducible factors used for differentiation of NSCs depending on the targeted subtype of neurons. For example, either co-culturing of ESCs with PA6 cells [146] or by exposure to fibroblast growth factor 8 (FGF8) and sonic hedgehog (SHH) directs the cells towards a dopaminergic subtype [147], whereas treatment with SHH [148] or brain-derived neurotrophic factor (BDNF) yields a greater percentage of GABAergic interneurons [114]. For NPC transplantation after a focal cortical injury, the more pertinent cell subtype is glutamatergic cortical neurons, which can be generated through treatment with retinoic acid (RA) [149]. There are multiple methods for differentiation of stem cells, including the adherent (AKA monolayer) method, the embryoid body (EB) method, and the five stage method [114, 149] (*Figure 2-1*). The adherent method involves plating stem cells on 0.1% gelatin-coated dishes in N2B27 medium for 7 days [150]. The EB method (AKA 4-/4+) involves seeding the stem cells onto uncoated dishes in normal stem cell maintenance media without the pluripotency

maintenance factor, leukemia inhibitory factor (LIF) for 4 days. During this time, the cells tend to aggregate into spherical floating clusters, known as EBs, and then RA is added on the 4th day for another 4 days to promote neural differentiation [151]. More recently, a modified version of the EB method was developed by Mohamad et al. that involved continuous shaking of the EBs on a revolving motor, which produced improvements in survival and differentiation speed [152]. Finally, the five stage method was first described by Okabe et al. [153] and was modified by Lee et al. [154]. Stem cells are plated during stage 1, followed by formation of EBs for 4 days (stage 2). Then 24 hr later, stage 3 is neural induction, in which the stem cell medium is replaced with ITSFn medium (insulin, apo-transferrin, sodium selenite, fibronectin, L-glutamine) for another 4 days. Then, cells are dissociated and plated in mN3FL medium (stage 4), which includes basic fibroblast growth factor (bFGF), for 6 days. The final stage (stage 5) involves removal of bFGF for another 6 days [154]. The All three methods generate predominantly glutamatergic neurons, although there are about 25-35% GABAergic neurons [114].

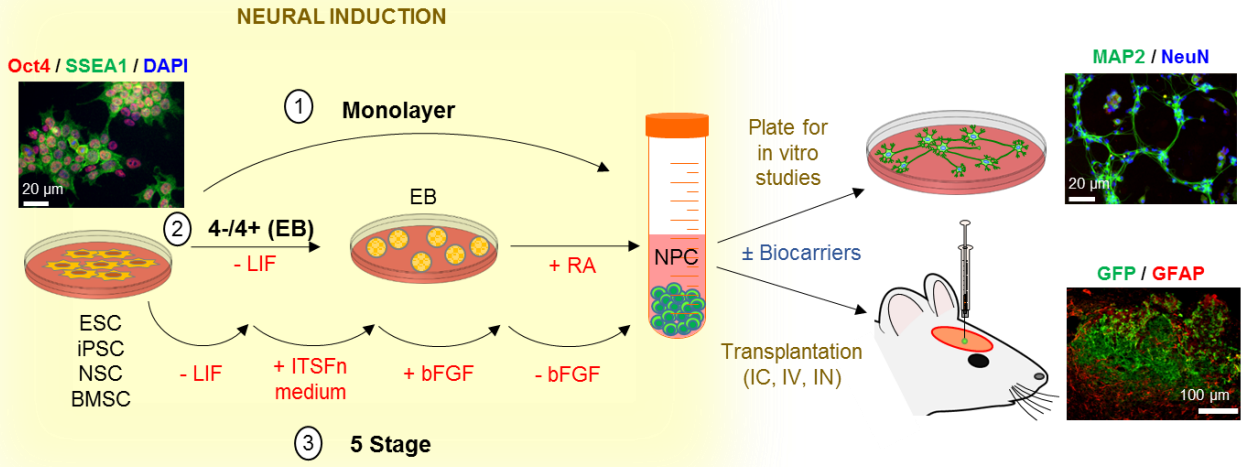

Figure 2-1: Neural differentiation of stem cells for basic science studies or transplantation.

There are 3 major methods for differentiation of pluripotent or multipotent stem cells, including 1) monolayer method, 2) 4-/4+ (AKA EB) method, and 3) 5 stage method. The more widely adopted approach is the EB method, which utilizes treatment of the cells with retinoic acid (RA) for neuronal differentiation. Once the cells have been pre-differentiated into neural progenitor cells (NPCs), they are harvested for either in vitro studies or transplantation into animal models or humans. LIF: leukemia inhibitory factory. ITSFn: insulin, apo-transferrin, sodium selenite, fibronectin, L-glutamine. bFGF: basic fibroblast growth factor. IC: intracranial. IV: intravenous. IN: intranasal.

2.4 Transplantation Routes

2.4.1 Intracranial (intracerebral or intraventricular)

The route of delivery remains an important factor for the clinical success of stem cell therapy [80]. Intracranial (IC), or direct, implantation offers the most direct method of

transplantation and can be intracerebral or intraventricular, where it circulates and deposits into the brain parenchyma via the cerebrospinal fluid (CSF). Intracranial transplantation offers a highly efficient and targeted method to treat brain injuries. Most cells are delivered directly to the infarct [155] and selectively increase progenitor cell proliferation in the SVZ compared to other methods such as intravenous transplantation [156]. However, this method is evidently invasive, and introduces the possibility of further tissue damage during stem cell transplantation [145].

2.4.2 Intravenous or Intra-arterial

Intravenous (IV) administration is one of the most thoroughly studied and safest exogenous cellular therapies, and allows for the systemic distribution of stem cells throughout the body and multiple tissues [157, 158]. Stem cell therapies through intravenous administration have been shown to modulate inflammation, growth factor production, endogenous neurogenesis, and angiogenesis, with even clinical trials showing therapeutic benefit [155]. However, the clinical implications of intravenous administration of stem cells is highly limited by the potential for cells to obstruct pulmonary vasculature [159], the buildup of cells in unintended targets [155, 160], and high pulmonary first-pass effect [145, 161]. Intra-arterial administration addresses these concerns by further localizing stem cell placement and decreasing the pulmonary first-pass effect [162]. However, even with intra-arterial infusion, treatment is limited by stem cell obstruction of arterial vasculature, as well as the high variability in cell delivery and therapeutic outcomes [163].

2.4.3 Intranasal

Intranasal (IN) administration is perhaps the best current compromise between decreased invasiveness and target specificity in terms of stem cell delivery. Although the exact route of

intranasal delivery is poorly understood, it has been demonstrated that small peptides [164] and stem cells [77, 165, 166] can bypass the BBB by permeating the olfactory epithelium and then entering direct axonal uptake or circulating through the CSF to be delivered to the CNS [167, 168]. Additionally, intranasal stem cell delivery has shown therapeutic benefit in various models of neurological injury and disease such as stroke and Parkinson's disease [169, 170]. Consequently, the non-invasiveness and direct pathway to the brain make intranasal delivery an effective method of stem cell administration [168].

2.5 Timing of Transplantation

The timing of stem cell treatment after initial TBI is also important for clinical success, and should be determined according to the primary goal of treatment. As mentioned previously, TBI comprises the primary injury from mechanical or inertial damage, and the secondary injury, characterized by biochemical processes that can lead to neurodegeneration and cell death, but also plasticity and repair [171]. These post-TBI processes can include widely detrimental effects such as excitotoxicity, oxidative stress, BBB disruption, inflammation, and glial scarring [172-176]. These processes, in part, contribute to the hostile microenvironment mentioned earlier that reduce cell viability and impair the success of stem cell therapy [177]. However, compensatory pathways are also upregulated after injury, such as increased expression of growth factors such as BDNF and endogenous neurogenesis and plasticity [178]. In these cases, acute administration of treatment immediately after initial TBI would be ideal for neuroprotection [86]. However, treatments aimed at regulating the more drawn out secondary injury processes would most likely call for delayed administration.

In one study, undifferentiated ES cells were implanted 72 hours after fluid percussion injury [76]. This decision was based on reports demonstrating that the initial inflammatory reaction decreases three days after the trauma of nervous tissue, and is succeeded by the development of astroglial scar within 2 days [175]. The relatively early time point was chosen in order to avoid the peak of any inflammatory reaction and to allow for the migration and differentiation of stem cells that might be obstructed by later formation of astroglial scars [175, 176].

2.6 Mechanisms Underlying Cell Therapy

2.6.1 Trophic support: neuroprotection and suppression of inflammation

There are several putative mechanisms for which stem cells confer their beneficial effects, including trophic support, enhancement of endogenous neurogenesis and plasticity, and ideally, cell replacement. The most well-established mechanism underlying cell therapy has been trophic support. In animal models, transplanted NSCs (IV) mediate beneficial effects by production and release of growth factors, such as BDNF, nerve growth factor (NGF), and neurotrophin-3 (NT-3) [179], with upregulation of BDNF enhancing the positive effects of stem cell therapy [180-182]. In fact, BDNF has been implicated as a potential critical component of the therapeutic potential, with BDNF knockdown in NSCs resulting in an exacerbation of cellular pathologies and functional deficits [183]. Aside from neurotrophins, transplanted stem cells also secrete other trophic factors, including the vascular endothelial growth factor (VEGF), which is major activator of endothelial proliferation and neovascularization [184].

These trophic factors naturally expressed by and secreted by stem cells have pleiotrophic beneficial effects, including neuroprotection and suppression of the inflammatory response. Trophic factors can prevent cell death through their intersection with apoptosis pathways. For example, there is evidence that VEGF prevents apoptosis by inhibiting the expression of pro-apoptotic genes, such as p53 and caspases, through its binding and activation of VEGFR-1, one subtype of VEGF receptors [185]. VEGF has also been shown to promote neurogenesis in the SVZ and SGZ, as well as endogenous migration of neural progenitors from the SVZ [186]. Thus, VEGF has neurogenic, neuroprotective, and angiogenic abilities. BDNF is another trophic factor released by stem cells that have been shown to provide neurotrophic properties and play a role in neurogenesis [187, 188]. BDNF intersects with apoptotic pathways to prevent cell death, as evidenced in cerebellar neurons treated with BDNF [189]. There was more survival with granule neurons treated with 50 ng/ml of BDNF compared to cells with no treatment [189].

Another way that stem cell transplantation can be protective is through the reduction of inflammation. Transplanted BMSCs have been shown to provide a direct immunosuppression effect by modulating a broad profile of cytokines, including pro-inflammatory cytokines such as interleukin-1β (IL-1β), IL-6, IL-17, and tumor necrosis factor-α (TNF-α) [190, 191]. There are other mechanisms by which stem cells may modulate the immune system, including through the reduction of proliferation of peripheral blood mononuclear cells (PBMCs), especially the reactive T- [192-194] and B-lymphocytes [193, 195], which play important roles in mounting the immune response [196]. Furthermore, MSCs also reduce cytokine release from a variety of cell types, including TNF-α in dendritic cells and interferon-γ (IFN-γ) in differentiating type 1 helper T-cells (T_H1) and natural killer (NK) cells [196]. They may also confer anti-inflammatory effects by upregulating anti-inflammatory cytokines, such as IL-10 in DCs [196] and macrophages [197], as

well as IL-4 in differentiating T_H2 cells [196]. Because MSCs have thus far been predominantly administered through the IV or IA routes, it is of particular importance to note the variety of trophic support that is conferred from the circulating cells, which allow for more systemic indirect modulation that can lead to beneficial effects within the CNS as well. Furthermore, the immunosuppressive effects of stem cells is of particular importance for treating TBI, which results in a strong inflammatory response that leads to delayed secondary cell and potentially neurodegenerative sequelae [198].

2.6.2 Stimulation of Angiogenesis

In order for stem cell transplantation to improve upon a stroke injury, several reparative events must take place. One of the major events of tissue regeneration involves rebuilding the vasculature, particularly the neurovascular unit of the stroke injury [20]. A major trophic factor involved in this process is VEGF, which stimulates angiogenesis. In particular, VEGF activates the tubule formation of endothelial cells within an *in vitro* model (human umbilical vein endothelial cells, HUVEC) to increase vessel numbers [199]. The effect is attenuated with the addition of a VEGF inhibitor [199]. In an *in vivo* example of stem cell transplantation, VEGF secreted from neural stem cells increased neovascularization and the attenuation of inflammation in the penumbra [200]. In animals that received neural stem cell transplantation in the penumbra, there was a greater blood vessel density compared to naïve and control animals at two weeks post-transplantation. Further, animals with neural stem cell transplantation demonstrated enhanced angiogenic signaling pathways exhibiting greater levels of phosphor-VEGFR2, Tie-2, and both cognate receptors for ligands VEGF and Angiopoietin 1 and 2. Increases in the phosphorylated form of VEGF indicate increased levels of signaling through the receptor in animals with cell

transplantation [200]. Neuroepithelial-like stem cells derived from human iPS cells express VEGF [201]. Their transplantation into the stroke mouse brain also shows increased levels of VEGF in astrocytes and blood vessels within the area surrounding the graft. However, interestingly in this specific study, they were not able to find increased angiogenesis associated with the greater VEGF levels. This suggests that while not enough VEGF was secreted by the transplanted cells to cause an angiogenic effect, VEGF possibly provides an additional non-angiogenic role in the improved functional recovery that was observed. Although VEGF has mainly been studied in the context of angiogenesis, VEGF plays a role as a neuroprotective and neurogenic factor as well. Mice over-expressing VEGF had fewer neurological deficits and smaller infarct volumes than mice without over-expression [202]. In all, the contribution of VEGF and stem cells to angiogenesis after the stroke site can be measured and evaluated by several methods: blood vessel density, Western blot of angiogenic receptors, functional recovery, local cerebral blood flow [203], or vessel and 5-bromo-2-deoxyuridine (BrdU) colocalization analyses via immunohistochemistry (*Figure 2-2*).

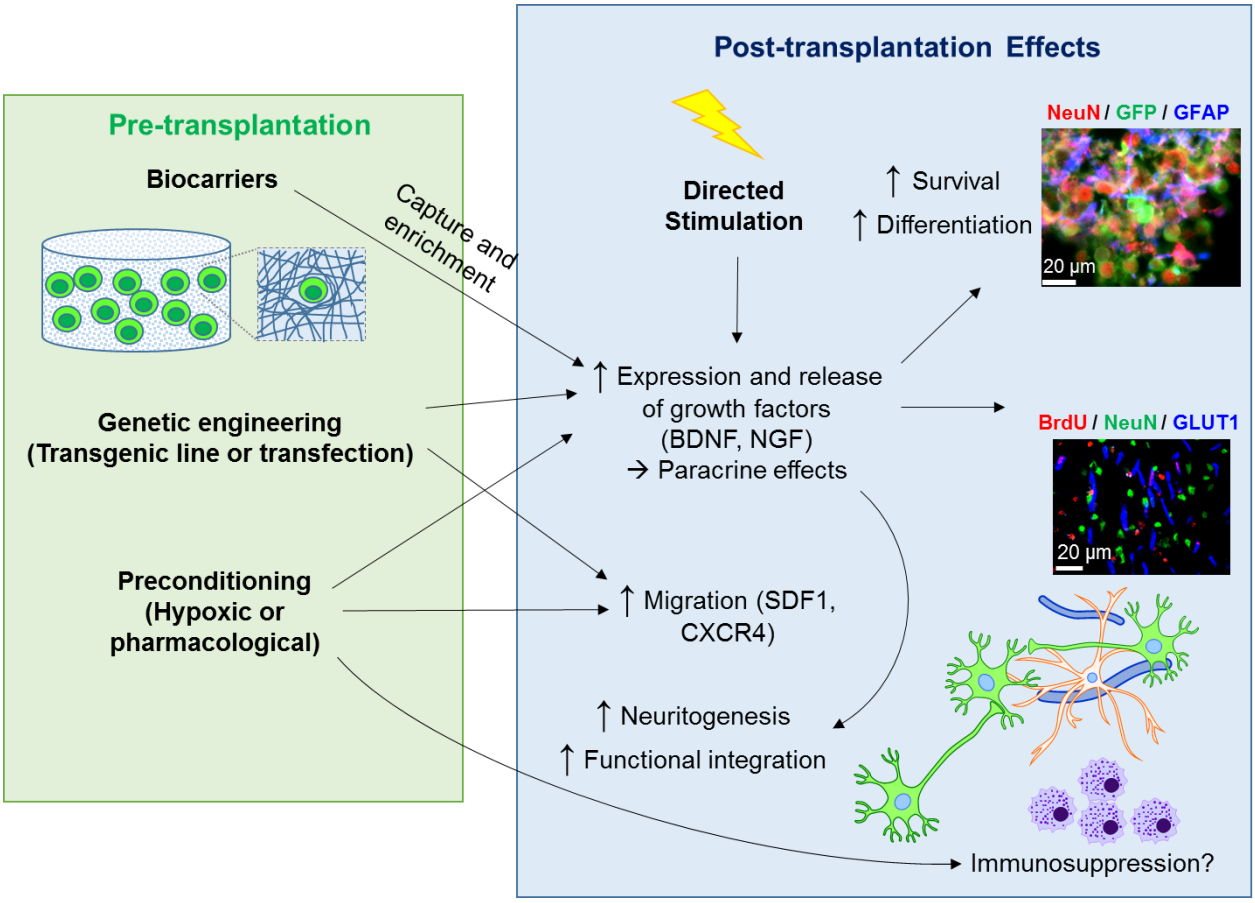

Figure 2-2: Domains for combination approach with stem cell therapy and synergistic post-transplantation effects.

Prior to transplantation, there are 3 main modifications that can be applied, including genetic engineering (by transfection or an overexpression stable cell line), encapsulation into biocarriers, or preconditioning. After transplantation, another combination therapy is directed stimulation with electrical, light, or pharmacological stimulation. These combination therapies have demonstrated a variety of putative effects, including upregulation of trophic factors to confer paracrine effects, such as enhanced survival and differentiation of grafted cells, increased angiogenesis and neovascularization around the lesion site, and bolstered neurite outgrowth and cell-cell engagement. Immunosuppression may also be a downstream effect of preconditioning, although this mechanism has not been well-established.

2.6.2 Enhancement of endogenous neurovascular regeneration

Furthermore, stem cell transplantation has been shown to improve local cell survival and augment endogenous neurogenesis [156] as a result of either direct cell contact or paracrine effects from neurotrophin release. The grafted cells also promote the formation of a “biobridge” between the endogenous neurogenic niche and the lesion site by the transplanted cells, which can form a conduit between the two zones to direct neuroblast migration towards the lesion [204].

2.6.3 Cell Replacement

Finally, while the ultimate goal of transplantation is for cell replacement, the degree of functional integration for grafted cells has been only a fraction of the total grafted cells [205-209]. Although only a small percentage of NPCs fully differentiated and integrated, this may already be sufficient to provide a noticeable functional effect. For example, Steinbeck et al. demonstrated that the grafted NPCs successfully managed to differentiate into mesencephalic dopaminergic (mesDA) neurons that resulted in improved functional outcomes which were abolished upon optogenetic silencing of these grafted cells [209].

Now that we have identified and corroborated the multitude of beneficial effects conferred by NS/NPCs, the next frontier is to formulate and optimize approaches to upregulate or manufacture NSCs to augment our endogenous healing mechanisms [210]. One of the most viable strategies that is under fervent exploration is the pre-differentiation of pluripotent stem cells into NS/NPCs. There are many different sources for NS/NPCs, including ESCs, iPSCs, BMSCs, or adult NS/NPCs.

2.7 Transplantations in Animal Models and Outcomes

Given the irreversible and multifactorial nature of cell death in brain injury, a regenerative therapy approach will be more clinically amenable than neuroprotection. While our CNS upregulates its own regenerative mechanisms after an injury, the extent of repair is usually too limited and insufficient for preventing functional or psychiatric deterioration [211, 212]. As a paragon of regenerative medicine, transplantation of stem cells has been widely explored, especially within varying animal models of TBI. In nearly all of these studies, stem cell therapy were observed to be safe and efficacious, with minimal side effects. One of the primary concerns of stem cell therapy is the formation of tumors, but out of dozens of investigations, only one study found any incidences of tumorigenesis [213]. Another major concern specific to TBI is the hyperexcitability of injured neurons, which makes them susceptible to excitotoxicity or formation of seizure foci [214, 215]. Thus, it needs to be ensured that this hyperexcitable state does not 1) cause excessive graft cell death, or 2) exacerbate host cell death after transplantation. From the preclinical rodent studies, there were no reports of heightened cell death for either population after transplantation.

Different routes of transplantation have successfully delivered the cell into the brain parenchyma, with chemoattractants like SDF1 guiding transplanted cells toward the lesion site. While IV injection is less invasive, the preferred route is usually the more direct intracranial implantation of cells, which results in greater cell retention around the injury zone. However, IV injections of BMSCs have demonstrated multifactorial benefits given their capacity for trophic support, such as upregulation of BDNF and NGF [216, 217], which have led to enhancements in functional recovery [218-220]. The BMSCs were also observed to successfully penetrate the BBB and engraft into the peri-contusion region [217]. For the most part, the number of cells used for IV

injections is an order of magnitude (on the order of 10^6) greater than the number used for IC injections of NSCs. This is to ensure great cortical bioavailability of the cells, given the systemic distribution of the circulatory system. However, despite accounting for the greater number of cells required, Harting et al. failed to replicate some of the positive findings that previous studies had reported for IV injection of BMSCs [221]. They found that <4% of cells actually traversed the lungs to enter arterial circulation (termed the "pulmonary first-pass effect"), and only a fraction of that number (0.0005% of total) managed to reach the brain parenchyma [221]. Similar effects of limited stem cell engraftment to the target site were observed by other studies, although Park et al. only measure BMSC uptake at 4 hr post-injection, which may have been too early of a timepoint [161, 222, 223]. Thus, while IV cell delivery is indeed exciting and translationally feasible, it would be prudent to be cognizant of the potential challenges associated with this particular delivery route and prepare appropriate alternatives or solutions when proceeding with clinical trials.

BMSCs are ideal vehicles for trophic support given their relatively low immunogenicity and tolerance by the recipient [217, 218, 224, 225]. In fact, BMSCs appear to confer immunosuppressive effects that can dampen the deleterious inflammatory response that occurs during the acute and chronic phases of TBI [190, 191]. However, NPCs derived from ESCs, iPSCs, or adult NSCs provide greater differentiation potency and a greater capacity for cell replacement and tissue repair after transplantation. For in vitro differentiation protocols, neuronal induction of BMSCs with retinoids usually yields only approximately 2-4% neuron-like cells, whereas neuronal induction of ESCs yields approximately 66-90% neuron-like cells, together with extensive neurite outgrowth [151, 226]. Transplantation of ES-NPCs also leads to greater co-expression of the grafted cells with neuronal markers, including the NSC marker Nestin, or the marker of mature neurons, such as neuronal nuclear antigen (NeuN) or microtubule-associated protein 2 (MAP2)

[227]. These markers are not as evident following BMSC transplantation, although there is a great degree of variability depending on the route of administration as well [217, 218, 226, 228, 229]. Nevertheless, transplantations of NPCs from any source and through varying routes of administration have consistently demonstrated robust efficacy across multiple models of TBI, including CCI, LFPI, and the weight-drop model. Furthermore, many different beneficial mechanisms have been implicated, including upregulation of growth factors [179, 216, 217, 230], restoration of BBB integrity [231], immunosuppression [190, 191, 231], reduced astrocytosis [232], neuroprotection [233], and neovascularization [225]. The multitude of beneficial effects makes stem cell therapy such an appealing candidate, because it provides simpler yet more versatile translational paradigm than a multi-faceted pharmacological or neuroprotective approach.

2.8 Clinical Trials of Stem Cell Therapy for TBI

Thus far, investigations of stem cells in TBI patients lag far behind that of stroke [234, 235] and spinal cord injury [236]. While stem cell therapy for stroke and spinal cord injury have already progressed to evaluation of more versatile cell types, such as with ES-NPCs and iPS-NPCs, nearly all of the research in the realm of TBI has been with either MSCs or BMSCs. Many of the trials involving stem cell therapy for stroke have already proceeded into or have completed Phase 2 clinical trials, which entails the evaluation of therapeutic efficacy, rather than just safety and feasibility. This is in contrast to the state of TBI clinical trials, in which only one has proceeded to begin Phase 2 testing (NCT02525432).

Nevertheless, the findings from the early phase clinical trials have proven fruitful and promising. The vast majority of TBI patients have been very tolerant and receptive to the stem cell

therapy from multiple routes, even invasive procedures such as stereotactic intracranial transplantations (studies currently in progress). More importantly, there have been minimal reports of adverse events or side effects, with the only incidental findings coming from a stroke clinical trial by Savitz et al., in which there were an increased risk of seizures and exacerbation of motor deficits [237]. There were no adverse events reported in any of the TBI clinical trials.

There remain many challenges that need to be addressed before widespread adoption of stem cell therapy for brain injury. For one, the observed beneficial effects seem to be very sporadic and minor, lacking the degree of impact expected from the regenerative capacity of stem cell therapy. While the studies are well-controlled, it is difficult to perfectly match patients, and possibly the different injury phenotypes or genetic makeup of the patients may account for the discrepancies observed in outcomes. Next, many different parameters still need to be optimized to determine possible indications and contraindications of stem cell therapy for brain injury. These include timing and dosage of transplantation, route of administration, subtype/severity of injuries, combination therapies (eg. biocarriers, transgenic cell lines), and so on.

In TBI, the studies varied widely in their window of administration, ranging from 24 hr post-TBI [238] sometimes up to even 1 month post-TBI [239], whereas the promising outcomes observed in animal models resulted from transplantations performed a maximum of 7 days post-injury. Dosage is also an important concern, given the inherent risk of tumorigenesis and immunoreactivity. Thus, establishing the balance for the optimal concentration and volume of cells, as well as the optimal number of injections, remains an ongoing and important consideration. So far, patients are receiving on the order of 10^7 cells for BMSCs in approximately 2 mL, and up to 4 dosings, without any apparent side effects [240]. However, because the beneficial effects were also relatively minor, there may still be margin for calibration and improvement.

Systemic delivery of stem cells (such as with IV or intra-arterial injections) can lead to widespread engraftment of the cells, potentially leading to disruption of other organs, especially with ectopic deposition of neuronally-differentiated cell type, although this has not yet been reported. Furthermore, there are extensive reports of the pulmonary first-pass effect of IV stem cell delivery, which leads to entrapment of cells within non-CNS organs, such as the lungs and heart, diminishing the overall effectiveness of the transplantation [161, 222, 223]. This can be possibly overcome with greater dosages of cells, but the optimal transplantation route may be the more direct intracranial implantation, which has so far proven safe with stereotactic guiding and a skilled neurosurgeon technique.

Other considerations include the severity of the injuries, as well as the different subtypes. For TBI, the vast majority of injuries are concussions or repeated concussions, which are considered mild TBI [1, 2]. However, the clinical trials have focused on severe TBI, in which there are more evident functional deficits. However, because concussions, and especially repetitive concussions, as is common for athletes and veterans, are more prevalent and result in insidious neuropsychiatric comorbidities, there is a great need to launch clinical trials that investigate cell therapy in this context as well.

2.9 Summary

Stem cell therapy holds vast potential for the treatment of brain injuries and other neurological conditions. However, there remains many challenges to be addressed within the near future in order to guide this therapy closer towards translational realization. The different cell types have been extensively studied through in vitro studies, but there is a great need to optimize the

transplantation protocol. There are many parameters at play, including the timing and route of administration, different cell types and dosages, and the different possible combination approaches. At the same time, it is exactly because this field is so nascent and unexplored that it is also filled with such tremendous possibilities and intrigue. Stem cell therapy has come a long way since its discovery, and we are finally beginning to realize the fruition of the accumulation of many decades of research. However, progress is oftentimes slowest during the infancy stage. Now that stem cell research has become more ripe, and with the accelerated progress in interdisciplinary fields such as genomics, proteomics, connectomics, and tissue engineering, we can anticipate more translational applications and breakthroughs for stem cell therapy in the decades to come.

Chapter 3: Evolving Frontiers of Cell Therapy

While stem cell therapy is a promising field, it remains imperfect and subpar for translational efficacy. Therefore, many combinatorial approaches that have been explored to advance cell therapy by addressing challenges involving stem cells through both extrinsic and intrinsic modifications. We highlight the four primary classes of combination therapies, including upregulation of growth factors, stem cell precondtioning, cellular biocarriers, and activity supplementation.

3.1 Performance Enhancing Factors

One of the earliest improvements is the upregulation of factors that promote the survival, differentiation, or neuritogenesis of the transplanted cells. In fact, while there are other distinct classes of improvements, For the success of cell therapy in the CNS, the most fundamental requirement is cell viability, because living cells will not only produce and secrete factors to provide beneficial paracrine effects on nearby cells [241, 242], but conversely dying or injured cells will release factors into the microenvironment that will halter surrounding cell proliferation and differentiation [177]. BDNF is a primary activity-dependent factor of the CNS, and it has been implicated in a plethora of critical functions for development and maintenance of the CNS, including promotion of survival and axonal outgrowth, regulation of synaptic current [243] and synaptic plasticity [244], and enhancement of neurogenesis [245]. In fact, the translational potential of BDNF has already been explored in preclinical studies of brain injury, including pharmacological administration of BDNF [246, 247] and BDNF overexpression by AAV infection [248].

Several investigations have evaluated the synergistic effect of BDNF upregulation with stem cell therapy, both of MSCs [180-182] and of NSCs [249]. The initial studies with BDNF upregulation was first performed in MSCs by adenoviral infection, which resulted in approximately 23-fold increase in BDNF as compared to non-transduced controls [181, 182]. The combination of MSCs with BDNF upregulation resulted in diminished cell death and infarct volumes, as well as greater sensorimotor functional recovery after brain injury [182]. Furthermore, when other growth factors, including glial derived neurotrophic factor (GDNF), ciliary neurotrophic factor (CNTF), and NT-3, were overexpressed, only the upregulation of GDNF resulted in similar benefits as BDNF upregulation [181]. Similarly, overexpression of GDNF was

carried out in NSCs by transfection [250] and by a transgenic stable cell line [251], and both resulted in greater cell survival, greater synaptogenesis, and improved functional outcomes. Another report found that MSC with BDNF did not reduce infarct size greater than that of MSC alone, but the discrepancy may be attributed to varying routes of administration, with the latter being intranasal delivery, which is not as efficient as intracranial [180]. Finally, a recent study demonstrated that transplantation of a stable human NSC line overexpressing BDNF in a mouse model of hemorrhagic stroke results in 3-fold greater cell survival, greater differentiation of the hNSCs and angiogenesis surrounding the graft site, and enhance motor functional recovery [249]. Similarly, another canonical activity-dependent factor is NGF, which is also involved in many critical activities, such as the survival and differentiation of neurons, as well as neurogenesis [252]. When NSCs are transplanted together with NGF administration after ischemic stroke, rats that received the combination treatment displayed greater levels of recovery in neurological function as assessed by the Neurological Severity Score (NSS) [253].

Aside from neurotrophins, other growth factors, such as VEGF, has also been upregulated, both by lipofectamine transfection [254] and by overexpression in a transgenic stable cell line [255]. The transplantation of the transgenic NSCs resulted in greater VEGF expression, which corresponded with greater cell survival, improved angiogenesis [255], and greater motor functional recovery [254].

Other factors that have been upregulated target other specific pathways or mechanisms after transplantation, such as cell death and migration. The B-cell lymphoma (BCL) family is a conserved set of anti-apoptotic proteins that can be upregulated to improve cell survival after transplantation, especially within the hostile environment that persists after brain injury [256-258]. In several of our previous reports, we demonstrated that post-stroke transplantation of ES-NPCs

that have been genetically engineered to overexpress BCL-2 resulted in greater viability of the cells, as well as greater neuronal differentiation, and better functional outcomes [257, 258]. Other pro-survival genes, such as Survivin, have been investigated as well and have produced synergistic effects after injury [259]. The C-X-C chemokine receptor type 4 (CXCR4) is the cognate receptor for the chemoattractant SDF1. When the transplanted cells are primed with CXCR4, they are able to enhance angiogenesis and neurogenesis around the lesion site and reduce infarct volume [94].

3.2 Preconditioning Approaches

Preconditioning of stem cells is an alternative method of naturally augmenting pro-survival and pro-growth factors that is based on the old adage of "what doesn't kill you only makes you stronger". This approach relies on the cells' own machinery in order to synthesize and release factors conducive to survival and resilience upon exposure to a non-lethal insult. The more widely adopted approach is hypoxic preconditioning (HP), which is a simple procedure that involves exposure of the cells to oxygen-glucose deprivation (OGD, with 0.1-1% O_2) for 8-12 hrs prior to transplantation. We have demonstrated that OGD is a feasible strategy in BMSCs and other more pre-differentiated NPC types for upregulating specific beneficial factors, including the neurotrophins BDNF and GDNF, VEGF and its receptor VEGF-R (AKA FLK1), erythropoietin (EPO) and its receptor EPO-R, and the chemokine SDF-1 and its receptor CXCR4 [260, 261]. Thus, HP is an effective combinatorial strategy in increasing transplanted cell survival, accelerating differentiation [166, 262], homing towards the injury zone [263], promoting angiogenesis around the injury. These all ultimately contribute to bolster the functional recovery associated with stem cell therapy after brain injury [166, 260, 261]. Pharmacological preconditioning is a more recently developed strategy that exposes stem cells to certain drugs, such

as diazoxide [264] and minocycline [265], or chemokines to improve post-transplantation survival [266].

3.3 Cell Carriers for Improved Delivery

Currently, the vast majority of studies utilize modified culturing media as the stem cell vehicle for direct implantation [260, 267-269]. However, while this provides the ideal nourishment for cells in vitro, it does not mimic the natural microenvironment of the native CNS parenchyma after transplantation [270], which can impair grafted cell retention, viability, differentiation, and cell-cell engagement with host cells [257, 271]. Furthermore, the low viscosity of the medium provides inadequate protection of the cells against the rapid flow associated with injection through a narrow syringe needle or catheter, as is the conventional paradigm [272, 273]. New biomaterial carriers for delivery have been engineered to address some of these challenges. Early investigations were performed on scaffolds mimicking the endogenous extracellular matrix (ECM), which demonstrated greater axonal extensions and eventual "biobridging" between host and grafted cells, including enhancing connectivity and reciprocal interactions [271]. These resulted in a meshwork of arborized neurites, which also became vascularized and appeared to restore the lost parenchyma. Other matrices have been developed as well, including Matrigel scaffolding [274], which has shown syngergistic effects with stem cell transplantation after both stroke [275] and TBI [276]. While Matrigel provided a solid proof-of-concept for the scaffolds as feasible and effective cell carriers, they were not as clinically applicable given their derivation from mouse sarcoma lines [273], and other scaffolds were engineered, including plasma scaffolds [277], collagen/heparin sulfate scaffolds generated by 3D bioprinting [278], and other manufactured hydrogels. Not only do hydrogels provide the scaffold for local cell adhesion, they provide synergistic effects specific

to brain injury, including protecting against local inflammation and macrophage infiltration [279], reducing reactive astrocytosis, promoting vasculogenesis [280], and capturing and enriching growth factors [270]. Finally, another biocarrier under exploration is encapsulated biodelivery, which is the transplantation of cells within an alginate microcapsule that allows for the flow of nutrients and oxygen [281]. While the optimal biocarrier has yet to be determined and may differ across applications, hydrogels provide an especially promising avenue of improvement given their multitude of modifiable parameters, including polymer type (including degree of sulfation), porosity, stiffness, and biodegradability.

3.4 External Stimulation for Activity-Driven Plasticity

3.4.1 Activity-Dependent Plasticity During Development and After Injury

Endogenous neural activity and cell-cell interactivity are essential mediators of neuronal survival and differentiation and synaptic remodeling, especially during CNS development [282-284] . Both evoked [284] and spontaneous activity [285] are necessary for proper neuritogenesis and axon guidance during CNS development. While the relevance of neurogenesis becomes less pronounced in the healthy adult CNS, a brain injury such as stroke and TBI creates a sudden and irreversible loss of healthy tissue that necessitates the restoration of neurons and repair of neuronal connectivity. Indeed, endogenous neurogenesis is upregulated after injury [69], and the plasticity is contingent upon the similar activity-dependent factors that predominate during development [286-288]. Similarly, exogenous stem cells recapitulates the neural precursors and immature neurons that predominate throughout development, and as such, they rely on the comparable levels of neural activity for synaptogenesis and plasticity. During development, the expression and

release of neurotrophins such as BDNF and NGF are coupled with electrical activity, both evoked and spontaneous [242]. These activity-dependent factors both enhance survival of local neurons, neurite outgrowth and extension, and the formation and strengthening of new synaptic connections [252, 289-291]. The original connections that maintained the proper conduits for neuronal activity are lost following an injury such as TBI, and transplanted cells do not initially possess any graft-host connectivity, which warrants the supplementation of the activity by artificial stimulation (*Figure 3-1*). Indeed, direct electrical stimulation *in vitro* has demonstrated multiple beneficial effects, such as enhancement of magnitude and speed of neurite outgrowth and functional maturation in various neural cell types [292, 293], including NPCs [294, 295].

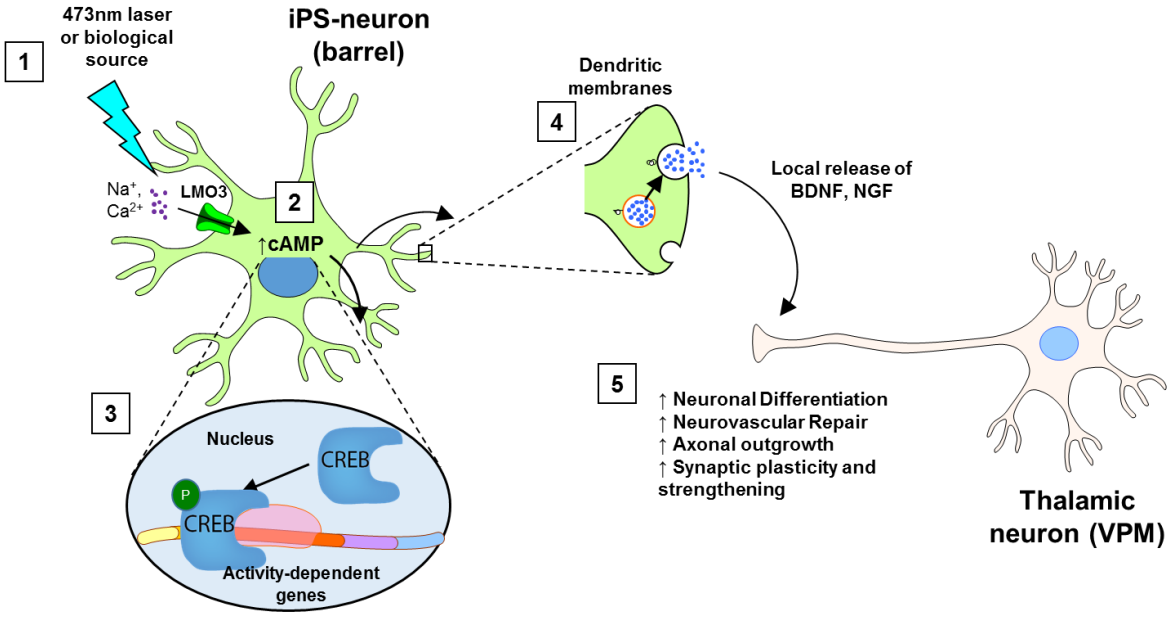

Figure 3-1: Mechanistic schematic of photostimulation-induced neurophysiological changes.

1) 473nm laser activates ChR2 encoded onto neuronal membranes, which opens and allows influx of cations Na+ and Ca2+. 2) Depolarization leads to an increase in cAMP and Ca2+-mediated CaMKII activation. 3) Both cAMP and CaMKII [296, 297] can phosphorylate and activate cAMP response element-binding protein (CREB). 4) CREB recognizes CRE sequences in BDNF and

NGF genes to promote BDNF and NGF transcription. 5) High CaMKII and cAMP levels also activate the secretion of activity-dependent factors such as BDNF and NGF from dendrites [284, 298, 299], resulting in enhanced local synapse formation and maintenance [252, 289-291], which promotes cell-cell engagement between host neurons and iPS-neurons.

3.4.2 Stimulation Modality: Neuroprosthetics

Multiple classes of stimulation modalities have been engineered, with most of the current conventional models relying on electrical stimulation, which has provided the basis behind the earlier examinations of the beneficial effects of stimulation. Neuroprosthetics such as implantable deep brain stimulating (DBS) electrodes, which has been a cornerstone of therapy for Parkinson's disease, epilepsy, and psychiatric disorders [300-303]. However, the therapeutic application is limited given the technical demands of implantation, as well as the invasive nature of the surgery. More recently, other modalities like magnetic and light stimulation have garnered attention as well, and there has been a shift towards non-invasive modes of stimulation, such as transcranial direct current stimulation (TDCS), transcranial magnetic stimulation (TMS), red-shifted or near-infrared (NIR) light stimulation [304, 305], or physiological stimulation (eg. whisker stimulation) [306, 307]. Different stimulation modalities will require optimization for different procedures. For example, TDCS and TMS may be very useful in conjunction with stem cells for treating more pathologies with more diffuse aberrations like neurodegenerative diseases or neuropsychiatric disorders such depression [308, 309]. However, focal injuries like stroke and TBI results in a subacute state of hyperexcitability, for which stimulation may lead to epileptiform activity [214, 215, 310]. Thus, modalities with poor spatial resolution, such as TDCS and TMS, may be contraindicated for stimulation of the transplanted cells [311, 312], whereas genetic engineering

approaches, such as optogenetics, could provide a feasible alternative for cell-specific level of stimulation precision [313].

3.4.3 Precision Stimulation by Genetic Engineering

Given the lack of precision associated with electrical or magnetic stimulation paradigms, there has been more attention focused on genetic delivery of actuators into specific cell populations that can be activated by a normally inert stimulus. The two major broad classes for targeting neural cell types are optogenetics and chemogenetics, though there are others that have emerged recently, including magnetogenetics and radiogenetics [314-316]. There has been much advancement made within and as a result of the field of optogenetics, and that will be the focus of the subsequent chapter. While optogenetics has been most heralded for dissecting complex neural circuits in both healthy and pathologic brains [317, 318], there is untapped potential for exploiting optogenetics for its photostimulatory capacity. Accordingly, there may be an anticipated paradigm shift of using optogenetics as a therapeutic actuator rather than just an interrogative tool.

Another similar arena involves chemogenetics, with the advent of designer receptors exclusively activated by designer drugs (DREADDs) [319], which creates a means for graft cell-specific pharmacological stimulation. DREADDs such as hM3Dq and hM4Di have both been incorporated into stem cells, but similar to optogenetics, it has only been exploited as an interrogative tool [320]. While DREADDs has great translational potential because of the non-invasive nature of drug delivery, it lacks the temporal specificity of optogenetics, and the off-target and adverse effects of the DREADD ligand must be thoroughly evaluated and minimized before proceeding to any clinical trials. One of the main challenges of DREADDs is the back metabolism of the ligand clozapine-N-oxide (CNO) to clozapine in humans (not as evident in animals), which

could lead to severe adverse psychiatric effects [321]. Nevertheless, the combination of either a chemogenetic or optogenetic stimulation paradigm and stem cell therapy could provide a promising means to drive neural activity in transplanted NPCs to enhance network remodeling and repair.

Chapter 4: Optogenetics

4.1 Introduction

Optogenetics is the genetic encoding of light-sensitive proteins, or opsins, into cells that may or may not natively respond to light. This groundbreaking method, whose importance has been reinforced after being deemed the Nature Method of the Year in 2010, has been critically important in neuroscience as an interrogative tool for dissecting nebulous and complex neural circuits in both healthy and pathological brains, allowing for accelerated advancement of the field of connectomics [318]. Optogenetics has also synergized well with stem cells to provide a means for evaluating functional integration after transplantation. Optogenetic probes such as *Chlamydomonas* channelrhodopsin 2 (ChR2) [206, 322, 323] and the Natronobacterium halorhodopsin (NpHR) [209] have already been encoded into stem cells in order to directly excite or silence, respectively, the cells after transplantation.

4.2 The Expanding Optogenetic Toolbox

Optogenetic derives from the fact that the light-sensitive proteins (hence "opto") are packaged into genetic plasmids or viruses that can be used to encode genetic information into specific populations nontransgenic cells. Because the opsins respond to light, rather than the diffusion of chemicals, they can operate at an unprecedented temporal resolution, on a millisecond timescale, which allows for dissection of neural circuits by coupling the stimulus with the response [324]. Although Karl Deisseroth is considered to be the original pioneer of optogenetics for the field of neuroscience [324, 325], opsins have been studied since the 1970s for biophysical insights, and ChR2 was actually first characterized and engineered by Nagel et al. in 2003 [326] and the engineered form of ChR2 wsa demonstrated in oocytes from *Xenopus laevis*. From there, many other opsins have been discovered or synthesized, including excitatory and inhibitory ion channels, ion transporters, and even chimeric fused to G-protein coupled receptors (or optoXRs, or RH-CTs) [327], which allow for exquisite control and interrogation of intracellular signaling mechanisms, such as for serotonin (5-HT1A) receptor signaling [328]. By far, the most widely used opsins in neuroscience research has been the excitatory and inhibitory opsins.

For excitatory opsins, ChR2 remains the benchmark for comparison, given its ability to be expressed in multiple cell types and robustly drive cell activity and elucidate biophysical function, this has led to the discovery and creation of many variants of channelrhodopsins (*Figure 4-1*) [329]. These variants address some of the limitations of ChR2, including its sensitivity to a certain wavelength and intensity of light and its on/off kinetics. The variants of excitatory opsins include those that exhibit greater sensitivity and higher amplitude currents, such as ChR2(H134R), ChR2(T159C), ChRGR (ChR2 producing Channelrhodopsin-green receiver), [330, 331] or opsins that have either faster or slower off-kinetics, and ChETA, step-function opsins (SFOs), ChIEF,

and the ChR2(D156A) mutant [332-335]. There are also channelrhodopsins that have enhancement of permeability to Ca^{2+}, such as CatCh [336]. Then there are color shifted channelrhodopsins that allow for activity using different wavelengths of light, such as light of a longer wavelength (ie. red-shifted), including VChR1, MChR1, C1V1, and ReaChR, an opsin that has been red-shifted such that it enables non-invasive deep transcranial optogenetic activation [304].

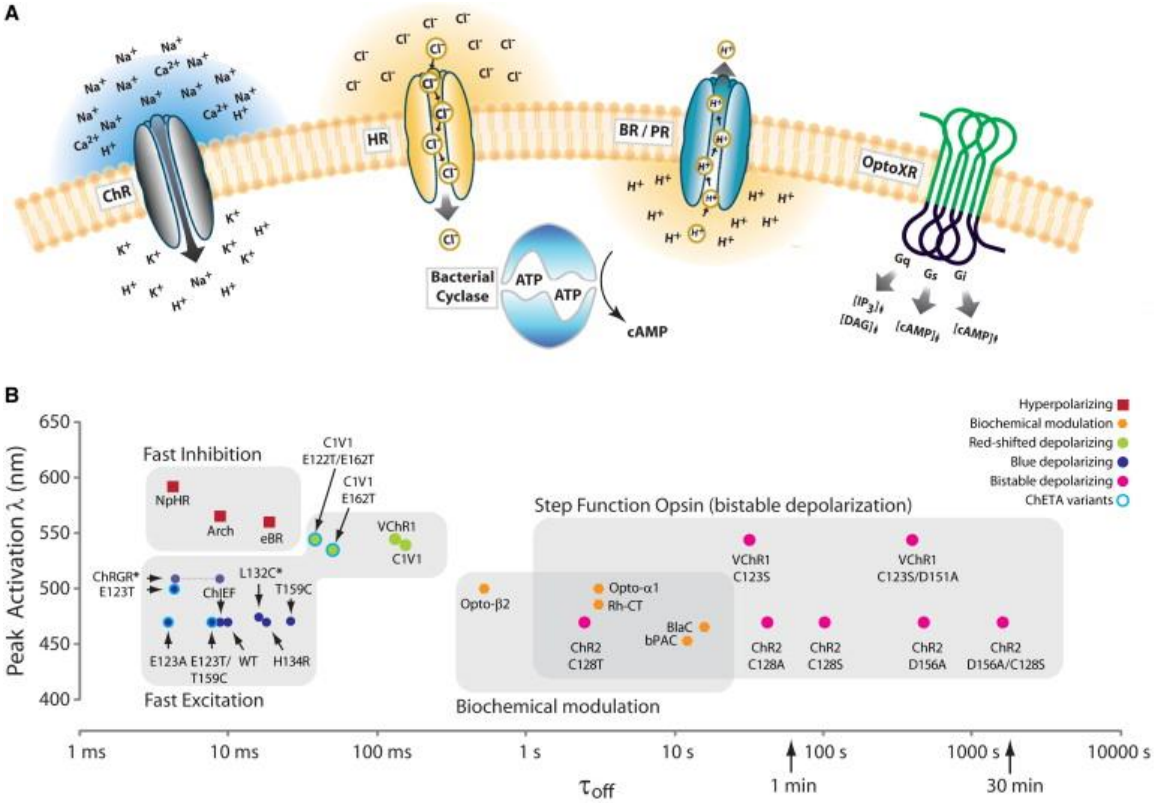

Figure 4-1: Overview of major classes within the optogenetic toolbox.

Credit: Yizhar et al. [329] Four major classes of opsins are currently predominant, including excitatory channelrhodopsins, halorhodopsins, bacteriorhodopsins, and optoXRs, which are type II fusion protein that combine light-sensitive opsins with G protein coupled receptors. Furthermore, the different variants of the four classes are stratified according to their wavelength

of activity (ie. color of light) and their on/off kinetics. SFOs provide the best option for extended periods of stimulation, whereas fast excitation variants, such as ChRGR and ChETA allow for higher-frequency excitation.

In the realm of inhibitory opsins, the two most common classes are the halorhodopsins, which are light-driven inward chloride pumps derived from archaea species (also known as halobacteria), and the archaerhodopsins, which are light-drive outward proton pumps. The first to be used extensively in neuroscience is the halorhodopsin from the archaeabacteria *Natromonus pharaonis* (NpHR), which is activated by yellow light [337]. In general, they have lower efficiency of expression as compared to channelrhodopsins and require trafficking sequences (TS), such as Golgi TS or endoplasmic reticulum (ER) export motifs or both, in order to enable for greater membrane localization and greater silencing function [338-340]. The most commonly used archaerhodopsin is archaerhodopsin-3 (Arch) from Halorubrum sodomense, which has been shown to enable near 100% silencing of neurons in awake mice brains [341]. It is activated by green/yellow light and differs from NpHR in that it spontaneously recovers from light-dependent inactivation, making it more resilient against desensitization. Improved variants of Arch has also been engineered with added TS motifs, but moreso in the context of voltage-sensitive fluorescence for monitoring that rather than eliciting activity [342].

4.3 Targeted Delivery of Opsins

There are multiple mechanisms by which transgenes can be engineered into specific cell types. These include plasmid transfection, such as through lipofectamine or electroporation, or more commonly for in vivo paradigms, viral infection. Two major classes of viruses that have been used include recombinant adeno-associated virus (AAV) [343, 344] and lentivirus (LV) [345, 346].

For retrograde delivery of viruses from axon terminals back to cell bodies, opsins packaged into herpes simplex virus (HSV) vectors have also been utilized [347, 348]. For AAVs, there are 9 different serotypes that possess varying degrees of tropism for different organ systems [349]. In the brain, the rAAV2 and 9 serotypes seem to possess the greatest magnitude of transduction into cortical neurons, making this a suitable option for packaging optogenetic transgenes [350]. The tropism also varies between rAAV and LVs, with rAAVs seeming to be less discriminatory between excitatory vs. inhibitory neurons in the cortical region, while LVs preferentially transduce excitatory neurons [351]. Another major difference between AAVs and LVs is that AAVs tend to replicate episomally while LV vectors integrate into the host genome, potentially leading to interference from surrounding chromatin and unintentional disruption of host genes. Furthermore, the maximum capacity of each viral vector must be accounted for, which is around 5 kb for AAVs and 8 kb for LVs [352, 353].

While tropism certainly plays an important role in directing genetic transfer, another important consideration is the promoter chosen to drive the expression of the transgene. There are many different options, including ubiquitously-expressing promoters, such as elongation factor 1-α (EF1α), the cytomegalovirus immediate-early enhancer (CMV), or the combination of chicken β-actin promoter, the CMV immediate-early enhancer, and the splice acceptor of the rabbit β-globin gene (CAG) [354]. Furthermore, there neuron specific promoters, such as human synapsin (hSyn) [355], human thymocyte differentiation antigen 1 (Thy-1) [356]. Finally, there are promoters specific for neuronal subpopulations, such as those for excitatory neurons, α-calcium/calmodulin-dependent protein kinase II (CAMKIIα) [357].

4.4 Delivery of Light

The dependence on light for stimulation is a double-edged sword. While it allows for the selective stimulation of specific cell types, it requires a source of light and a delivery system for that light to reach the cells. The light delivery can be separated into two different categories: invasive and non-invasive. During the nascent period of optogenetics, much of the research relied on fiber-coupled lasers that can be stereotactically implanted into specific regions of the brain via cannulas for acute stimulation, or can be cemented to the skull via dental acrylic after insertion for chronic stimulation [313]. Since then, light-emitting diode (LED)-coupled fibers have also emerged as a more cost-effective alternative to lasers, and while LEDs do not offer the same degree of light collimation, power output, and irradiance, utilizing an optical fiber that is plastic rather than glass and with a greater numerical aperture (NA) can help maintain the fidelity of light transmission [358]. As such, there are many different variables that should be taken into account in choosing the fiber, such as material, NA, inner and outer diameters, and whether the fiber should be jacketed for protection. Given the cost-effectiveness and improvement of light delivery with LEDs, there is a trend towards greater adoption of LED-coupled fibers in the future.

The other major category is non-invasive delivery, which is also a burgeoning area of research, given its latent potential for translational applications. Non-invasive light delivery would be able to address some of the challenges associated with optogenetics, including the requirement of a skilled neurosurgeon hand to implant the optical device. There has also been a shift towards untethering the light source so that the implanted device is completely wireless, and this has been achieved through a radio-frequency (RF) power source [359, 360]. Some of the existing alternatives to optical fibers include completely non-invasive options such as injectable LEDs or optoelectronics [361] or partially non-invasive options that involve the subcutaneous implantation

of a wireless optogenetic device that is RF-powered and can stimulate cells within the brain [359]. Furthermore, there are also mechanically soft and stretchable optoelectronic systems developed that also operate on RF power and can be fully implanted on top of the spine or elsewhere to allow for stimulation of even peripheral targets [360] to treat pain and other patholgies, such as glucose homeostasis or vascular dysregulation [362].

Finally, another non-invasive option involves another light source altogether. Rather than relying on a biomedically engineered device for light generation, several groups have tapped into natural phenomena to capitalize on the light sources that are already found in certain biological organisms, such as fireflies and marine crustaceans [363].

4.5 Luminopsins: Next-Generation Optogenetic Fusion Proteins

Luminopsins are a recently developed class of proteins that is comprised of a light-responsive opsin coupled to a light-generating luciferase [364]. Once the luciferase substrate, luciferin, is available, the luciferase will oxidize the reaction of luciferin into photons of light, and given its proximity, the opsin will then be activated. The primary luciferin that is utilized is coelenterazine (CTZ). Multiple subtypes of luminopsins have already been developed, including ones for inhibition [365] and excitation [366, 367].

Berglund et al. first demonstrated the feasibility of this fusion protein within an in vitro system using ChR2 and a *Gaussia* luciferase (GLuc), which produced robust photocurrents with lamp stimulation, but demonstrated very limited response to CTZ (only a few pA) [366]. Building off of this, they switched to the more sensitive *Volvox* channelrhodopsin 1 (VChR1) and coupled that with the slow-burn variant of GLuc (sb-GLuc), which provided more sustained emission of

light (*Figure 4-2*). This new LMO version (LMO3) demonstrated a much greater photocurrent response (on the order of 100-200 pA in vitro, and 10-50 pA in slice recordings), and a much greater coupling efficiency (essentially the ratio of the photocurrent response to CTZ vs. to lamp stimulation), which was 10-fold higher as compared to previous generations of excitatory LMOs [367].

Tung et al. and Berglund et al. both also demonstrated the feasibility of inhibiting neural activity using LMOs. Tung et al. created a optimized version of inhibitory LMO (iLMO2) that comprised an NpHR fused to a brighter *Renilla* luciferase variant, Nano-lantern [365]. The iLMO2 was able to provide peak photocurrents of ~50 pA and coupling efficiency of ~20%. Furthermore, iLMO2 was able to suppress neural activity in vitro with CTZ stimulation (complete suppression of spontaneous action potentials and partial suppression of evoked action potentials), and also suppressed activity in vivo with CTZ stimulation by ~60% and resulted in functional differences in rotational behavior [365]. Another iLMO was developed by Berglund et al., which was made up of a photosensitive proton pump (Mac) and the super luminescent GLuc (slGLuc), and they demonstrated that CTZ stimulation resulted in hyperpolarization and elimination of action potential in vitro, as well as suppression of neural activity in vivo and modulation of turning behavior [367].

The advantages for luminopsins is especially apparent when considering the therapeutic applications of optogenetics, such as for providing artificially-driven stimulation after stem cell transplantation or to correct aberrant cell activity either through excitation or suppression (eg. for epilepsy). Having a system in which the light source is directly tethered to the opsin and can be pharmacologically delivered can resolves many of the translational challenges associated with optogenetics, including 1) hardware dependence, whether wired or wireless (eg. power source

and/or optical fiber), 2) potential invasive intracranial surgery (for implantation and for any maintenance), 3) possible tissue damage from the intensity of light stimulation (eg. heat from the laser), and 4) limited penetration of light in brain parenchyma, resulting in limited stimulation of deeper brain regions and a limited volume of influence. Luminopsins provide an elegant solution to all of these challenges by deriving its light source from a pharmacologically administered biological source, such as CTZ. While there is an initial invasive surgery required to deliver the transgene vector to the anatomical target, it is not as intrusive as implantation of a neuroprosthetic. Furthermore, luminopsins maintain the versatility associated with optogenetics, because both the transgene vector concentration (eg. viral titer) and the CTZ dosage can be titrated to fit individual requirements. One drawback of this combination of pharmacogenetic and optogenetic approach is that the temporal specificity of light stimulation is lost, and there is less control over the frequency of stimulation. However, this is not as important for therapeutic applications, in which the goals may be just to broadly upregulate spontaneous activity of transplanted NPCs to promote greater trophic support or to suppress epileptiform activity. Thus, luminopsins provide an ideal system for optimizing the translational value of optogenetics.

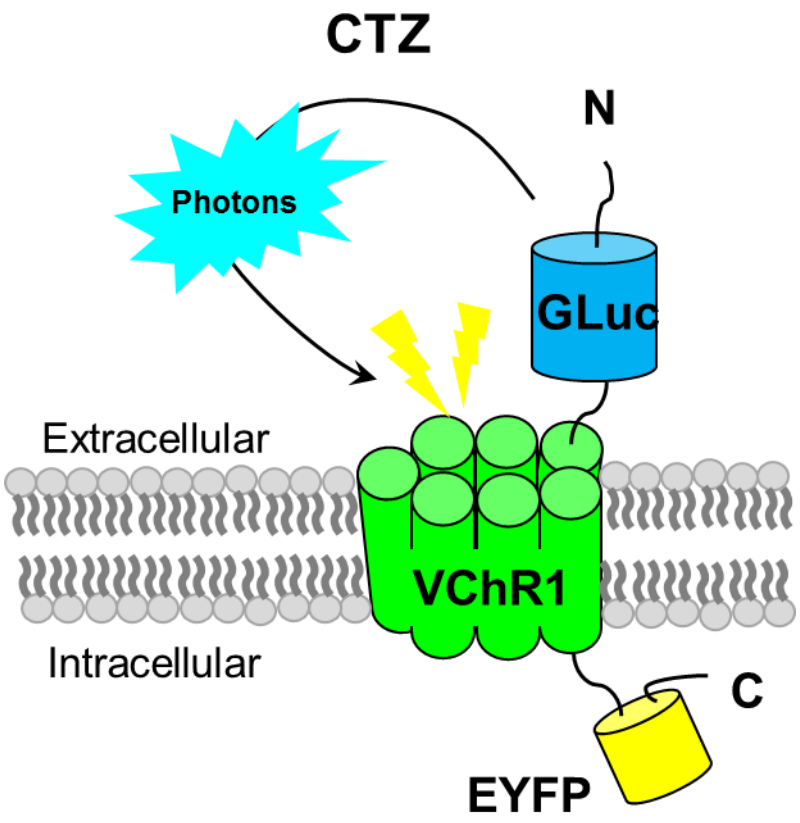

Figure 4-2: Luminopsins allows for non-invasive activation of channelrhodopsins.

Adapted from Figure 1 of Berglund et al. (2013) [366]. Luminopsins are a class of fusion proteins that contain a bioluminescent *Gaussia* luciferase (GLuc) that is directly attached to the N-terminus of the photosensitive *Volvox* channelrhodopsin (VChR1), which is an excitatory ion channel. Coelenterazine (CTZ, administered via IV or IP or IN) will be oxidized by GLuc to produce photons that can activate the VChR1 to allow cation influx. An enhanced yellow fluorescent protein (EYFP) tag at the C-terminus will be used to confirmation of expression efficiency.

4.6 Optogenetics and Stem Cells

Although they are interdisciplinary fields, optogenetics synergizes well with stem cells given the ease of genetic manipulation of the mitotic stem cell population, as well as the demands

for either interrogating or stimulating stem cells following transplantation. So far, the primary utility of optogenetics for stem cells has been to evaluate functional integration after transplantation. This has been done in both normal brains [322, 323, 368] and neuropathological models, such as Parkinson's disease [209]. These studies have been crucial in demonstrating that transplanted stem cells, even human ESC xenografts [368], are capable to integrating into host circuitry and driving neural activity.

While this has continued to provide useful information about the fate of NPCs after transplantation, there is also a growing realization for the potential of optogenetics to also function as a stimulatory actuator of NPCs after transplantation. Optogenetic stimulation of remotely connected regions has already been shown to provide beneficial effects via enhancing neurogenesis and plasticity after stroke [369-371]. Thus, the combination of grafted cell driving activity and plasticity may play an important role in promoting neurovascular and functional repair.

In addition, optogenetics has already been investigated in NPC models in vitro, in which optogenetic stimulation of varying parameters and durations resulted in upregulation of neurotrophins, BDNF and NGF, as well as greater levels of neurite outgrowth and length [372]. Finally, Daadi et al. has investigated optogenetic stimulation of grafted NPCs after stroke and demonstrated an immunosuppressive effect, as well as a genetic profile suggestive of enhancement of neuronal differentiation, plasticity, and graft-host engagement [373]. While this is an important pilot study, more research is needed to characterize the cellular and physiological responses to optogenetic stimulation of grafted cells, especially within other pathological models, such as TBI.

Chapter 5: Rationale, Aims, and Experimental Methods

5.1 Rationale and Significance

TBI is the leading cause of morbidity and mortality among children and young adults in developed countries [1, 2]. TBI is a neurological disorder that uniquely afflicts otherwise healthy and high-functioning individuals, such as young adults, athletes, and soldiers in combat. After the primary insult, TBI results in secondary damage, such as blood-brain barrier disruption, inflammation, and reactive oxidative species release, that leads to the emergence of two distinct histological regions, similar to stroke pathophysiology [10]. The core region is comprised of complete or near-complete irreversible cell death due to both the primary and secondary effects [21]. The peri-contusional region (analogous to the stroke penumbra region) contains injured cells that can still be salvaged with intervention [17]. Most available therapies, such as hypothermia and hyperbaric oxygen therapy, are beneficial only for containing the spread of secondary effects in the peri-contusional region [23]. The drawbacks are that these therapies are time-sensitive and cannot reverse the cell death in the core. Although neuroprotection would be appropriate within a specific narrow time window that is often not possible for TBI. Thus, there is a great need for repairing or reversing TBI-induced neuronal damage. However, there are currently no effective therapies.

One promising approach for repairing brain damage is regenerative medicine, of which stem cell therapy remains the paragon. ESCs and MSCs have demonstrated efficacy in promoting neurogenesis and improving functional recovery for several brain pathologies such as spinal cord injury [233, 374] and ischemic stroke [257], and even TBI [218, 233]. More recently, induced

pluripotent stem cells (iPSCs) have emerged as superior translational candidates given their advantages over their stem cell counterparts. Through reprogramming of autologous fibroblast cells, iPSCs bypass immunoreactivity and ethical barriers, while still retaining the same pluripotent and proliferative potential [84, 91, 114]. Pluripotent iPSCs can be induced to differentiate into neural progenitor cells (NPCs) that can be transplanted into injury models. To our knowledge, this will be the first investigation delving into the therapeutic benefits of iPSC-derived NPCs (iPS-NPCs) for TBI.

Most of the recovery benefits observed with transplanted NPCs are believed to be primarily due to enhancement of trophic support, which ameliorates endogenous cell death and augments endogenous neurovascular repair [179-182]. This is primarily because most grafted cells do not survive in the hostile pathological environment [160, 257, 375, 376]. There is on the order of ~30% acute cell death of transplanted mouse ESCs, mainly through apoptosis, because upregulation of anti-apoptotic factor BCL-2 successfully reduces acute cell death to ~10% [257]. This can be very variable depending on the cell line used and route of administration, with another study using human human NSCs demonstrated a greater cell death rate of ~67% [376]. Nevertheless, some cells do survive and manage to advance past the NPC stage, and recent data have demonstrated the ability of grafted NSCs to differentiate into functional neurons and even incorporate into host circuitry. Maturation and functional integration occurs efficiently in healthy rodent models [377-379]. However, in pathological paradigms, the maturation and integration efficiency drastically declines, with the vast majority of stem cell-derived neurons failing to produce action potentials [205, 380]. This may be largely due to the absence of healthy neural activity in the injury area, particularly in the atrophied core region [11, 87]. Cell-cell interactivity is an essential mediator of synaptic remodeling, by promoting neurite outgrowth and guidance, as well as formation and

maintenance of new synaptic contacts [282-284, 288]. Without the trophic and stimulatory support, grafted cells fail to mature and engage with existing host circuitry [284, 285, 291]. Understanding and improving upon graft-host integration will be a critical step in repairing the irreversible damage to neuronal networks in the core, an area previously thought to be irreparable [10, 381]. Previous *in vitro* studies have shown that direct electrical stimulation is able to augment axon regeneration in different neuronal subtypes, as well as enhance maturation and neurite outgrowth of neural progenitor cells (NPCs) [291, 293-295]. As an incremental advancement to these discoveries, there is a need for external stimulation of transplanted iPS-NPCs to drive neural activity in order to promote activity-dependent plasticity and repair after TBI.

Conventional modes of stimulation carry many disadvantages. Implantable electrodes, such as deep brain stimulating electrodes, are invasive and cumbersome [301-303]. Other methods may be non-invasive, such as transcranial direct-current stimulation and transcranial magnetic stimulation, but do not provide enough spatial resolution [311, 312]. Nonspecific stimulation may exacerbate the hyperexcitability of cells in the pericontusional region and increase seizure frequency after TBI [214, 215]. Optogenetics, on the other hand, provides cell-level spatial resolution because of the ability to engineer photosensitive ion channels (opsins) into specific cells [325]. A translational obstacle is that activation of the opsin requires the intracranial implantation of a light source, such as a fiber optic cable [313]. This is invasive and will likely further exacerbate the injury due to physical penetration and heat production. Furthermore, light photons are scattered upon penetration of even a few hundred microns of cerebral tissue [317]. Transplanted stem cells may disseminate rapidly after injection and can migrate even longer distances (~1mm), thus reducing their sensitivity to a conventional light source [376]. Luminopsins (LMOs) are a novel class of fusion proteins that link channelrhodopsins with bioluminescent luciferase proteins that

convert the coelenterazine (CTZ) substrate) into light photons (*Figure 4-2*), allowing for non-invasive opsin activation [365-367]. Once LMOs are transgenically introduced into neurons, the cells can then be pharmacologically-activated through controlled injections of CTZ. In this dissertation, I demonstrate and evaluate the novel application of engineering LMOs into mouse iPSC-derived NPCs (miPS-NPCs), which will provide a non-invasive and cell-specific method of artificial stimulation.

5.2 Specific Aims

Central Objective

The primary objective of this dissertation is to evaluate a novel strategy to overcome a key obstacle: the limited ability of grafted stem cells to engage with host cells and promote endogenous neurovascular repair. After transplantation of iPS-NPCs into our established mouse barrel cortex TBI model in mice, I hypothesize that bioluminescence-derived photostimulation (CTZ stimulation) of the iPS-NPCs will result in enhanced graft-host plasticity and repair *in vivo* and improved functional outcomes. The results of this dissertation could yield broad implications for clinical applications of stem cell therapy.

Specific Aim 1

To develop an iPS cell line that is sensitive to biologically derived (ie. CTZ) photostimulation, and characterize the photoresponse. Hypothesis: CTZ stimulation LMO3-expressing iPS-NPCs will upregulate neurotrophins, axonal outgrowth, and plasticity.

1.1: Create and validate an LMO3 plasmid containing the fused VChR1-sbGLuc transgene.

1.2: Establish an iPS cell line that expresses LMO3, which will be functionally validated by performing *in vitro* luminescence and electrophysiology studies.

1.3: Determine neurotrophic responses to photostimulation at different stages of neural progenitor cell differentiation

Specific Aim 2

Evaluate cellular and functional outcomes using CTZ-induced stimulation following iPS-NPC transplantation in barrel cortex TBI model. Hypothesis: CTZ stimulation of the whisker thalamocortical pathway will enhance graft-host plasticity, endogenous neurovascular repair, and functional recovery after CCI.

2.1: Validate cell viability and LMO function after transplantation of LMO3-expressing iPS-NPCs in a mouse barrel cortex TBI model

2.2: Assess effectiveness of CTZ stimulation for upregulating activity-dependent neurotrophin release and enhancing endogenous plasticity and neurovascular repair in vivo

2.3: Compare functional recovery of TBI animals treated with combination therapy of LMO3-expressing iPS-NPC transplantation and CTZ stimulation vs. iPS-NPC transplantation alone

Specific Aim 3

To develop a superior version of the LMO3 that contains the Golgi trafficking sequence (TS) to improve membrane localization.

3.1: To create the virus containing LMO3 with an inserted Golgi TS motif and assess the membrane localization by fluorescence imaging.

3.2: To evaluate the functional improvements of membrane localization by electrophysiology and behavioral assay.

5.3 Experimental Methods

Maintenance and differentiation of iPS Cells

Mouse WP5 iPS cells were purchased from Stemgent (Stemgent Inc, Lexington, MA, USA). Undifferentiated iPS cells were cultured in 0.1% gelatin coated T25 flasks in stem cell culture media consisting of DMEM (Corning Inc, Corning, NY, USA), 10% ES cell FBS (Life Technologies, Grand Island, NY, USA), 10% NCS (Sigma-Aldrich, St. Louis, MO, USA), 2 mM glutamine (Stemcell Technologies, Vancouver, BC, Canada), 0.1mM NEAA (Stemcell Technologies), 55 μM 2-mercaptoethanol (Sigma-Aldrich), 2000U/ml LIF (Miltenyi Biotec, Auburn, CA, USA) and 100U/ml pen/strep (Corning). For neuronal differentiation, iPS cells were differentiated in suspension culture with a "4-/4+" (4 days without/4 days with) retinoic acid (RA, 1μM) (all trans-RA, Sigma-Aldrich) protocol in LIF-free medium under rotary condition as

previously described [382, 383]. Briefly, cells were dissociated from the growth flasks by trypsinization with 0.25% trypsin-EDTA (Life Technologies) for 2 min. Then cells were seeded onto standard 10-cm bacterial Petri dishes in stem cell culture media lacking LIF and β-mercaptoethanol. Within the first day, the cells formed embryoid bodies in suspension culture. In the last 4 days, 500 nM of all-trans RA was added to the media. After 4-/4+ culture, the iPS-NPCs were ready to be dissociated and harvested for transplantation or in vitro terminal differentiation on poly-D-Lysine (PDL, 0.1 mg/mL)/Laminin coated dishes in modified SATO media (containing 100 mM MEM pyruvate, 1× SATO (final concentrations: 100 µg/mL BSA, 60 ng/mL progesterone, 16 µg/mL putrescine, 40 ng/mL thyroxine, 30 ng/mL tri-iodothyronine, 10 µg/mL insulin, 10 µg/mL transferrin, 10 µg/mL sodium selenite – all dissolved in DMEM), N-acetyl cysteine, 1 M HEPES stock, 5% fetal bovine serum and 5% newborn calf serum in DMEM) [384] for 3 days before changing to neuronal maintenance media, consisting of Neurobasal medium (Life Technologies, Carlsbad, CA, USA), + 1:50 B27 (Life Technologies), and 0.5 mM L-glutamine (Life Technologies) for the duration of the culturing. For electrophysiology recordings, iPS-NPCs were plated on a layer of astrocytes for longer terminal differentiation up to 12 days after the "4-/4+" neural induction.

Primary neuronal culture

Primary neuronal culture was made using the neocortex dissected from the mouse embryonic brains (embryonic day: E14–16; strain: C57BL6/J) as previously described [385]. Cells were seeded onto poly-D-lysine coated 18-mm coverslips (neuVitro, Vancouver, WA, USA) in 12-well plates or 96-well plates (Corning, Corning, NY, USA) and were initially maintained in Neurobasal medium (Life Technologies) with GlutaMAX (Life Technologies), heat-inactivated

fetal bovine serum (5% v/v), and gentamicin (final concentration: 1 µg/ml; Life Technologies). One day after seeding, culture medium was fully changed with serum/antibiotics-free Neurobasal with B-27 serum-free culture supplement (Life Technologies), followed by half-volume medium changes every 7 day.

The transgenes were delivered to the cultured cells by either electroporation or AAV infection. Electroporation was done with the 4D-Nucleofector System (Lonza, Basel, Switzerland) following the manufacturer's instructions with minor modifications. For each reaction, immediately after dissociation, ~6 million cells were spun down at 100 relative centrifugal force for 10 minutes, resuspended in 100 µl of Dulbecco's PBS (Sigma, St. Louis, MO, USA) supplemented with 3 µg of a DNA plasmid (1 µg/µl in Tris-EDTA buffer, Life Technologies), transferred to a cuvette and then electroporated using either the program CU-133 (with high viability for patch clamp experiments) or EM-110 (with high expression levels for bioluminescent assays). The cells were added with 500 µl of pre-equilibrated RPMI 1640 Medium (Life Technologies) and placed in a CO_2 incubator for ~5 minutes. After this recovery step, the cells were plated at the density of 1.5 million cells/well (12-well plate for patch clamping) or 40 thousand cells/well (96-well plate for bioluminescent assays). Bioluminescence was measured with a plate reader (FLUOstar Optima, BMG Labtech, Ortenberg, Germany) immediately after adding CTZ to each well (final concentration 33 µM in the same culture medium).

Alternatively, neurons were infected with an AAV vector 1 day in vitro (DIV). This was done by adding 100 nl of AAV suspension per ml of culture medium at the time of full medium change. This corresponds to multiplicity of infection of ~10^3.

Cloning and creation of stable cell line

DNA plasmids were made using conventional molecular biology techniques. TWe received the luminopsin (LMO3) sequence containing both the Volvox channelrhodopsin 1 (VChR1) and the slow-burn Gaussia luciferase (sb-GLuc) as an adeno-associated virus (AAV) vector (generous gift from Dr. Ute Hochgeschwender of Duke University) [366, 367]. For the backbone, we used the episomal cassette, pPyCAG-Nanog-IP (Addgene #13838), which has been demonstrated to maintain expression across multiple division cycles and differentiation stages [386, 387]. We amplified out the transgene insert by PCR with primers containing BsrgI sites (forward: GGGTGTACAATGGGAGTCAAAGT-TCTGTTT; reverse: GGGTGTACATTACTTATACAGCTCGTCCAT) and then digested both the insert plasmid and the backbone with BsrgI, followed by ligation. This resulted in an episomal plasmid containing LMO3 and the puromycin resistance gene under the control of a CAG promoter (pPyCAG-VChR1-sbGLuc-PuroR). The correct orientation and sequences were confirmed by reverse transcriptase polymerase chain reaction (RT-PCR) and Basic Local Alignment Search Tool (BLAST) DNA sequencing.

Lipofectamine 2000 (Life technologies) was used for transduction of the transgene into mouse iPSCs that had already been thawed and passaged multiple times. Two days after transfection with the episomal LMO3 plasmid, positive clones were selected by puromycin (1 ug/ml, Sigma) for at least 2 weeks and the highest expression clones were assessed by fluorescence and inoculated for expansion of the new stable cell line, LMO-iPSC. From that point forward, the LMO-iPSCs were maintained in culture medium containing puromycin (0.5 µg/ml) to prevent loss of the transgene.

Subcloning of eLMO3

DNA plasmids were made using conventional molecular biology. The correct sequences were confirmed by digestion with restriction enzymes (RE) and DNA sequencing.

To insert the $K_{ir}2.1$ TS in LMO3, the TS-EYFP cassette within pAAV-CaMKIIα-SwiChR$_{CA}$-TS-EYFP (Addgene plasmid #: 55630; a gift from Karl Deisseroth) [388] was cut with RE, NotI and BsrGI, agarose gel-purified, and then ligated into pCAG-LMO3 using the respective RE sites, resulting in a mammalian expression vector with enhanced LMO3 under control of the CAG promoter (pCAG-eLMO3). To obtain an AAV vector with eLMO3, the whole eLMO3 cassette in pCAG-eLMO3 was cut using BglII and BsrGI and then ligated into compatible RE sites (BamHI and BsrGI) of pAAV-LMO3 [2], resulting an AAV vector with eLMO3 under control of the human synapsin I promoter (pAAV-eLMO3).

GLuc is a secreted protein. To delete the secretion signal (AA2-17) in sbGLuc in LMO3, the sbGLuc cassette without the secretion signal in pCAG-sbGLuc$_{\Delta SS}$-tdTomato (a gift from Ute Hochgeschwender) was PCR-amplified with the primers containing the HindIII and BamHI RE sites (HindIII forward: ataaagcttgccaccatgaagcccaccgagaaca-acgaag; BamHI reverse: aatggatccccgtcaccaccggccccctt), digested with the enzymes, and ligated into pCAG-LMO3 using the respective RE sites, resulting in a mammalian expression vector with LMO3 without the secretion signal under control of the CAG promoter (pCAG-LMO3$_{\Delta SS}$).

Viral vector

AAV vectors pseudotyped with recombinant AAV2/9 were made from pAAV-LMO3 and pAAV-eLMO3 through the Emory Viral Vector Core, with both of the titers determined by qPCR

to be 1.8×10^{13} viral genomes (vg)/ml. AAV vectors were resuspended in sterile phosphate-buffered saline (PBS).

Light and CTZ stimulation of iPS-NPCs in vitro

In vitro experiments were performed on LMO3-iPS derived neural progenitor cell (iPS-NPC) cultures. Starting one day after the "4-/4+" neural induction (1 DIV) [389], cells were subjected to daily blue light stimulation (473 nm wavelength, ~1 mW/mm^2, 5 ms pulse-width, at 10 Hz for 12 sec followed by a 48-sec off period for 15 repetitions) until collection for experiment. The 200 μm (core diameter) optical fiber, connected to a laser source (Class IIIb laser, model BL473T3-100FC, SLOC, Shanghai, China), was placed 5 mm below the culture dish. The peak irradiance at the level of the specimen (i.e. at the bottom of culture dish) was determined by an optical power meter console (ThorLabs, Newton, NJ, USA) to be ~1 mW/mm^2. The same procedure was used for all in vitro light stimulation experiments. Cells in the CTZ group received CTZ administration (1.5 μM) for 15 min daily starting 1 DIV until collection for experiment. Cells in control group received medium changes following the same schedule.

Bioluminescence imaging in vitro

Bioluminescence imaging for in vitro systems was carried out using a chemiluminescence reader, LAS-3000 (Fujifilm, Tokyo, Japan), which is equipped with a charge-coupled device camera for ultra-resolution detection of light emissions. For each experiment, a baseline image was acquired over 60 seconds with the chemiluminescence mode at ultrasensitivity. Then, either CTZ (3 μM) or (2-Hydroxypropyl)-β-cyclodextrin (CyD, same volume) was added into the wells.

Using the chemiluminescence mode, the images were acquired as precision detection intensities every 30 seconds over the course of 60 min. The region of interest (ie. areas of emission) were then normalized to the baseline image.

Fluorescence microscopy and electrophysiology

At DIV14, the coverslips containing cortical neurons were imaged by an inverted epifluorescent microscope (Leica DM-IRB, Leica, Weitzlar, Germany or Olympus IX53, Waltham, MA, USA) equipped with a charge-coupled device (CCD) or a scientific complementary metal-oxide-semiconductor (sCMOS) camera (OptiMOS, QImaging, Surrey, BC, Canada), respectively, and a mercury lamp. Fluorescent images were taken with 10x, 20x, or 40x fluorescence objective lens with an FITC filter cube (41001, Chroma, Bellows Falls, VT, USA). Bright field images were also acquired with phase contrast.

Whole-cell patch clamp recording was performed using the Olympus IX53 inverted microscope equipped with a micromanipulator (Sutter Instrument, Novato, CA, USA). The membrane currents or potentials were collected using an EPC9 amplifier and Pulse software (HEKA Elektronik, Lambrecht, Germany) at room temperature (~22°C). The external solution contained 150 mM NaCl, 3 mM KCl, 2 mM $MgCl_2$, 2 mM $CaCl_2$, 10 mM HEPES, and 20 mM glucose at a pH of 7.35. The internal solution consisted of 140 mM K-gluconate, 2 mM $MgCl_2$, 0.5 mM $CaCl_2$, 4 mM Na_2-ATP, 0.4 mM Na_3-GTP, 5 mM EGTA, and 10 mM HEPES at a pH of 7.15. Recording electrodes pulled from borosilicate glass pipettes (World Precision Instruments, Sarasota, FL, USA) had a tip resistance between 5 and 7 MΩ when filled with the internal solution. Series resistance was compensated by up to 50%. Data was filtered at 3 kHz and digitized at

sampling rates of 10 kHz. Widefield photostimulation was delivered through an oil-immersion objective lens (40x; 1.35NA; UApo/340, Olympus) using a bandpass excitation filter (460-500 nm) in the FITC filter cube. Intensity was adjusted by ND filters (ND25 and ND6, Olympus). CTZ stock solution (50 mM in Fuel Solvent, #303, Nanolight, Pinetop, AZ, USA) was diluted in the extracellular solution at final concentration of 100 µM and bath-applied to the recording chamber.

Stereotactic AAV injections

Stereotactic injections into the mouse barrel cortex was performed according to previously established protocols [367]. Anesthesia in mice was induced by 3.5% isoflurane in oxygen and maintained by 1.5% isoflurane, during which the mice were placed in a stereotactic apparatus (David Kopf Instruments). For injection of viruses, a 33-gauge syringe needle in a Nanofil syringe (World Precision Instruments) was used to infuse 2 µl of virus suspension into the deep layers of the barrel cortex (coordinates from the bregma: -1 mm AP, +3.5 mm ML; depth from the dura: 0.5 mm) at a rate of 100 nl/min. The needle was left in place for 10 min after injection before being slowly withdrawn. The incision was closed with tissue adhesive (3M Vetbond, Maplewood, MN, USA). After surgery, mice were given daily doses of meloxicam (1 mg/kg body weight) for analgesia until they fully recovered from surgery.

Isolation of total RNA and reverse transcriptase polymerase chain reaction

Reverse transcriptase polymerase chain reaction (RT-PCR) was carried out as described previously [390]. Total RNA from tissues of stroke mice or neuronal cells was isolated according to manufacturer's instruction (P/N 4387406; A&B Applied Biosystems, ThermoFisher). RNA

integrity was confirmed by detection of 28S and 18S rRNA bands. RNA was confirmed to be free of genomic DNA contamination using PCR in the absence of reverse transcriptase. The RNA samples were reverse transcribed in 20 μl at 37 °C for 60 min then incubated at 95 °C for 5 min and transferred to 4 °C. RT product (1 μl) was subjected to PCR amplification with 10 pmol primer, 10 × standard Taq reaction buffer, 10 mM dNTP, and 0.625 unit Taq polymerase in 20 μl PCR reaction buffer (#M0273L, #N0447S, #B9014S; New England Biolabs Inc., Ipswich, MA, USA). PCR primers were used as shown in Table 5-1: Sequences of all primers used for RT-PCR., and in our previous study (Chen et al., 2015; Lee et al., 2016a). PCR mixtures were heated to 95 °C for 10 min and cycled 30–37 times for each primer; cycles consisted of 95 °C for 15 s, 58 °C for 1 min, and 68 °C for 30 s. After additional incubation at 68 °C for 10 min, the PCR samples were transferred to 4 °C. PCR products were subjected to electrophoresis in 2% agarose gel with ethidium bromide (EtBr). Relative intensity of each PCR band was analyzed using InGenius3 manual gel documentation systems (Syngene, Frederick, MD, USA).

Genes		**Primers 5' – 3'**
BDNF	Forward	ATGTTTGCGGCATCCAGGTA
	Reverse	CGACATCACTGGCTGACACT
NGF	Forward	GTGGCTGTGGTCTTATCTCC
	Reverse	AACTTCAGCATTCCCTTGAC
TrkB	Forward	CACCAGACACCCTCAAATAAG
	Reverse	TGAATAACGGAGACTACACCC
vGLUT1	Forward	TACACCAGAGCGTTTATTGG

	Reverse	TTCCCAGGACTGATTCTCAC
GDNF	Forward	CAGTTCCTCCTTGGTTTCATAG
	Reverse	GAAGTTATGGGATGTCGTGG
18S	Forward	GACTCAACACGGGAAACCTC
	Reverse	ATGCCAGAGTCTCGTTCGTT

Table 5-1: Sequences of all primers used for RT-PCR.

Chondroitin sulfate proteoglycan droplet assay

The chondroitin sulfuate proteoglycan (CSPG) droplet assay was adapted from Silver et al. [391]. Briefly, spots were prepared by placing four, 1.5 µl droplets of Hank's balanced salt solution (HBSS, Sigma) containing mixed CSPGs (10 µg/mL; Millipore) and laminin (5 µg/ml; Invitrogen) onto poly-D-lysine (0.1 mg/mL) pretreated 12mm glass coverslips and allowed to dry completely. Additionally, negative control spots consisting of bovine serum albumin (BSA: 25–500 µg/ml; Sigma) and laminin (5 µg/ml) as well as laminin-alone (5 µg/ml) were prepared in parallel with the experimental groups. The entire coverslip was then suffused with a solution of laminin (5 µg/ml) in DMEM and incubated at 37°C for at least 3 h. The laminin solution was then aspirated, and the coverslips were washed with molecular grade water 1x and allowed to dry completely before plating. After neuronal induction, 100,000 iPS-NPCs were seeded onto the coverslips with SATO medium. Media was exchanged every other day until the 5DIV, in which the completed assay was then fixed with 4% formaldehyde and immunostained for β-III tubulin (Tuj1) and DAPI.

Scratch assay

A modified version of the previously described scratch wound healing assay was carried out [165]. For the modified scratch assay, ~1.5 million iPS-NPCs were seeded into 35-mm dishes (Cellstar/Sigma) immediately following the 4-/4+ neural induction protocol. At 2 DIV, the monolayer of cells was scratched along a central vertical line using a 20-µl pipette tip. The debris was removed, and the edges of the scratch was smoothed by washing the cells once with 1 ml of SATO and then replaced with 2 ml of fresh SATO. Pictures along the entire scratch line were acquired prior to the scratch, and immediately at time 0, 12, 36, 60, and 84 hr after the scratch. The cells were stimulated with either HP-CyD (5 µl, equal volume as CTZ), CTZ (1.5 µM), or laser (15 min, 10 Hz) daily starting at 12 hr post-scratch. Pictures were acquired 1 hr after stimulation. After the final image acquisition at the 84 hr timepoint, all cells were fixed with 4% PFA and prepped for immunocytochemistry. The images were then analyzed by a blinded scorer in order to determine the width of the gap zone, the total number of neurite extensions into the gap zone (demarcated by the cell bodies), and the total number of axons crossing the midline of the gap zone, which is a marker of axonal outgrowth and plasticity. The data is presented as the density of neurite entries and axonal crossings per mm of the scratch zone. All experiments were carried out in triplicates.

Immunocytochemistry

Culture cells were fixed with 4% paraformaldehyde in phosphate buffered saline (PBS) and post-fixed with 2:1 mixture of ethanol:acetic acid for 5 min, then permeabilized with 0.2% Triton-X 100 and blocked with 1% fish gelatin. Cells were incubated overnight at 4°C with primary antibodies against GFP (1:200; Novus Biologicals, Littleton, CO, USA; used to stain for the EYFP tag in LMO3), NeuN (1:400; Millipore, Billerica, MA, USA), Tuj1 (1:400; Covance,

Princeton, NJ, USA), GFAP (1:500; Novus Biologicals), Synapsin-1 (1:400; Millipore), neurofilament (1:400; Millipore), CAMKIIα (1:400; Millipore), SSEA-1 (1:200; Abcam), Oct3/4 (1:100; Santa Cruz), vesicular glutamate transporter 1 (VGLUT1, 1:200; Abcam), and vesicular glutamate transporter 2 (VGLUT2, 1:200; Abcam). For the secondary antibodies, either Alexa Fluor 488 (1:100; Life technology) or Cy-3 (1:400; Jackson ImmunoResearch, West Grove, PA, USA) conjugated antibody against the respective IgG was used. DAPI within the DAPI-Vectashield (Vector Labs, Burlingame, CA, USA) was used to stain cell nuclei.

Controlled cortical impact model in mice

Controlled cortical impact (CCI) was induced in mice as previously described [392]. C57BL/6 mice (8-12 week old, 160 total) were housed in standard cages with 12-hr light/dark cycle and had access to food and water *ad libitum*. The animal protocol was approved by the Emory University Institutional Animal Care and Use Committee (IACUC), in compliance with the National Institutes of Health (NIH) guidelines. For TBI surgery, mice were anesthetized with isoflurane (3% induction, 1.5% maintenance) and placed on a stereotaxic frame. After a midline skin incision, a 3.5 mm circular craniotomy was performed midway between the lambda and bregma, 2.0 mm to the right of the central suture using an electric microdrill (Dremel, Mount Prospect, IL). During the craniotomy, mice were excluded from the study if the dura mater was breached. CCI was induced with an electric impact device using a steel cylindrical flat impact tip. In this study, I used a PCI3000 precision cortical impactor (Hatteras Instruments, Cary, NC) and a 2.8mm diameter impact tip (velocity = 3.0 m/s, depth = 0.5 mm, and contact duration = 150 ms). Body temperature was maintained during surgery by a feedback-controlled homeothermic blanket (Harvard Apparatus, Holliston, MA). After the injury, the skin was sealed using Vetbond (3M, St.

Paul, MN), and mice were allowed to recover in a humidity and temperature controlled incubator (Thermocare, Incline Village, NV). Sham animals received the craniotomy, but no impact was applied.

Transplantation of iPS-NPCs into the post-ischemic brain

Cell transplantation was performed at 3 days after the TBI induction. Experimental groups included the TBI + Sato vehicle control, TBI + Sato + CTZ control, TBI + LMO-iPS-NPC transplantation with vehicle (saline), and TBI + LMO-iPS-NPC transplantation + CTZ. Animals were randomly assigned to groups. After the "4-/4+" neural induction, $4x10^5$ LMO3-iPS-NPCs were resuspended in 4 µL Sato medium and transplanted to the peri-contusion regions using by a modified stereotactic injection technique with a Hamilton syringe with injections of 2 µL each at two locations. TBI + Sato control animals received vehicle injection (4 µl of Sato medium). The LMO-iPS-NPCs were pre-labeled with Hoechst 33342 (1:10,000 v/v) for one hour, which facilitated tracking of these cells after transplantation. In accordance with our established transplantation protocol for enhanced cell survival and regenerative property, all iPS-NPCs were exposed to hypoxic preconditioning (1% O_2) for 8 hrs before transplantation [393, 394]. For some experiments, to label proliferating cells in the brain, animals received daily administration of 5-bromo-2-deoxyuridine (BrdU, 50 mg/kg; i.p.) starting the day of transplantation until the day of sacrifice.

Intranasal administration of CTZ

The nasal route is an established method for brain specific drug delivery, bypassing the BBB [77, 164-166]. CTZ intranasal administration (water-soluble CTZ, Promega, Madison, WI, USA) was carried out according to previously described procedures [395] at a dosage of 50 µg per animal (2 mg/kg, dissolved in molecular grade H_2O at 5 µg/µL) each time. For each injection, the mouse was scruffed by the ears and inverted to expose the nostrils. A 25 µL Hamilton syringe was used to administer 5 µL of either water-soluble CTZ or 0.9% saline into alternating nostrils, starting with the left, and repeating for 2 injections, for a total of 10 µL. Animals received one CTZ treatment per day starting at 1d post-transplantation and continuing for 2 wks.

Bioluminescence imaging in vivo

The same chemiluminescence reader, LAS-3000, used for in vitro bioluminescence imaging was also used for in vivo bioluminescence readouts. For each experiment, the animals were anesthetized with isoflurane (5% induction, 1.5% maintenance, with 100% O_2 gas) and given 250 µg of CTZ (intranasal) at 5 min prior to the imaging. Then, their scalps were shaved and a midline incision was made to expose the skull before the animals were placed into the imager. Using the chemiluminescence mode, the images were acquired as precision detection intensities every 30 seconds over the course of 60 min. The region of interest (ie. area of emission) were then normalized to a hypointense region outside of the region of interest.

Terminal deoxynucleotidyl transferase dUTP nick end labeling (TUNEL) staining

A TUNEL assay kit was used to examine cell death by detecting fragmented DNA in 10-µM-thick coronal fresh frozen sections as described previously [396]. After fixation (10% buffered

formalin for 10 min and then ethanol:acetic acid (2:1) solution for 5 min) and permeabilization (0.2% Triton X-100 solution), brain sections were incubated in the equilibration buffer for 10 min. Recombinant terminal deoxynucleotidyl transferase (rTdT) and nucleotide mixture were then added on the slide at 37°C for 60 min in the dark. Reactions were terminated by 2X SSC solution for 15 min. Nuclei were counterstained with Hoechst 33342 (1:20,000; Molecular Probes, Eugene, OR) for 5 min.

Immunohistochemistry

Immunohistochemistry (IHC) procedures were carried out to measure proliferation as previously described [392]. Mice were subjected to cardiac perfusion with 0.9% saline followed by 10% formalin, and then immersion fixed in 10% formalin for 24 hr before transferring into 30% sucrose until the brains settled to the bottom of the container. Brains were then flash frozen using Tissue-Tek optimal cutting temperature compound (VWR International, Radnor, PA) using powdered dry ice and kept overnight in a -80°C freezer. Brain tissue was then sliced into 15 µm-thick coronal sections using a cryostat vibratome (Leica CM 1950; Leica Microsystems, Buffalo Grove, IL). Sections were dried on a slide warmer for 30 min, fixed with 10% formalin buffer, and then permeabilized with 0.2% Triton-X 100 solution (diluted in PBS) for 60 min, followed by blocking with 1% fish gelatin (diluted in PBS; Sigma) for 60 min at room temperature. For BrdU staining, the slides were also fixed with methanol for 15 minutes after the 10% formalin fixation step, and then treated with 2N hydrochloric acid in 37°C, and washed with 0.1M borate buffer (11:9 ratio of 0.2M boric acid and 0.05M Borax) and permeabilized with 0.2% Triton-X 100 solution for 60 min and blocked with 1% fish gelatin at room temperature. Then, the slides incubated with the following primary antibodies: rabbit anti-Beclin-1 (1:200, BD Biosciences, East

Rutherford, NJ), rat anti-BrdU (1:400; ABD Serotec, Raleigh, NC), rabbit anti-glucose transporter 1 (GLUT1; 1:200; Millipore, Billerica, MA), rabbit anti-myelin basic protein (MBP, 1:200; Abcam), goat anti-GFP (1:200; Novus Biologicals), chicken anti-GFAP (1:500; Novus Biologicals), and/or mouse anti-neuronal nuclear antigen (NeuN, 1:300; Millipore) overnight at 4°C. Next day, the slides were washed 3 times with PBS for at least 10 min each wash, then reacted with the secondary antibodies specific to the host species of the primary antibodies for 90 min at room temperature. After washing with PBS 3 times for at least 10 minutes each, the slides were then mounted with Vectashield fluorescent mounting medium with or without DAPI (without DAPI for the slides containing Hoechst-prelabeled cells; Vector Laboratory, Burlingame, CA), and coverslipped for microscopy and image analysis. Pictures were taken by using fluorescence microscopy (BX61; Olympus, Tokyo, Japan) along the length of the penumbra region defined morphologically as the region just outside the stroke core. Colocalization of signals were confirmed using the confocal microscope (FV1000, Olympus). For systematic random sampling in design-based stereological cell counting, six coronal brain sections per mouse were selected, spaced 90 μm apart across the same region of interest in each animal. For multistage random sampling, six fields per brain section were randomly chosen in the peri-infarct/penumbra region of the brain. The fluorescence density was measured using NIH Image J software.

Western blot analysis

Western blot analysis was used to detect the activation of the canonical Wnt pathway, as well as for factors involved in apoptosis, blood-brain barrier disruption, and neurovascular regeneration. Western blot was carried out using the protocols as outlined previously [396]. Either cell lysates or tissue lysates were used to isolate protein samples. To collect tissue lysates, the cells

were treated with lysis buffer containing 0.02 M Na_4P2O7, 10 mM Tris-HCl (pH 7.4), 100 mM NaCl, 1 mM EDTA (pH 8.0), 1% Triton, 1 mM EGTA, 2 mM $Na3VO_4$, and a protease inhibitor cocktail (Sigma). Then, a cell scraper was used to remove all attached cells for collection and subsequent homogenization. Animals were sacrificed at day 2 or day 14 after TBI. The peri-injury cortical tissue was isolated and homogenized in lysis buffer. The supernatant was collected after centrifugation at 15000 g for 10 min at 4°C. Protein concentration was determined with a bicinchoninic acid assay (Pierce Biotechnology, Rockford, IL). Equivalent amounts of total protein were separated by molecular weight on an SDS-polyacrylamide gradient gel, and then transferred to a PVDF membrane. The blot was incubated in 5% BSA for 1 hr and then treated with primary antibodies at 4°C overnight.

The primary antibodies used and the dilutions for each were rabbit anti-phospho-CREB (1:1000, Cell Signaling Technology, Danvers, MA, USA), rabbit anti-CREB (1:1000, CST), rabbit anti-CXCR4 (1:100, Abcam, Cambridge, UK), rabbit anti-BDNF (1:500, Santa Cruz Biotechnologies, Dallas, TX, USA), rabbit anti-NGF (1:1000, Abcam), rabbit anti-TrkA (1:1000, CST), rabbit anti-TrkB (1:1000, CST), rabbit anti-Synaptophysin (1:1000, Abcam), rabbit anti-PSD95 (1:2000, CST), and rabbit anti-VEGF antibody (1:1000, Sigma), and mouse anti-β-actin (1:5000, Sigma). After washing with TBST, membranes were incubated with AP-conjugated or HRP-conjugated secondary antibodies (GE Healthcare, Piscataway, NJ) for 2 hrs at room temperature. After final washing with TBST, the signals were detected with bromochloroidolyl-phosphate/nitroblue tetrazolium (BCIP/NBP) solution (Sigma) or film. Signal intensity was measured by ImageJ (NIH) and normalized to the actin signal intensity.

Local cerebral blood flow measurement

Laser Doppler scanner imaging of cortical cerebral blood flow was conducted as previously described [397, 398] at two time points: immediately prior to CCI induction, and 21 days after iPS-NPC transplantation. Briefly, animals were anesthetized with an injection of isoflurane (5% induction, 1.5% maintenance), and an incision was made to expose the skull surrounding the contusion region. The laser was centered over the anterior medial zone of the injury, in the peri-contusion region. Different from the conventional Laser Doppler probe that measures a small point of blood flow, the scanner method measures a 2.4 × 2.4 mm square area using the laser Doppler perfusion imaging system (PeriFlux System 5000 - PF5010 LDPM unit, Perimed, Stockholm, Sweden). This scanning measurement largely avoids inaccurate or bias results caused by inconsistent location of the laser probe. Data was analyzed using the LDPI Win 2 software (Perimed AB, Stockholm, Sweden).

Nissl staining and contusion volume quantification

Contusion volume was quantified using volumetric Nissl staining analysis as previously described [392]. The brains were collected at 21d post-transplantation, and 10 μm-thick coronal sections were taken using the cryostat vibratome, with 200 μm separation between each section. The sections were then treated with a 1:1 mixture of 10% formalin and acetic acid, followed by staining with the working solution comprised of a buffer solution (94:6 ratio of sodium acetate and acetic acid) and cresyl violet at a ratio of 5:1. Sections were scanned and imported into ImageJ for area and total volume quantification. For each section, the contusion area was demarcated and normalized using an imported image of a standard ruler. Volumetric analysis was carried out using

the Cavalieri method: V = ā x t x k, where ā is the average contusion area for each animal, t is the section thickness (200 μm), and k is the number of sections[399]. To account for edema and hemorrhage, hemispheric tissue loss was calculated by the following equation: (contralateral hemispheric volume - ipsilateral hemispheric volume)/contralateral hemispheric volume x 100%.

Adhesive removal test for sensorimotor functions

The adhesive removal test is a sensitive assay for sensorimotor deficits [392, 400]. Prior to the injury, mice were trained to remove a quarter-circle adhesive tape (Genesee Scientific, San Diego, CA) from alternating forelimb paws. The training was repeated 3 times for each paw for 3 days. Two latencies were recorded: 1) latency to contact, which indicated the time the mouse took to recognize and demonstrate the conviction to remove the adhesive, and 2) latency to removal. The maximum recording latency was 180 seconds. Mice that were unable to rapidly remove the adhesive (<10s) after the training period were excluded from behavior testing. Following the injury, the adhesive removal task was performed at 14d and 21d post-transplantation. The latencies were scored with the experimenter blinded to the treatment conditions. Animals were randomly assigned to each group prior to the injury.

Corner test

A modified version of the well-established corner test was carried out at baseline, and at 7d, 14d, and 21d post-transplantation [401]. Rather than creating a single corner, 10 12 × 12 × ¼ in. black, opaque plexiglass panels were placed together in the shape of a star with 5 30° corners.

This arena was then placed into a TopScan chamber, with an overhead camera recording. The animals were individually placed into the center of the arena and allowed to roam freely for 10 min while being recorded. The video was later played back and a blinded observer scored the animals on their turning behavior according to the following criteria:

1. Turning behavior was assessed when the animal fully entered the corner to allow bilateral whisker deflection, and only after the animal reared forward and up prior to turning towards the open end. The turn was not scored if the animal turned directly without rearing. Only unambiguous full turns that were immediately preceded by rearing behavior were counted.
2. If the animal rear and began turning towards one side and then changed direction, the turn was not scored.
3. If the animal waited an extended period of time (>5 seconds) after rearing up to turn, that turn was not scored.

After the total counts were tallied, the laterality index (LI) and the normalized laterality index [402] were determined according to the following equations:

$$LI = \frac{Number\ of\ right\ turns - Number\ of\ left\ turns}{Total\ number\ of\ turns}$$

$$Normalized\ LI = \frac{LI + 2}{LI_{D0} + 2}$$

Where LI_{D0} is the laterality index as determined at baseline prior to the TBI induction. An LI closer to 0 reflects a non-preferential turning bias, whereas an LI > 0 reflects a bias towards the right side, and an LI < 0 reflects a bias towards the left side. For the normalized LI, a value closer to 1 reflects no lateral discrimination in turning, while an LI closer to 2 or 0 reflects preferential turning for the right or left side, respectively.

Rotarod test for locomotor function

The rotarod test is sensitive for deficits in gross motor skills and motor coordination [403]. Mice are placed onto a spinning cylindrical beam (Ugo Basile, Italy) that accelerated from 4 rpm to 40 rpm over the course of 5 minutes. Prior to the injury, mice were trained on the rotarod for 3 days for 3 trials per day, and animals that were unable to remain on the beam for 5 min after the training period were excluded from future testing. Following the injury, 3 trials of the rotarod test were performed at 1d, 2d, 3d, 7d, and 10d post-injury.

Whisker response behavior

Whisker touching behavior was recorded and analyzed using the HomeCageScan system (Clever Sys Inc, Reston, VA, USA). The system had four cameras that simultaneously monitored and recorded four cages, with each cage (dimension: 191 mm x 292 mm x 127 mm) containing one mouse. This system has been extensively calibrated and validated to provide accurate and

automated and reliable behavioral output analyses (*e.g.* [392]). Mice received viral injections for either LMO3 or eLMO3 expression in the barrel cortex as described above. I used 4-6 animals per group. Mice were injected with either water-soluble isotonic CTZ (3 mg/kg, 2.5 µg/µl, dissolved in sterile water, Nanolight, Pinetop, AZ, USA) or equal volumes of saline (sterile 0.9% w/v NaCl solution) via the intranasal route according to previously established protocols [166]. After the final injection of CTZ, the animals were placed into the individual cages and allowed to acclimate for 5 minutes before simultaneous behavior recording and analysis for a total of 1 hour. The settings for the data acquisition system were set as the following: 1) animal size threshold (pixel) = 160; 2) contrast threshold = 23. The whisker response behavior was defined as the total grooming behavior automatically detected by the system, and the duration was summed over the whole 1-hr episode.

Statistical analysis

GraphPad Prism 6 (GraphPad Software, San Diego, CA) was used for statistical analysis and graphic presentation. Student's two-tailed t-test was used for comparison of two experimental groups. For multiple comparisons, a one-way ANOVA was used, followed by Tukey's correction. For repeated measurements, two-way ANOVA followed by Bonferroni's correction for pairwise comparisons was used. Significance was defined to be a P value ≤ 0.05. All data are presented as mean ± SEM.

Chapter 6: TBI Model and the Neurovascular Response

6.1 Introduction

TBI is a leading cause of mortality and morbidity amongst children and young adults [1]. While neuroprotective strategies are being investigated, there currently exists no effective treatments for TBI [2]. TBI originates from the primary physical deformation which causes irreversible cell death, but aside from this, there are also prolonged insults, such as excitotoxicity, inflammation, oxidative and endoplasmic reticulum (ER) stress, BBB disruption and resulting edema and hypoxia, and lysosomal and autophagic dysfunction during the acute and subacute phase of TBI (hrs to days post-injury) that causes further cell death [3, 404]. Furthermore, the central nervous system is inadequate in replacing the lost neurons and restoring original connectivity and function [78, 79], which warrants the need for regenerative approaches. This chapter highlights the establishment of the chosen TBI model, controlled cortical impact (CCI) that sets up all future transplantation experiments for treatment of TBI. Furthermore, there are many endogenous compensatory mechanisms that are upregulated following a focal injury, and these were investigated thoroughly beforehand in order to establish a baseline and develop a better understanding of the neurovascular response and how to exploit it for treatment.

6.2 Controlled Cortical Impact Model

Animal models are imperative for studying the pathophysiology and time course of particularly nebulous disease, such as TBI and neurodegenerative diseases, but they are also useful for innovating breakthroughs in treatment [33]. In order for an animal model to be effective, it must have high face validity, by properly reflecting the etiology of the disorder, and high construct

validity, by producing information or tools that can be clinically translated. Furthermore, the ease of use and accessibility and reliability of the animal models must be considered as well. Although many TBI models exist, the CCI model was chosen for this dissertation given its high face validity and construct validity to represent penetrating head wounds, such as gunshot wounds, and for its simplicity and reproducibility given that it is completely automated [34]. The modifiable parameters include the depth of impact, speed of impact, duration of impact, and diameter of impact. Any of these can be adjusted to change the severity of injury, allowing for much margin for manipulation. Furthermore, the CCI model has been shown to demonstrate consistent contusion volumes and functional deficits as assessed by behavioral assays [174] that are graded according to the severity of injury.

After carrying out the established CCI model of TBI, I demonstrated consistent and reliable induction of contusion volumes and hemispheric tissue loss ratios that were dependent upon injury severity, mild vs. moderate (*Figure 6-1*). Moderate injuries resulted in an approximate 10-fold increase in contusion volume ($t(14) = 6.788$, $p < 0.0001$, for Mod vs. Mild) and an approximate 15-fold increase in hemispheric loss ratio (Student's t-test: $t(14) = 8.013$, $p < 0.0001$, for Mod vs. Mild). Furthermore, functional deficits were evaluated by the behavioral assays, adhesive removal task (AKA sticky dot task) and the rotarod task. In the adhesive removal task, longer latencies to contact and removal correspond to greater sensory and sensorimotor deficits, respectively. Mice that suffered a TBI demonstrated significantly higher latency to contact at 3d post-TBI (*Figure 6-2*, Two-way repeated measures ANOVA with Bonferroni's c;orrection for pairwise comparisons: $t(18) = 3.046$, $p = 0.0208$), and significantly higher latency to removal at 3d post-TBI ($t(24) = 2.637$, $p = 0.0433$).

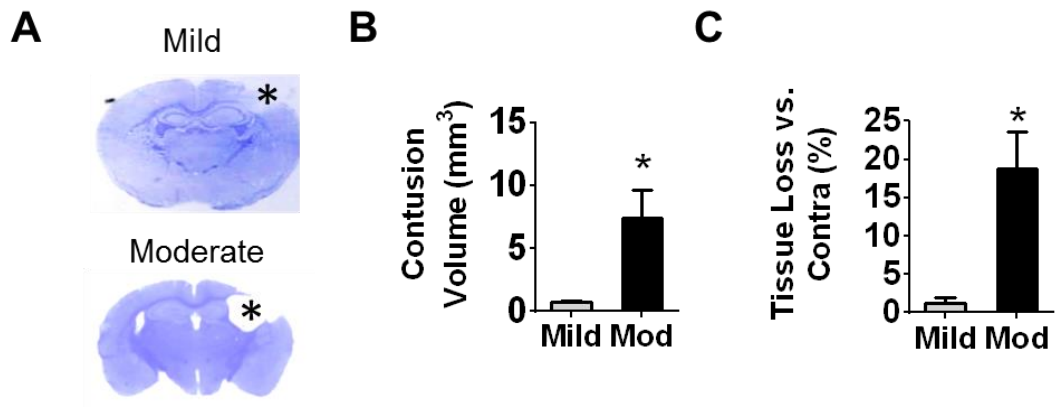

Figure 6-1: The CCI model of TBI produces a reliable and severity-dependent contusion volume in mice.

A-C. Nissl staining was carried out following sacrifice of the animals at 2d post-injury after induction of either a mild (1mm depth, 2.8mm diameter, 3 m/s impact speed, 150 ms impact duration) or a moderate severity injury (2mm depth, 2.8mm diameter, 3 m/s impact speed, 150 ms impact duration). **A.** Representative images of Nissl-stained sections Tissue loss can be observed in the ipslateral hemisphere (bordered by dashed line). **B.** Volumetric analysis by the Cavalieri method was used to calculate total injury volumes from cumulative summation of injury areas of adjacent sections spanning the length of the contusion. **C.** Hemispheric tissue loss was calculated by comparing the difference in volume between the ipsilateral hemisphere and the contralateral hemisphere. *: $p<0.05$, compared to Mild. n=5 for Mild and 10 for Moderate.

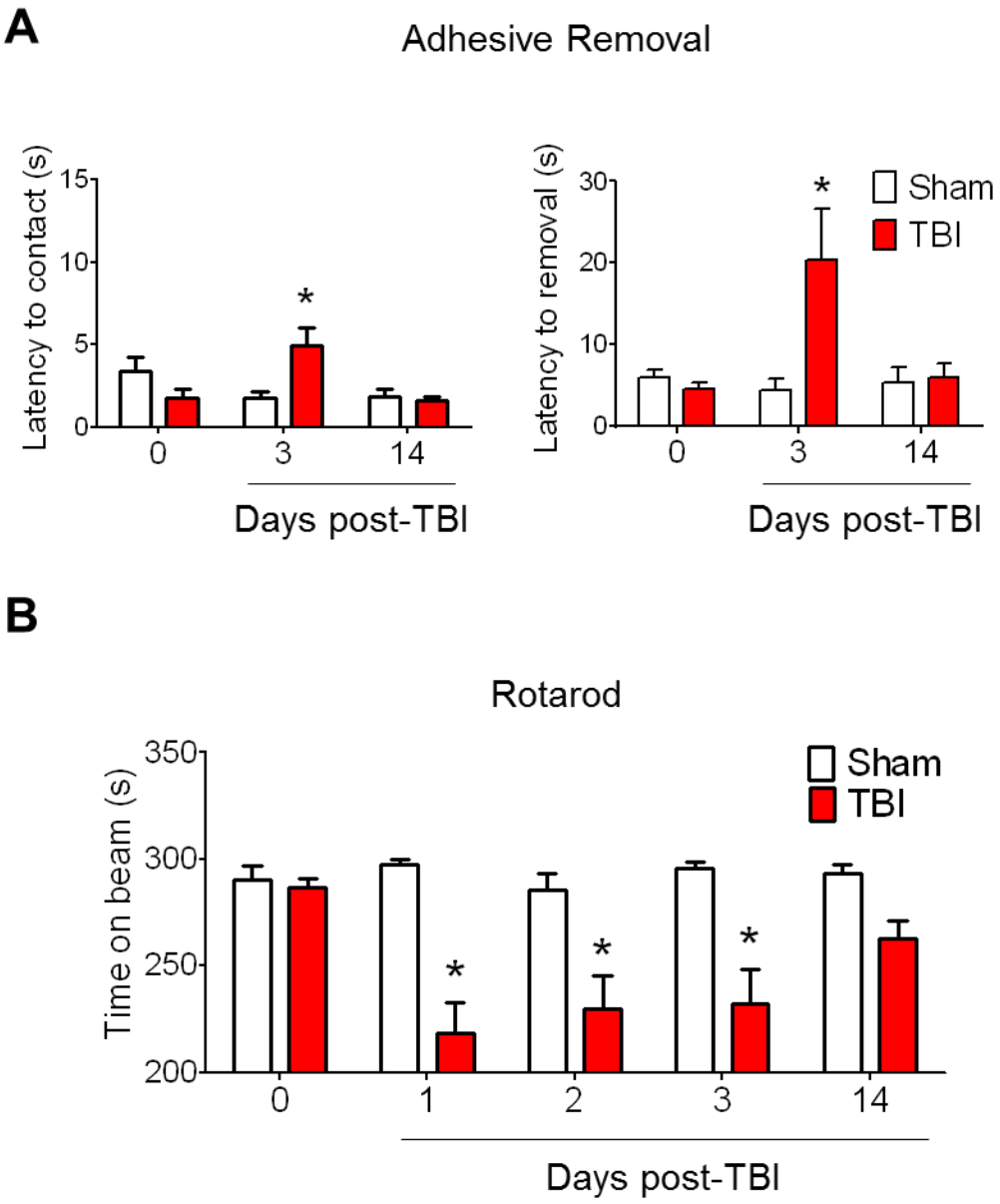

Figure 6-2: Mild TBI results in reproducible functional deficits that can be objectively quantified with behavioral assays, adhesive removal (sticky dot) task and the rotarod task.

A. All animals were pre-trained in the adhesive removal task prior to the injury to ensure competent removal. Baseline latencies (day 0) were measured to ensure no significant differences across groups. TBI resulted in deficits in mouse forelimb sensorimotor function, as indicated by the significantly longer latencies to removal in the contralateral forepaw of the TBI animals, especially

at earlier timepoints. In the mild model of TBI, the animals had all spontaneously recovered to the point where the TBI performance at 14 days post-TBI were equal to that of sham animals. **B.** Mice were prescreened and pretrained on the rotarod task to ensure adequate performance of ≥90% maximum running time (ie. ≥270 sec, day 0). Then at varying timepoints post-TBI, the animals were evaluated for rotarod performance. Animals induced with TBI demonstrated attenuated ability to remain on the accelerating beam, resulting in significant reductions in time on beam during the early timepoints. Similar to the adhesive removal task, the animals had nearly spontaneously recovered by 14 days post-TBI such that no significant differences were observed between the TBI and sham groups, although there remained a trend for impaired performance in TBI animals. *: $p<0.05$, compared to Sham. n=6 for Sham group, and 12 for TBI group.

6.3 TBI-Induced Autophagy and Cell Death

Next, I investigated the cellular damage that manifest following TBI. Autophagy is a conserved adaptive response to stress, such as nutrient deprivation and hypoxia, through which proteins and organelles are degraded in autophagosomes and recycled [405, 406]. However, TBI results in dysregulated autophagy, which manifests as lysosomal dysfunction, impaired clearance of autophagosomes, and increased autophagic cell death [404, 407]. I carried out IHC for the autophagosome protein Beclin-1 and TUNEL to measure the levels of autophagy and autophagic cell death after mouse TBI. The IHC showed that there was an approximately 10-fold increase in the number of Beclin-1+ cells within the peri-contusion region at 2d post-TBI, as well as greatly elevated numbers of colocalized Beclin+/TUNEL+ cells, which are indicative of autophagic cell death (*Figure 6-3*). Next, I characterized the total cell death, as well as the neuronal-specific cell death after TBI at the 2d post-TBI timepoint. Even at this delayed stage, there was significant elevation of TUNEL+ cells and colocalized TUNEL+/NeuN+ cells, suggesting ongoing cell death and neuronal cell death (*Figure 6-4*). Furthermore, there was a significant reduction in NeuN+

cells, which corroborates the persistent loss of neurons in the peri-contusion region, as a result of delayed cell death from the secondary effects of TBI.

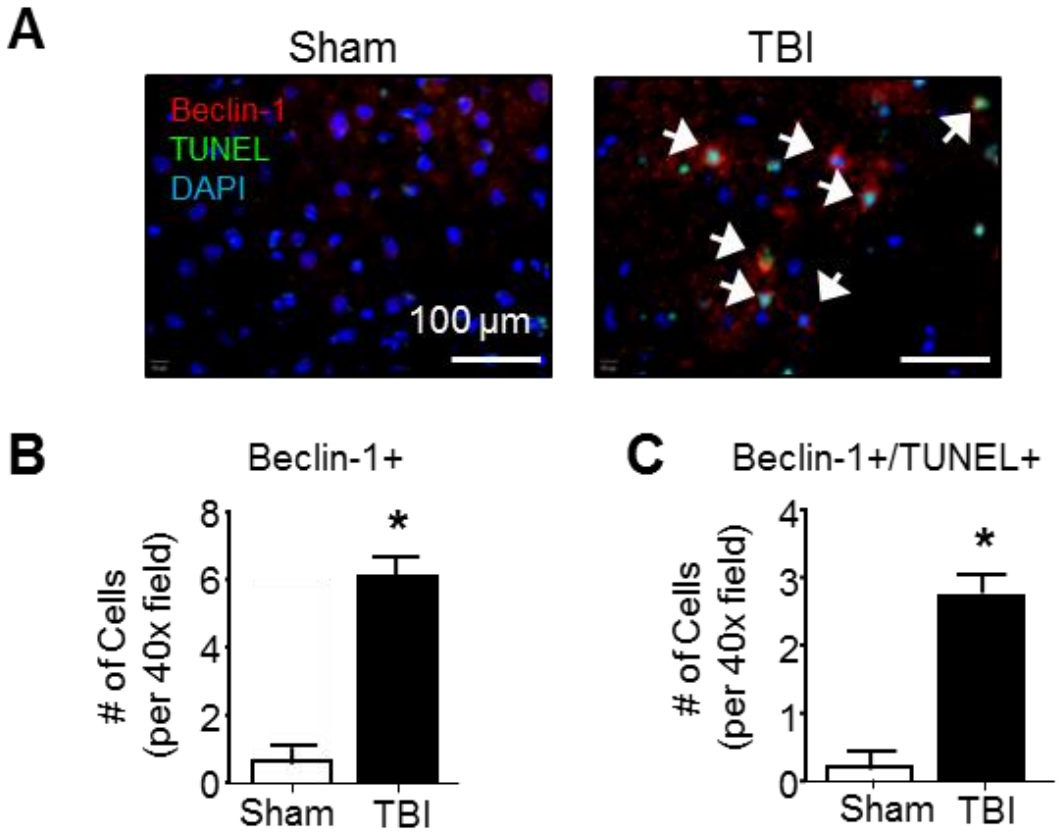

Figure 6-3: Mild TBI results in autophagic cell death.

A-C. The presence of autophagic cell death in the peri-contusion zone was visualized by immunohistochemistry at 2 days post-TBI. **A**. Representative images of immunofluorescence (red: Beclin-1, green: TUNEL, blue: DAPI). **B.** Quantification of Beclin-1+ cells per 40x field. **C.** Quantification of Beclin-1+/TUNEL+ colabeled cells per 40x field (arrow: colabeled cells). Mild TBI resulted in significantly elevated overall autophagic activity, as well as pathological

autophagic cell death. *: p<0.05, compared to Sham. #: p<0.05, compared to Sham. n = 4 for Sham, and 7 for TBI. Scale bar = 100 µm.

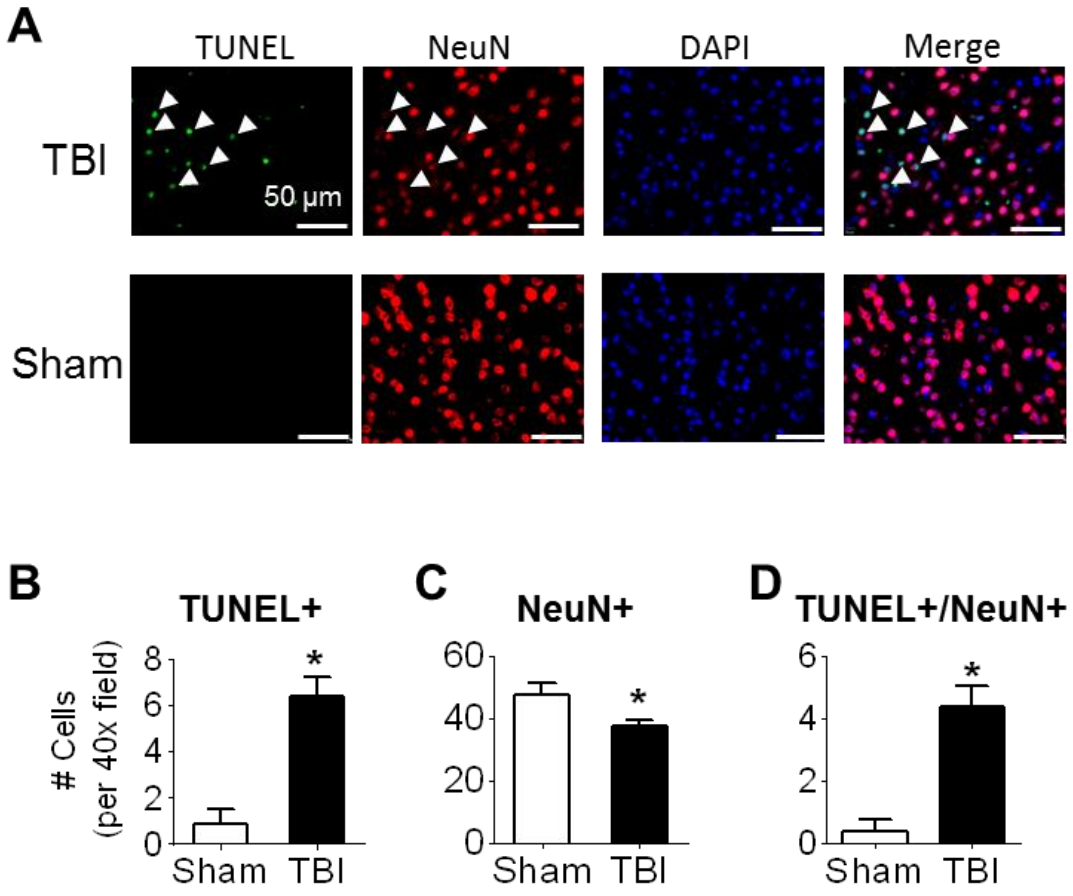

Figure 6-4: Mild TBI results in continuous cell death within the peri-contusion zone, including neuronal cell death.

A-C. The presence of cell death in the area directly adjacent to the injury was visualized by immunohistochemistry and co-staining with TUNEL at 2 days post-TBI. **A.** Representative immunofluorescence images are shown (green: TUNEL, red: NeuN, blue: DAPI) revealed significantly greater levels of TUNEL+ cells, as well as TUNEL+/NeuN+ colabeled cells (arrows). **B.** Quantification of total number of TUNEL+ cells. There is significantly elevated general cell death within the peri-contusion region. **C.** Quantification of total number of NeuN+ cells. There is

a significant loss of neurons in injured tissue. **D.** Quantification of total number of TUNEL+/NeuN+ colocalized cells. There are significantly elevated levels of neuronal-specific cell death during the subacute phase after injury. *: $p<0.05$, compared to Sham. #: $p<0.05$, compared to TBI+Saline. A total of 500-600 images were quantified. n=5 per group. Scale bar = 50 μm.

6.4 Endogenous Repair Mechanisms After TBI

The neurovascular unit is a fundamental subunit of the CNS, and it includes the neurons and the blood vessels they are coupled with, as well as the associated astrocytes and pericytes, which all coexist and integrate together dynamically for proper function [408]. This unit becomes disrupted as a result of the primary and secondary insults following TBI, but the CNS possesses endogenous repair pathways to partially restore and repair the neurovascular network. To establish the baseline for endogenous regeneration and repair, I performed a series of studies to characterize the subacute (days-weeks) and longterm (weeks-months) features that manifest following TBI.

First, I evaluated the changes in vascular-related factors, including VEGF and EPO, as well as their cognate receptors VEGF-R2 and EPO-R, for various timepoints within the subacute phase of TBI (*Figure 6-5*, A). Interestingly, the profiles for VEGF and EPO differed slightly, with VEGF expression being upregulated after TBI and peaking at 7d post-TBI, while EPO expression had a much more delayed upregulation, with a peak at 14d post-TBI (*Figure 6-5*, B). This suggests that VEGF may be more associated with short-term rapid changes in neovascularization, such as proliferation of endothelial cells, whereas EPO may be more involved with longterm chronic vascular remodeling, such as recruitment of pericytes and extension of blood vessels, as well as re-establishment of the neurovascular unit. This seemed to be further corroborated by investigation of the cognate receptors. While there was no significant change in VEGF-R2, the expression of

EPO-R gradually increased and peaked at 14d post-TBI (*Figure 6-5*, B), suggestive of longterm remodeling.

Next, I examined the changes in the macrovessels surrounding the injury region at chronic timepoints, including at 2, 5, and 8 wk post-TBI. CCI was performed on smooth muscle actin (SMA)-GFP animals that allowed for immunofluorescence visualization of SMA+ structures, including arteries and arterioles, as well as SMA+ pericytes at higher magnifications. Both the number of feeding vessels (arterioles entering into contusion zone) and the diameters of surrounding arterioles were quantified (*Figure 6-6*, A). No significant changes were observed for the number of feeding vessels, though there was a trend for an increase from 2 to 8 weeks. However, there was a significant change in the diameters of the surrounding macrovessels as compared to sham (*Figure 6-6*, B). TBI resulted in a shift in the distribution of vessel diameters, such that there were reduced numbers of smaller diameter vessels (0-10 units as measured by ImageJ) and greater numbers of larger diameter vessels (>10 units) (*Figure 6-6*, C). This shift demonstrates the collateralization and arteriogenesis that occurs due to BBB disruption and the continuous ischemic damage that results from TBI.

IHC was also performed to examine the regeneration of the neurovascular network on a cellular level. To this end, I carried out immunostaining for glutamate transporter 1 (GLUT1), glial fibrillary acidic protein (GFAP), SMA, and BrdU, which are markers of endothelial cells, astrocytes, pericytes, and newly divided cells, respectively. No significant differences were observed either in the number of vessels or the levels of angiogenesis within the peri-contusion region from 2 to 8 wk post-TBI (*Figure 6-7*, A-B). However, the numbers of proliferating astrocytes increased from 2 to 8 wk post-TBI (*Figure 6-7*, B). This was likely because the neovascularization scales up early on (peaking by 4 d following injury and stabilizing and tapering

off within 1 wk) [409], with a similar profile as the VEGF upregulation. This was further corroborated by the subsequent study that characterized the progression of maturation of the neurovascular unit. By quantifying the varying ratios of triple-labeled GLUT1+/SMA+/GFAP+ units to either total GLUT1+/SMA+ or GLUT1+/GFAP+ units, I discovered that while there were still a significant proportion of GLUT1+/GFAP+ units not associated with pericytes (left graph), only ~3% of vessels associated with pericytes were not associated with astrocytes (right graph) (*Figure 6-8*, A-B). This suggests that the maturation of the neurovascular unit occurs first between the astrocytes and the endothelial cells, followed by the recruitment of the pericytes. In fact, the astrocytes may be integral to the recruitment and stabilization of the pericytes within the neurovascular unit. Thus, the hypothetical timeline may be that angiogenesis rapidly occurs within the first week post-TBI, followed by a slower and chronic formation and maturation of the blood vessels in conjunction with the neurovascular network.

To evaluate the function of the blood vessels around the injury, I also characterized the changes in local cerebral blood flow (LCBF) around the contusion by laser Doppler imaging. There was a significant attenuation in LCBF in the peri-contusion region during the 1-3 weeks following TBI, with a gradual elevation of perfusion within that timeframe (*Figure 6-9*, A-B). By 5 weeks post-TBI, the LCBF had returned to ~85% of baseline levels (*Figure 6-9*, A-B). Because blood flow appears to be restored relatively quickly (by 5 wk), this data altogether suggests that the maturation of blood vessels continues even for weeks after (at 8 wk), potentially to promote future neurogenesis within the peri-contusion region.

Finally, I characterized the glial scar formation. Previous reports have indicated that astrogliosis peaks at around 7d post-TBI and subsides afterwards to appear nearly normal around the cortical injury by 28d post-TBI [409]. However, when I immunostained for reactive astrocytes

with GFAP, I found sustained elevations of gliosis even at the 5 wk post-TBI timepoint, although the scar was significantly contracted by 8 wk post-TBI (*Figure 6-10*, A-C). Specifically, the scarring thickness peaked at 2 wk post-TBI and then gradually thinned from 5-8 wk post-TBI, although the contraction rate was more prominent from 5-8 wk post-TBI (*Figure 6-10*, C). While it is difficult to demarcate the distinct margins of the scar, this analysis demonstrates that reactive astrocytosis response remains upregulated for weeks-months after the initial injury. This is especially relevant for cell therapy studies given the inhibitory microenvironment established by the astrocytes, such as through the release of axon growth inhibitors like chondroitin sulfate proteoglycans (CSPGs) [410]. Thus, to promote plasticity after transplantation, it will be imperative to design approaches that can resolve the persistent challenge of the glial scar.

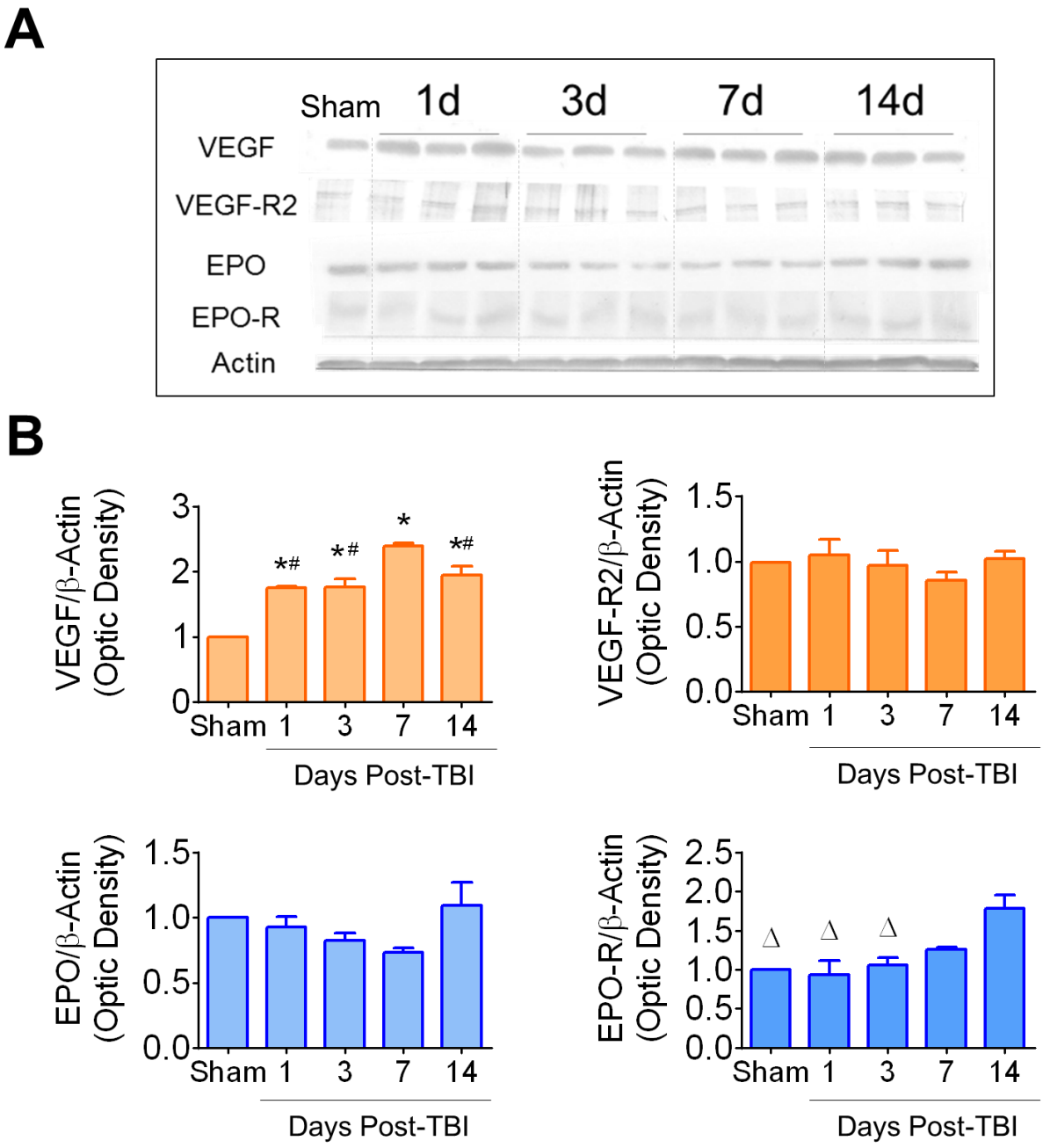

Figure 6-5: Peri-contusion expression of proteins related to angiogenesis and vessel maturation.

A. Representative immunoblot images after staining for VEGF, VEGF-R2, EPO, and EPO-R, as well as β-actin loading control. B. Quantification of the densitometry analyses for the different markers across the different timepoints. *: $p<0.05$, as compared to Sham. #: $p<0.05$, as compared to 7 d post-TBI. Δ: $p<0.05$, as compared to 14d post-TBI. N = 1 for sham, 3 for all other groups.

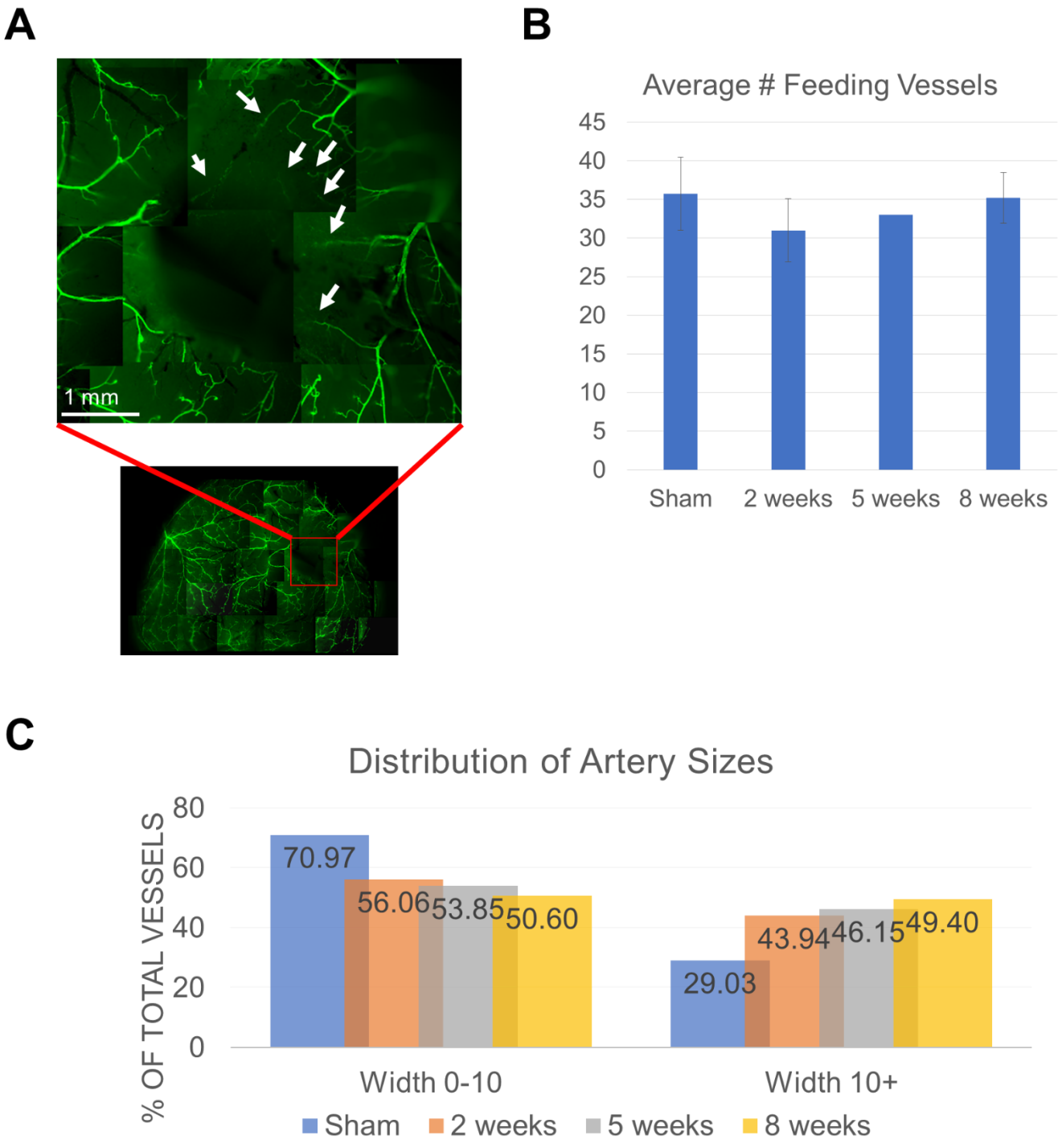

Figure 6-6: Development of macrovessels in the injury region.

A. Whole brain images were taken at each time point. Vessels supplying the contusion region (arrows) were counted and diameters of the peri-contusion arteries were measured. B. Quantification of the average number of feeding vessels into the contusion region. N = 4 Sham, 4 for 2 weeks, 1 for 5 weeks, and 4 for 8 weeks. C. Quantification and histogram representation of the size distribution of the arteries around the peri-contusion region. N = 1 per group. While there was no significant difference between the total # of vessels feeding the injury region, injured animals had a distinct loss of smaller vessels (0-10 units), and an enrichment of larger vessels (>10 units).

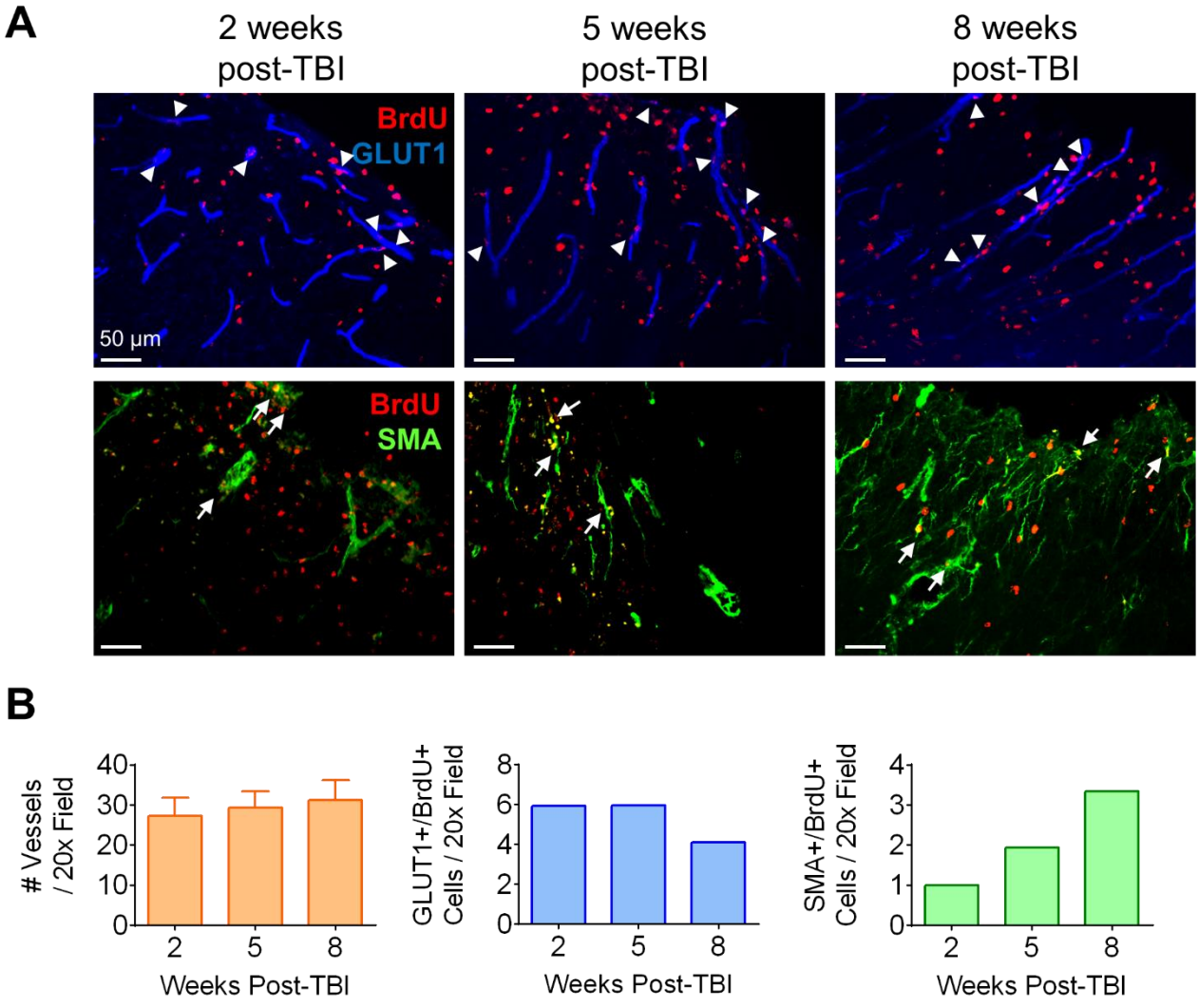

Figure 6-7: Progression of neovascularization after injury.

A. Representative immunofluorescence images demonstrating either GLUT1/BrdU colocalization (top panels, arrowheads) or SMA/BrdU colocalization (bottom panels, arrows). B. Quantification of the average numbers of vessels, GLUT1+/BrdU+ colocalized cells, or SMA+/BrdU+ colocalized cells per 20x image. For # vessel count, N = 4-5 per timepoint. For other quantifications, N = 1 per timepoint.

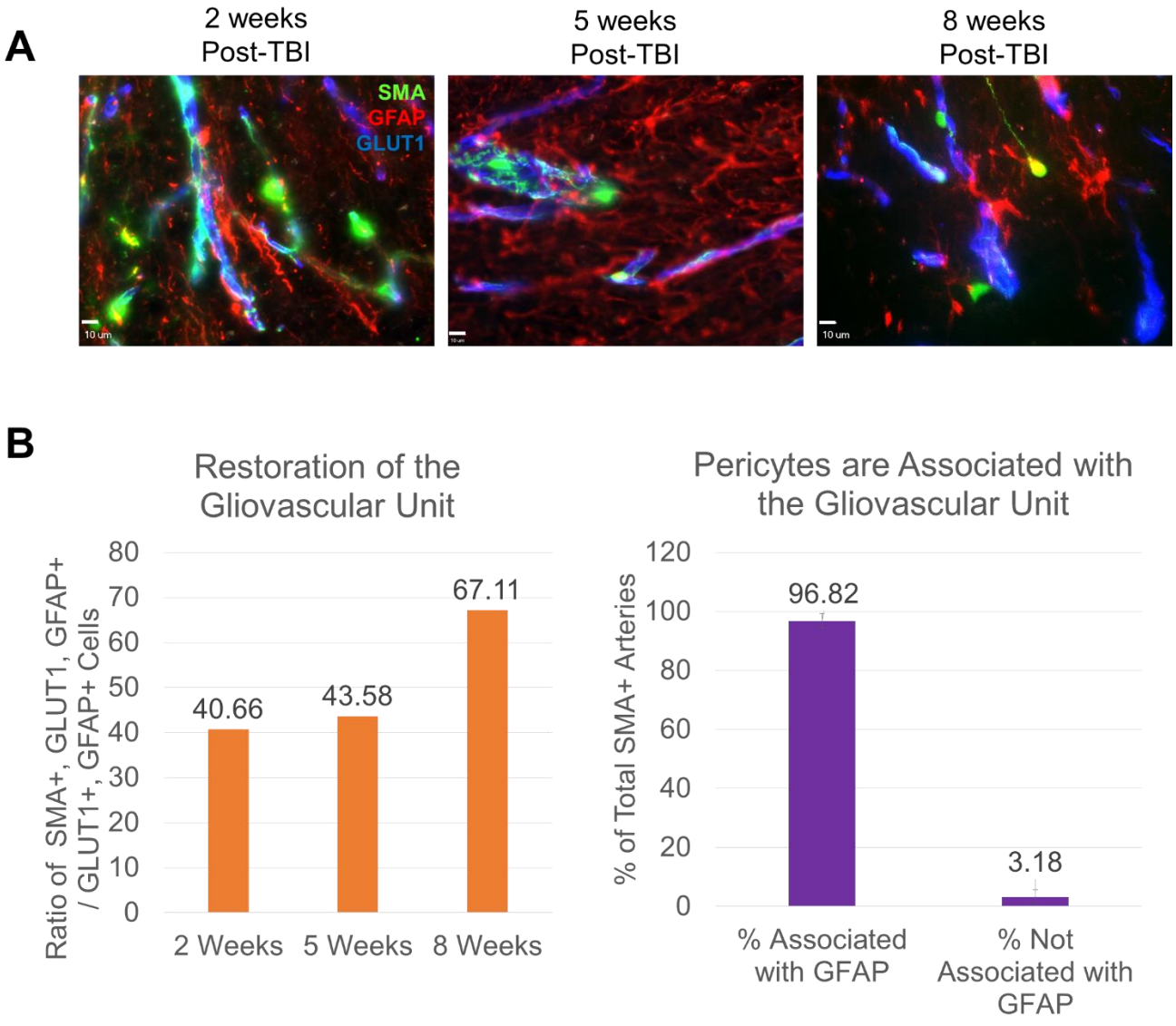

Figure 6-8: Pericytes are essential to reforming the BBB.

A. Representative immunofluorescence images of the peri-contusion region demonstrating colocalization of either GFAP with GLUT1, or triple colabeling of GFAP, SMA, and GLUT1. B.

Left panel: Quantification of the ratio of triple-labeled SMA+/GLUT1+/GFAP+ cells to the total colabeled GLUT1+/GFAP+ cells. Right panel: Quantification of the total % of SMA+/GLUT1+ cells that are either also GFAP+ or not GFAP+. The vast majority of the SMA+/GLUT1+ cells are also GFAP+. N = 1 per timepoint.

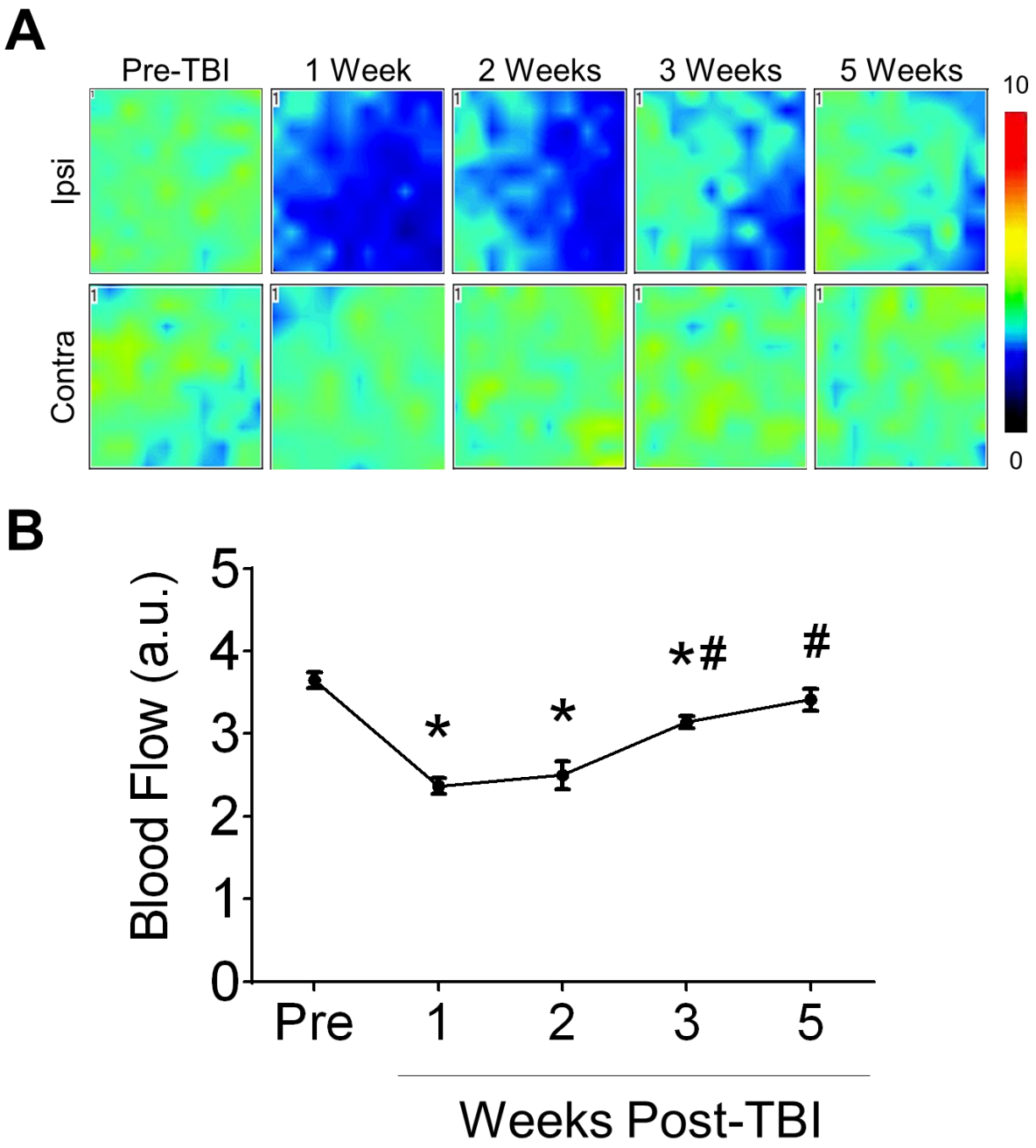

Figure 6-9: The cerebral blood flow gradually returns to near-baseline within the peri-contusion area.

A. Representative images of the local cerebral blood flow (LCBF) within peri-contusion region either prior to injury or at various timepoints following TBI (green and yellow indicate greater levels of flow, whereas blue and purple indicate decreased flow). **B.** Quantification of LCBF at the different timepoints. *: $p<0.05$, compared to Pre. #: $p<0.05$, compared to 1 week post-TBI. N = 6-7 animals per timepoint.

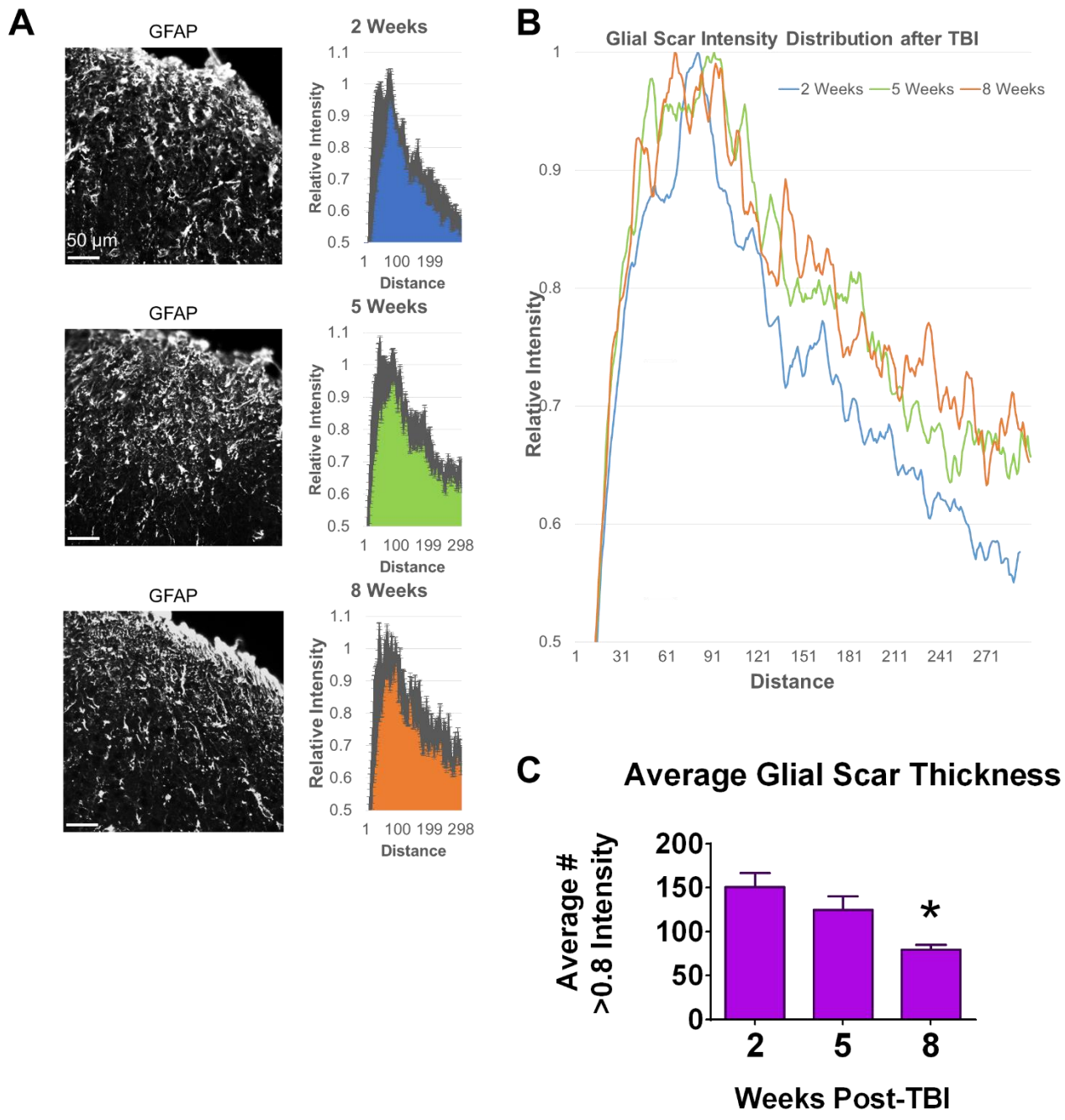

Figure 6-10: The astroglial scar continues to evolve even months after TBI.

A. Left panel: Representative images of the GFAP immunofluorescence at 2, 5, and 8 weeks post-TBI. Right panel: to determine the relative intensity profiles, an orthogonal reference line (relative to the parenchymal surface) was drawn, and then the signal intensities at each point along the line was measured. The signal intensities were normalized to a region outside the brain that had no signal. B. Superimposed relative intensity profiles. C. Quantification of average glial scar

thickness by blinded scoring of the thickness of pixel aggregates of >0.8 intensity. *: $p<0.05$, as compared to 2 weeks post-TBI. N = 7 for 2 and 8 weeks post-TBI, 5 for 5 week post-TBI

Chapter 7: Aim 1 – Creation and in vitro Characterization of LMO3-expression Stable iPS Cell Line

7.1 Introduction

Stem cells provide an unprecedented therapeutic approach for regeneration and repair following intractable disorders such as TBI. With these brain injuries currently lacking in long-term treatment options, there is a mounting unmet clinical need to address these prevalent healthcare scourges. Transplantation of pre-differentiated neural progenitor cells promotes neural remodeling and repair of damaged neural circuits through multiple mechanisms, including trophic support, facilitating endogenous neurogenesis and plasticity, and cell replacement [86, 235]. Although stem cell therapy confers many benefits, several key challenges must be resolved prior to clinical translation. Some of these challenges involve optimizing the parameters for transplantation, including the therapeutic window, therapeutic index for dosing, and the route of administration. Furthermore, stem cell therapy alone results in subpar viability, differentiation, and functional integration rates. Several classes of advancements have been innovated to augment stem cell survival function after transplantation, including genetic engineering, preconditioning, biocarriers, and external stimulation.

One of the most evident challenges for cell therapy in treating focal brain injury is the hostile environment of the core zone and the surrounding penumbra zone in which the stem cells are usually transplanted into [177]. These hostile factors include the upregulated inflammation, which impairs survival and differentiation and neurite extension, as well as reactive astrocytosis, which releases inhibitory factors such as chondroitin sulfate proteoglycans (CSPGs) that hinder axon outgrowth both outwards and inwards [410]. However, stimulation of NPCs has been shown to improve survival, differentiation, and neurite extensions [295, 372], as well as plasticity and cell-cell engagement after transplantation [373]. Furthermore, eliciting the release of neurotrophins, such as NGF, has demonstrated efficacy in promoting axonal outgrowth beyond the glial scar [292, 411], which is especially valuable in the context of focal brain injury. Creation of a new CTZ-responsive cell line may be a viable approach for continuous and long-term stimulation of NPCs and even differentiated neurons after transplantation to augment the beneficial effects of cell therapy.

In this chapter, I will highlight the cloning of a new episomal plasmid carrying the LMO3 transgene, followed by the generation of a new LMO3-expression stable iPS cell line. This cell line will provide the means for non-invasive pharmacologically-derived optogenetic stimulation after transplantation of the cells, which will be able to drive graft cell activity to promote trophic support and graft-host cell-cell engagement.

7.2 Results

7.2.1 Aim 1.1 – Create and validate an LMO3 plasmid containing the fused VChR1-sbGLuc transgene.

Construction of the episomal pPyCAG-LMO3-EYFP plasmid.

Different vectors were considered for use as the backbone for the LMO3 transgene, including lentiviral (LV), AAV, and various plasmid vectors. I first attempted to create the stable cell line using the LV vector pLenti-CAG-LMO3 that was obtained from Duke University (kind gift of Dr. Ute Hochgeschwender). However, there were several factors that precluded this option from being feasible: 1) low rate of infection efficiency with the lack of ability to select for the mammalian positive clones, 2) loss of the viral copies and expression levels across mitotic divisions and with differentiation into neuronal products. Although infecting the cells for multiple rounds allowed for slightly higher expression, I ultimately decided to pursue a more cost-effective alternative. Our lab and prior studies had previously shown that the pPyCAG-Nanog-IP episomal plasmid (Addgene #13838) is a viable option to maintain expression across multiple division cycles and differentiation stages [386, 387]. Furthermore, our lab corroborated this stability of expression by creating a pPyCAG-mCherry cell line with the episomal backbone (unpublished data). Therefore, this vector was selected to be the ideal candidate to be the backbone of choice for LMO3.

Aside from being an episomal plasmid, pPyCAG-Nanog-IP also contains the puromycin resistance gene, a mammalian selection marker, in order to create stable iPS cell lines with 100% transgene expression, as well as an internal ribosomal entry site (IRES) motif to allow for co-

translation of multiple genes (LMO3 and the puromycin resistance gene). I will use this vector as a backbone for the proposed LMO3 expression vector. To create this novel vector, our lab has obtained the VChR1-GLuc (LMO3) coding sequence from Duke University (kind gift of Dr. Ute Hochgeschwender). The LMO3 coding sequence was amplified using PCR using primers with BsrgI recognition sequences encoded into the ends to allow for restriction enzyme digestion of the insert to be inserted into our established pPyCAG plasmid backbone (*Figure 7-1*), using standard molecular cloning techniques (PCR amplification, digestion, ligation, competent cell transformation and expansion, and finally DNA extraction and purification). Positive clones were confirmed through restriction enzyme analysis and PCR amplification (same forward and reverse primers as for amplification of the insertion fragment (*Figure 7-2*) and BLAST analysis to verify the sequence of the LMO3 transgene. Similarly, a control GFP transgene (insert fragment derived from previous plasmids available in lab) was also cloned into the identical episomal pPyCAG backbone (minus the LMO3-EYFP gene) as a vector control. Finally, the expression of both the LMO3 and GFP transgenes were verified within a highly proliferative and easily maintained human embryonic kidney (HEK)-293T cell line. Using Lipofectamine 2000, the HEK-293T cells were transfected with either the pPyCAG-GFP plasmid or the pPyCAG-LMO3 plasmid, and fluorescence images were taken to evaluate the transfection efficiency, as well as to partially validate the function of LMO3 by bioluminescence readout (*Figure 7-3*). The comparative fluorescence images demonstrate robust GFP and YFP expression in the GFP and LMO3 cells, respectively, and that both plasmids result in similar levels of transfection efficiency in HEK-293T cells (*Figure 7-3*, A). Furthermore, the LMO3-HEK cells responded rapidly to CTZ administration and produced easily identifiable bioluminescence (*Figure 7-3*, B).

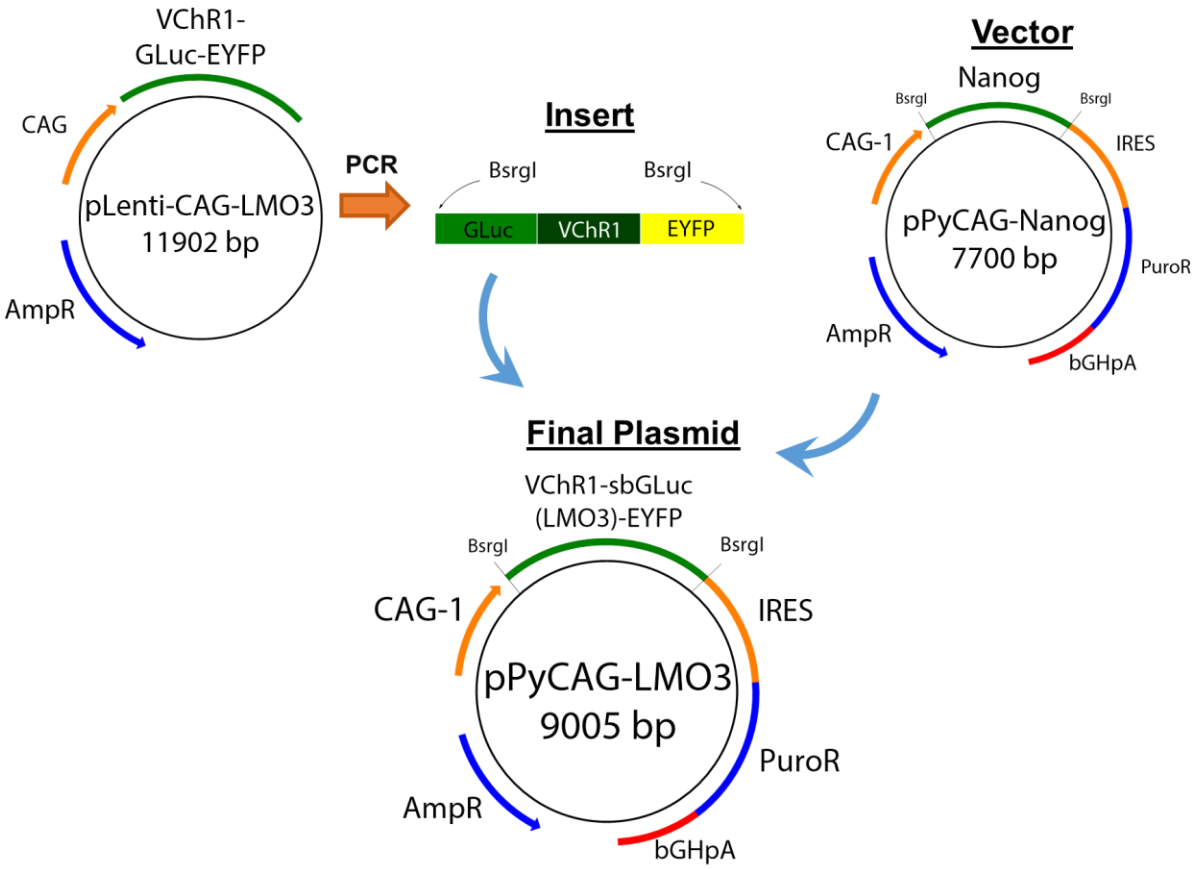

Figure 7-1: Summary schematic of the construction of the episomal LMO3 plasmid.

The VChR1-Gluc (LMO3) transgene was amplified out of the original pLenti-CAG-LMO3 vector by PCR with the insertion of BsrgI recognition sequences on the ends of the transgene. The vector of choice is the episomal plasmid pPyCAG-Nanog-IP, which carries the CAG-1 promoter, an internal ribosomal entry site (IRES) motif, the bovine growth hormone polyadenylation (bGHpA, a termination signal), an ampicillin resistance gene, and a puromycin resistance gene, which allows for the selection of mammalian cells. Both the pLenti vector and the backbone was digested with BsrgI to create complementary sequences for ligation. Then the digested products were ligated together to create the final episomal pPyCAG-LMO3-EYFP plasmid.

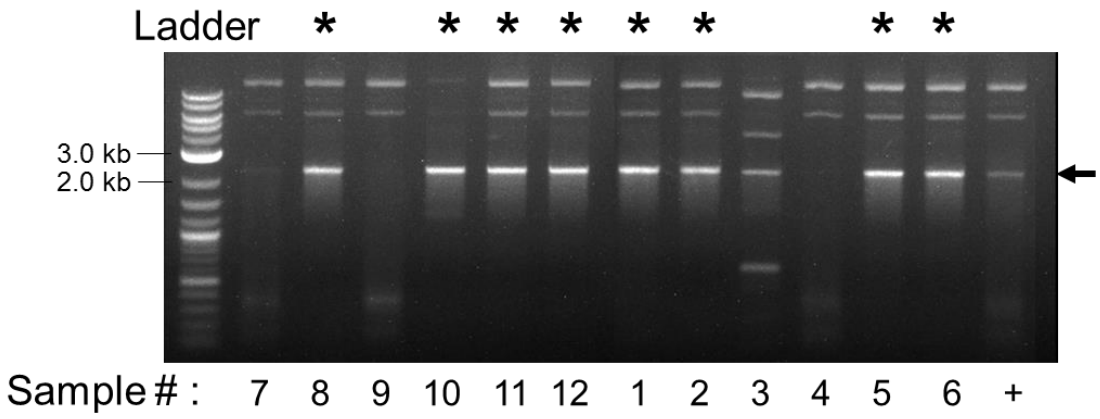

Figure 7-2: PCR confirmation of the transgene orientation in the final pPyCAG-LMO3 plasmid.

Primers that flanked the LMO3 gene (same as the forward and reverse primers used to amplify the insert fragment) were used to confirm the orientation of the insertion of the transgene into the backbone. The expected target fragment size is 2226 bp (as indicated by the arrow). A total of 12 samples were tested, and the final lane was the positive control of the original pLenti vector, in which the target fragment can be observed. In total, 8/12 of the samples were positive clones. 4 were chosen to proceed with BLAST analysis for confirmation of the LMO3 sequence.

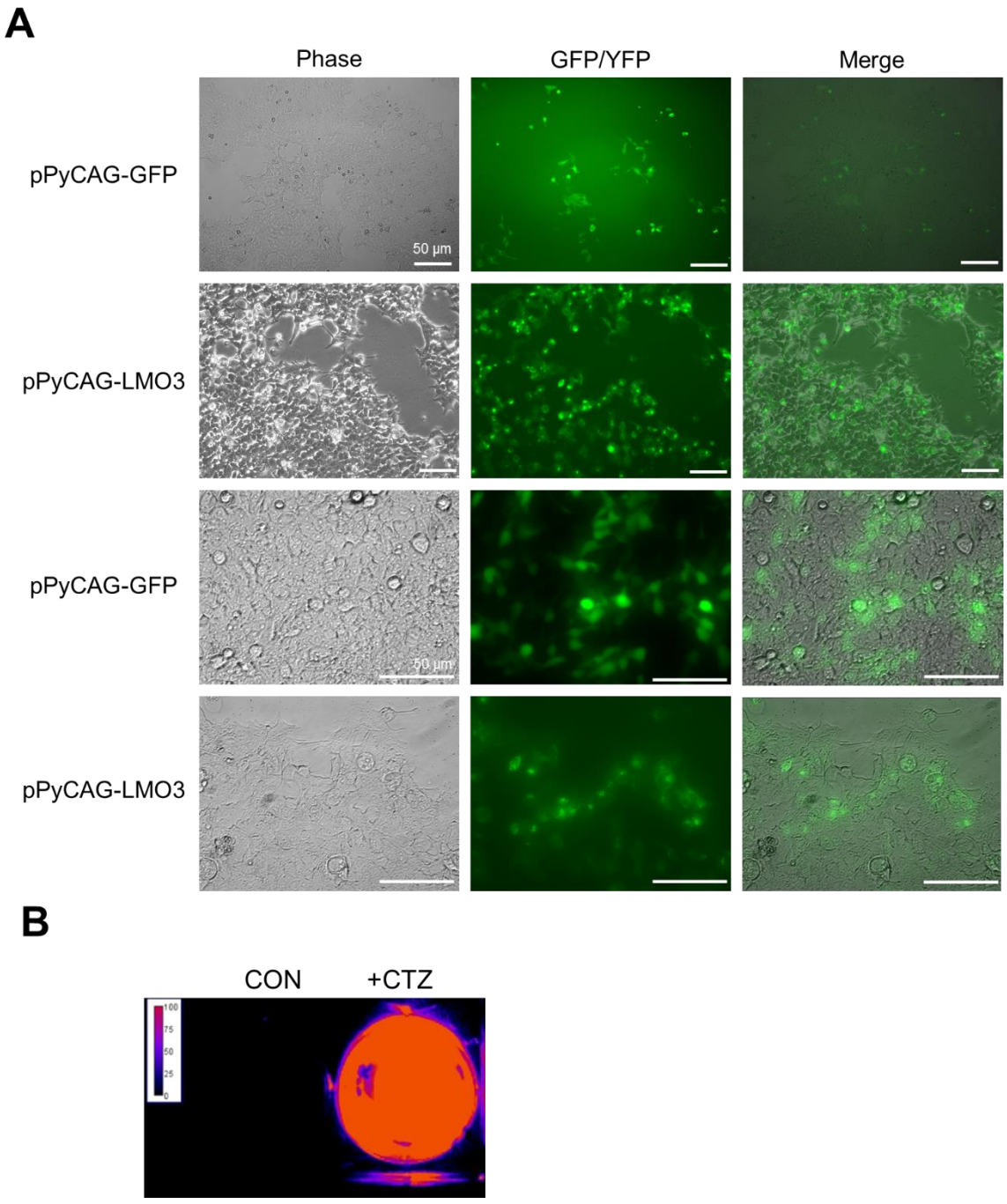

Figure 7-3: Transfection of HEK-293T cells to confirm expression and CTZ response of the pPyCAG-LMO3-EYFP plasmid.

A-B. HEK-293T cells were cultured and maintained using normal DMEM (with 4.5 g/L glucose, L-glutamine and sodium pyruvate, and 1:100 FBS, and 1:100 penicillin/streptomycin). **A.** HEK-293T cells were transfected with either the pPyCAG-GFP plasmid or the pPyCAG-LMO3-EYFP

plasmid using Lipofectamine 2000 (1:2 DNA:lipofectamine ratio). Fluorescence images were acquired at 3 days post-transfection at either 10x (top 2 panels) or 20x (bottom 2 panels) magnifications. Both plasmids resulted in efficient transduction of the transgene, as indicated by the number of cells that were GFP+ or YFP+ compared to the total number of cells observed on phase contrast. **B.** At 5d post-transfection, bioluminescence emission was measured using a chemiluminescence reader. CTZ (10 µM) was applied to one well of the LMO-HEK cells, while the other well of LMO-HEK cells were untreated. Within minutes (image acquisition shown at 5 min with a 30 sec exposure period), robust bioluminescence was observed from the CTZ-treated well, while no response was observed in the untreated well.

7.2.2 Aim 1.2 – Establish an iPS cell line that expresses LMO3, which will be functionally validated by performing *in vitro* luminescence and electrophysiology studies.

Generation of stable LMO3-expression iPS cell line

Two lines of iPS cells will be prepared according to our standard culturing protocol in order to create two distinct transgenic stable cell lines [152]. One iPSC line was transfected using Lipofectamine 2000 with the pPyCAG-LMO3 plasmid, while the second will be transfected with the pPyCAG-GFP control vector. In order to create stable cell lines, the cells were allowed to expand for 3d following transfection, and then positive clones were selected for both cultures by puromycin application (1 µg/mL) and then through live fluorescence imaging, the highest GFP- or YFP-expression cells were inoculated for further expansion (*Figure 7-4*). To prevent spontaneous mutation and proliferation of negative clones, the stable cell lines were maintained with continuous puromycin application (0.5 µg/mL).

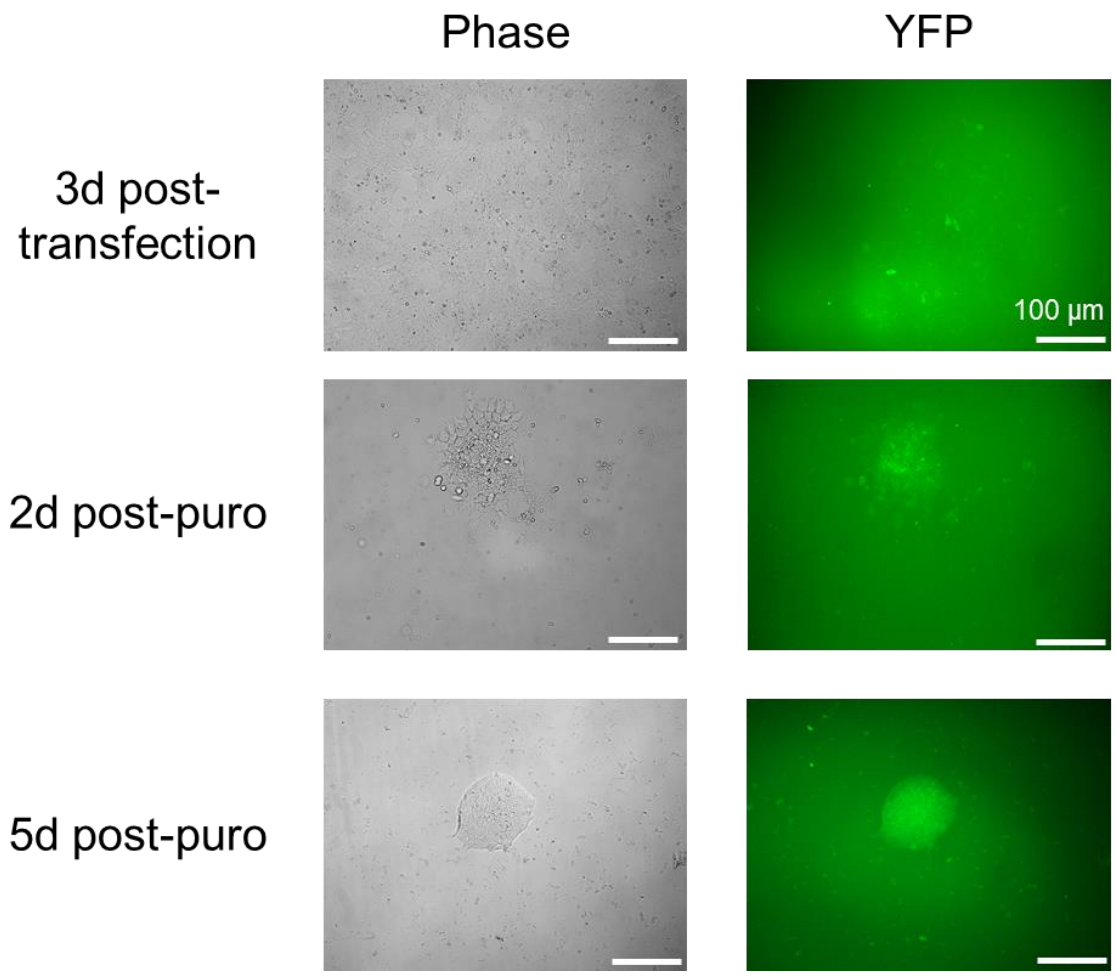

Figure 7-4: Creation of the LMO3-expression stable iPS cell line.

Mouse iPS cells (WP5 line) were thawed and cultured until passage 8 (P8), for which they were transfected with the pPyCAG-LMO3-EYFP plasmid using Lipofectamine 2000 (1:4 DNA:lipofectamine ratio). At 3d post-transfection (top panels), the cells were treated with puromycin for 2d with daily washes with stem cell maintenance media to remove dying cells and debris. At 2d post-puro administration (middle panels), there was nearly a 100% expression of YFP+ cells, and the greatest expression cells were inoculated for further expansion. By 5d post-puro administration (bottom panels), the colonies demonstrated 100% GFP expression with high consistency of expression levels.

Maintenance of expression across differentiation stages

After stable cell line creation, both lines of iPSCs, LMO3-iPSCs will be induced to become cortical neurons using our lab's established 4-/4+ method [152]. Upon removal of LIF, the shaken dissociated stem cells aggregate together form embryoid bodies, which then form neurospheres with the addition of retinoic acid. After 4 days of retinoic acid treatment, the neurospheres were collected, dissociated, and seeded onto PDL/laminin coated dishes for immunostaining to confirm expression of neuronal markers. The cells demonstrated 100% expression of YFP across all stages, starting from the pluripotent stage, as verified by colocalization with pluripotency markers Oct4 and stage-specific embryonic antigen 1 (SSEA1) (*Figure 7-5*).

Similar differentiation and immunocytochemistry protocols were carried out for the GFP-iPSCs, and the expression of GFP was confirmed across all three major phases as well, including the pluripotent phase, differentiating neurosphere phase, and the mature neuronal phase (*Figure 7-6*). Furthermore, additional immunostaining was carried out to confirm neuronal differentiation and to characterize the neuronal subtypes. Fluorescence microscopy demonstrated that approximately 80-90% of the neuronal products of LMO-iPS-NPC differentiation are glutamatergic neurons (*Figure 7-7*).

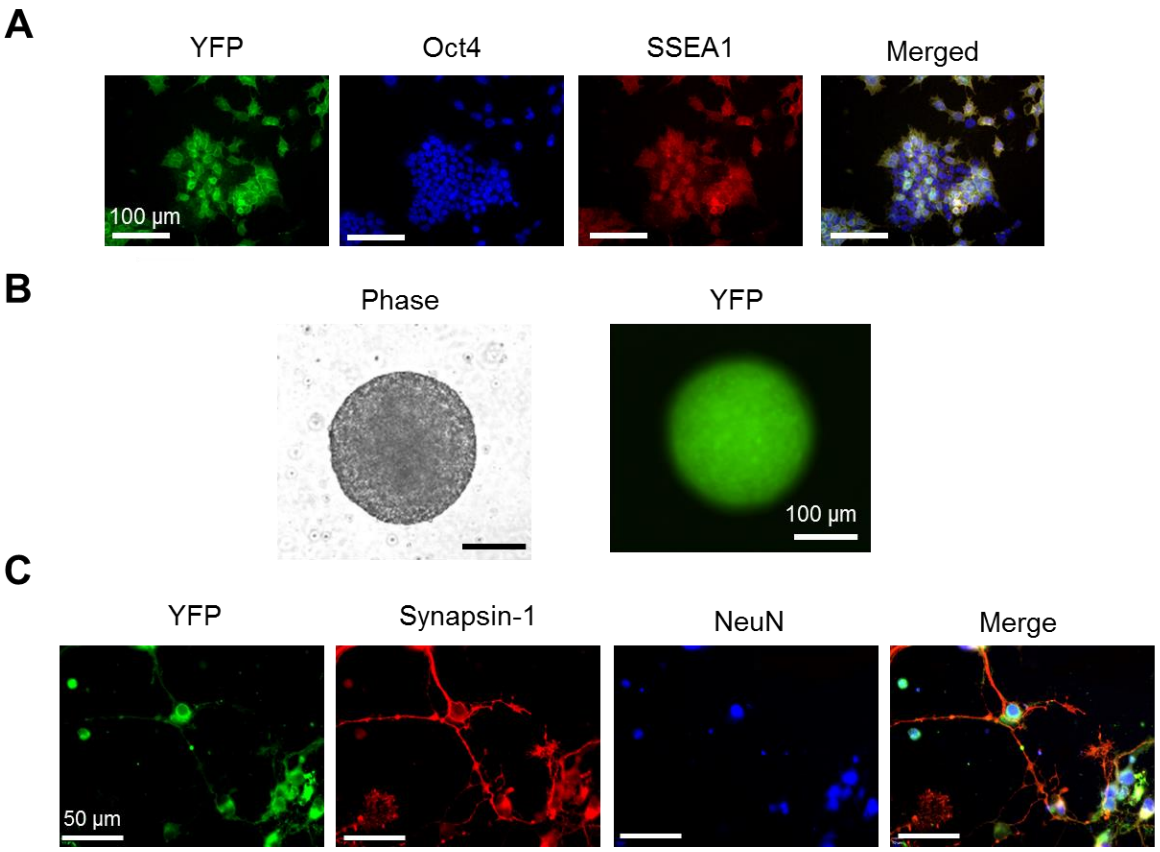

Figure 7-5: Neuronally differentiated LMO3-iPSCs maintain expression across all stages.

A-C. LMO3-expression iPSCs were induced to differentiate into cortical neurons by the 4-/4+ protocol. A. Undifferentiated iPSCs expressed YFP that 100% colocalized with Oct4 and SSEA1. **B.** Differentiating neurospheres demonstrated high expression levels of YFP through 20+ passages. **C.** Finally, fully mature neurons that expressed neuronal markers Synapsin-1 and NeuN displayed retention of YFP expression as well.

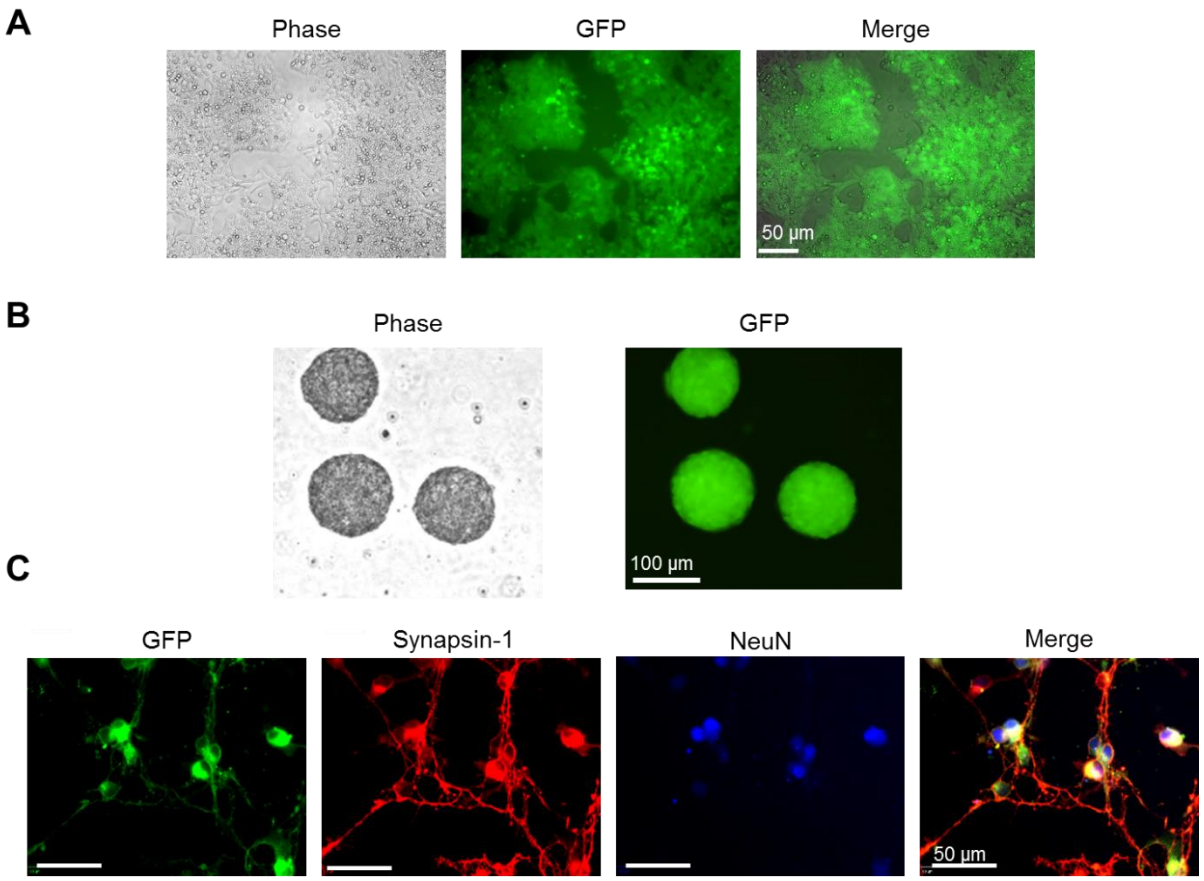

Figure 7-6: Neuronally differentiated GFP-iPSCs maintain expression across all stages.

A-C. GFP-expression iPSCs were induced to differentiate into cortical neurons by the 4-/4+ protocol. **A.** Undifferentiated iPSCs demonstrated approximately 100% GFP expression. **B.** Differentiating neurospheres demonstrated high expression levels of YFP. **C.** Finally, fully mature neurons (11 DIV) that expressed neuronal markers Synapsin-1 and NeuN displayed retention of YFP expression as well.

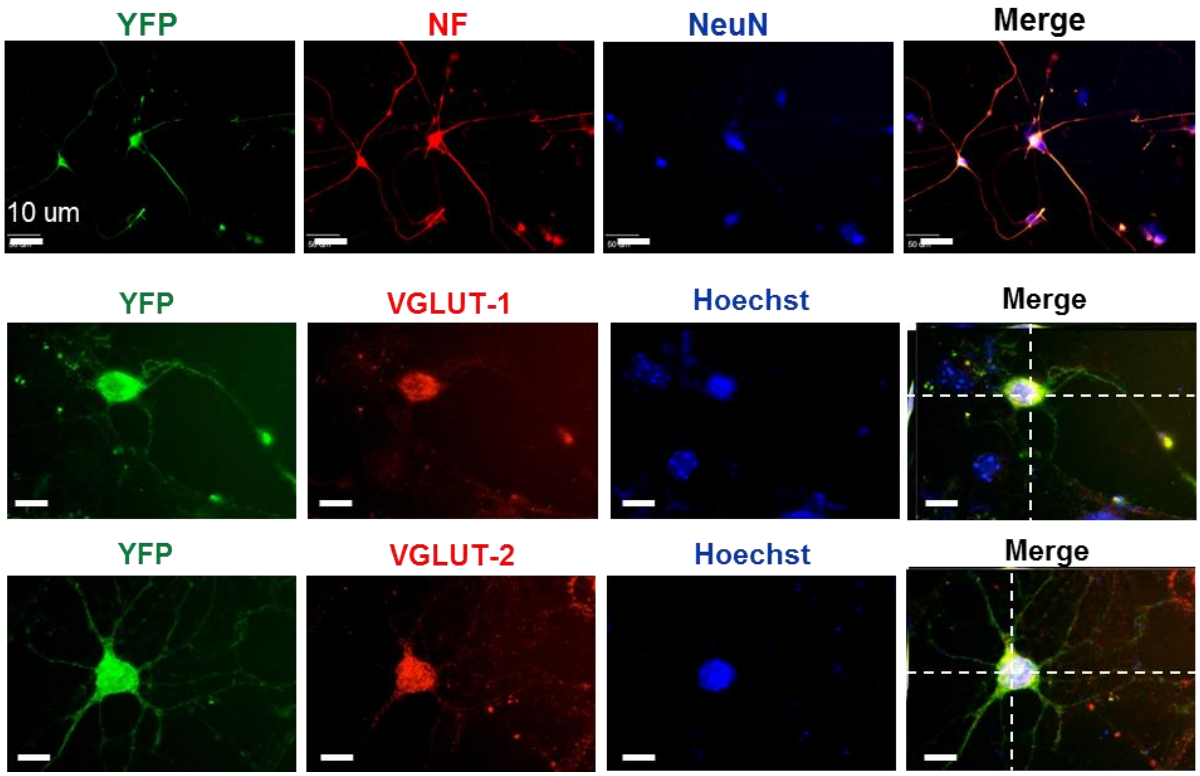

Figure 7-7: Differentiated products of LMO3-iPS-NPCs express additional neuronal markers and markers of glutamatergic neurons.

At 11 DIV, the LMO-iPS-neurons were also stained for neurofilament (NF), another marker of neurons, and vesicular glutamate transporters 1 and 2 (VGLUT1 and 2), markers of glutamatergic neurons. It was observed that ~80-90% of the YFP+ cells colabeled with VGLUT1/2, suggesting that the vast majority of the LMO3-iPS-NPCs differentiate into glutamatergic neurons.

Validation of LMO3 function in iPS-neurons.

The functional activity of the various components of the LMO3 fusion probe was validated within the differentiated iPS-neurons. At 11DIV, the sbGLuc activity was assessed by bioluminescence imaging within an ultrasensitive chemilumiscence reader. Upon addition of CTZ (3 µM), there was a strong bioluminescence emission response that was sustained for approximately 60 min before reaching 10% of the peak luminescence readout (*Figure 7-8*). By

contrast, no bioluminescence response was observed in either the YFP-iPS-neuron + CTZ control or the LMO + CyD vehicle control. The experiment was prepared with duplicate cultures (n = 2).

Next, electrophysiology was carried out to confirm both the VChR1 function, as well as the coupling of VChR1 with sbGLuc. Again, 11DIV LMO3-iPS-neurons were prepared on coverslips for experimentation. The functionality of the VChR1 was confirmed in the mature neurons by patch clamp recordings on both voltage clamp mode and current clamp modes. The LMO3-iPS-neurons demonstrated strong photocurrents in response to laser stimulation (473 nm) on the order of ~100 pA, as well as a train of evoked action potentials (*Figure 7-9*, B). Furthermore, in order to validate the coupling of the luciferase with the opsin, spontaneous action potentials were recorded with administration of either CTZ (3 µM) or internal solution vehicle control. Nearly immediately following bath application of CTZ, there was a marked increase in the firing rate of the iPS-neurons, whereas no changes in activity were observed for the control solution (*Figure 7-9*, C).

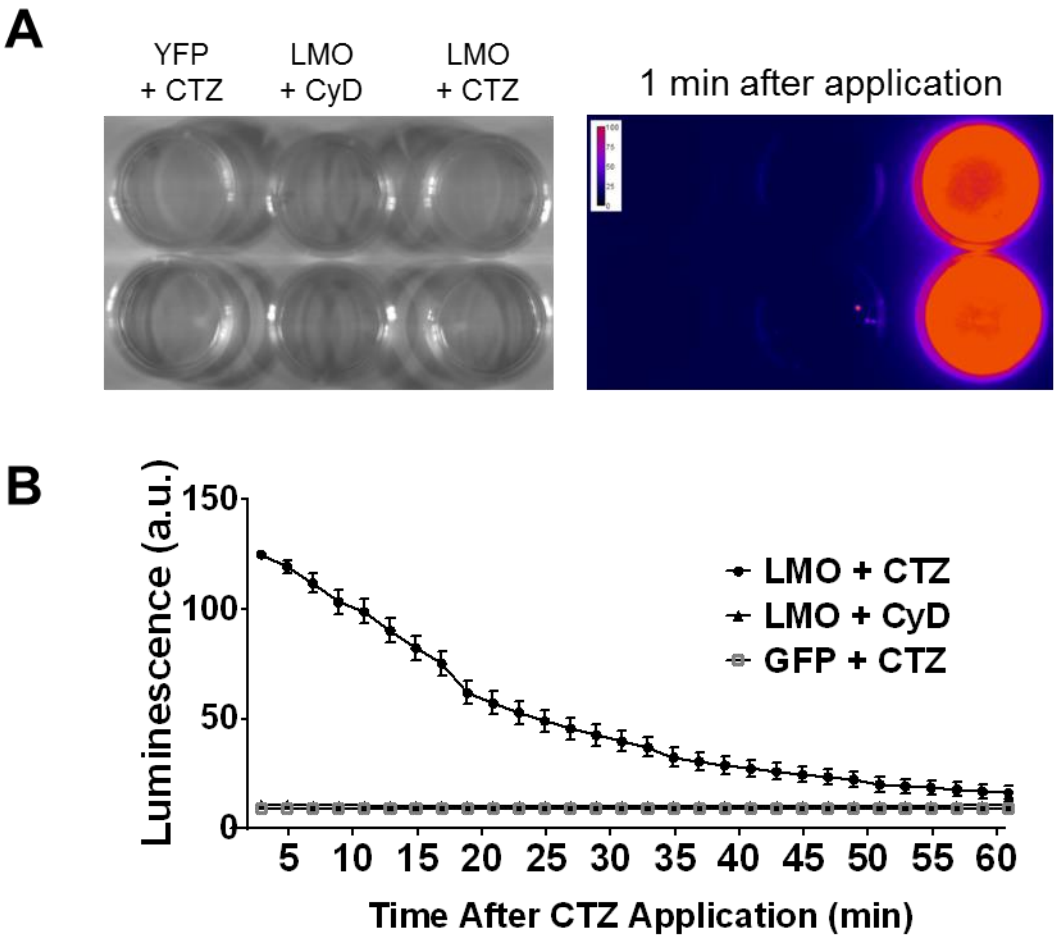

Figure 7-8: CTZ administration triggers bioluminescence emission in LMO-iPS-NPCs.

A-B. LMO-expressing iPS-NPCs were seeded at equal densities onto each well of a 6-well plate (n=2 per group) and used for bioluminescence imaging at 11 DIV. **A.** The background image was acquired to demonstrate the layout of the plate (left panel), in which there were 3 groups: YFP-iPS-neurons + CTZ (3 µM), LMO-iPS-neurons + CyD ((2-Hydroxypropyl)-β-cyclodextrin), and LMO-iPS-neurons + CTZ (3 µM). An adjusted luminescence readout image was acquired 1 min after application (with 30 sec exposure time at ultrasensitive precision, right panel). **B.** The quantification of the luminescence readout over the course of the image acquisition. The experiment was stopped when the luminescence levels returned to within 10% of baseline. The data was normalized to a control region in which no noticeable luminescence was observed. N = 2 per group.

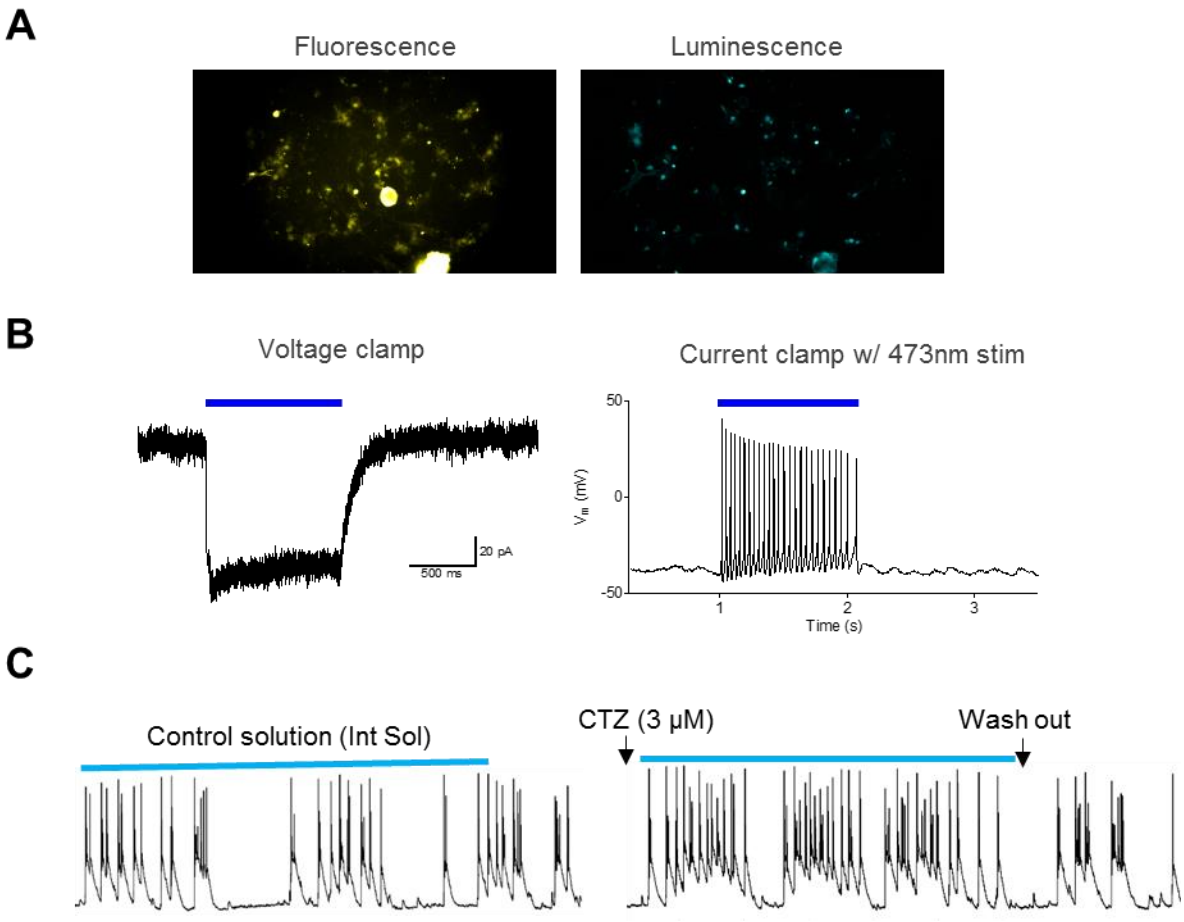

Figure 7-9: LMO3-iPS-neurons demonstrate functional activity following both laser stimulation and CTZ stimulation.

A-D. At 11DIV, LMO3-iPS-neurons were prepared for electrophysiology. A. Representative images of the YFP fluorescence (left panel) and the emitted bioluminescence (right panel) after CTZ (3 µM) perfusion. **B.** A single LMO-iPS-neuron was patched and on voltage clamp mode with a holding potential of -60 mV, the inward current was measured with a 1 s pulse of laser stimulation (473 nm), resulting in a strong inward current (left panel). Then, on current clamp mode, a 1 s pulse of laser stimulation (473 nm) resulted in a train of action potentials (right panel). **C.** Either internal solution control (left panel) or CTZ (3 µM, right panel) was added to the coverslip. Bathing the cells in internal solution did not result in changes in firing rate, while CTZ administration elicited modest increases in spontaneous action potentials.

7.2.3 Aim 1.3 – Determine neurotrophic responses to photostimulation at different stages of neural progenitor cell differentiation

Activation of intracellular CREB signaling and neurotrophins after photostimulation

Firstly, I carried out RT-PCR to evaluate whether the temporal dependency of stimulation paradigms (10 min vs 30 min) for regulating the mRNA of neurotrophins and their cognate receptors. 3DIV LMO3-iPS-neurons were stimulated by one round of laser stimulation (10 Hz, 5 ms pulse-width; each sweep consisted of 12 second of stim, followed by 48 sec of rest for each sweep; either 10 or 30 sweeps total for each round). Then, cells were collected for RT-PCR 30 min after the end of the stimulation (*Figure 7-10,* A). Stimulation with both paradigms resulted in upregulation of TrkB, and the 30 min stimulation resulted in significantly greater levels of BDNF (*Figure 7-10*, B). The 10 min stimulation resulted in a trend of upregulation of BDNF. For both stimulation paradigms, there was a strong trend of upregulation of NGF (*Figure 7-10*, B).

Afterwards, GFP-iPS-neurons and LMO3-iPS-neurons were collected at different timepoints after the 4-/4+ protocol for Western blot analysis: an early timepoint (3DIV) and a mature timepoint (7DIV). Both the GFP and LMO3 groups underwent either CTZ stimulation (3 µM) or laser stimulation ((10 Hz, 5 ms pulse-width; each sweep consisted of 12 second of stim, followed by 48 sec of rest for each sweep; 15 sweeps total for each round). At the early timepoint, the total protein isolated from the cell lysates were probed for phospho-cAMP responsive element binding protein (p-CREB), total CREB, the neurotrophins BDNF and NGF, as well as their cognate receptors TrkB and TrkA, respectively (*Figure 7-10*) . The immunoblots instantiated significantly greater levels of p-CREB in the LMO-CTZ and LMO-laser groups, as compared to the GFP-CTZ and the LMO-CyD groups (*Figure 7-11*, B), suggesting greater activation of the intracellular CREB signaling pathway, which is activated following neural activity as a result of cAMP

upregulation. Total CREB levels did not change across groups. Additionally, both CTZ and laser stimulation of LMO cells resulted in upregulation of BDNF and NGF, both of which are activity-dependent factors (*Figure 7-11*, C). Finally, both CTZ and laser stimulation of LMO cells resulted in upregulation of the TrkB and TrkA, suggestive of sustained plasticity changes that correlates with enhanced network remodeling (*Figure 7-11*, D).

Next, I investigated the more longterm effects of photostimulation. Cell lysates were collected from 7DIV GFP-iPS-neurons and LMO3-iPS-neurons for Western blot analysis of synaptic maturation markers, post-synaptic density protein-95 (PSD-95) and the synaptic vesicular protein synaptophysin (*Figure 7-12*, A). The Western blot demonstrated that both CTZ and laser stimulation of LMO cells resulted in greater levels of both PSD95 and synaptophysin (*Figure 7-12*, B), suggesting greater levels of synaptic contact formation and strengthening in the photostimulated cells.

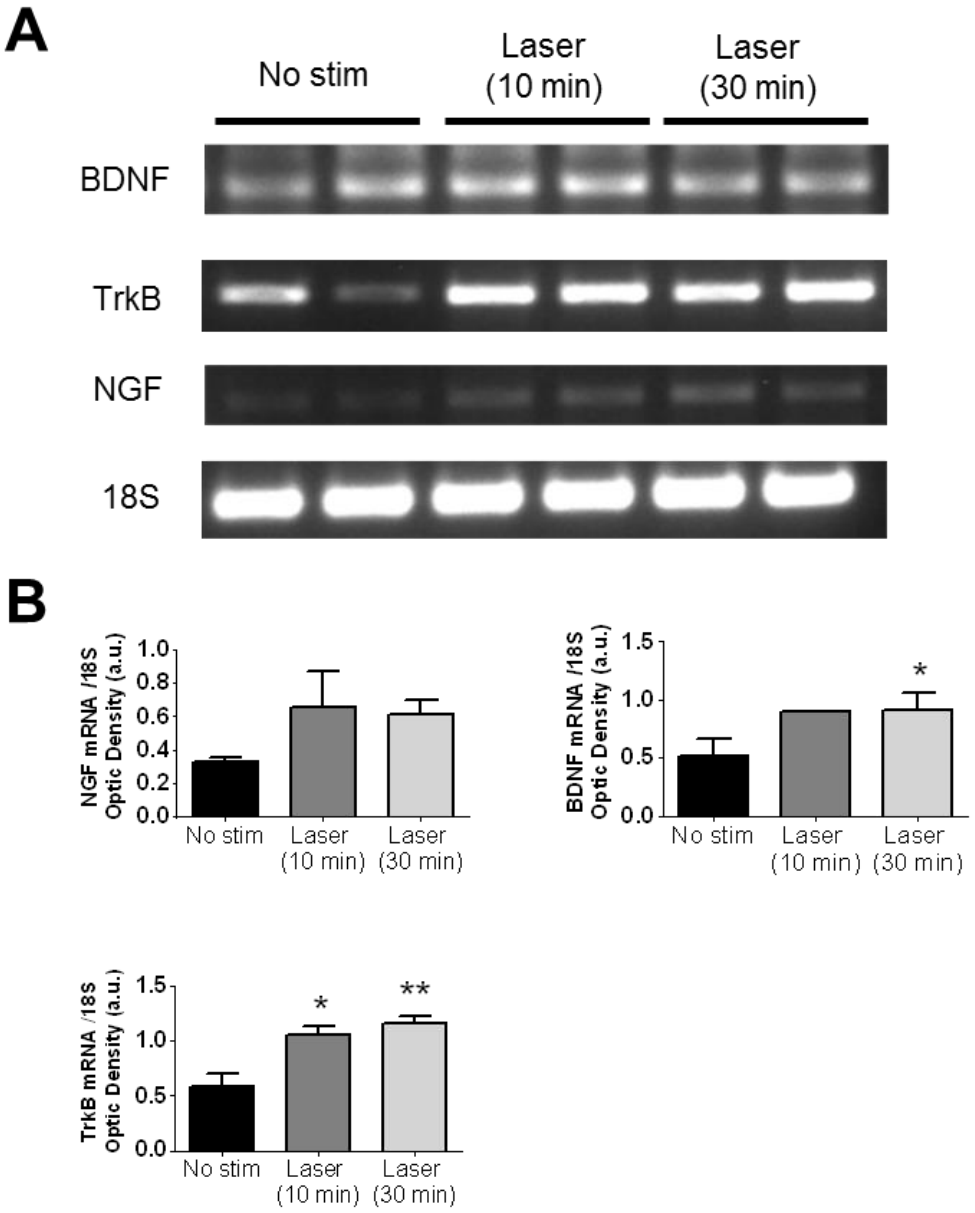

Figure 7-10: Greater levels of neurotrophin mRNA following laser stimulation.

A-B. As a preliminary experiment, at 3DIV, LMO3-iPS-neurons were stimulated with one round of laser stimulation (either 10 min or 30 min), followed by cell collection for RT-PCR. Multiple markers were probed, including neurotrophins BDNF and NGF, and the cognate receptor of BDNF, TrkB. **A.** Representative bands from the DNA electrophoresis is shown. **B** Both 30 min and 10 min stimulation paradigms produced similar effects on upregulation of neurotrophin and TrkB mRNA. Both 30 min and 10 min stimulation resulted in significant upregulation of TrkB

mRNA, while only 30 min stimulation produced a significant effect on increasing BDNF mRNA, although there was an increasing trend for the 10 min stimulation. Both 30 and 10 min stimulation resulted in a trend of elevated NGF expression, although neither was significant as compared to the No Stim group (One-way ANOVA with Tukey's correction for pairwise comparisons. *: $p < 0.05$, compared to No Stim group. N = 5 for No Stim group, and 4 for both Laser groups).

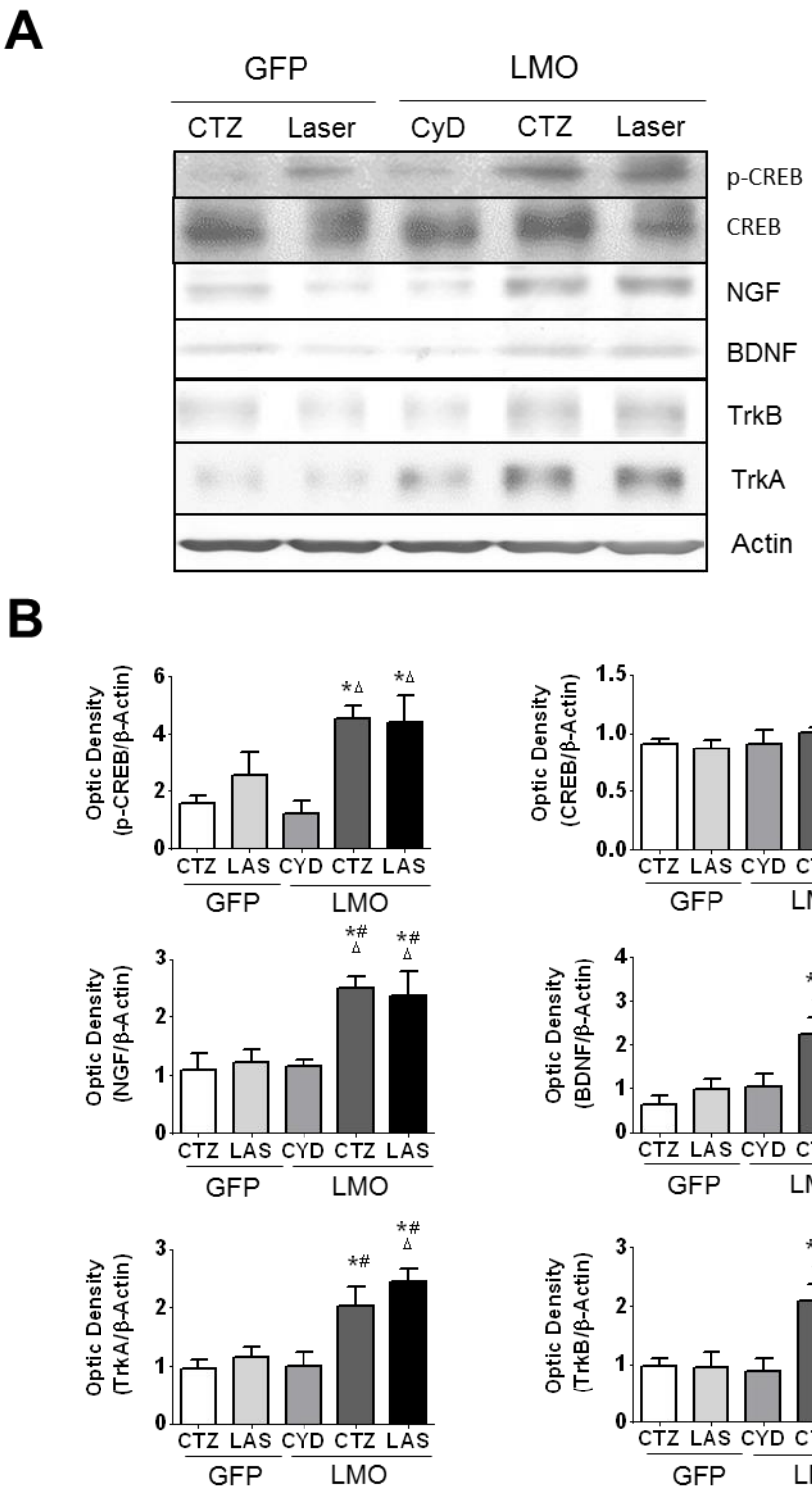

Figure 7-11: CTZ and laser stimulation enhanced the CREB signaling pathway, neurotrophins, and their cognate receptors.

A-B. Cell lysates were collected from 3DIV GFP-iPS-neurons or LMO3-iPS-neurons at 30 min following the final round of daily stimulation with either laser, CTZ, or CyD vehicle control (total 3 rounds of daily stimulation started at 1DIV). **A.** Representative images of Western blots for all p-CREB, CREB, NGF, BDNF, TrkB, TrkA, and actin loading control. **B.** Densitometry quantification of blots as normalized to actin, followed by normalization to GFP + CTZ group. *: $p < 0.05$, vs. GFP + CTZ; #: $p < 0.05$, vs. GFP + laser (LAS); Δ: $p < 0.05$, vs. LMO + CyD. N = 4 for all GFP groups, and 5 for all LMO groups.

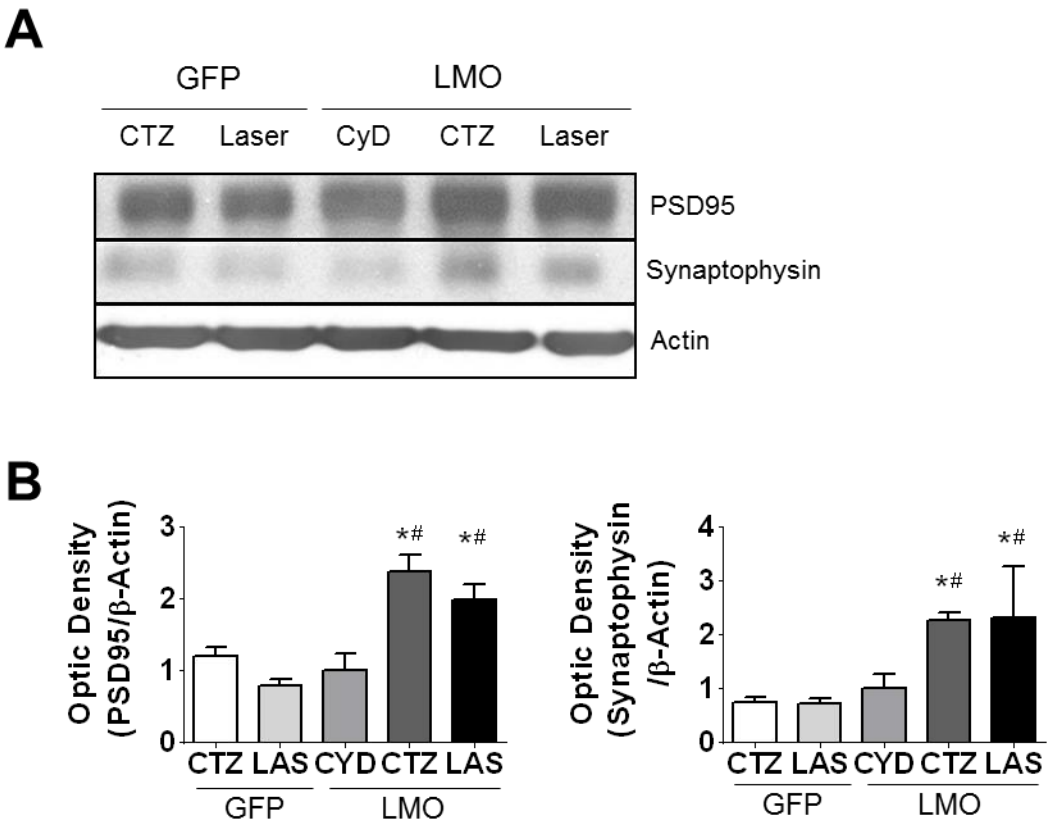

Figure 7-12: CTZ and laser stimulation of light-responsive iPS-neurons promoted synaptogenesis and plasticity.

A-B. Cell lysates were collected from 7DIV GFP-iPS-neurons or LMO3-iPS-neurons at 30 min following the final round of daily stimulation with either laser, CTZ, or CyD vehicle control (total 7 rounds of daily stimulation started at 1DIV). **A.** Representative images of Western blots for

PSD95, synaptophysin, and actin. **B.** Densitometry quantification of blots as normalized to actin, followed by normalization to GFP + CTZ group. *: $p < 0.05$, vs. GFP + CTZ; #: $p < 0.05$, vs. GFP + laser (LAS). N = 4 for all GFP groups, and 5 for all LMO groups.

Photostimulation results in enhanced neurite outgrowth, even across axon inhibitors

First, I characterized the differentiation products of the LMO3-iPS-NPCs after the 4-/4+ protocol, and whether CTZ stimulation can promote neuronal differentiation. To this end, multiplexed immunostaining was carried out against YFP, the immature neuronal marker Tuj1, and the astrocyte marker GFAP, as well as a counter-staining for all nuclei with DAPI. While both CTZ and CyD administration resulted in neuronal differentiation efficiency of > 90%, CTZ stimulation did not produce significant enhancements as compared to the CyD control (*Figure 7-13*). This may be due in part to the ceiling effect of the high baseline rate of neuronal differentiation in this iPS cell line.

Next, an axon investigation system (AXIS) microfluidic device was used to isolate measure axon outgrowth of LMO3-iPS-NPCs following laser or CTZ stimulation. Using the aforementioned stimulation paradigm, the devices were immunostained with Tuj1 and DAPI (*Figure 7-14*, A). Laser stimulation in increased axon crossings, as well as greater axon length, diameter, and branching numbers (*Figure 7-14*, B). CTZ stimulation similarly resulted in higher numbers of axon crossings and enhanced axon length and diameter, as well as a trend for greater branching numbers (*Figure 7-14*).

To model the inhibitory microenvironment faced by transplanted cells after TBI, a CSPG droplet assay was carried out. The iPS-neurons were seeded onto a coverslip containing 4 CSPG droplets and stimulated with either CyD, CTZ, or laser following the same paradigms. Immunocytochemistry demonstrated that the CSPG droplet resulted in a marked loss of neuronal

survival and axon growth within the spot region. However, there were still noticeable neurite entries into the CSPG zone (*Figure 7-15*, A). While stimulation did not noticeably improve the length of axon entries or survival or neurons within the CSPG zone, there was a 2-3 fold increase in number of neurite entries for the CTZ and laser stimulated LMO3-iPS-neurons, as compared to the controls (*Figure 7-15*, B).

Finally, a modified version of the scratch test was carried out to evaluate the plasticity response following an in vitro model of a traumatic insult involving diffuse cellular damage and axonal injury, and whether stimulation can augment the adaptive response. Both iPS-neurons were plated onto 35mm dishes and then following a full-length midline scratch at 2DIV, the cells were stimulated and imaged every day until 6DIV, in which they were fixed and immunostained (*Figure 7-16*, A). Three metrics were considered: the length of the gap, the number of neurite entries, and the number of midline axon crossings (a proxy of axon length). Both CTZ and laser stimulation resulted in greater numbers of neurite entries and midline axon crossings per mm, suggesting greater morphogenesis into and cell-cell engagement across the injury zone (*Figure 7-16*, B).

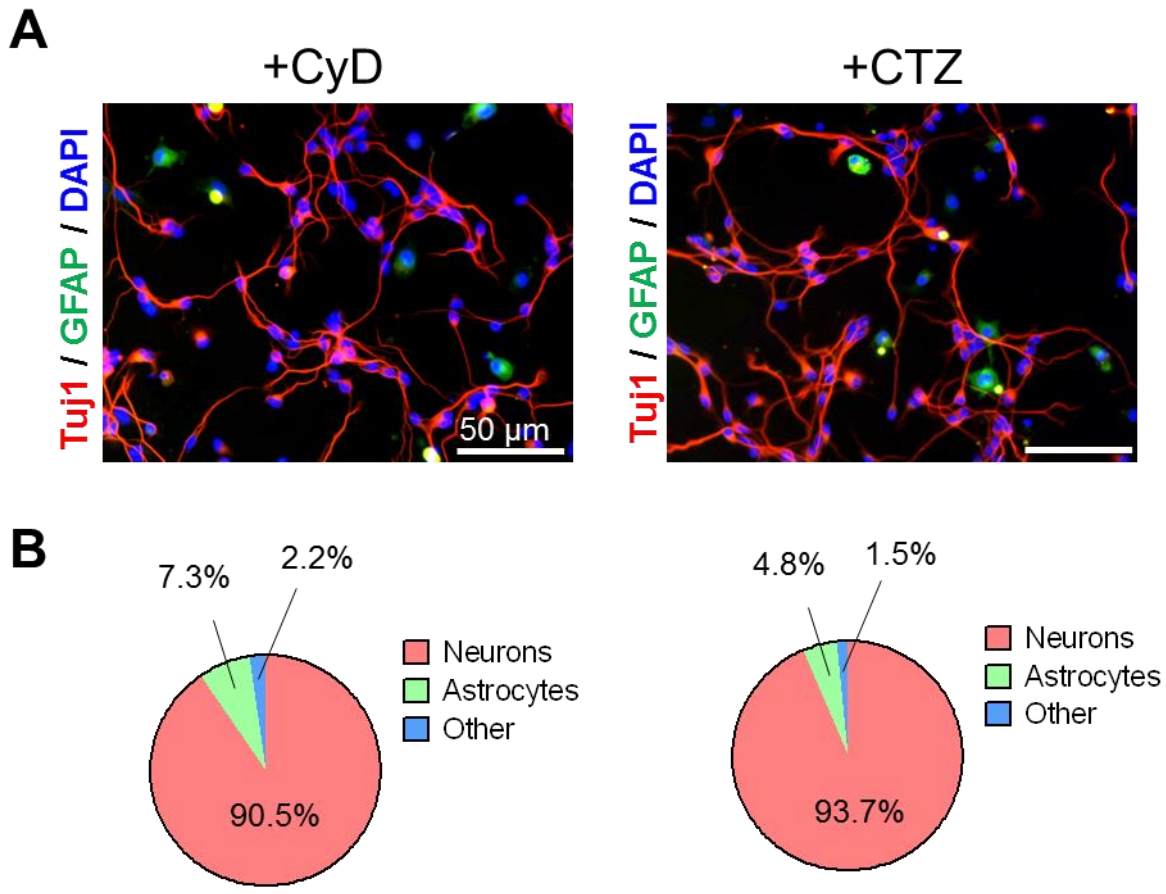

Figure 7-13: CTZ stimulation did not significantly enhance neuronal differentiation after the 4-/4+ protocol.

A. Representative fluorescent images of immunostained LMO3-iPS-neurons at 3DIV following either CyD or CTZ stimulation. **B.** Quantification of Tuj1+/DAPI+ cells (neurons), GFAP+/DAPI+ cells (astrocytes), or just DAPI+ cells (other).

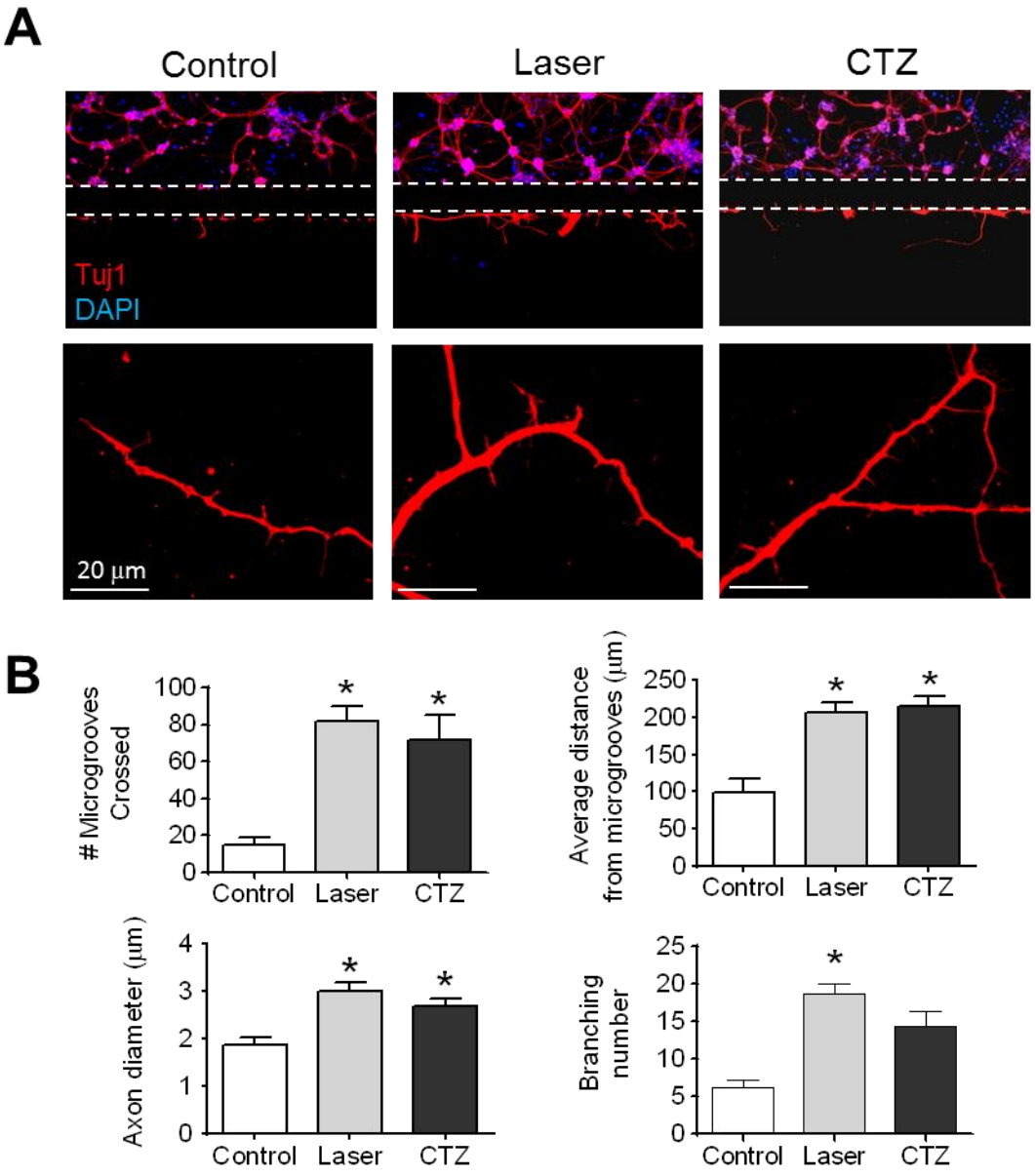

Figure 7-14: Laser stimulation and CTZ stimulation promote axonal outgrowth in the AXIS system.

A-B, LMO3-iPS-NP cells were plated in AXIS axon isolation device after "4-/4+" differentiation. One day after plating, cells in the laser group received blue light (10 Hz, 15 min) daily for 5 consecutive days. Cells in the CTZ group were exposed to CTZ (3 µM, 15 min) daily for 5 days. Cells in control group received medium changes at the same time as the CTZ group. Representative images of the acquired fluorescence images are shown. The dashed lines in lower magnification

images outline the microgrooves in the AXIS device, which separated the cell body and axons. The images with higher magnification show samples of axons in each group (lower panels). **B.** Quantification of number of axon entries into the axon compartment (number of microgroove crossings), average length of axons (distance from microgrooves), axon diameter, and axonal branching number. N = 2 per group.

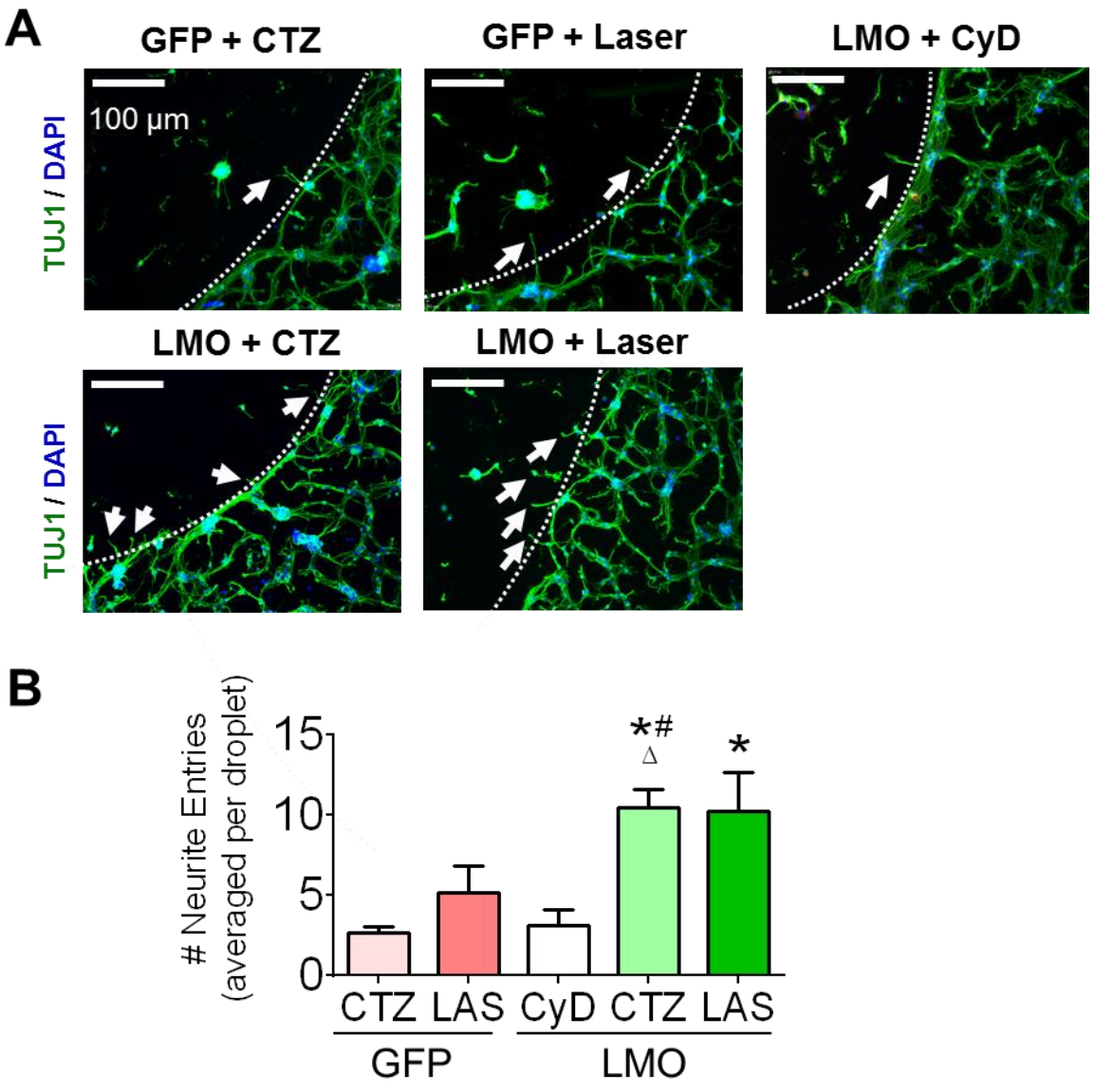

Figure 7-15: Photostimulation promoted neurite extension into CSPG droplet.

A-B. LMO3-iPS-NPCs were seeded onto coverslips containing 4 droplets of CSPG and immunostaining was performed at 5 DIV. **A.** Representative fluorescence images of the neurite penetration (arrows) into the CSPG droplet at the spot boundary (demarcated by the dashed line). **B.** Quantification of the total number of neurite entries around the entire circumference of the CSPG droplet. *: $p < 0.05$, vs. GFP + CTZ; #: $p < 0.05$, vs. GFP + laser (LAS), Δ: $p < 0.05$, vs. LMO + CyD. N = 3 per group.

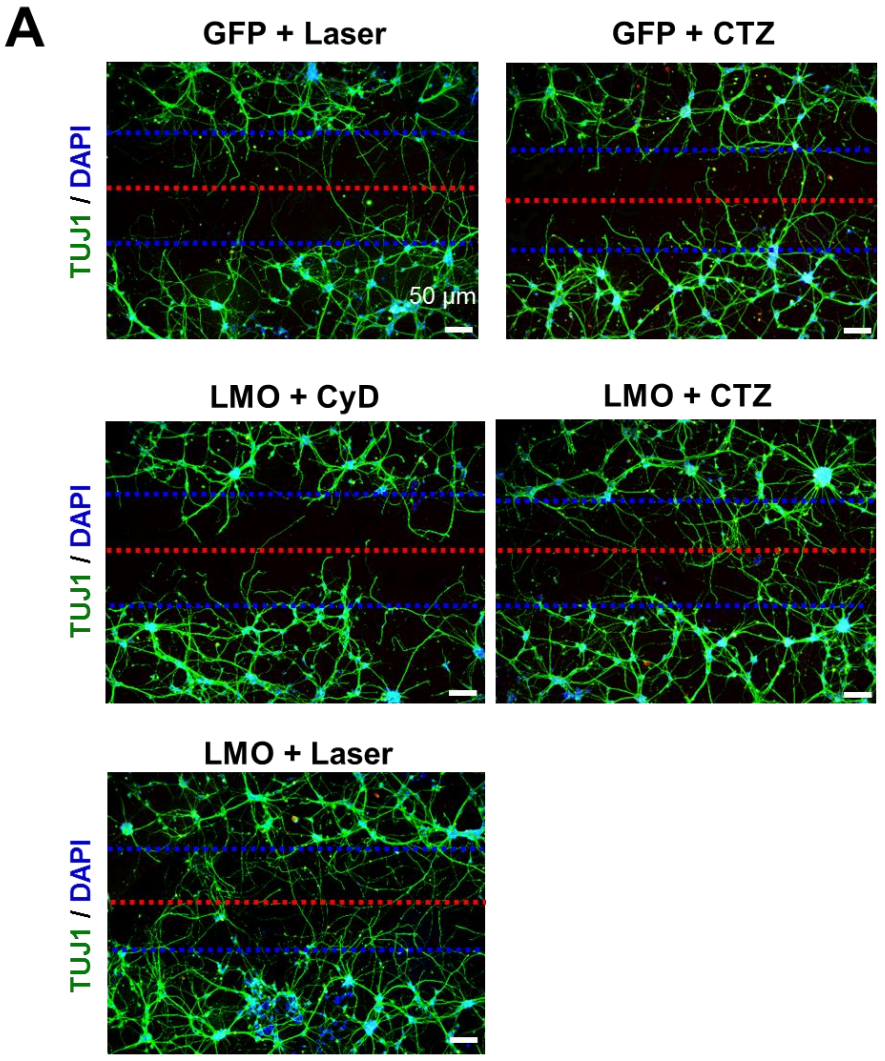
A
GFP + Laser
GFP + CTZ
TUJ1 / DAPI
50 µm
LMO + CyD
LMO + CTZ
LMO + Laser
B
Gap Length (mm)
0.8
0.6
0.4
0.2
0.0
0
1.5
3.5
Days post-scratch
GFP + CTZ
GFP + Laser
LMO + CyD
LMO + CTZ
LMO + Laser
Neurite Entries (/ mm)
300
200
100
0
*#Δ
Midline Axon Crossings (/ mm)
100
75
50
25

Figure 7-16: CTZ and laser stimulation enhanced axon growth into a focal injury zone in vitro.

A-B. The scratch assay was performed on 2DIV neurons, followed by daily stimulation and imaging for 3.5 days (until 5DIV). A. Representative fluorescence images taken after immunostaining for Tuj1 and DAPI of the iPS-neurons at 5DIV. The gap was still evident based on the separation of the DAPI+ cell bodies (delineated by blue dashed lines). The red dashed line demarcates the gap midpoint to assess axonal crossings. **B.** Quantification of the neurite entries (# of neurites that crossed into the gap zones), axonal midline crossings (intersections with the red dashed line), and the length of the gap zone (distance between the blue dashed lines). *: $p < 0.05$, vs. GFP + CTZ; #: $p < 0.05$, vs. GFP + laser (LAS), Δ: $p < 0.05$, vs. LMO + CyD. N = 3 per group per timepoint.

7.3 Discussion

In this chapter, I have established the foundations of the stable LMO3-expressing iPS cell line before proceeding with transplantation studies. Importantly, the characteristics of the LMO3 cell line is highly comparable to those of the control GFP cell line, as demonstrated by the multiple initial immunocytochemistry analyses. Both cell lines are able to maintain expression of the transgene across many passages, as well as across differentiation stages. This was a significant improvement over prior trials of establishing a stable cell line using lentiviral or other plasmid vectors. Furthermore, both cell lines successful differentiate at high rates into neurons, specifically cortical glutamatergic neurons. Interestingly, stimulation did not provide a significant improvement in the differentiation efficiencies, but that may be due in part to the high efficiency of neuronal differentiation even at baseline, which was already over 90%. While the focus of this study was on stimulation to confer beneficial effects, several other standardized protocols that were implemented may have contributed to the high differentiation efficiencies, including rotary

shaking during the 4-/4+ period [152] and hypoxic preconditioning of the iPS-NPCs just prior to dissociation and harvesting [266].

While photostimulation did not produce significant effects on differentiation, probing deeper into the molecular level did yield some insight into the neurophysiological response to stimulation. During the early stages of stimulation, there was a robust upregulation of activity-dependent factors BDNF and NGF. While there are many other neurotrophins, such as glial-derived neurotrophic factor (GDNF), and neurotrophin 3-6 (NT3-6), only BDNF and NGF have been consistently demonstrated to be responsive to neural activity [242]. Another concern is the importance of the window of maturity for which stimulation would confer maximum benefit, or even benefit at all. Multiple studies have demonstrated pro-morphogenic and pro-plasticity effects of stimulation in various cell lines, including regeneration of post-mitotic cells, such as motor neurons [294], retinal ganglion cells [291] and dorsal root ganglion neurons [412, 413]. However, stimulation can also improve neurite outgrowth even in immature differentiating cells, such as NS/NPCs [295]. Thus, even without generation of evoked action potentials and synaptic transmission, stimulation may confer beneficial effects by directly increasing BDNF expression [414] and providing ionic or chemical gradients [415]. The depolarizing effect alone through the electric field may also provide beneficial effects [416].

Optogenetics is a superior option compared to electrical stimulation given its capacity for precision cell-specific stimulation, as well as its direct manipulation of cellular physiology. Because optogenetics involves the direct insertion of ionic channels into the cell membrane, this is similar to the process of neuronal maturation itself, during which Na+ and Ca2+ channels are recruited, transported to the membrane, and activated to allow for ionic influx [417]. These ion channels and the developmental and regenerative processes mediated by ion channels, including

differentiation, axon outgrowth and guidance, and cell migration, can be potentially controlled, or at least facilitated, by optogenetic stimulation [418]. Indeed, optogenetic stimulation of maturing neurons have demonstrated robust neuritogenic effects [372]. Aside from the neurotrophin upregulation, my findings demonstrated that photostimulation by either the conventional laser light source or the new biologically derived CTZ source results in greater markers of synaptogenesis and synaptic strengthening. Also, photostimulation markedly enhances axonal outgrowth, both in the normal neuron culturing conditions, as well as in injury models, such as extension into high CSPG zones and over a scratch injury zone.

In summary, I have created and characterized a novel LMO3-expression stable iPS cell line that is capable of maintaining high levels of transgene expression, even across differentiation stages. I have also demonstrated that photostimulation is able to induce intracellular signaling cascades that leads to upregulation of activity-dependent neurotrophins and downstream enhancement of morphogenesis and plasticity, which can even overcome inhibitory factors. Thus, the photoresponsive NPCs derived from this cell line provide a viable option for transplantation and cell-specific stimulation following TBI.

Chapter 8: Aim 2 – Enhancement of iPS Cell Therapy by CTZ Stimulation After TBI

8.1 Introduction

Stem cells provide a unique regenerative option to treat prevalent intractable neurological disorders such as stroke and traumatic brain injury (TBI). Following transplantation, stem cells provide two major therapeutic benefits: 1) trophic support, and 2) potential for cell replacement. Enhanced trophic support attenuates endogenous cell death and augments endogenous neurovascular repair [145, 235, 375], while cell replacement can in theory restore lost neural circuits, together promoting functional recovery. Indeed, transplantation of stem cells into injured regions promotes neurogenesis and improves functional outcomes for multiple pathologies, including spinal cord injury [374], stroke [180, 257, 373], and TBI [85, 190, 211]. Induced pluripotent stem cells (iPSCs), in particular, are highly viable translational targets, because they can be reprogrammed from autologous host cells, thus minimizing immunogenicity [84, 91, 114]. Transplanted iPS-derived neural progenitor cells (iPS-NPCs) are able to differentiate into functional neurons [201] that are capable of integrating with host circuitry [201, 205, 377, 378, 380]. Under pathological conditions, however, the cell replacement efficacy of transplanted iPS-NPCs remains limited and do not directly improve functional outcomes [205, 380]. Solving the challenge of graft-host functional integration and network repair could be a critical step in moving stem cell therapy forward to clinical translation.

Neural activity is an essential mediator of neuronal survival and differentiation and synapse formation [284]. During development and NPC differentiation, the expression and release of neurotrophins, such as brain-derived neurotrophic factor (BDNF) and nerve growth factor (NGF), are dependent on electrical activity and Ca^{2+}-mediated signaling cascades [242, 297, 299, 419]. These target-derived factors (with the grafted iPS-neurons being the “target”) enhance survival of local neurons, outgrowth of nearby neurites, and establishment/maintenance of synaptic

connections , as well as promote neurite growth across the inhibitory glial scar [292, 411]. Release of target-derived factors are a post-synaptic response due to input stimuli from afferent connections [291]. These connections are lost following a focal injury such as TBI, necessitating the need for an external source of post-synaptic stimulation. Direct electrical stimulation in vitro has already demonstrated beneficial neurophysiological effects, such as enhancement of magnitude and speed of neurite outgrowth and functional maturation in various neural cell types [293, 294], including NPCs [295]. Electrical stimulation in animal models of traumatic injury also resulted in greater plasticity of the injured pathway and enhanced functional recovery [420, 421]. Thus, stimulation of transplanted cells presents a novel, comprehensive approach for promoting network repair by enhancing circuit remodeling, in particular the stabilization and extension of pre-synaptic axons to the post-synaptic iPS-NPC targets.

Conventional modes of stimulation carry translational limitations, including low spatial resolution [311, 312], which can trigger seizure episodes given the hyperexcitable state of damaged neurons following brain injury [214, 215]. Optogenetics is a recently developed tool that utilizes genetic engineering to encode light-sensitive ion channels into a specific subpopulation of cells, allowing for cell-level spatial resolution [325]. However, activation of the opsin is hardware dependent, requiring a power source and/or the intracranial implantation of a light guide, such as a fiber optic cable [313, 358]. Fiber implantation is invasive and heat from the laser can further exacerbate the injury. I propose to develop an iPS cell line expressing a novel fusion protein, luminopsin (LMO), which addresses these challenges. LMOs are comprised of a bioluminescent luciferase protein link to a channelrhodopsin. The luciferase oxidizes its substrate, coelenterazine (CTZ), to produce light photons, allowing for pharmacologically-derived channelrhodopsin activation [366]. CTZ is capable of crossing the blood-brain barrier (BBB) [363], so it can be

administered via an intravenous (IV) route or the intranasal (IN) route, which bypasses the BBB to allow CTZ to enter directly into the brain parenchyma [167]. Both routes of administration would be more translationally feasible than intracranial fiber implantations or chronic skull cementation with dental acrylic. Not only does this novel construct resolve the hardware requirements of optogenetics, it also provides a light source that is closely apposed to the light-responsive opsin (by nature of the fusion protein). This resolves two major limitations of conventional optogenetics: 1) limited tissue penetration of light (few hundred microns) [317], and 2) graft cell migration after transplantation (up to ~1mm), which decreases cell response to a fixed light source [376].

In this chapter, I explore the transplantation and non-invasive optogenetic stimulation of a novel LMO3-expression iPS cell line within a mouse model of TBI, and whether the combination therapy can provide additional therapeutic benefits for endogenous regeneration, plasticity, and functional repair.

8.2 Results

8.2.1 Establishment of improved transplantation technique and evaluation of iPS-neuronal migration after transplantation

Firstly, given the gross morphological changes and tissue deformation following TBI, it was imperative to ensure adequate transplantation and retention of viable iPS-NPCs within the proximity of the injury area. To this end, I evaluated transplantation with the conventional vertical stereotactic injections of iPS-NPCs. However, because of the deformation or loss of the cortical tissue, this resulted in inconsistent and oftentimes excessively deep transplantations of the cell

boluses (*Figure 8-1*). Thus, to rectify this issue, a modified transplantation protocol was implemented using a separated stereotaxic frame to hold the Hamilton syringe, allowing for insertion of the needle into the brain parenchyma at a 30° angle (*Figure 8-2*, A). As a result, the needle could be inserted further into the parenchyma without penetrating too great a depth via the superior-inferior axis (*Figure 8-2*, B). Thus, the cells could be delivered reliably into the superficial areas of the brain, such as the barrel cortex. Two boluses were injected in total at 3 days post-TBI, both anterior to the injury, and one medial and one lateral to the core zone (*Figure 8-3*, A).

Following the transplantation, the locations of the cells were determined by IHC. Through immunostaining of YFP, the iPS-neurons could be visualized after transplantation at various timepoints, including 2d, 3d, and 5d post-transplantation (*Figure 8-3*, B). Interestingly, CTZ stimulation accelerated the migration of the grafted cells towards the margins of the injury, and the shortest distance between the cell bolus and the cerebral surface was significantly reduced at the 3d post-transplantation time point in the CTZ group as compared to the saline vehicle control group (*Figure 8-3*, C). Next, I investigated further into the mechanisms underlying the improved migration associated with stimulation. I carried out a Western blot to examine a key chemokine receptor, the C-X-C chemokine receptor type 4 (CXCR4, *Figure 8-3*, D), which is the cognate receptor for stromal-derived factor 1α (SDF-1α), a chemoattractant that is highly secreted in the injury region by astrocytes and endothelial cells to create a chemical gradient for migrating neuroblasts [75, 422]. Western blot analysis instantiated that CXCR4 expression is upregulated by iPS-NPC transplantation alone, possibly by trophic support, but this upregulation is augmented even further by CTZ stimulation (*Figure 8-3*, E).

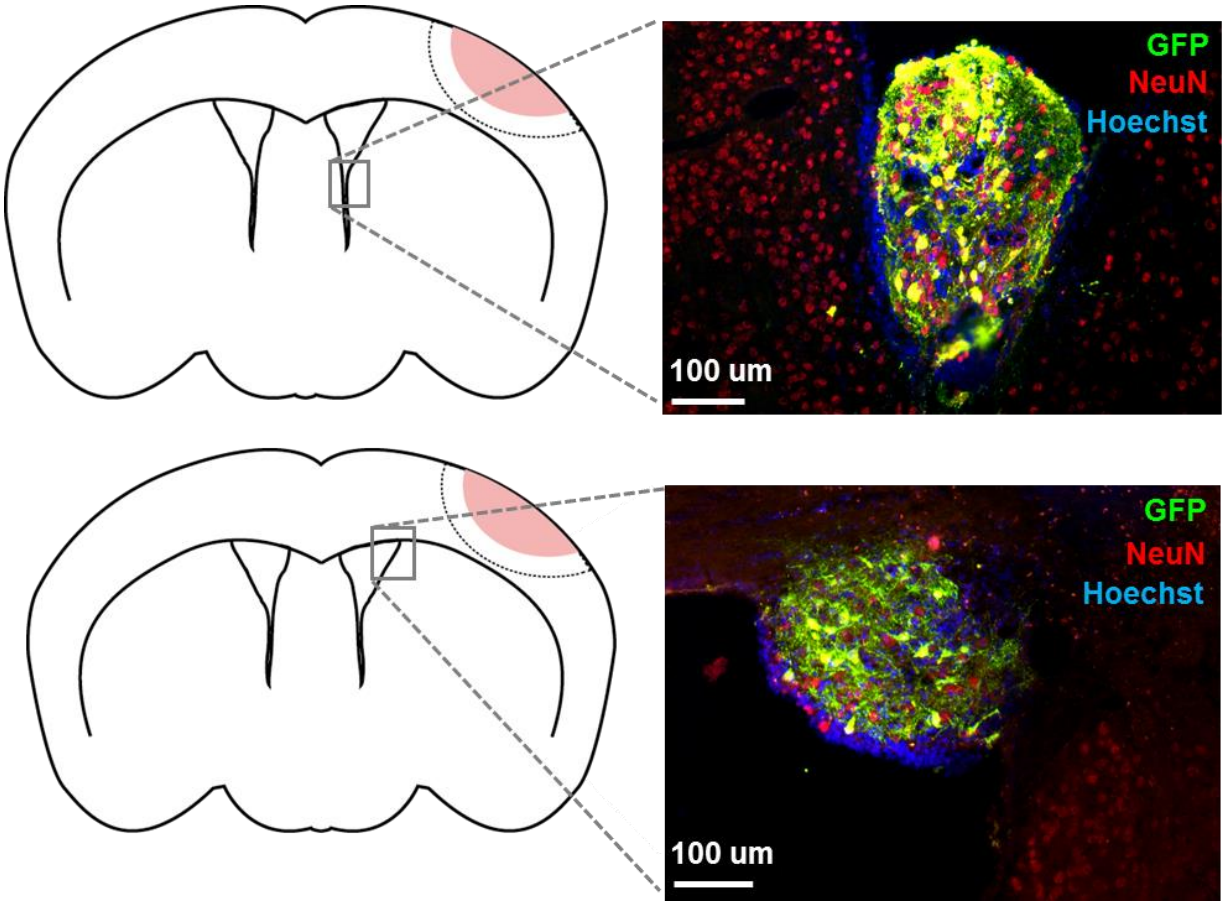

Figure 8-1: Vertical stereotactic injections of iPS-NPCs resulted in inconsistent and off-target injections.

The conventional method of vertical stereotactic injections in which cells were delivered orthogonal to the brain surface resulted in off-target transplantations, such as those in the inferior portions of the lateral ventricles (top panel) and inconsistent delivery (compare top with bottom panels) due to the likelihood of efflux of cells given the loss of cortical tissue.

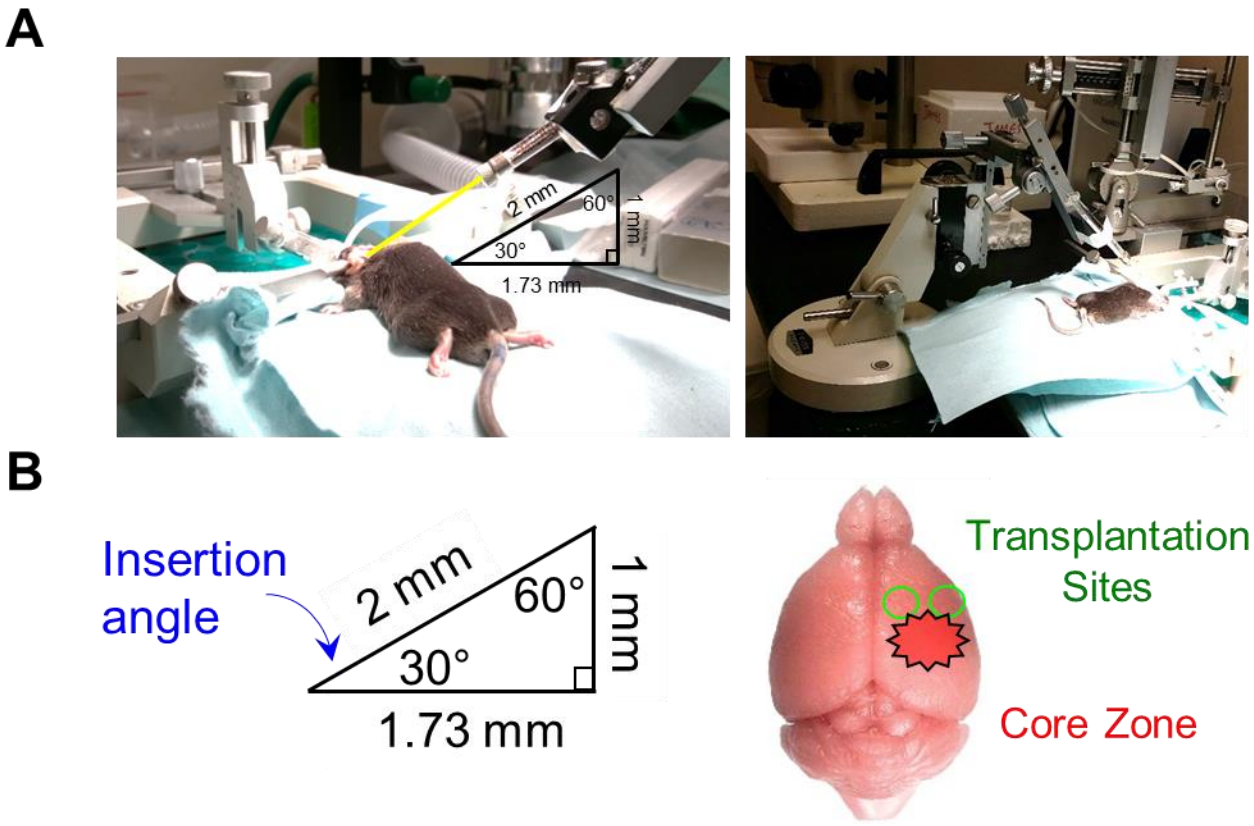

Figure 8-2: Modified inclined transplantation protocol to deliver cells consistently into peri-contusion region.

A. Representative photographic images of the modified transplantation surgery using a disconnected stereotaxic frame for holding the Hamilton syringe. The needle (yellow line) is inserted into the existing craniotomy at a 30° angle and penetrated into the brain a distance of 2 mm, resulting in 1.73 mm anterior to the injection point, and a depth of 1 mm. **B.** Two bolus injections (green circles) are made anterior to the injury core zone (red area).

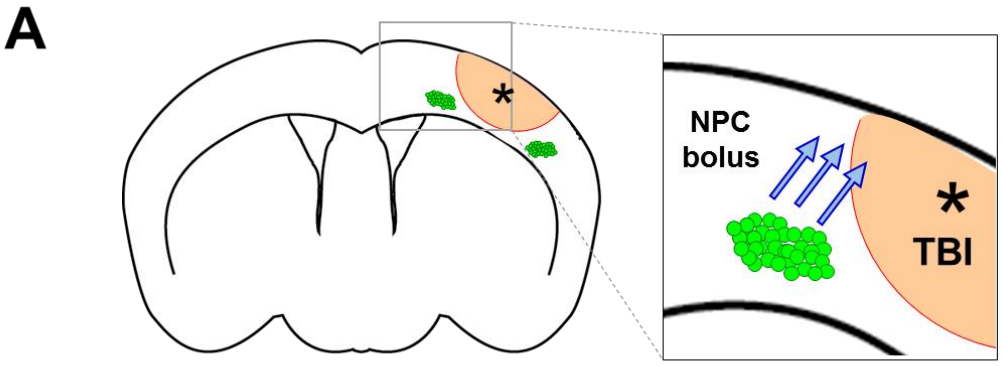
A
NPC
bolus
TBI

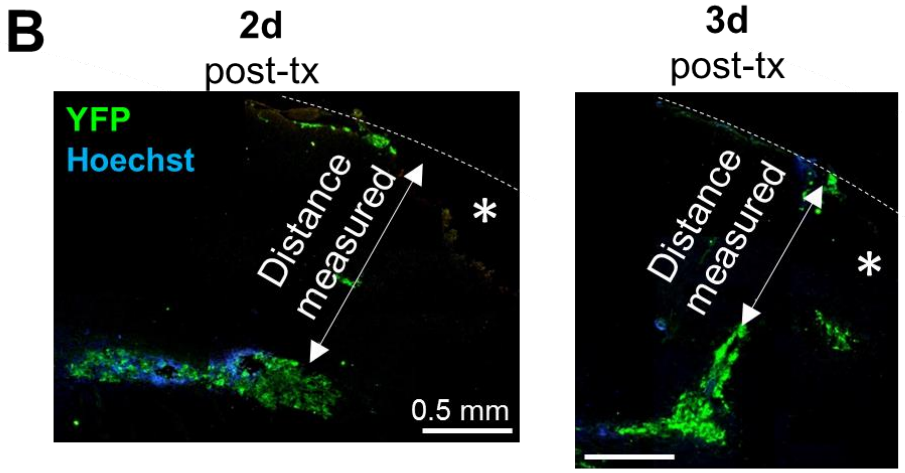
B
2d
post-tx
YFP
Hoechst
Distance
measured
0.5 mm
3d
post-tx
Distance
measured
5d
post-tx

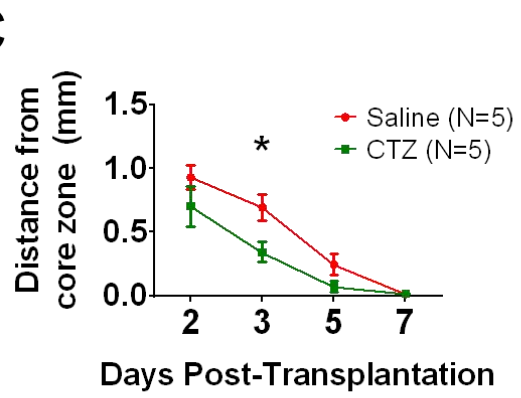
C
Distance from
core zone (mm)
1.5
1.0
0.5
0.0
2
3
5
7
Saline (N=5)
CTZ (N=5)
Days Post-Transplantation

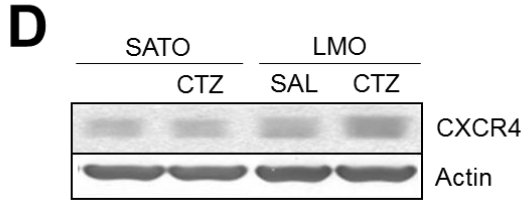
D
SATO
LMO
CTZ
SAL
CTZ
CXCR4
Actin

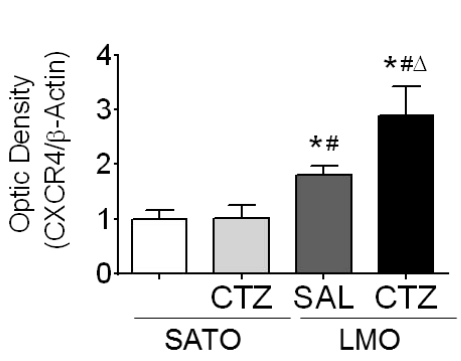
E
Optic Density
(CXCR4/β-Actin)
4
3
2
1
0
CTZ
SAL
CTZ
SATO
LMO

Figure 8-3: CTZ stimulation promotes migration of transplanted iPS-NPCs toward the injury margins.

A. Cartoon depiction of the injection targets relative to the injury region (red zone). 2 boluses of Hoechst-prelabeled iPS-NPCs were injected anterior and either lateral or medial to the core zone, within the peri-contusion region, at a depth of ~1 mm. Due to chemoattractant gradients, the cells gradually migrated towards the boundaries of the injury core (blue arrows = migration path). The shortest distance between the bolus of cells and the surface of the brain was measured. **B.** Representative fluorescent images of brain sections from CTZ stimulated animal at varying timepoints, including 2d, 3d, and 5d post-transplantation (post-tx). Note wash out of Hoechst due to staining procedures. **C.** Quantification of the measured distance for saline-treated and CTZ-treated groups. *: $p < 0.05$, vs. Saline. N = 5 per group. **D.** Representative Western blots for expression of CXCR4. **E.** Quantification of densitometry analysis of Western blots. *: $p < 0.05$, vs. SATO; #: $p < 0.05$, vs. SATO + CTZ; Δ: $p < 0.05$, vs. LMO + Saline (SAL). N = 6 for all groups.

8.2.2 Aim 2.1 –Validate cell viability and differentiation and LMO3 function after transplantation of LMO-expressing iPS-NPCs in a mouse barrel cortex TBI model

After establishing a reliable transplantation paradigm and verifying the correct location of the grafted cells, I next investigated the effects that CTZ stimulation had on grafted cell death. This was also important to ensure that stimulation did not exacerbate grafted cell death, given the excitotoxic effects of excess activity, as well as the potential secondary effects of TBI. To this end, a TUNEL immunostaining assay was carried out, multiplexed with YFP staining to label grafted cells (*Figure 8-4*, A). The fluorescence images demonstrated that CTZ stimulation had no effect on total cell death, including that of the iPS-neurons. Interestingly, very little cell death was observed in both groups (1-2% during the subacute stages; *Figure 8-4*, B) , reaching a ceiling effect

similar to that of the neuronal differentiation efficiency, possibly due to the combination of rotary shaking during differentiation and hypoxic preconditioning.

Next, I evaluated the differentiation of the transplanted LMO3-iPS-NPCs into the peri-contusion region. At 7d post-transplantation, sections from the grafted region was immunostained for YFP and NeuN, and dense clusters of YFP+/NeuN+ cells were observed at the margins of the injury (*Figure 8-5,* A), suggesting that the grafted iPS cells were able to differentiate into mature neurons. Colocalization of the the YFP and NeuN signals were confirmed by z-stack images with confocal microscopy (*Figure 8-5*, B).

Finally, as part of the first aim, it was necessary to ensure the function of the LMO3 protein in the transplanted cells in vivo and to validate the intranasal delivery of CTZ (*Figure 8-6,* A). To this end, bioluminescence imaging using the chemiluminescence reader was performed in mice at 14d post-transplantation. The mouse was given intranasal CTZ (2 mg/kg), followed by an incision to expose the skull. Then, the mouse was placed into the chemiluminescence reader for an hr, with images acquired every min with 1 min exposure time (*Figure 8-6*, B). Given the period of waiting during intranasal administration, the animal was placed into the reader 5 min after the initial injection (starting timepoint = 5 min), by which point the bioluminescence emission had already peaked and slowly declined over the course of an hr until it reached ~60% of the peak emission (*Figure 8-6,* C).

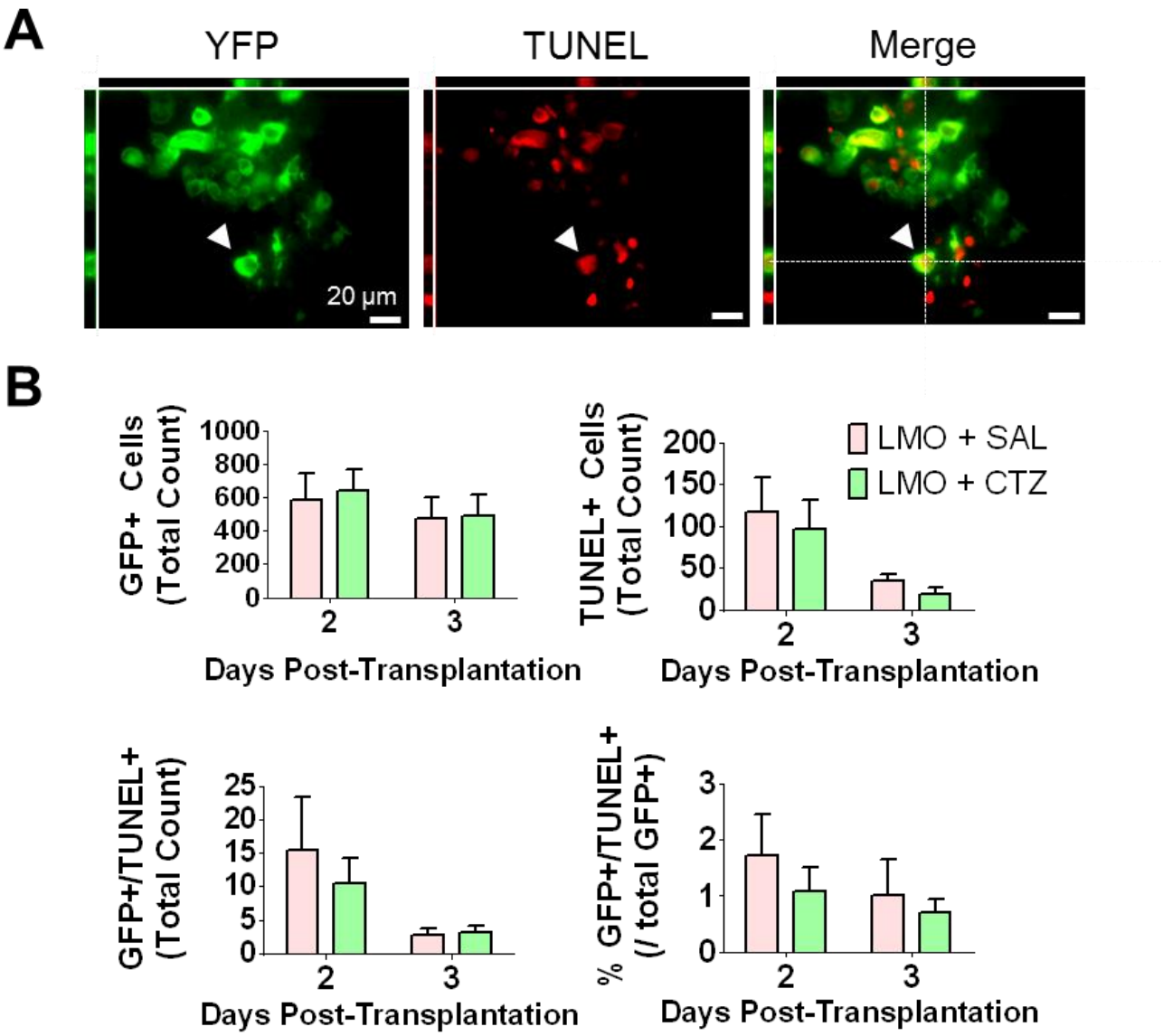

Figure 8-4: CTZ stimulation did not reduce or exacerbate graft cell death after transplantation.

A-B. LMO3-iPS-NPCs were transplanted as 2 boluses into the peri-contusion region and animals were sacrificed at 2 and 3 days post-transplantation for TUNEL immunohistochemistry. **A.** Representative pseudo-confocal images of the YFP+ graft cells costained with TUNEL, with the z-stack image to confirm colocalization (arrow). **B.** Quantification of the following total cell counts within a single section: GFP+ cells, TUNEL+ cells, GFP+/TUNEL+ colabeled cells, and the ratio of GFP+/TUNEL+ cells to total GFP+ cells. N = 4 per group per timepoint.

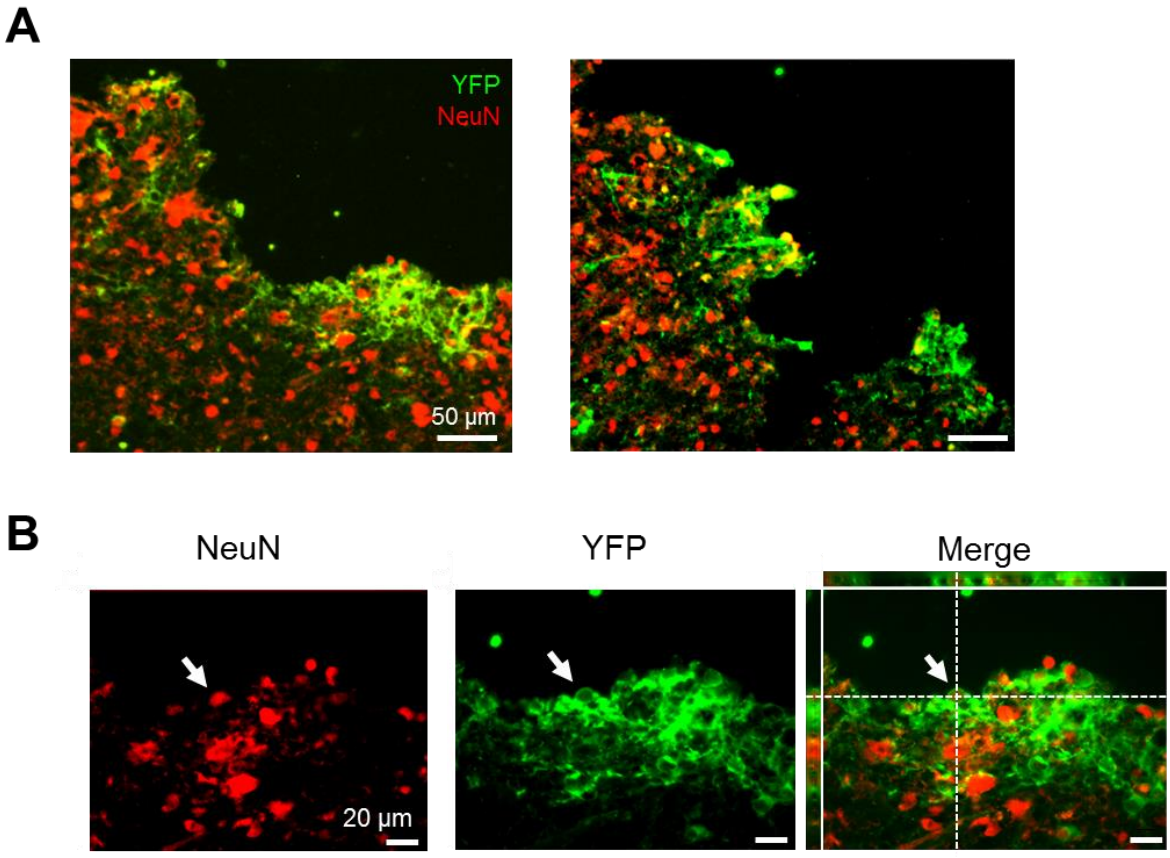

Figure 8-5: Transplanted LMO3-iPS-NPCs differentiate into mature neurons.

A. Representative immunohistochemical images of transplanted LMO3-iPS-neurons at 7 days post-transplantation to demonstrate colocalization of NeuNand YFP, suggesting full differentiation of the iPS-NPCs into mature neurons. **B.** Colocalization of NeuN(red) and YFP (green) was confirmed by confocal microscopy with z-stack images.

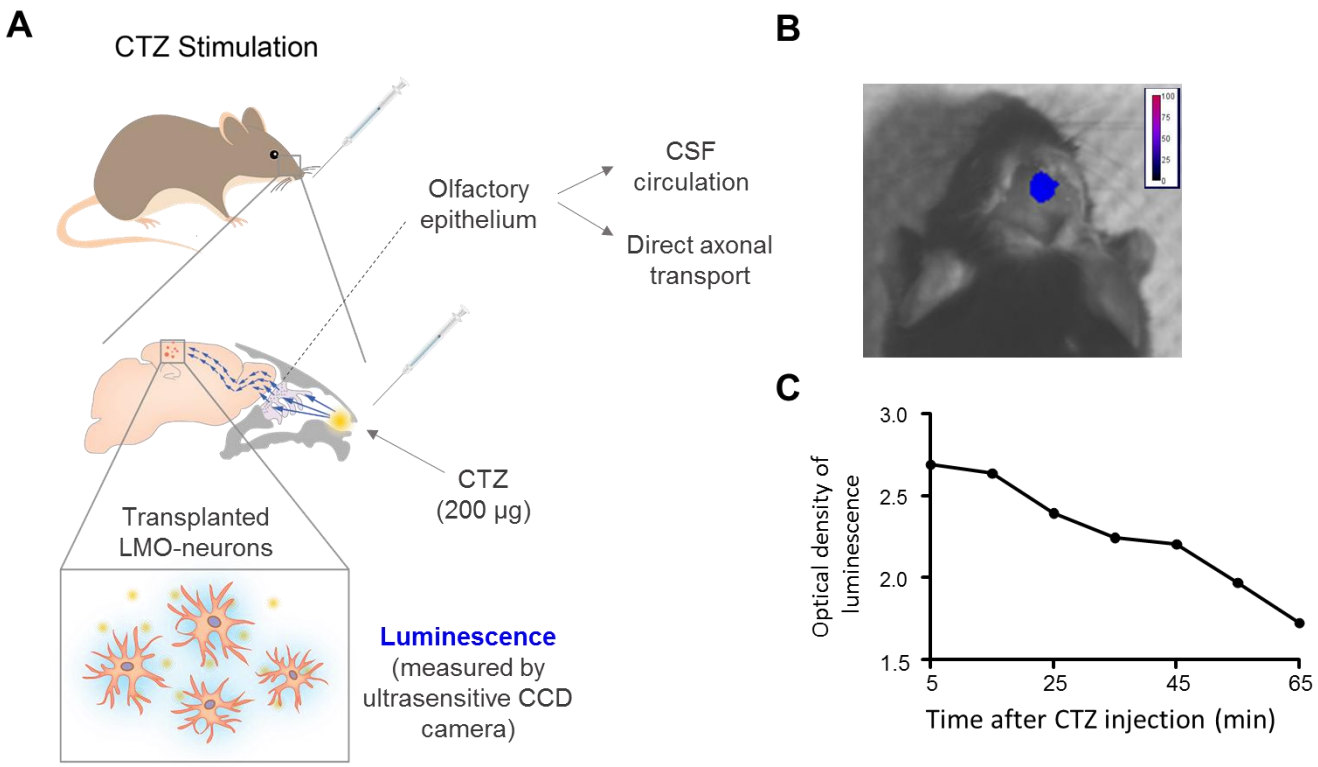

Figure 8-6: Validation of intranasal administration of CTZ in mouse model after brain injury.

A. Cartoon depiction of the intranasal pathway through which CTZ enters into the CNS. After CTZ is inhaled through the nostrils, it then crosses the BBB by absorption through the porous olfactory epithelium. Afterwards, it either enters the CSF circulation through the perineural spaces or gets directly taken up and transported through the axons of cranial nerves. Once CTZ reaches CSF circulation, it can reach more distal sites, such as the region containing the transplanted cells. **B**. Intranasal of administration of CTZ (2 mg/kg) induced bioluminescence in the cell grafted area. **C.** Quantification of the intensity of luminescence for 60 min of the individual animal. The intensity of luminescence verified that the CTZ-induced luminescence persisted for approximately one hour until it reached 10% of peak emission intensity in the post-injury brain.

8.2.3 Aim 2.2. – Assess effectiveness of CTZ stimulation for upregulating activity-dependent neurotrophin release and enhancing endogenous plasticity and neurovascular repair

Cell therapy and early intranasal CTZ administration activated neurotrophin expression

I next investigated the physiological responses of both grafted and host cells to intranasal CTZ-derived photostimulation. Western blot analyses using tissue lysates from the transplantation region were performed at two different timepoints after transplantation, 3d (acute) and 7d (chronic). The animals were stimulated with either daily CTZ (2 mg/kg, IN) or normal saline vehicle control until the date of sacrifice, on which they were sacrificed 30 min following the intranasal injections. At 3d post-transplantation, there was significant upregulation of BDNF and NGF in the CTZ stimulated groups, as compared to the SATO, SATO + CTZ, and LMO + Saline controls (*Figure 8-7*, A-B). Transplantation of LMO cells with saline control also increased BDNF levels, which corroborates the trophic support provided by stem cell therapy (*Figure 8-7*, B). Furthermore, transplantation of LMO cells increased levels of growth-associated protein 43 (GAP43), which is a marker of axonal extension and synaptic reorganization (*Figure 8-7*, B). CTZ stimulation augmented this effect even further than that of cell therapy alone.

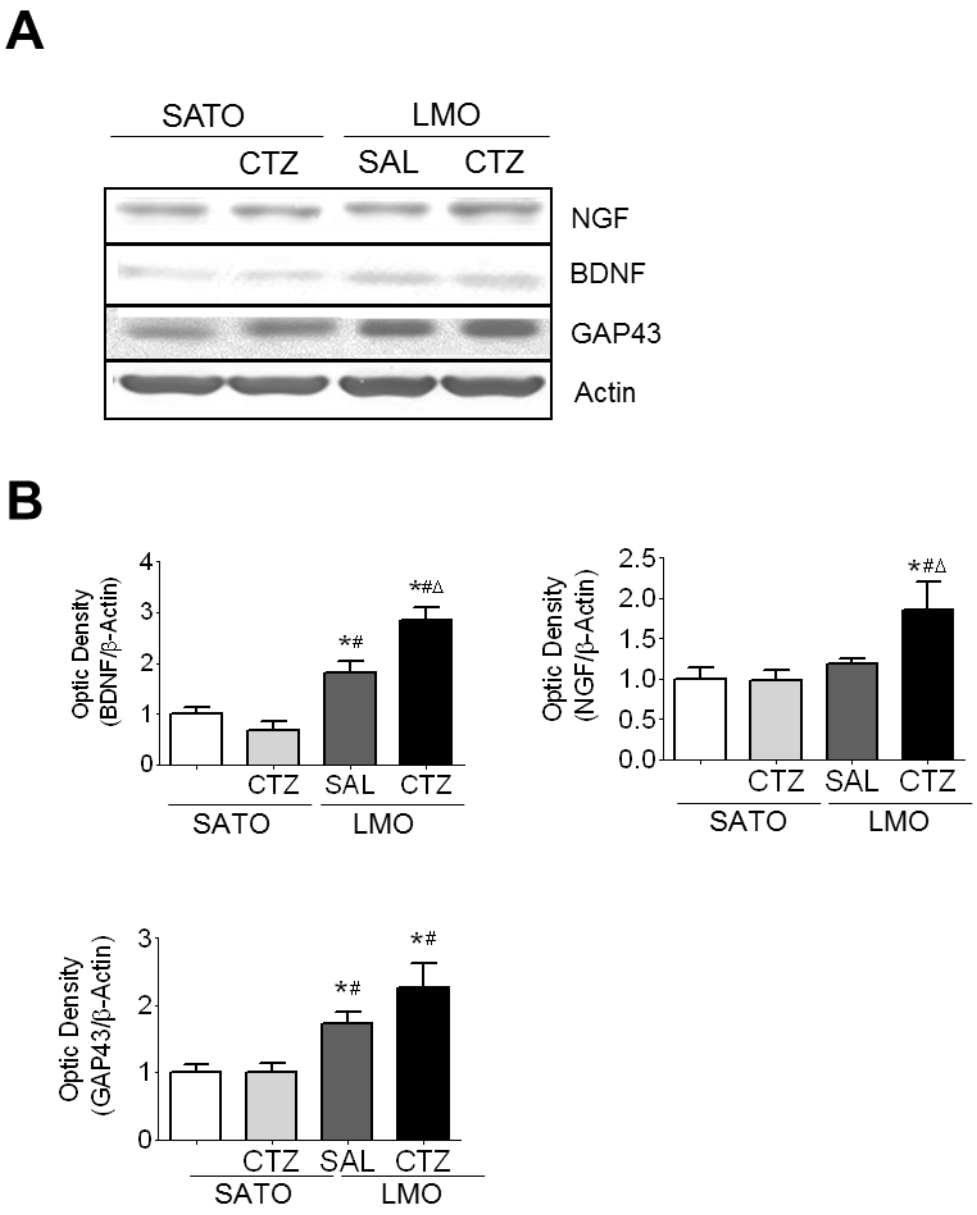

Figure 8-7: CTZ stimulation upregulated activity-dependent neurotrophins and enhanced axonal outgrowth.

A-B. Tissue lysate for Western blot analysis was collected from the transplantation region at 3d post-transplantation 30 min following a round of CTZ stimulation. **A.** Representative bands from the Western blot probing for NGF, BDNF, and GAP43. **B.** Densitometry quantification of the Western blots. *: $p < 0.05$, vs. TBI + SATO; #: $p < 0.05$, vs. TBI + SATO + CTZ; Δ: $p < 0.05$, vs. TBI + LMO + SAL. N = 6 for all groups.

Transplantation of iPS-NPCs and longterm CTZ administration promoted neuronal plasticity and remodeling

Additional markers were probed at 7d post-transplantation, including the cognate receptors for BDNF and NGF, TrkB and TrkA, respectively, and synaptic proteins, all of which respond to extended neural activity and plasticity. Western blot demonstrated that CTZ stimulation upregulated TrkB and TrkA, while LMO + saline only upregulated TrkA, as compared to controls (*Figure 8-8*, A-B). Furthermore, cell therapy significantly elevated levels of synaptic markers, synaptophysin and PSD95, and CTZ stimulation was able to further augment the increase in synaptophysin (*Figure 8-8*, A-B).

To confirm the Western blot data, IHC was carried out at 21d post-transplantation following a 7d stimulation paradigm to investigate the axonal reorganization after TBI. Brain sections around the transplanted region were immunostained for myelin basic protein (MBP), which labels axons, and NeuN. Through the fluorescence images, one of the most notable features was the reorganization of the axons, in particular the parallelism or conformity of the projections. In the TBI + SATO control group, there appeared to be a high degree of discordance in the axonal projections, resulting in high variance when the relative angles (0° = horizontal) were measured (*Figure 8-9*, A). Transplantation of LMO cells resulted in improved conformity amongst the projections (equivalent of decreased angle variance), and CTZ was able to augment this effect even further (*Figure 8-9*, B). While not quantified, it also appeared there was greater quantities and densities of axonogenesis and axonal tract formation in the LMO groups as well (*Figure 8-9*, A).

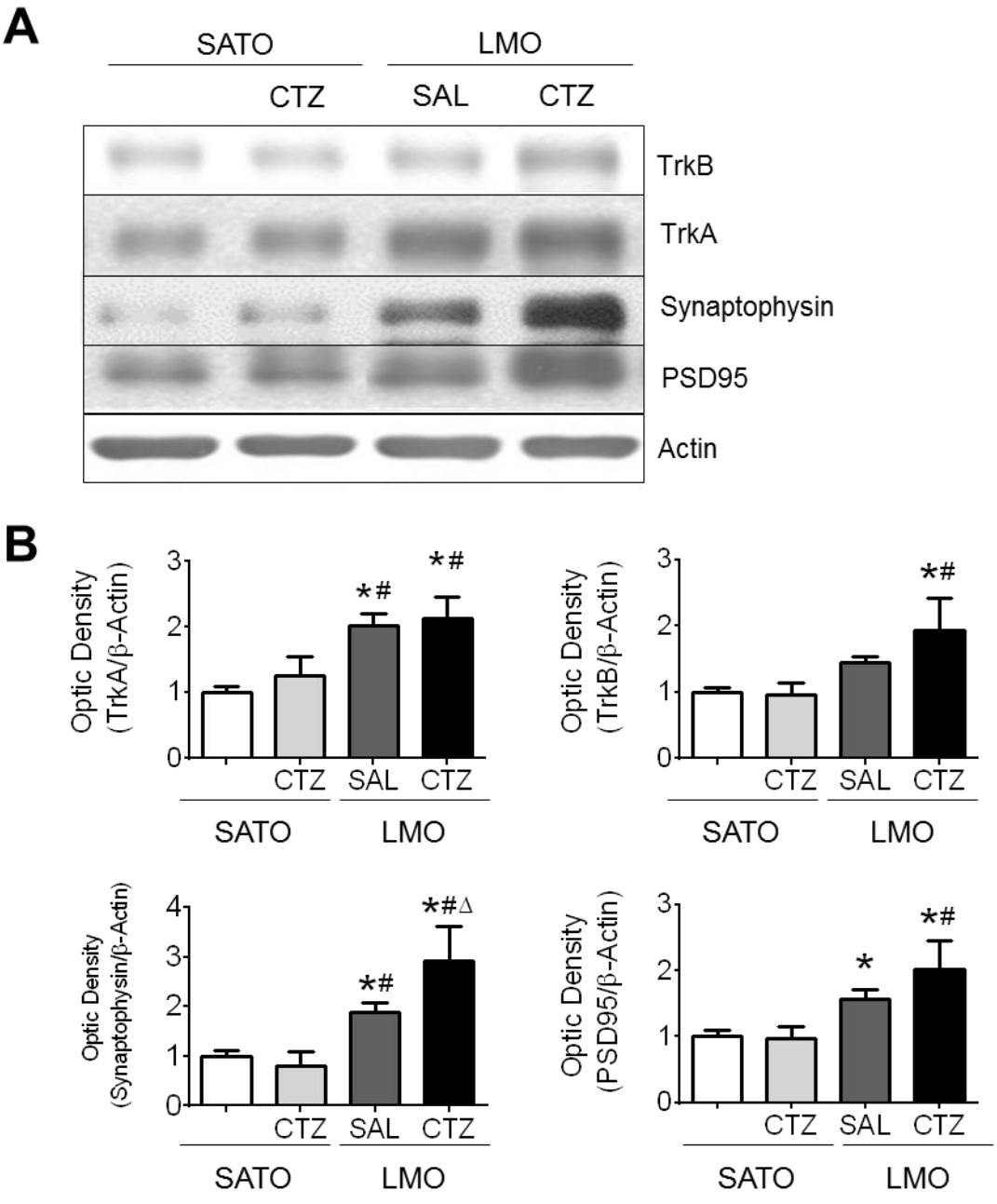

Figure 8-8: Longterm CTZ stimulation resulted in upregulation of neurotrophin receptors and synaptic plasticity.

A-B. Tissue lysate for Western blot analysis was collected from the transplantation region at 7d post-transplantation 30 min following a round of CTZ stimulation. **A.** Representative bands from the Western blot probing for TrkB, TrkA, synaptophysin, and PSD95. **B.** Densitometry quantification of the Western blots. *: $p < 0.05$, vs. TBI + SATO; #: $p < 0.05$, vs. TBI + SATO + CTZ; Δ: $p < 0.05$, vs. TBI + LMO + SAL. N = 6 for all groups.

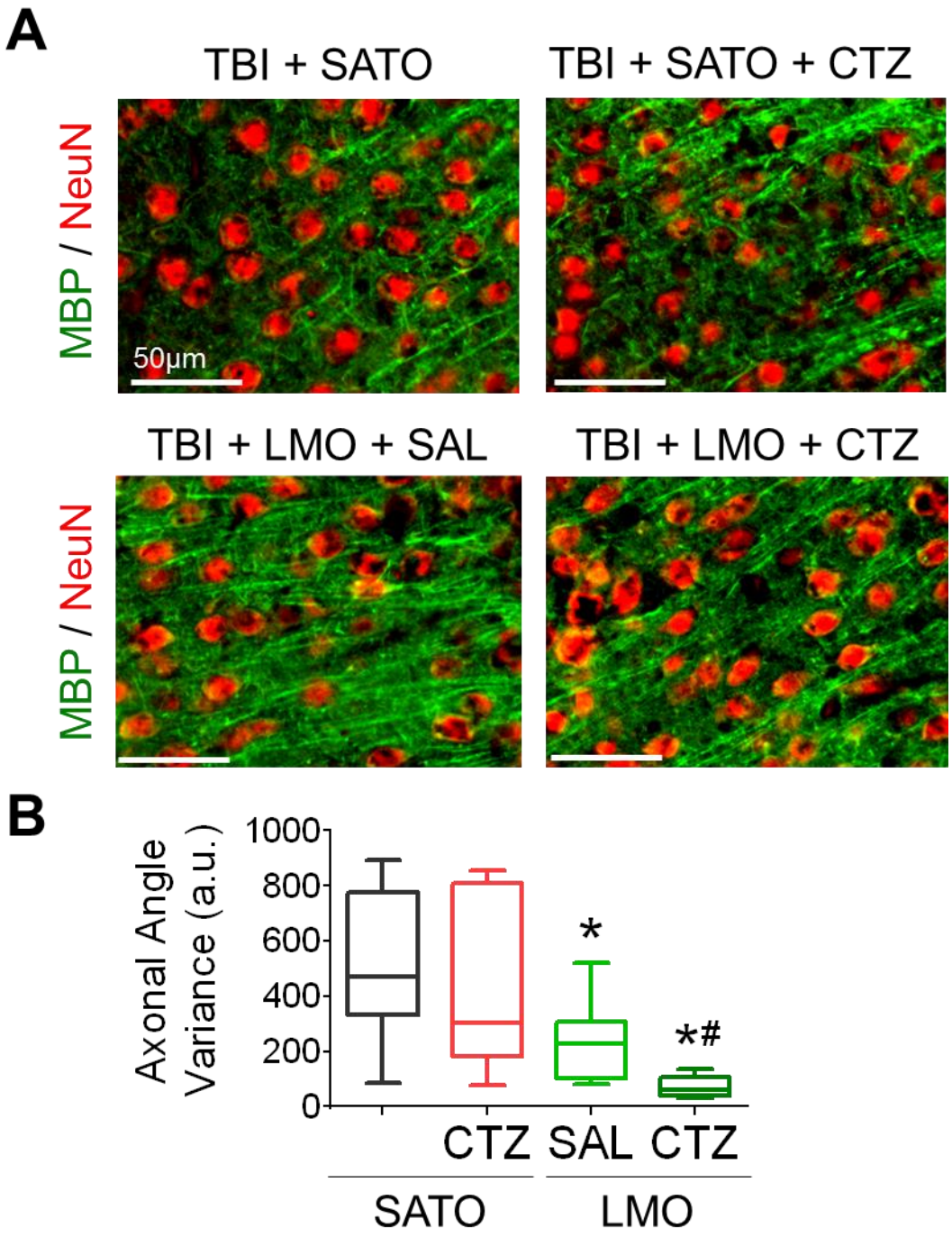

Figure 8-9: Cell therapy and CTZ stimulation demonstrated a synergistic effect in promoting axonal reorganization after TBI.

A. Representative immunostained images of the area around the transplantation region demonstrating features of axonal projections towards the injury zone. The relative angles of 10

axons were measured for each 40x image. **B.** Quantification of the angular variances for each of the groups. *: $p < 0.05$, vs. TBI + SATO; #: $p < 0.05$, vs. TBI + SATO + CTZ. N = 10 for SATO groups, 9 for LMO groups.

Cell therapy and CTZ stimulation promotes angiogenesis and restoration of blood flow after injury

Endogenous neurovascular regeneration was assessed by IHC at 14d post-transplantation. Sections from the anterior peri-contusion region was immunostained for NeuN, BrdU (5-bromo-2'-deoxyuridine), which labels proliferating cells treated with BrdU, and glutamate transporter 1 (GLUT1), which labels endothelial cells (*Figure 8-10*, A). Colocalization of NeuN/BrdU represents newly generated neurons, and NeuN/GLUT1 represents newly generated blood vessels (*Figure 8-10*, B). Quantification of the IHC instantiated that iPS-NPC transplantation enhanced the number of proliferating cells (BrdU+), in particular the number of newly divided endothelial cells (*Figure 8-10*, C). CTZ stimulation of the transplanted cells augmented both the endogenous proliferation and angiogenesis even further (*Figure 8-10*, C).

Given the increased angiogenesis, it was important to ensure that the neovascularization correlated with functional blood vessels. To this end, I performed laser Doppler imaging to evaluate the local cerebral blood flow (LCBF) around the anterior peri-contusion region, the region of interest (ROI) that demonstrated robust angiogenesis. The cerebral blood flow was measured at baseline (on the ipsilateral side), as well as in the ipsilesional and contralesional side of all animals at 14d post-transplantation following the described 7d stimulation paradigm (*Figure 8-11*, A). I observed there was an increasing trend for iPS-NPC transplantation to restore LCBF within the ROI (*Figure 8-11*, B). However, CTZ stimulation augmented this effect such that there was a

significant increase in LCBF in the LMO + CTZ group as compared to the SATO group (*Figure 8-11*, B).

Finally, I investigated the mechanisms underlying the enhanced angiogenesis on a molecular level by carrying out a Western blot for a key angiogenic factor, vascular endothelial growth factor (VEGF), which is upregulated in hypoxic states. Using tissue lysates collected from the anterior peri-contusion region at 7d post-transplantation, the Western blot demonstrated that cell therapy alone was able to significantly promote the expression of VEGF, and there was no further enhancement from cell therapy (*Figure 8-12*). Thus, the augmented neovascularization and LCBF observed from CTZ stimulation may have stemmed from another biomolecular mechanism, such as increased neural activity, which is directly coupled to angiogenesis as part of the neurovascular unit [20].

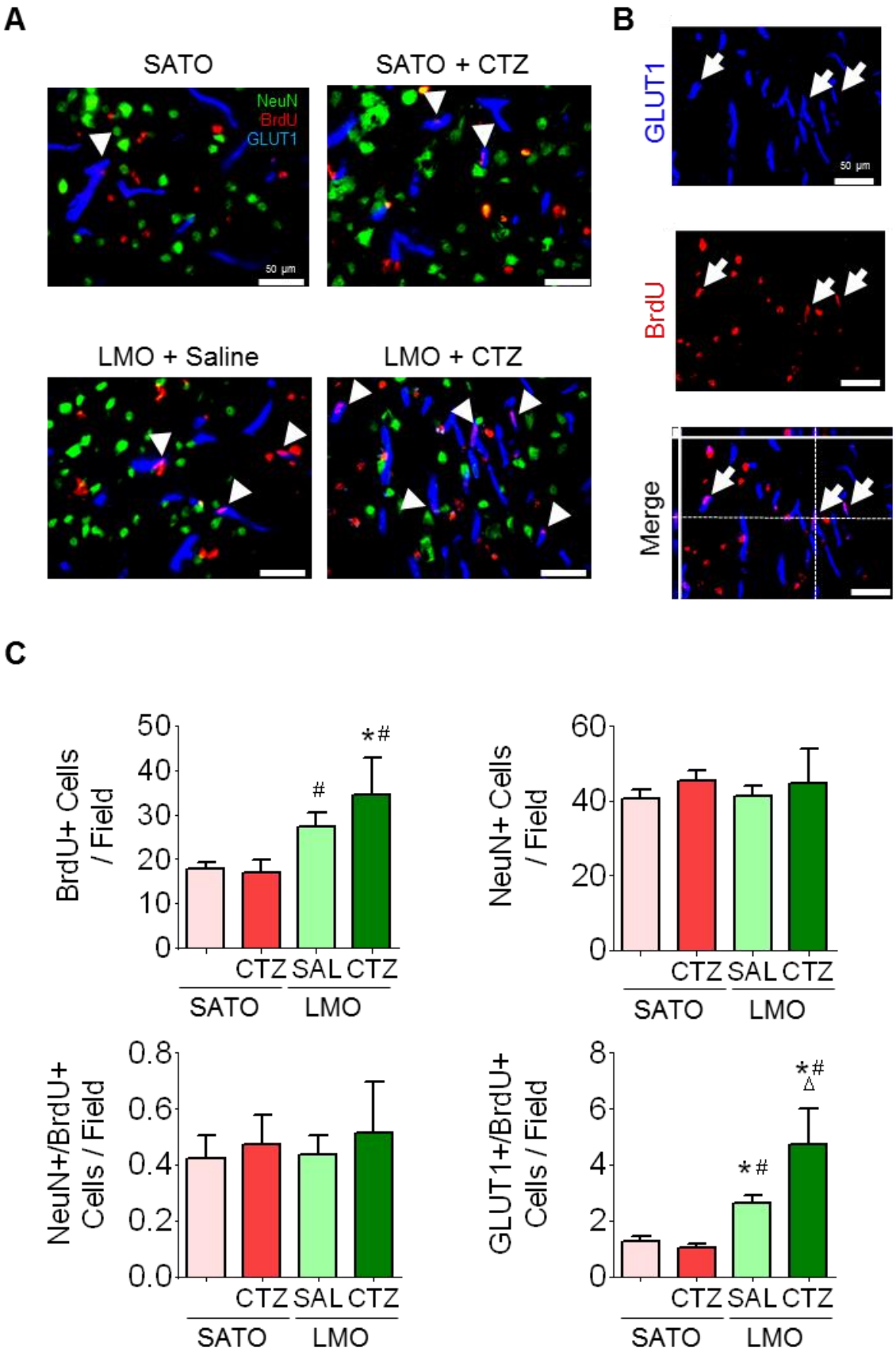
A
SATO
SATO + CTZ
NeuN
BrdU
GLUT1
50 μm
LMO + Saline
LMO + CTZ
B
GLUT1
BrdU
Merge
50 μm
C
BrdU+ Cells / Field
NeuN+ Cells / Field
NeuN+/BrdU+ Cells / Field
GLUT1+/BrdU+ Cells / Field
CTZ
SAL
CTZ
SATO
LMO

Figure 8-10: CTZ stimulation augmented angiogenesis, but not neurogenesis, in the peri-contusion zone.

A. Representative images of IHC carried out on brain sections from the peri-contusion region at 14d post-transplantation. **B.** Z-stack images from confocal microscopy to confirm GLUT1 (blue) and BrdU (red) colocalization. **C.** Quantification of the average number the following types of cells in each 40x field: BrdU+, NeuN+, NeuN+/BrdU+, GLUT1+/BrdU+. *: $p < 0.05$, vs. TBI + Sato; #: $p < 0.05$, vs. TBI + Sato + CTZ; Δ: $p < 0.05$, vs. TBI + LMO + SAL. N = 9 for SATO and LMO + SAL groups, 8 for SATO + CTZ group, and 10 for LMO + CTZ group.

A

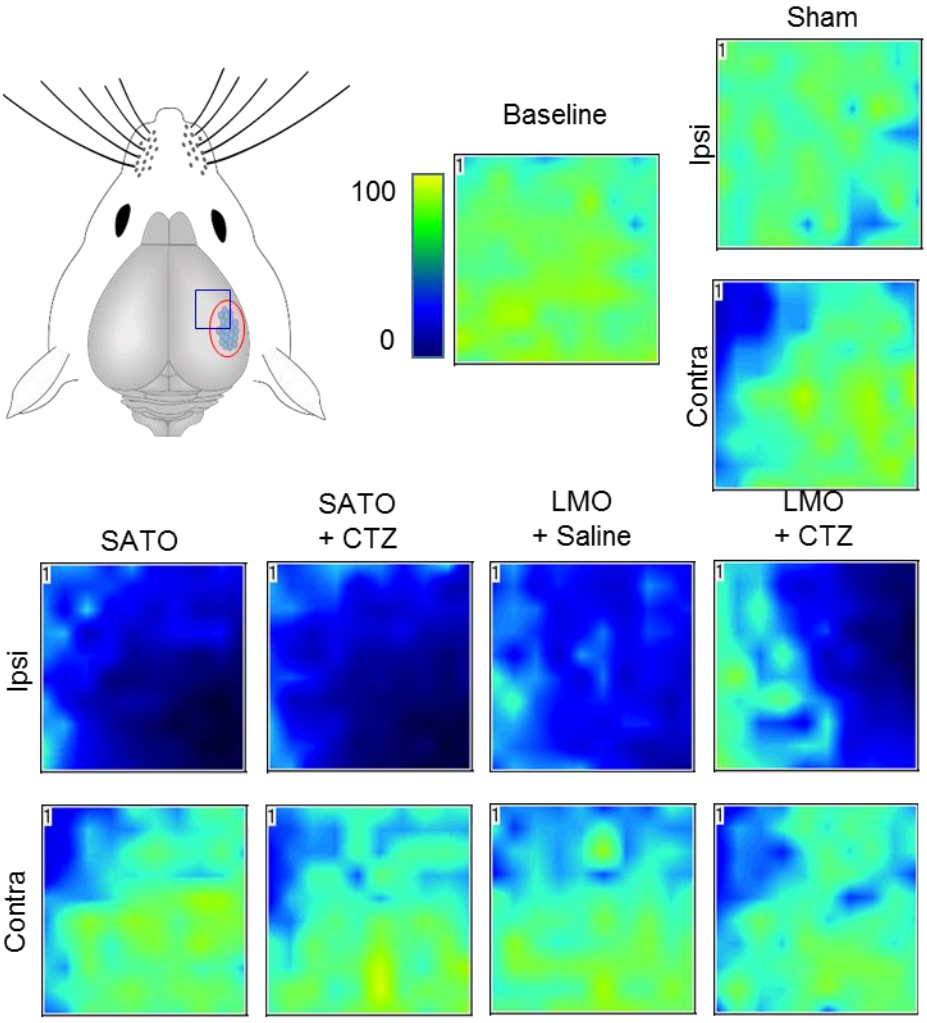
Sham
Baseline
100
0
Ipsi
Contra
SATO
SATO
+ CTZ
LMO
+ Saline
LMO
+ CTZ
Ipsi
Contra

B

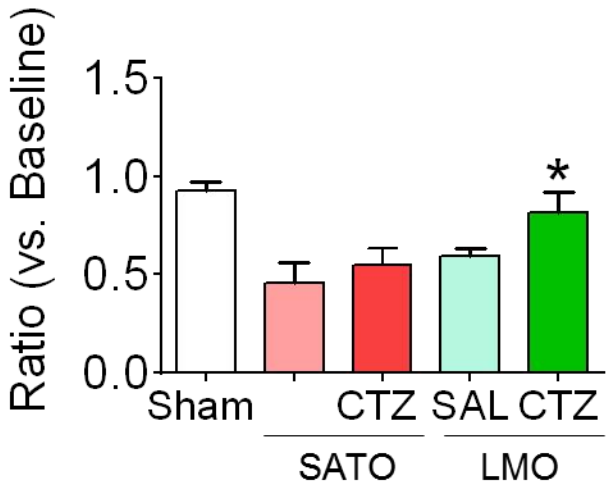
Ratio (vs. Baseline)
1.5
1.0
0.5
0.0
*
Sham
CTZ
SAL
CTZ
SATO
LMO

Figure 8-11: Enhanced angiogenesis correlated with greater restoration of blood flow within the anterior peri-contusion region.

A-B. Laser Doppler imaging was carried out to evaluate blood flow reduction and recovery. **A.** Representative images of the blood flow at baseline (prior to injury), as well as the ipsilesional and contralesional images acquired at 14d post-transplantation. The bottom panel depicts the region of interest (ROI) for all image acquisition, which was the anterior medial peri-contusion region (blue box; red circle = core zone). **B.** Quantification of mean blood flow within the ROI, as normalized to baseline. *: $p < 0.05$, vs. TBI + SATO. N = 5 per group.

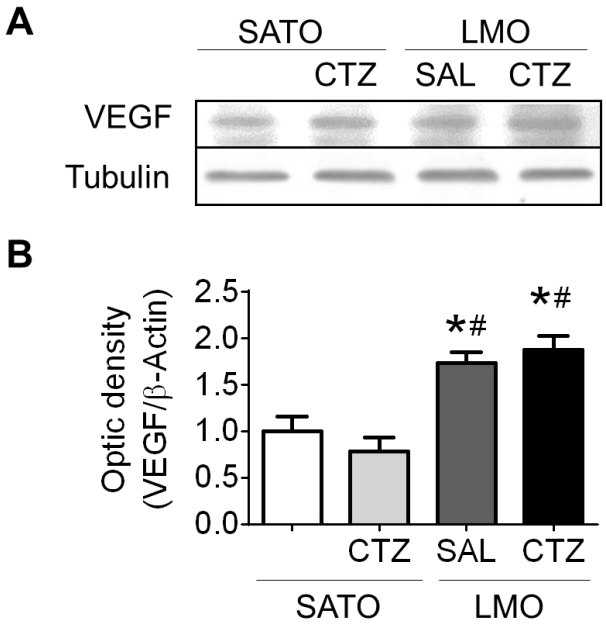

Figure 8-12: Transplantation of iPS-NPCs upregulated VEGF expression in the peri-contusion zone.

A-B. Western blot analysis was performed on tissue lysates from the peri-contusion zone at 7d post-transplantation. **A.** Representative immunoblot images after probing for VEGF. **B.** Quantification of blot densitometry for all the groups. *: $p < 0.05$, vs. TBI + SATO; #: $p < 0.05$, vs. TBI + SATO + CTZ. N = 4 for all groups.

8.2.4 Aim 2.3 – Compare functional recovery of TBI animals treated with combination therapy of iPS-NPC transplantation and CTZ stimulation vs. iPS-NPC transplantation alone

The ultimate goal of translational medicine is to repair the damaged organ and improve functional outcomes. For the first metric, I carried out Nissl staining for brain sections (15 µm thick) that spanned the entire contusion area. ImageJ was used to quantify the injury area, as well as the ratio of hemispheric tissue loss (vs. the contralesional side, in order to account for edema formation), followed by Cavalieri method of summation to convert the measurements into a total volume (*Figure 8-13*, A). Transplantation of iPS-NPCs provided a robust neuroprotective effect and decreased both the contusion volumes and hemispheric ratio loss, while CTZ stimulation bolstered this effect even greater (*Figure 8-13*, B).

Behavior testing was also carried at timepoints prior to sacrifice, including pre-injury (0d, baseline), and at 7d, 14d, and 21d for corner testing, or 14d and 21d for adhesive removal testing. For the adhesive removal task, the injured animals demonstrated elevated latencies for both contact and removal of their contralesional forepaw, suggestive of sensorimotor deficits. At 14d post-transplantation, both iPS-NPC therapy alone and the combination of iPS-NPC therapy with CTZ stimulation resulted in similar levels of performance improvement, in latency to contact and removal, although there was a greater improvement trend in the combination therapy group for latency to removal (*Figure 8-14*, A). A similar outcome was observed at 21d post-transplantation, although the spontaneous recovery in the nontreatment control groups resulted in diminishment of the differences observed at the 14d timepoint. At 21d post-transplantation, only the combination therapy demonstrated significantly improved functional outcomes as compared to the other 3

groups (*Figure 8-14*, A). No differences were observed in the control ipsilesional forepaw adhesive removal performance (*Figure 8-14*, B).

Finally, whisker sensation function was evaluated using the modified high-throughput corner test system. At baseline, the mice demonstrated lateral nondiscrimination and turned towards both sides approximately equally, resulting in a baseline laterality index (LI) close to 0. After TBI, the injured mice demonstrated greater preference towards ipsilesional turning, as expected from a unilateral injury, resulting in LI > 0. At 14d post-transplantation, there was an improving trend for both the iPS-NPC alone group and the combination therapy group, and at 21d post-transplantation, the combination therapy group demonstrated significant improvements as compared to SATO control, with the LI returning to 0, suggesting nearly full recovery of whisker sensation (*Figure 8-15*, A). Interestingly, the significance was not observed after normalizing the LI to baseline, although there was still a marked trend in improved functional recovery in the combination therapy group (*Figure 8-15*, B).

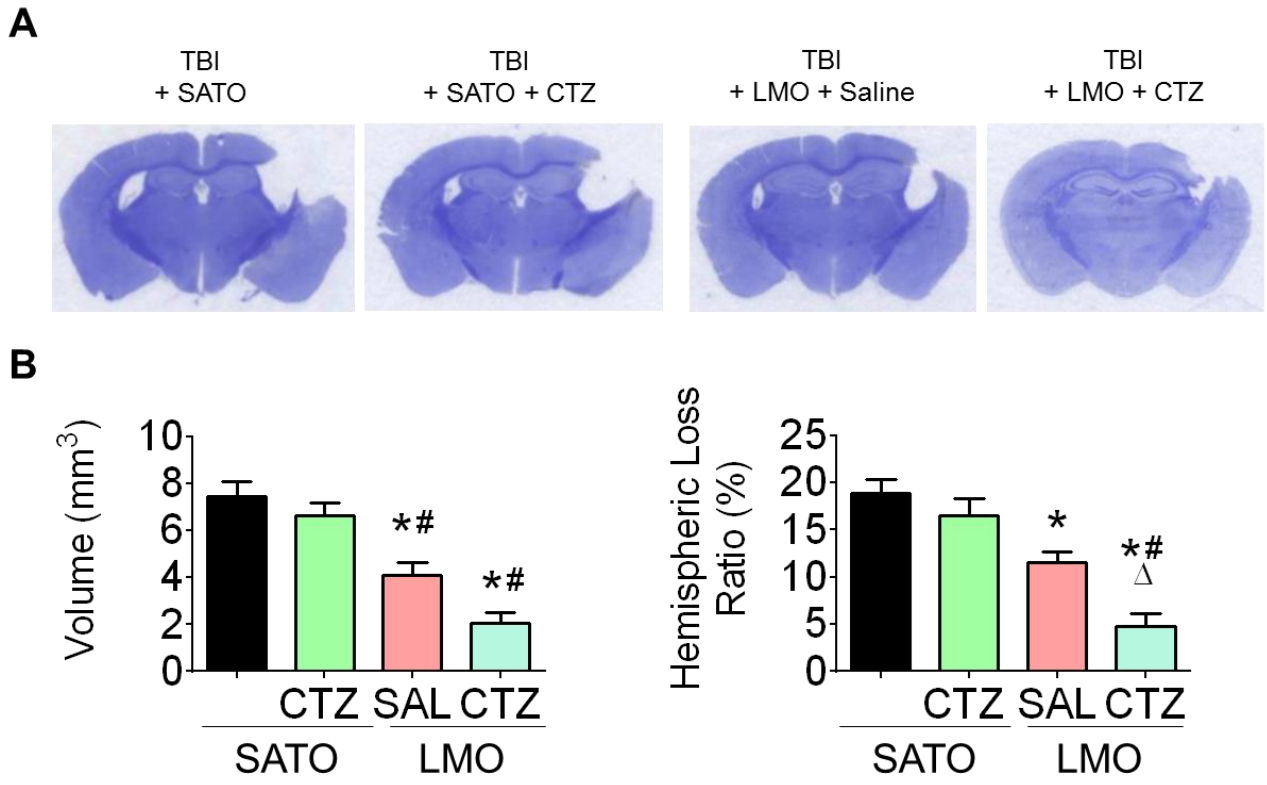

Figure 8-13: Both iPS-NPC transplantation and CTZ stimulation reduced the tissue damage after TBI.

A. Representative images of Nissl stains carried out at 21d post-transplantation. **B.** Quantification of the contusion volume for all groups (left panel) and the ratio of hemispheric volume loss (vs. the contralesional side). *: $p < 0.05$, vs. TBI + Sato; #: $p < 0.05$, vs. TBI + Sato + CTZ; Δ: $p < 0.05$, vs. TBI + LMO + SAL. N = 10 for all SATO groups, 11 for all LMO groups.

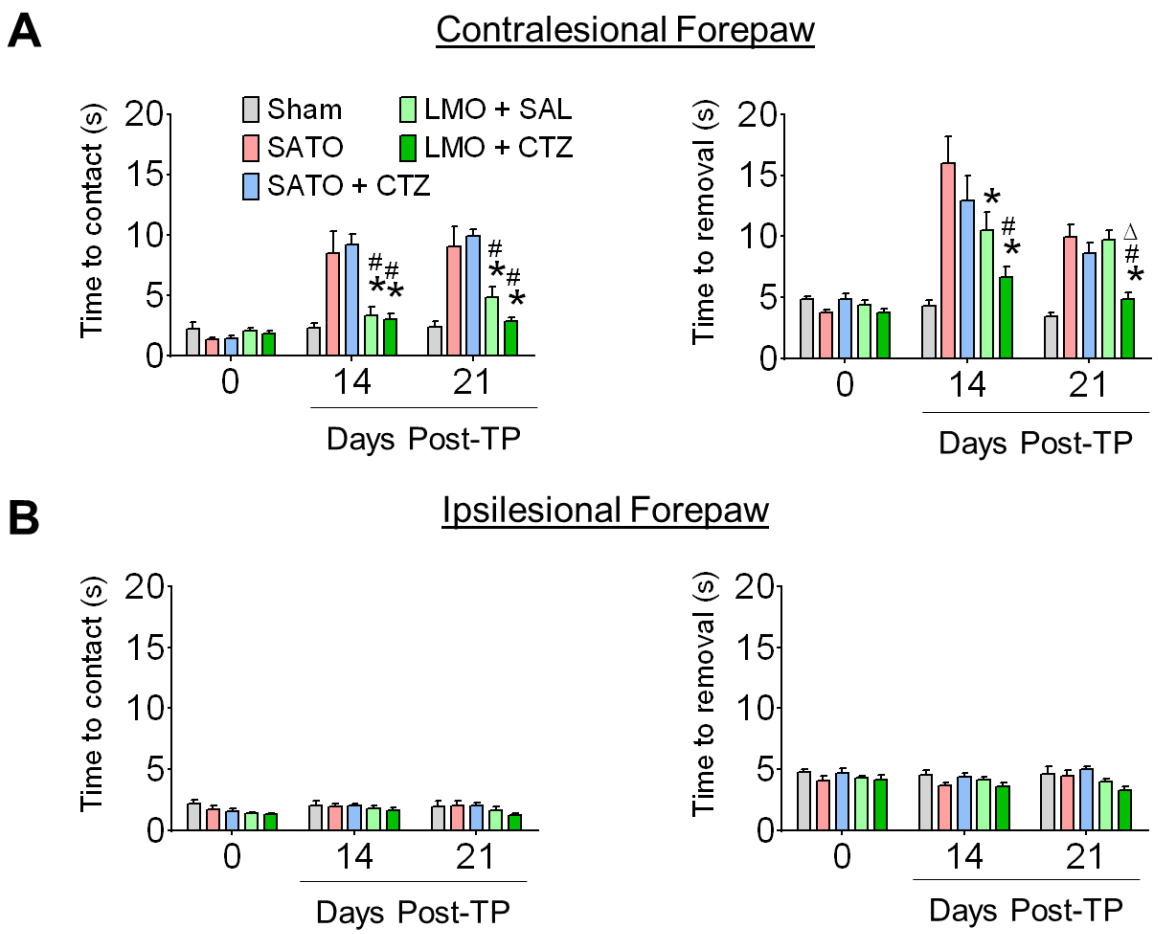

Figure 8-14: Transplantation of iPS-NPCs and CTZ stimulation conferred synergistic effects for improving sensorimotor function.

A-B. The adhesive removal test was carried out for all groups prior to TBI (baseline), and at 14 and 21d post-transplantation (TP). **A.** Quantification of latencies to contact and removal of the contralesional forepaw. **B.** Quantification of latencies to contact and removal of the control ipsilesional forepaw. *: $p < 0.05$, vs. TBI + Sato. N = 9 for Sham group, 10 for all other groups.

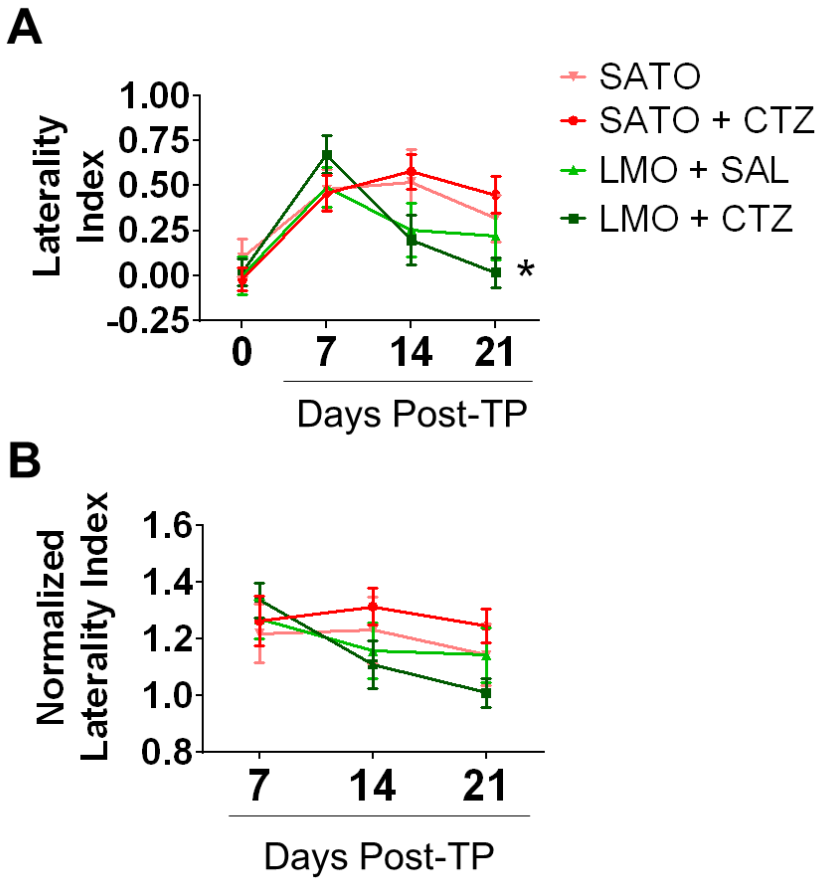

Figure 8-15: The combination of cell therapy and CTZ stimulation accelerated whisker sensation restoration after TBI.

A-B. The high-throughput automated corner test was carried out for all groups prior to TBI (baseline), and at 7, 14, and 21d post-transplantation (TP). **A.** Quantification of the laterality index for all groups (0 = complete lateral nondiscrimination). **B.** Quantification of the normalized laterality index for all groups (normalized to baseline). *: $p < 0.05$, vs. TBI + Sato. N = 9 for Sham group, 10 for all other groups.

8.3 Discussion

Stem cells have great potential to transform modern medicine and treat a variety of irreversible disorders. However, their underwhelming efficacy in clinical trials [69-71], suggest

there is still a significant treatment gap. One potential approach to bridge this gap may be to facilitate endogenous stem cell function after transplantation. For transplantation of NPCs into the CNS, this entails exogenous stimulation of the transplanted cells to promote grafted cell activity. Neural activity is a crucial regulator of differentiation and plasticity during development [19], and stimulation has been demonstrated to promote neurogenesis, neuritogenesis, and synaptic remodeling for tissue repair after injuries [19, 72-74]. To be able to drive neural activity after transplantation, I have established the new light-responsive LMO3 iPS cell line that can be activated via a pharmacological approach. Furthermore, not only have we validated the function of the LMO3 fusion probe, I also characterized the physiological responses to CTZ stimulation in vitro and within a mouse TBI model.

I first used the well-controlled and simpler in vitro system of differentiated iPS-neuron cultures to compare the response to CTZ stimulation with that of laser stimulation, which is the gold standard for optogenetics. I found that the cells responded favorably for both stimulation modalities. Both resulted in upregulation of the CREB intracellular pathway and activity-dependent factors BDNF and NGF, which confer a multitude of beneficial effects including promoting survival, NSC proliferation and differentiation [75], axonal outgrowth [24, 25], and synaptic plasticity [20]. Interestingly, while I observed enhanced axon outgrowth and extension and synaptogenesis, I did not observe a greater rate of neuronal differentiation or cell survival (with in vivo experiments) for the photostimulated group. This could both be attributed to a ceiling effect from implementing protocols that have been standardized in our iPSC differentiation and transplantation routine, including hypoxic preconditioning and rotary shaking, both of which increase survival and differentiation [67, 76]. Hypoxic preconditioning has also been shown to increase compensatory and pro-survival factors, such as erythropoietin (EPO) and hypoxia-

inducible factor 1α (HIF1α), which both promote restoration of blood flow, and B-cell lymphoma 2 (BCL-2), a key anti-apoptotic factor [76]. Notably, photostimulation was able to promote axon outgrowth despite potential inhibitory forces, such as high CSPG concentrations and areas of cell death and axonal injury. While the mechanisms behind axonal sprouting and guidance are still being elucidated, it is known signals that are normally repulsive for axon growth cones can switch to become attractors, a reversal that can be mediated by Ca2+ and cAMP levels [77]. Furthermore, growth factors like NGF can override the inhibitory microenvironment of the glial scar to promote axon growth into and out of the injury region [292, 411]. This makes stimulation such a viable target for improving stem cell therapy for brain injuries, because this provides an organic approach to upregulating NGF to improve connectivity beyond the glial scar.

While TBI is a highly prevalent healthcare burden, there currently exists no effective treatments. The only current therapeutic options for managing TBI are prophylactic hypothermia and hyperbaric oxygen therapy during the early phases and physical rehabilitation during the later phases [78]. Hypothermia has more thoroughly established for treating other brain injuries, such as ischemic stroke [79], but it may be a feasible option for TBI as well, given the similarity in some of the hypothermia-responsive pathophysiological mechanisms between stroke and TBI, such as thermo-pooling, BBB disruption and subsequent ischemia and edema, and glutamate excitotoxicity [2, 80, 81]. However, there is evidence that hypothermia has little effect [82] or may actually exacerbate the deficits from TBI [83]. One of the major challenges with TBI is the persistence of the secondary effects, especially the decreased perfusion within the peri-contusion region, causing ischemic cytotoxic damage and edema that peaks around 1 week post-injury [84]. This results in continuous longterm damage that entails, resulting in gradual injury expansion and tissue loss [85]. This tissue expansion could also explain why the size of the contusion volumes

measured by Nissl staining appeared to be disproportionately greater than the impact size, given the elasticity of brain parenchyma. During the transplantations of the cell, while there was already some initial tissue loss, it was not nearly as extreme as what was observed at the 21d post-transplantation timepoint, in which all the cortical layers around the impact zone was absent. Thus, the continuous loss of tissue may in part be due to the ongoing secondary effects and ensuing cell death that persists long after the initial injury. While cell therapy and stimulation are not administered within a short enough therapeutic window to overturn the irreversible cell death of the initial impact and acute cell death within the first 3 days, both cell therapy and stimulation still demonstrated neuroprotective effects, suggesting that a significant proportion of the damage from TBI occurs during the subacute and chronic phases, and that regenerative therapy during this phase can still provide marked neuroprotection.

Furthermore, stimulation also conferred regenerative effects that combatted the deleterious secondary effects associated with injury expansion. While stimulation did not markedly enhance neurogenesis, it did significantly elevate levels of angiogenesis and the restoration of blood flow within the peri-contusion region, which is particularly important after TBI given the BBB disruption and persistent hypoperfusion within that region [84]. The mechanisms behind the enhancements in neovascularization is not clearly elucidated, although I did find that both cell therapy and combination therapy similarly upregulated VEGF levels. The compounded effect of stimulation may be due to the coupling of the neurovascular unit, with neural activity closely paired with angiogenesis [68].

While this study demonstrated proof-of-concept for the LMO3 iPS cell line, as well as the synergistic effects of cell therapy and noninvasive CTZ stimulation, there are still areas for improvement for future studies. These include the dosage and anatomic targets for transplantation.

I chose the anterior peri-contusion region given its proximity to the SVZ and the potential greater paracrine effects to facilitate endogenous neurovascular regeneration and plasticity [86]. However, other regions may be more appropriate, especially given the goal of therapy. For example, one of the longterm effects of TBI is depression, which is associated with a more global activity disturbance, especially in the reward pathway involving the prefrontal cortex (PFC), nucleus accumbens (NAcc), ventral tegmental area (VTA), and the amygdala [87]. Therefore, those neuroanatomical targets may be better suited for directing therapy towards comorbidities like depression. Furthermore, the timing of transplantation post-TBI still needs to be optimized, especially because cell therapy within a clinical setting is unlikely to happen within days, given the need to harvest autologous cells and potentially genetically re-engineer them [70, 88]. Thus, it may be necessary to investigate delayed paradigms of cell transplantation in animals, such as weeks or even months post-TBI.

Another approach for driving neural activity that has garnered attention in recent years is chemogenetics, especially designer receptors exclusively activated by designer drugs (DREADDs) [89]. Indeed, DREADDs such as hM3Dq and hM4Di have both been incorporated into stem cells, but similar to optogenetics, it has only been exploited as an interrogative tool [90]. While DREADDs has great translational potential because of the noninvasive nature of drug delivery, it lags behind the expansive and versatile toolbox of optogenetics, and the off-target and adverse effects of the DREADD ligand must be thoroughly evaluated and minimized before proceeding to any clinical trials. One of the main challenges of DREADDs is the back metabolism of the ligand clozapine-N-oxide (CNO) to clozapine in humans (not as evident in animals), which could lead to severe adverse psychiatric effects [91]. Furthermore, CNO stimulation results in high-frequency burst activation of DREADD-expressing cells [92], which could result in greater likelihood of

desensitization and excitotoxicity, or even induce epileptiform actvity after injury. However, if these challenges are addressed in the future, the combination of either a chemogenetic or optogenetic stimulation paradigm with stem cell therapy could provide a promising means to implement multimodal systems for controlling activity, such as a paradigm in which optogenetics is used for chronic low-frequency stimulation, while DREADDs might be exploited for burst activity or even silencing.

In summary, I have demonstrated the efficacy of the combination therapy of iPS-NPC transplantation with external stimulation for promoting neurovascular repair, endogenous plasticity, and functionary recovery after TBI. While primarily as a proof-of-concept, this therapy already possesses the essentials for clinical translation, including minimal invasiveness, ease of use, and efficacy. With an expanding and ever-improving optogenetic and chemogenetic toolbox, there will be greater efficacy and precision for stimulation. I envision there to be further developments around external stimulation of genetically modified stem cells to drive cellular and network activity after transplantation to treat brain injuries and other intractable disorders.

Chapter 9: Aim 3 - Enhancement of Luminopsins by Addition of Golgi Trafficking Element

9.1 Introduction

Luminopsins (LMOs) are molecular tools that enable both chemogenetic and optogenetic control of neuronal activity. They consist of a luciferase enzyme fused to an opsin and therefore allow optogenetic activation by both external light illumination as well as by internal bioluminescence with a chemical substrate, coelenterazine (CTZ). These chimeric probes are therefore well-suited for long-term in vivo studies requiring chronic optogenetic stimulation or stimulation in multiple areas of the brain. Both excitatory [367, 423] and inhibitory LMOs [367, 424] have been successfully utilized to modulate neuronal activity in vitro and in vivo.

LMO3 is an excitatory luminopsin that consists of a light-sensitive cation channel (Volvox channelrhodopsin 1, VChR1) coupled to a variant of bioluminescent enzyme (slow-burn Gaussia luciferase, sbGLuc). This optogenetic probe therefore allows multi-modal control of membrane potential with either external blue/green light illumination or by CTZ-derived bioluminescence. The degree of opsin activation by either direct external light illumination or chemically derived bioluminescence has been previously demonstrated to be sufficient for excitation of neurons in vitro and in vivo [367]. However, long-term expression of LMO3 has been associated with globular accumulations of the protein inside the cells (unpublished observations), similar to other unmodified optogenetic probes which form blebs in the endoplasmic reticulum (ER) due to poor membrane trafficking [339, 340]. This poses a concern for long-term cellular health as well as limited photocurrent responses resulting from suboptimal membrane expression.

In this study, we sought to improve membrane trafficking of LMO3 using cellular trafficking methods previously utilized by Gradinaru et. al.[338] Specifically, the Golgi export trafficking signal (TS) from a neuronal potassium channel ($K_{ir}2.1$)[425] was added to the LMO3 fusion protein to create an enhanced LMO3 (eLMO3). We tested whether decreased ER

accumulations and improved membrane trafficking of LMO3 would result in more robust excitation of neuronal activity and indeed found that eLMO3 produced greater photoresponses in vitro and in vivo.

9.2 Results

9.2.1 Aim 3.1 – To create the virus containing eLMO3 with an inserted Golgi TS motif and evaluate the membrane localization and elicited photocurrents

Enhanced improved membrane localization of LMO3 with the membrane trafficking signal in cultured neurons in vitro

Previous studies on optogenetic probes have shown that the endoplasmic reticulum (ER) and Golgi export motifs in the $K_{ir}2.1$ sequence improves trafficking of the foreign membrane proteins from the ER to the cell membrane [338, 425, 426]. To improve membrane expression, we inserted the Golgi export trafficking signal (TS) from $K_{ir}2.1$ into the original LMO3 backbone to create the enhanced LMO3 (eLMO3) in a mammalian expression plasmid (*Figure 9-1,* A). The eLMO3 cassette was then subcloned into an adeno-associated viral (AAV) vector with the human synapsin 1 promoter for neuronal specificity and viral vectors pseudotyped with recombinant AAV2/9 was produced. Then, we infected primary culture of cortical neurons with either the original LMO3 AAV or the eLMO3 AAV one day after seeding by adding the same volume of virus suspension to culture medium. Viral titers were approximately equal (1.8×10^{13} vg/ml for both LMO3 and eLMO3) and we assumed that multiplicity of infection were very similar between the two conditions. We first characterized the distribution of both transgene products in neurons

15-16 days in vitro (DIV). LMO3 was seen in multiple neuronal compartments, including the putative ER in the soma (*Figure 9-1*, B, top right, arrows), but more so within the neurite branching points typically enriched with the ER (*Figure 9-1*, B, top right, arrowheads). The addition of the TS nearly completely abolished the presence of protein aggregates and fluorescence from the EFYP tag of eLMO3 was predominantly observed around the soma and in processes (*Figure 9-1*, B, bottom right), consistent with proper membrane targeting of the protein.

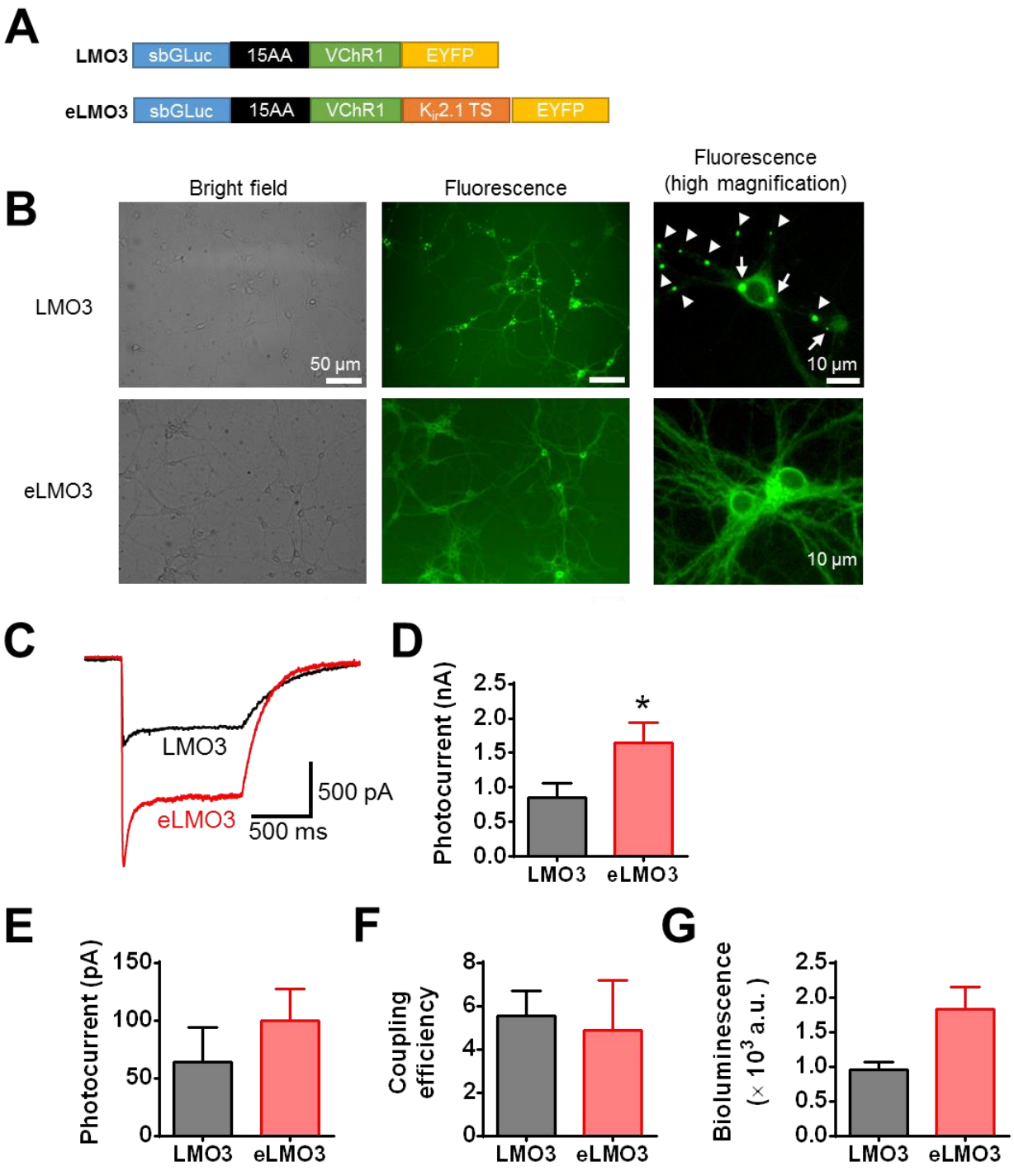

Figure 9-1: Insertion of trafficking signal improved membrane targeting and photocurrents from multimodal sources.

A. Linear map of original LMO3 plasmid backbone (top) and the modified eLMO3 construct with the Kir2.1 trafficking signal (TS) insertion (bottom). **B.** Representative epi-fluorescent images of cortical neurons infected with either LMO3 or eLMO3 AAV. Note the distribution of high-density YFP blebs across multiple neuronal compartments, including the soma (arrows) and neurites (arrowheads). **C.** Raw photocurrent trace after lamp-induced stimulation of a patched LMO3-expression or eLMO3-expression cortical neuron. **D.** Quantification of photocurrents after lamp-induced stimulation. **E.** Quantification of photocurrents after CTZ-induced stimulation. **F.** Quantification of coupling efficiency. **G.** Bioluminescence output measured as absorbance by plate reader. All data represented as Mean ± SEM. *: $p < 0.05$.

Next, we assessed whether the improved membrane targeting also enhanced the function of luminopsin. Either LMO3- or eLMO3-expressing neuron was patch-clamped. We first measured the photocurrent to saturating photostimulation with an arc lamp (300 µW/mm^2; 460-500 nm). Photocurrent with LMO3 was larger than in the experiments in the previous section, probably due to differences in modes of transfection (electroporation vs. viral infection) and promoters (CAG vs. hSynI). We observed a nearly 2-fold increase in the photocurrent of eLMO3 over that of LMO3 (*Figure 9-1*, C). The increase was statistically significant (two-tailed Student's *t*-test; *$p = 0.042$; $t(19) = 19.04$; $n = 10$ and 12 for LMO3 and eLMO3, respectively; *Figure 9-1*, D). Next, we applied coelenterazine (CTZ; final concentration: 100 µM), substrate for luminopsin, to the bath solution, which resulted in bioluminescence and bioluminescence-mediated photocurrent. Similar to the responses to physical light, eLMO3 resulted in larger photocurrent (~1.6 times) than LMO3 (*Figure 9-1*, E), although the difference was not statistically significant (two-tailed Student's *t*-test; $p > 0.4$; $t(6) = 0.874$; $n = 4$ each). We also calculated the coupling efficiency, which is defined as the photocurrent induced by a saturating concentration of CTZ (100 µM) divided by that evoked by a saturating intensity of lamp (300 µW/mm^2) [367]. The coupling

efficiency was similar between the two versions of luminopsin and was not significantly different (Student's t-test; $p > 0.8$; $t(8) = 0.263$; $n = 4$ each; *Figure 9-1*, F). Finally, we evaluated bioluminescence from the sbGLuc with a plate reader and found that eLMO3-expressing cortical neurons emitted approximately 2-fold greater luminescence as compared to LMO3-expressing cortical neurons when CTZ (3 μM) applied (Student's t-test; $p = 0.0177$; $t(11) = 2.787$; $n = 7$ for LMO3 and 6 for eLMO3; *Figure 9-1*, G).

These experiments indicate that surface expression of LMO3 was significantly enhanced by adding the TS. The TS did not affect efficiency of the channel to be activated by bioluminescence as proportions of the channels activated by bioluminescence was similar between the two versions of luminopsin (~5%), but improved surface expression resulted in larger CTZ-induced responses.

9.2.2 Aim 3.2 – To investigate the distribution of eLMO3 following AAV infection of the mouse S1 cortex and assess the functional differences between LMO3 and eLMO3

Improved membrane trafficking of LMO3 in the mouse brain

To confirm the efficacy of the TS in an *in vivo* setting, we injected the AAV vector, either with LMO3 or eLMO3, into the mouse primary somatosensory cortex (S1; *Figure 9-2*, A). Histological sections were prepared 35 days after injections and the fluorescence signal was amplified by immunostaining against the EFYP tag of LMO3 and the distribution of the expressed protein was evaluated within the injection sites (*Figure 9-2*, A, green box). Fluorescence was primarily observed in pyramidal cells of the deep cortical layers. Sections were location-matched and counting of protein aggregates was performed only of deeper-layer neurons around the

epicenter of the AAV injection. Similar to what was observed *in vitro*, aggregates of LMO3 were observed in both the cell body and neurites (Fig. 3B, top right, arrowheads and arrows, respectively). These dense puncta were not observed in neurons expressing eLMO3 (*Figure 9-2*, B, bottom right). We quantified the total numbers of puncta and EYFP-positive somata, as well as the ratio of puncta to cell bodies in each microscopic field. The $K_{ir}2.1$ TS in eLMO3 resulted in greatly improved membrane targeting of the fusion protein, which manifested as significantly decreased numbers of total puncta and more pronounced somatic expression of luminopsin (*Figure 9-2*, C) (two-tailed Student's *t*-test; $*p < 0.0001$ and $*p < 0.0001$; $t(14) = 9.863$ and $t(14) = 5.351$; $n = 8$ images for both the LMO3 and eLMO3 groups; for the numbers of puncta and puncta-to-somata ratio, respectively). Thus, addition of the TS significantly reduced protein aggregates and improved surface expression of LMO3 *in vivo* after virus-mediated chronic expression, similar to dissociated neurons in culture.

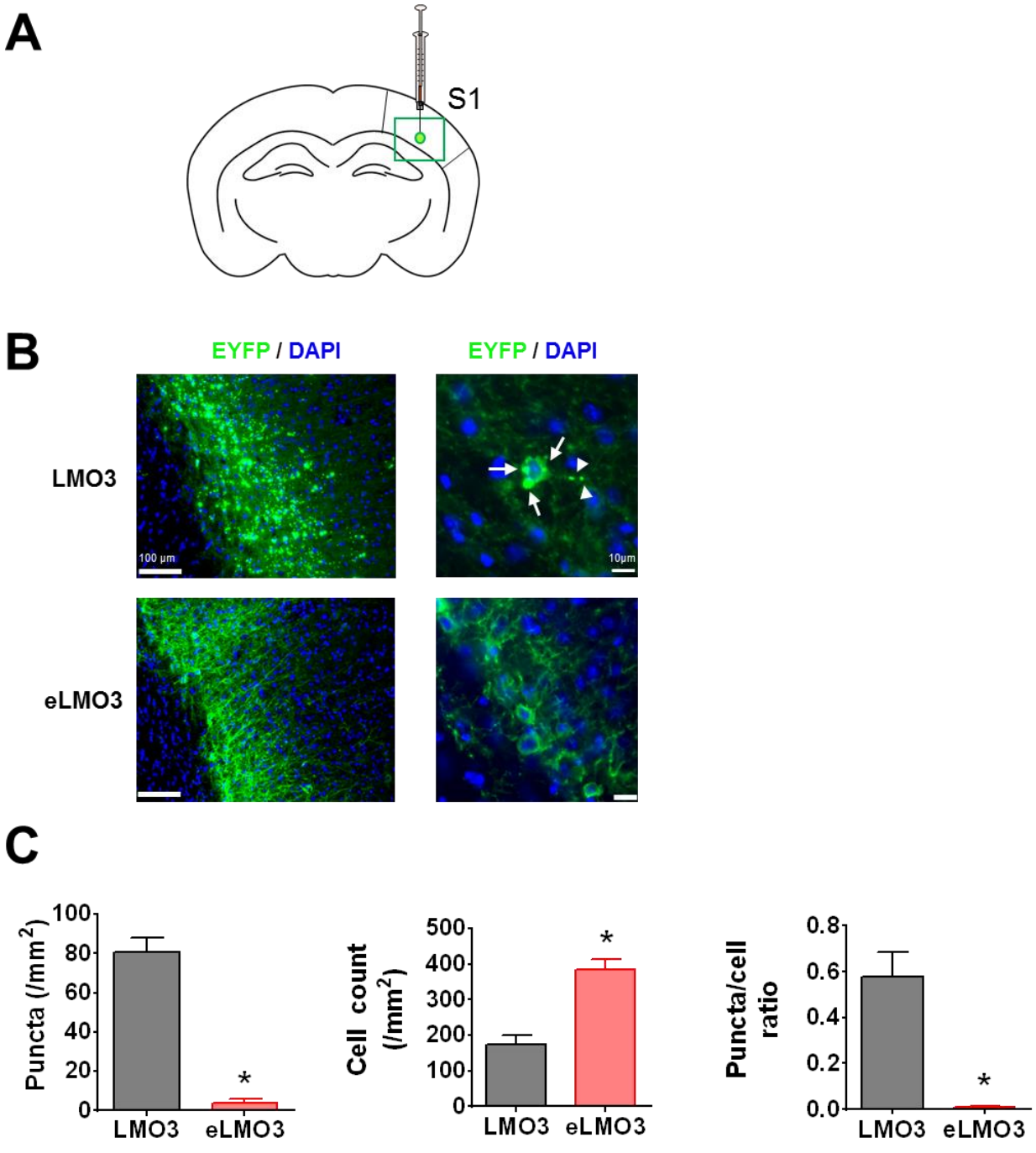

Figure 9-2: Cortical expression of eLMO3 in mice displayed enhanced membrane trafficking and near abolishment of aggregate formation.

A. The injection site of the AAV was the somatosensory cortex (S1), with the target layer being the deeper cortical layers (green box: region of interest). **B.** Representative immunohistochemical images displaying the presence of prolific aggregate formation within the injected region. Upon

higher magnification, blebs could be observed in both the cell bodies (arrows) and neurites (arrowheads). **C.** Quantification of the total puncta in each 40x ROI, the total YFP+ cells in each 40x ROI (YFP+ defined as YFP expression observable in soma), and ratio of puncta to cells. All data represented as Mean ± SEM. *: $p < 0.05$. N=8 per group.

9.2.3 Improved expression of LMO3 elicits greater behavioral responses

AAV injection into the S1, specifically the barrel cortex (BC), allowed for examination of behavioral effects of the CTZ-induced activity of transduced cortical neurons. The BC is the tertiary structure in the whisker thalamocortical pathway, for which sensory signals from the whisker ascend the barrelettes of the brainstem to the ventroposteromedial (VPM) nucleus of the thalamus, and finally to the deep layers of the BC (*Figure 9-3*, A). Thus, by stimulating the target neurons in the BC, we expected to induce an artificial sensation of repetitive whisker deflections, which would produce a slight irritation for the mouse and evoke a continuous whisker brushing or grooming-like behavior, which we defined as "whisker response" (*Figure 9-3*, B). To test this hypothesis, we injected CTZ (30 µl of 6 µM in 0.9% saline) via intranasal delivery and quantified duration of whisker response through an automated behavior observation system. Intranasal injections are a well-established route for delivering blood-brain barrier-permeable agents, such as CTZ, directly into the brain, and they provide more bioavailability of the injected agent in the neocortex than intraperitoneal injections [166, 427, 428]. Furthermore, it is less invasive and allows for convenience of access as well as ability of behavioral observation with minimal disturbance. After recovery of AAV injection with LMO3 or eLMO3, half of the mice were intranasally injected with CTZ and then was monitored for 1 hour. The other half received saline injection as a control. The experiments were repeated the following day with the experimental groups switched, such that animals that received saline the prior day would then receive CTZ, and

vice versa. Then, after allowing the mice to wait for a week, the trials for both CTZ and saline injections were repeated. The CTZ groups were repeated for 3 trials in total, while the saline groups and the naïve animals + CTZ group were repeated for 2 trials. All data were combined for analysis, and 2 mice were used per group, creating a total of 4-6 trials/group. We observed longer whisker responses in animals with both LMO3 and eLMO3 after CTZ administration compared to the saline controls, corroborating the stimulatory effect of CTZ (*Figure 9-3*, C). We observed a statistically significant increase of whisker responses with CTZ in both groups of mice, LMO3 and eLMO3 (two-way ANOVA; the main effect of interaction: $p = 0.0014$; $F(1,16) = 14.85$ for LMO3/eLMO3 and SAL/CTZ; the main effect of treatment for SAL vs. CTZ: $p < 0.0001$; $F(1,16) = 73.14$; pairwise comparisons with Tukey's corrections: *: $p = 0.0202$; $q(16) = 4.699$ for LMO3 + SAL vs. LMO3 + CTZ; #: $p < 0.0001$; $q(16) = 12.41$ for eLMO3 + SAL vs. eLMO3 + CTZ; $n = 4$ for CTZ (naïve) group; $n = 4$ for LMO3 + SAL group; $n = 6$ for LMO3 + CTZ group; $n = 4$ for eLMO3 + SAL group; $n = 6$ for eLMO3 + CTZ group). When eLMO3 animals were compared with LMO3 animals, they showed significantly longer whisker response times (*Figure 9-3*, C) (two-way ANOVA; the main effect of genetics for LMO3 vs. eLMO3: $p = 0.5466$; $F(1,16) = 0.3794$; Δ: $p = 0.0132$; $q(16) = 4.997$ for LMO3 + CTZ vs. eLMO3 + CTZ), suggesting prolonged and elevated neuronal activity in the BC of the eLMO3 group after CTZ injection. The more robust response in mouse behavior was consistent with improved membrane-localized expression of LMO3.

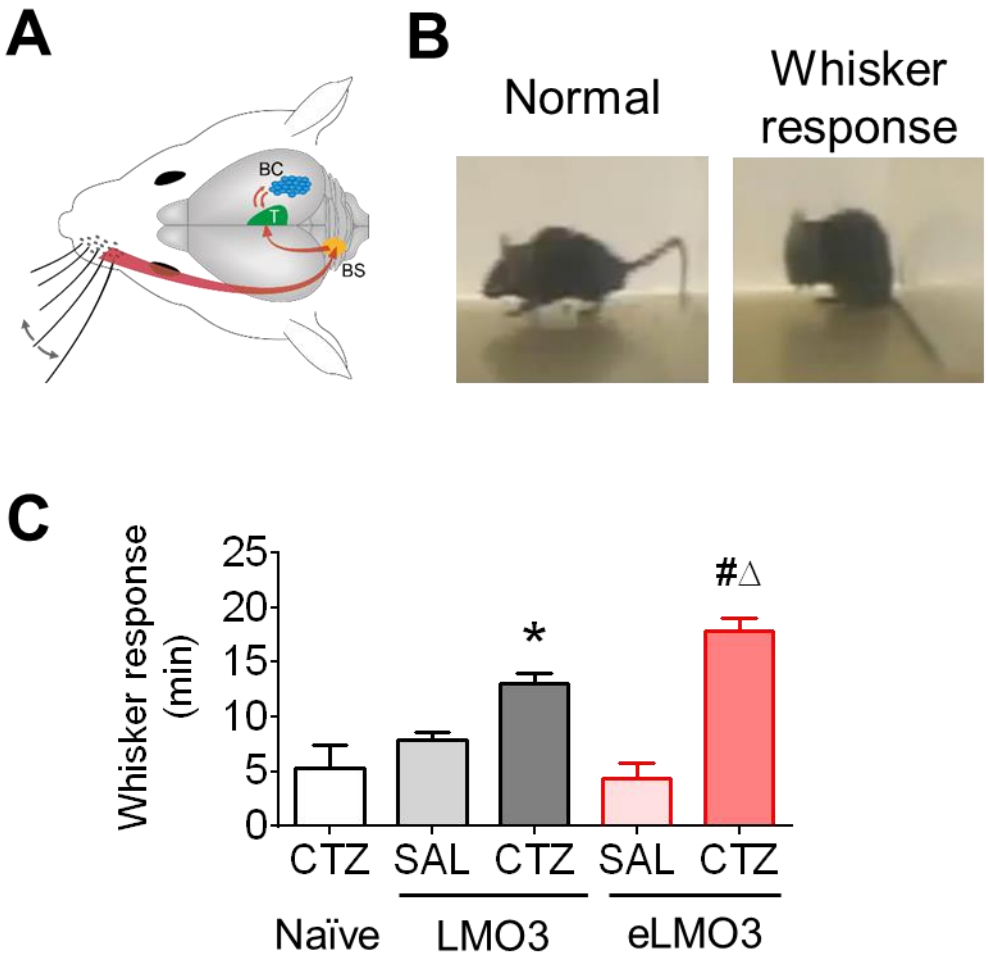

Figure 9-3: Greater functional readout after CTZ-induced stimulation in eLMO3-transduced mice. **A.** The whisker thalamocortical pathway initiates with whisker deflection signals in the vibrissal mechanoreceptors, which ascends to the brainstem (BS), and then the ventroposteromedial (VPM) nucleus of the thalamus (T), and finally to the barrels of the barrel cortex (BC). **B.** Representative screen captures of the mouse during normal exploratory behavior and the whisker response behavior associated with excessive BC activity. **C.** Quantification of the whisker response times as measured and analyzed using the automated Home Cage Monitoring System. All data represented as Mean ± SEM. *: $p < 0.05$, as compared to LMO3 + Saline group. #: $p < 0.05$, as compared to eLMO3 + Saline group. Δ: $p < 0.05$, as compared to LMO3 + CTZ group. N=4-6 trials per group.

9.3 Discussion

The LMO3 fusion protein was previously developed and characterized and responsiveness to CTZ was demonstrated both *in vitro* and *in vivo* [367, 423]. However, we noted the perseverance of LMO3 aggregates in ER-rich regions of infected cells, which we believed to impair the efficiency of photostimulation. In this study, we improved membrane expression of LMO3 by adding the Golgi TS sequence and created an improved version, eLMO3. Transduction of eLMO3 resulted in greater photocurrents with either CTZ or external light stimulation (*Figure 9-1*) and was also able to elicit more robust behavioral responses upon CTZ-derived stimulation as compared to LMO3 (*Figure 9-3*).

The increased membrane expression of eLMO3 means that less light or CTZ is required to achieve the same levels of neuronal activation. A given cell expressing eLMO3 therefore requires less light than a cell expressing LMO3 molecules to reach the same level of effect, therefore mitigating potential heat-induced injury of tissue and potentially allowing for more non-invasive methods of light delivery (*e.g.* transdermal or transcranial). The same applies for chemogenetic activation of LMO3 with CTZ substrate as the same dosage of CTZ has a greater effect with eLMO3, which is advantageous in chronic long-term in vivo studies.

In this study, we also noticed that levels of membrane expression varied depending on the method of transduction when they were assessed as photocurrent (*Figure 9-1*). Viral-mediated transduction of LMO3 resulted in greater photocurrents than electroporation of the same transgene, possibly due to the higher copy numbers of the transgene, higher promoter activity, and better integrity and overall health of neurons after transfection. Thus, the benefit of eLMO3, namely a higher degree of membrane expression is best complemented by virus-mediated transduction.

Multiple prior studies have explored the creation of superior optogenetic tools that have improved trafficking properties, including using ER export sequences [340], the Golgi export TS sequence [338], or the combination of the two [340, 426]. In this study, we improved membrane trafficking by including the Golgi TS sequence. Despite no evidence of aggregations of eLMO3 in the ER by fluorescence microscopy, there may still be aggregations present below levels of detection, and membrane trafficking could therefore be potentially further improved by utilizing ER export motifs as previously described. Other genetic modifications may also be investigated, such as a combinatorial approach with other transport/trafficking motifs, or even altering the insertion site for the motifs, which has been shown to affect the functionality of the motifs [425, 429] [338].

Since the bioluminescence-induced photocurrents of eLMO3 were unable to reach saturating levels (*i.e.* below photocurrents induced by lamp illumination), the substrate induced photocurrents could be potentially further improved with the use of brighter luciferase enzymes. Indeed, a new line of luciferase has been developed from a brighter luciferase, NanoLuc (Promega, Madison, MI, USA) [430, 431], and have the appropriate emission spectrum to be paired with VChR1. We hope that the current study and future engineering of luminopsin will further increase utility of the molecular probe in both conventional optogenetic paradigms as well as in chemogenetic activation.

Chapter 10: Summary and Conclusions

The advent of stem cells have ushered in a new era of possibility for both basic science and translational research. While pluripotent stem cells, and especially iPSCs provide unprecedented possibilities for differentiation potency and utility, there are still many approaches that can be taken to improve upon their function and efficiency, especially for treating intractable diseases such as TBI. Some of these approaches include preconditioning, biocarriers, cotreatment with trophic factors or other biochemical buttresses, and genetic engineering, and as an extension, the potential for cell-specific activity modulation. While these are different classes of improvements, there exists much overlap. For example, stimulation of transplanted NPCs also leads to upregulation of neurotrophins, which can be captured and enriched by biocarriers as well. In our study, we implemented two different approaches, hypoxic preconditioning and activity modulation, specifically a noninvasive optogenetic means to drive neural activity.

TBI represents a costly unmet clinical need that not only exhausts financial resources, but deprives the quality of life and productivity of millions of young and otherwise high-functioning individuals each year. Given the damage from both the initial impact as well as lingering secondary injuries, it will be fruitful to implement longterm therapeutic strategies that can both delay or halt further injury expansion and promote neurovascular remodeling and functional repair. The pleiotropic effects associated with cell therapy make it an ideal target for therapy. While clinical trials have repeatedly corroborated the safety and efficacy of the delivery and biocompatibility of stem cell transplantation, the state of cell therapy currently remains suboptimal, especially with the underwhelming outcomes of clinical trials for TBI [237-239, 350]. Thus, this dissertation has focused on a promising and translationally feasible approach towards building upon cell therapy.

In Aim 1, I created and validated the LMO3-expressing iPS cell line and demonstrated that it is capable of maintaining robust LMO3 expression across multiple passages and across differentiation stages, including as fully differentiated glutamatergic neurons. The LMO3 transgenic fusion protein allows for the CTZ-driven stimulation of the iPS-derived neurons. Next, through a variety of IHC and Western blots, I characterized the response of the iPS-neurons to both CTZ and laser-driven stimulation. Both photostimulation modalities were able to upregulate activity-dependent factors BDNF and NGF, as well as promote markers of plasticity and migration. Furthermore, photostimulation enhanced axon outgrowth and extension across inhibitory zones, such as CSPG spots and scratch-injured regions.

In Aim 2, I transplanted the LMO3-expressing iPS-NPCs into a mouse TBI model and evaluated the physiological response to CTZ stimulation on a molecular, cellular, and functional level. Western blots demonstrated that CTZ stimulation induced the expression of BDNF and NGF and promoted factors of axon extension and synaptogenesis. While CTZ stimulation did not significantly improve cell viability, it did confer other benefits, including enhancing axonal reorganization and vascular remodeling around the peri-contusion region. These effects resulted in greater blood flow around the injury, decreased contusion volumes, and enhanced behavioral recovery as compared to just cell therapy alone.

Overall, this dissertation has accomplished its primary objective to implement an innovative and clinically viable approach to enhance the beneficial effects of cell therapy. Although the efficacy of the combination therapy of CTZ stimulation and cell therapy has been demonstrated in the mouse TBI model, there are many other pathologic conditions in which this synergy can be investigated, such as neurodegenerative disease and spinal cord injury. Moreover, this dissertation establishes a potential precedence for stem cell therapy for all organ systems –

rather than passively transplanting cells into the native organ system, it may be prudent to adopt a more active approach of inducing the grafted cells to behave like host cells to promote graft-host engagement and functional repair. This is of particular importance in the CNS, in which the interconnections within neural networks are essential and intricately vast. While this dissertation highlighted a promising strategy for bridging the treatment gap for cell therapy, there are other synergistic approaches that can be implemented, including transplantation of stem cells within biocarriers like hydrogels. These scaffold supports that mimic the endogenous extracellular matrix could provide the structural support to promote graft-host cell-cell engagement, especially with concomitant stimulation of the grafted cells. Furthermore, the scaffolds can be designed to establish a discrete organization of cells, such as the lamellar structure of the cortex, which can further contribute to tissue repair. Nevertheless, many of these combination approaches for cell therapy have yet to be evaluated in clinical trials, though that may be conducted in the near future. It has been just over a decade since the discovery of iPSCs, but the stem cell field has made tremendous strides, and with the continued acceleration and integration of interdisciplinary fields, the vast regenerative potential of stem cell therapy may soon at least be partially be realized.

Chapter 11: References

1. Langlois, J.A., W. Rutland-Brown, and K.E. Thomas, *Traumatic brain injury in the United States: emergency department visits, hospitalizations, and deaths*. 2004: Department of Health and Human Services, Centers for Disease Control and Prevention, Division of Acute Care, Rehabilitation Research and Disability Prevention, National Center for Injury Prevention and Control.

2. Selassie, A.W., et al., *Incidence of Long-term Disability Following Traumatic Brain Injury Hospitalization, United States, 2003.* The Journal of head trauma rehabilitation, 2008. **23**(2): p. 123-131.

3. Morales, D., et al., *Experimental models of traumatic brain injury: do we really need to build a better mousetrap?* Neuroscience, 2005. **136**(4): p. 971-989.

4. Sharma, A.P., *Penetrating brain injury.* Journal of Lumbini Medical College, 2013. **1**(2): p. 112-117.

5. Teasdale, G. and B. Jennett, *Assessment of coma and impaired consciousness: a practical scale.* The Lancet, 1974. **304**(7872): p. 81-84.

6. Jones, C., *Glasgow coma scale*. 1979, LWW.

7. Mena, J.H., et al., *Effect of the modified Glasgow Coma Scale score criteria for mild traumatic brain injury on mortality prediction: comparing classic and modified Glasgow Coma Scale score model scores of 13.* The Journal of trauma, 2011. **71**(5): p. 1185.

8. Davis, A.E., *Mechanisms of traumatic brain injury: biomechanical, structural and cellular considerations.* Critical care nursing quarterly, 2000. **23**(3): p. 1-13.

9. Gaetz, M., *The neurophysiology of brain injury.* Clinical Neurophysiology, 2004. **115**(1): p. 4-18.

10. Greve, M.W. and B.J. Zink, *Pathophysiology of traumatic brain injury.* Mount Sinai Journal of Medicine: A Journal of Translational and Personalized Medicine, 2009. **76**(2): p. 97-104.

11. Raghupathi, R., D.I. Graham, and T.K. McIntosh, *Apoptosis after traumatic brain injury.* Journal of neurotrauma, 2000. **17**(10): p. 927-938.

12. Palmer, A.M., et al., *Traumatic Brain Injury-Induced Excitotoxicity Assessed in a Controlled Cortical Impact Model.* Journal of neurochemistry, 1993. **61**(6): p. 2015-2024.

13. O'Connell, K.M. and M.T. Littleton-Kearney, *The role of free radicals in traumatic brain injury.* Biological research for nursing, 2013. **15**(3): p. 253-263.

14. Marmarou, A., et al., *Impact of ICP instability and hypotension on outcome in patients with severe head trauma.* Special Supplements, 1991. **75**(1S): p. S59-S66.

15. Stahel, P.F., W.R. Smith, and E.E. Moore, *Hypoxia and hypotension, the "lethal duo" in traumatic brain injury: implications for prehospital care.* Intensive care medicine, 2008. **34**(3): p. 402-404.

16. Chodobski, A., B.J. Zink, and J. Szmydynger-Chodobska, *Blood–brain barrier pathophysiology in traumatic brain injury.* Translational stroke research, 2011. **2**(4): p. 492-516.

17. Newcombe, V.F., et al., *Microstructural basis of contusion expansion in traumatic brain injury: insights from diffusion tensor imaging.* Journal of Cerebral Blood Flow & Metabolism, 2013. **33**(6): p. 855-862.

18. Kurland, D., et al., *Hemorrhagic progression of a contusion after traumatic brain injury: a review.* Journal of neurotrauma, 2012. **29**(1): p. 19-31.

19. Plesnila, N., et al., *Relative cerebral blood flow during the secondary expansion of a cortical lesion in rats.* Neuroscience letters, 2003. **345**(2): p. 85-88.

20. Ohab, J.J., et al., *A neurovascular niche for neurogenesis after stroke.* J Neurosci, 2006. **26**(50): p. 13007-16.

21. Algattas, H. and J.H. Huang, *Traumatic brain injury pathophysiology and treatments: early, intermediate, and late phases post-injury.* International journal of molecular sciences, 2013. **15**(1): p. 309-341.

22. Alvis-Miranda, H., S.M. Castellar-Leones, and L.R. Moscote-Salazar, *Decompressive craniectomy and traumatic brain injury: a review.* Bulletin of emergency & trauma, 2013. **1**(2): p. 60.

23. Peterson, K., S. Carson, and N. Carney, *Hypothermia treatment for traumatic brain injury: a systematic review and meta-analysis.* Journal of neurotrauma, 2008. **25**(1): p. 62-71.

24. Maas, A.I., B. Roozenbeek, and G.T. Manley, *Clinical trials in traumatic brain injury: past experience and current developments.* Neurotherapeutics, 2010. **7**(1): p. 115-126.

25. Loane, D.J. and A.I. Faden, *Neuroprotection for traumatic brain injury: translational challenges and emerging therapeutic strategies.* Trends in pharmacological sciences, 2010. **31**(12): p. 596-604.

26. Sayeed, I. and D.G. Stein, *Progesterone as a neuroprotective factor in traumatic and ischemic brain injury.* Progress in Brain Research, 2009. **175**: p. 219-237.

27. Stein, D. and P. Hurn, *Effects of Sex Steroids on Damaged Neural Systems-69.* 2009.

28. Stein, D., *Progesterone in the treatment of acute traumatic brain injury: a clinical perspective and update.* Neuroscience, 2011. **191**: p. 101-106.

29. Hirst, J.J., et al., *Stress in pregnancy: a role for neuroactive steroids in protecting the fetal and neonatal brain.* Developmental neuroscience, 2009. **31**(5): p. 363-377.

30. Li, L.M., D.K. Menon, and T. Janowitz, *Cross-sectional analysis of data from the US clinical trials database reveals poor translational clinical trial effort for traumatic brain injury, compared with stroke.* PloS one, 2014. **9**(1): p. e84336.

31. Wright, D.W., et al., *Very early administration of progesterone for acute traumatic brain injury.* New England Journal of Medicine, 2014. **371**(26): p. 2457-2466.

32. Skolnick, B.E., et al., *A clinical trial of progesterone for severe traumatic brain injury.* New England Journal of Medicine, 2014. **371**(26): p. 2467-2476.

33. Xiong, Y., A. Mahmood, and M. Chopp, *Animal models of traumatic brain injury.* Nature Reviews Neuroscience, 2013. **14**(2): p. 128-142.

34. Lighthall, J.W., *Controlled cortical impact: a new experimental brain injury model.* Journal of neurotrauma, 1988. **5**(1): p. 1-15.

35. Brody, D.L., et al., *Electromagnetic controlled cortical impact device for precise, graded experimental traumatic brain injury.* Journal of neurotrauma, 2007. **24**(4): p. 657-673.

36. Dixon, C.E., et al., *A controlled cortical impact model of traumatic brain injury in the rat.* Journal of neuroscience methods, 1991. **39**(3): p. 253-262.

37. Kochanek, P.M., et al., *Cerebral blood flow at one year after controlled cortical impact in rats: assessment by magnetic resonance imaging.* Journal of neurotrauma, 2002. **19**(9): p. 1029-1037.

38. Saatman, K.E., et al., *Differential behavioral and histopathological responses to graded cortical impact injury in mice.* Journal of neurotrauma, 2006. **23**(8): p. 1241-1253.

39. Washington, P.M., et al., *The effect of injury severity on behavior: a phenotypic study of cognitive and emotional deficits after mild, moderate, and severe controlled cortical impact injury in mice.* Journal of neurotrauma, 2012. **29**(13): p. 2283-2296.

40. Dixon, C.E., et al., *A fluid percussion model of experimental brain injury in the rat.* Journal of neurosurgery, 1987. **67**(1): p. 110-119.

41. Mcintosh, T.K., et al., *Traumatic brain injury in the rat: characterization of a midline fluid-percussion model.* Central Nervous System Trauma, 1987. **4**(2): p. 119-134.

42. Thompson, H.J., et al., *Lateral fluid percussion brain injury: a 15-year review and evaluation.* Journal of neurotrauma, 2005. **22**(1): p. 42-75.

43. Hamm, R.J., *Neurobehavioral assessment of outcome following traumatic brain injury in rats: an evaluation of selected measures.* Journal of neurotrauma, 2001. **18**(11): p. 1207-1216.

44. Feeney, D.M., et al., *Responses to cortical injury: I. Methodology and local effects of contusions in the rat.* Brain research, 1981. **211**(1): p. 67-77.

45. Chen, Y., et al., *An experimental model of closed head injury in mice: pathophysiology, histopathology, and cognitive deficits.* Journal of neurotrauma, 1996. **13**(10): p. 557-568.

46. Marmarou, A., et al., *A new model of diffuse brain injury in rats: Part I: Pathophysiology and biomechanics.* Journal of neurosurgery, 1994. **80**(2): p. 291-300.

47. Shapira, Y., et al., *Experimental closed head injury in rats: mechanical, pathophysiologic, and neurologic properties.* Critical care medicine, 1988. **16**(3): p. 258-265.

48. Tang, Y.-p., et al., *A concussive-like brain injury model in mice (II): selective neuronal loss in the cortex and hippocampus.* Journal of neurotrauma, 1997. **14**(11): p. 863-873.

49. Warden, D., *Military TBI during the Iraq and Afghanistan wars.* The Journal of head trauma rehabilitation, 2006. **21**(5): p. 398-402.

50. Benzinger, T.L., et al., *Blast-related brain injury: imaging for clinical and research applications: report of the 2008 St. Louis workshop.* Journal of neurotrauma, 2009. **26**(12): p. 2127-2144.

51. Reneer, D.V., et al., *A multi-mode shock tube for investigation of blast-induced traumatic brain injury.* Journal of neurotrauma, 2011. **28**(1): p. 95-104.

52. Kuehn, R., et al., *Rodent model of direct cranial blast injury.* Journal of neurotrauma, 2011. **28**(10): p. 2155-2169.

53. Garman, R.H., et al., *Blast exposure in rats with body shielding is characterized primarily by diffuse axonal injury.* Journal of neurotrauma, 2011. **28**(6): p. 947-959.

54. Goldstein, L.E., et al., *Chronic traumatic encephalopathy in blast-exposed military veterans and a blast neurotrauma mouse model.* Science translational medicine, 2012. **4**(134): p. 134ra60-134ra60.

55. Lange, R.T., et al., *Risk factors for postconcussion symptom reporting after traumatic brain injury in US military service members.* Journal of neurotrauma, 2013. **30**(4): p. 237-246.

56. DeKosky, S.T., et al., *Acute and chronic traumatic encephalopathies: pathogenesis and biomarkers.* Nature Reviews Neurology, 2013. **9**(4): p. 192-200.

57. MacDonald, C.L., et al., *5-Year imaging sequelae of concussive blast injury and relation to early clinical outcome.* NeuroImage: Clinical, 2017. **14**: p. 371-378.

58. Taylor, B.C., et al., *Prevalence and costs of co-occurring traumatic brain injury with and without psychiatric disturbance and pain among Afghanistan and Iraq War Veteran VA users.* Medical care, 2012. **50**(4): p. 342-346.

59. Hermann, D.M. and M. Chopp, *Promoting brain remodelling and plasticity for stroke recovery: therapeutic promise and potential pitfalls of clinical translation.* The Lancet Neurology, 2012. **11**(4): p. 369-380.

60. Seri, B., et al., *Composition and organization of the SCZ: a large germinal layer containing neural stem cells in the adult mammalian brain.* Cerebral Cortex, 2006. **16**(suppl 1): p. i103-i111.

61. Ihrie, R.A. and A. Álvarez-Buylla, *Lake-front property: a unique germinal niche by the lateral ventricles of the adult brain.* Neuron, 2011. **70**(4): p. 674-686.

62. Young, C.C., et al., *Cellular and molecular determinants of stroke-induced changes in subventricular zone cell migration.* Antioxidants & redox signaling, 2011. **14**(10): p. 1877-1888.

63. Spalding, K.L., et al., *Dynamics of hippocampal neurogenesis in adult humans.* Cell, 2013. **153**(6): p. 1219-1227.

64. Dizon, M.L. and F.G. Szele, *The subventricular zone responds dynamically to mechanical brain injuries*, in *Mammalian Subventricular Zones*. 2006, Springer. p. 210-241.

65. Chang, E.H., et al., *Traumatic brain injury activation of the adult subventricular zone neurogenic niche.* Frontiers in Neuroscience, 2016. **10**.

66. McKay, R., *Stem cells in the central nervous system.* Science, 1997. **276**(5309): p. 66-71.

67. Fisher, L.J., *Neural precursor cells: applications for the study and repair of the central nervous system.* Neurobiology of disease, 1997. **4**(1): p. 1-22.

68. Gage, F.H., *Mammalian neural stem cells.* Science, 2000. **287**(5457): p. 1433-1438.

69. Gross, C.G., *Neurogenesis in the adult brain: death of a dogma.* Nature Reviews Neuroscience, 2000. **1**(1): p. 67-73.

70. Temple, S., *Division and differentiation of isolated CNS blast cells in microculture.* Nature, 1989. **340**(6233): p. 471-3.

71. Reynolds, B.A. and S. Weiss, *Generation of neurons and astrocytes from isolated cells of the adult mammalian central nervous system.* science, 1992. **255**(5052): p. 1707.

72. Wichterle, H., J.M. García-Verdugo, and A. Alvarez-Buylla, *Direct evidence for homotypic, glia-independent neuronal migration.* Neuron, 1997. **18**(5): p. 779-791.

73. Ponti, G., et al., *Cell cycle and lineage progression of neural progenitors in the ventricular-subventricular zones of adult mice.* Proceedings of the National Academy of Sciences, 2013. **110**(11): p. E1045-E1054.

74. Magavi, S.S., B.R. Leavitt, and J.D. Macklis, *Induction of neurogenesis in the neocortex of adult mice.* Nature, 2000. **405**(6789): p. 951-955.

75. Imitola, J., et al., *Directed migration of neural stem cells to sites of CNS injury by the stromal cell-derived factor 1α/CXC chemokine receptor 4 pathway.* Proceedings of the National Academy of Sciences, 2004. **101**(52): p. 18117-18122.

76. Obernier, K., C.K. Tong, and A. Alvarez-Buylla, *Restricted nature of adult neural stem cells: re-evaluation of their potential for brain repair.* Adult neurogenesis twenty years later: physiological function versus brain repair, 2015: p. 21.

77. Wei, Z.Z., et al., *Neuroprotective and regenerative roles of intranasal Wnt-3a Administration after focal ischemic stroke in mice.* Journal of Cerebral Blood Flow & Metabolism, 2017: p. 0271678X17702669.

78. Haas, S., N. Weidner, and J. Winkler, *Adult stem cell therapy in stroke.* Current opinion in neurology, 2005. **18**(1): p. 59-64.

79. Taylor, S.R., et al., *Maturation-dependent response of neurogenesis after traumatic brain injury in children: Laboratory investigation.* Journal of Neurosurgery: Pediatrics, 2013. **12**(6): p. 545-554.

80. Sahota, P. and S.I. Savitz, *Investigational therapies for ischemic stroke: neuroprotection and neurorecovery.* Neurotherapeutics, 2011. **8**(3): p. 434-451.

81. Prindull, G. and B. Prindull, *Haematopoietic stem cells (CFUc) in human cord blood.* Acta Paediatrica, 1978. **67**(4): p. 413-416.

82. Hilton, D., et al., *Myeloid leukemia inhibitory factor maintains the developmental potential of embryonic stem cells.* Nature, 1988. **336**: p. 684-687.

83. Doetschman, T., P. Williams, and N. Maeda, *Establishment of hamster blastocyst-derived embryonic stem (ES) cells.* Developmental biology, 1988. **127**(1): p. 224-227.

84. Takahashi, K. and S. Yamanaka, *Induction of pluripotent stem cells from mouse embryonic and adult fibroblast cultures by defined factors.* cell, 2006. **126**(4): p. 663-676.

85. Dekmak, A., et al., *Stem cells and combination therapy for the treatment of traumatic brain injury.* Behavioural Brain Research, 2016. **4328**(16): p. 31340-7.

86. Deveau, T., S.P. Yu, and L. Wei, *Cellular Therapy for Ischemic Stroke*, in *Translational Stroke Research*. 2012, Springer. p. 777-814.

87. Friendenstein, A., K. Petrakova, and A. Kurolesova, *Heterotopic transplants of bone marrow, Analysis of precursor cells, for osteogenic and hematotoxic tissues.* Transplantation, 1968. **6**(4): p. 230-247.

88. Thomson, J.A., et al., *Embryonic stem cell lines derived from human blastocysts.* science, 1998. **282**(5391): p. 1145-1147.

89. Thomson, J.A., et al., *Isolation of a primate embryonic stem cell line.* Proceedings of the National Academy of Sciences, 1995. **92**(17): p. 7844-7848.

90. Odorico, J.S., D.S. Kaufman, and J.A. Thomson, *Multilineage differentiation from human embryonic stem cell lines.* Stem cells, 2001. **19**(3): p. 193-204.

91. Yamanaka, S. and H.M. Blau, *Nuclear reprogramming to a pluripotent state by three approaches.* Nature, 2010. **465**(7299): p. 704-712.

92. Chu, G., *Embryonic stem-cell research and the moral status of embryos.* Internal medicine journal, 2003. **33**(11): p. 530-531.

93. Jain, K.K., *Ethical and regulatory aspects of embryonic stem cell research.* Expert opinion on biological therapy, 2005. **5**(2): p. 153-162.

94. Chen, J., et al., *Transfusion of CXCR4-primed endothelial progenitor cells reduces cerebral ischemic damage and promotes repair in db/db diabetic mice.* PLoS One, 2012. **7**(11): p. e50105.

95. Liu, Y., et al., *Medial ganglionic eminence-like cells derived from human embryonic stem cells correct learning and memory deficits.* Nature biotechnology, 2013. **31**(5): p. 440-447.

96. Nilbratt, M., et al., *Neurotrophic factors promote cholinergic differentiation in human embryonic stem cell-derived neurons.* Journal of cellular and molecular medicine, 2010. **14**(6b): p. 1476-1484.

97. Bissonnette, C.J., et al., *The controlled generation of functional basal forebrain cholinergic neurons from human embryonic stem cells.* Stem Cells, 2011. **29**(5): p. 802-811.

98. Roy, N.S., et al., *Enhancer-specified GFP-based FACS purification of human spinal motor neurons from embryonic stem cells.* Experimental neurology, 2005. **196**(2): p. 224-234.

99. Li, X.J., et al., *Directed differentiation of ventral spinal progenitors and motor neurons from human embryonic stem cells by small molecules.* Stem Cells, 2008. **26**(4): p. 886-893.

100. Hu, B.-Y., et al., *Human oligodendrocytes from embryonic stem cells: conserved SHH signaling networks and divergent FGF effects.* Development, 2009. **136**(9): p. 1443-1452.

101. Patani, R., et al., *Retinoid-independent motor neurogenesis from human embryonic stem cells reveals a medial columnar ground state.* Nature communications, 2011. **2**: p. 214.

102. Lu, J., et al., *Generation of serotonin neurons from human pluripotent stem cells.* Nature biotechnology, 2016. **34**(1): p. 89-94.

103. Hu, B.-Y. and S.-C. Zhang, *Differentiation of spinal motor neurons from pluripotent human stem cells.* Nature protocols, 2009. **4**(9): p. 1295-1304.

104. Krencik, R., et al., *Specification of transplantable astroglial subtypes from human pluripotent stem cells.* Nature biotechnology, 2011. **29**(6): p. 528-534.

105. Lee, H., et al., *Directed differentiation and transplantation of human embryonic stem cell-derived motoneurons.* Stem cells, 2007. **25**(8): p. 1931-1939.

106. Goldman, S.A. and N.J. Kuypers, *How to make an oligodendrocyte.* Development, 2015. **142**(23): p. 3983-3995.

107. Benraiss, A. and S.A. Goldman, *Cellular therapy and induced neuronal replacement for Huntington's disease.* Neurotherapeutics, 2011. **8**(4): p. 577-590.

108. Barker, R.A., et al., *The long-term safety and efficacy of bilateral transplantation of human fetal striatal tissue in patients with mild to moderate Huntington's disease.* Journal of Neurology, Neurosurgery & Psychiatry, 2013. **84**(6): p. 657-665.

109. Wang, S., et al., *Human iPSC-derived oligodendrocyte progenitor cells can myelinate and rescue a mouse model of congenital hypomyelination.* Cell stem cell, 2013. **12**(2): p. 252-264.

110. Barker, R.A., J. Drouin-Ouellet, and M. Parmar, *Cell-based therapies for Parkinson disease [mdash] past insights and future potential.* Nature Reviews Neurology, 2015. **11**(9): p. 492-503.

111. Z Barkho, B. and X. Zhao, *Adult neural stem cells: response to stroke injury and potential for therapeutic applications.* Current stem cell research & therapy, 2011. **6**(4): p. 327-338.

112. Hentze, H., R. Graichen, and A. Colman, *Cell therapy and the safety of embryonic stem cell-derived grafts.* Trends in biotechnology, 2007. **25**(1): p. 24-32.

113. Liu, H. and S.-C. Zhang, *Specification of neuronal and glial subtypes from human pluripotent stem cells.* Cellular and Molecular Life Sciences, 2011. **68**(24): p. 3995-4008.

114. Yamanaka, S., *Induced pluripotent stem cells: past, present, and future.* Cell stem cell, 2012. **10**(6): p. 678-684.

115. Lomax, G.P. and S.R. Peckman, *Stem cell policy exceptionalism: proceed with caution.* Stem Cell Reviews and Reports, 2012. **8**(2): p. 299-304.

116. Pei, Y., et al., *A platform for rapid generation of single and multiplexed reporters in human iPSC lines.* Scientific reports, 2015. **5**.

117. Chambers, S.M., et al., *Combined small-molecule inhibition accelerates developmental timing and converts human pluripotent stem cells into nociceptors.* Nature biotechnology, 2012. **30**(7): p. 715-720.

118. Ben-David, U., et al., *Selective elimination of human pluripotent stem cells by an oleate synthesis inhibitor discovered in a high-throughput screen.* Cell Stem Cell, 2013. **12**(2): p. 167-179.

119. Ranga, A., N. Gjorevski, and M.P. Lutolf, *Drug discovery through stem cell-based organoid models.* Advanced drug delivery reviews, 2014. **69**: p. 19-28.

120. Corti, S., et al., *Human pluripotent stem cells as tools for neurodegenerative and neurodevelopmental disease modeling and drug discovery.* Expert opinion on drug discovery, 2015. **10**(6): p. 615-629.

121. Zhao, T., et al., *Immunogenicity of induced pluripotent stem cells.* Nature, 2011. **474**(7350): p. 212-215.

122. Lee, G., et al., *Modelling pathogenesis and treatment of familial dysautonomia using patient-specific iPSCs.* nature, 2009. **461**(7262): p. 402-406.

123. Marchetto, M.C., et al., *A model for neural development and treatment of Rett syndrome using human induced pluripotent stem cells.* Cell, 2010. **143**(4): p. 527-539.

124. Brennand, K.J., et al., *Modelling schizophrenia using human induced pluripotent stem cells.* Nature, 2011. **473**(7346): p. 221-225.

125. Mitne-Neto, M., et al., *Downregulation of VAPB expression in motor neurons derived from induced pluripotent stem cells of ALS8 patients.* Human molecular genetics, 2011. **20**(18): p. 3642-3652.

126. Nguyen, H.N., et al., *LRRK2 mutant iPSC-derived DA neurons demonstrate increased susceptibility to oxidative stress.* Cell stem cell, 2011. **8**(3): p. 267-280.

127. Chae, J.-I., et al., *Quantitative proteomic analysis of induced pluripotent stem cells derived from a human Huntington's disease patient.* Biochemical Journal, 2012. **446**(3): p. 359-371.

128. Israel, M.A., et al., *Probing sporadic and familial Alzheimer/'s disease using induced pluripotent stem cells.* Nature, 2012. **482**(7384): p. 216-220.

129. Ricciardi, S., et al., *CDKL5 ensures excitatory synapse stability by reinforcing NGL-1–PSD95 interaction in the postsynaptic compartment and is impaired in patient iPSC-derived neurons.* Nature cell biology, 2012. **14**(9): p. 911-923.

130. Lowenthal, J., et al., *Specimen collection for induced pluripotent stem cell research: harmonizing the approach to informed consent.* Stem cells translational medicine, 2012. **1**(5): p. 409-421.

131. Altman, J., *Are new neurons formed in the brains of adult mammals.* Science, 1962. **135**(3509): p. 1127-1128.

132. Altman, J., *Autoradiographic and histological studies of postnatal neurogenesis. IV. Cell proliferation and migration in the anterior forebrain, with special reference to persisting neurogenesis in the olfactory bulb.* Journal of Comparative Neurology, 1969. **137**(4): p. 433-457.

133. Ming, G.-l. and H. Song, *Adult neurogenesis in the mammalian central nervous system.* Annu. Rev. Neurosci., 2005. **28**: p. 223-250.

134. Taupin, P., *Therapeutic potential of adult neural stem cells.* Recent patents on CNS drug discovery, 2006. **1**(3): p. 299-303.

135. Rolfe, A. and D. Sun, *Stem cell therapy in brain trauma: implications for repair and regeneration of injured brain in experimental TBI models*, in *Brain Neurotrauma: Molecular, Neuropsychological, and Rehabilitation Aspects*. 2015, CRC Press. p. 587-596.

136. De Filippis, L. and D. Delia, *Hypoxia in the regulation of neural stem cells.* Cellular and Molecular Life Sciences, 2011. **68**(17): p. 2831-2844.

137. Massirer, K.B., et al., *Maintenance and differentiation of neural stem cells.* Wiley Interdisciplinary Reviews: Systems Biology and Medicine, 2011. **3**(1): p. 107-114.

138. Hsu, Y.-C., D.-C. Lee, and I.-M. Chiu, *Neural stem cells, neural progenitors, and neurotrophic factors.* Cell transplantation, 2007. **16**(2): p. 133-150.

139. Kazanis, I., J. Lathia, and L. Moss, *The neural stem cell microenvironment.* 2008.

140. Bithell, A. and B.P. Williams, *Neural stem cells and cell replacement therapy: making the right cells.* Clinical science, 2005. **108**(1): p. 13-22.

141. Chang, C.-P., et al., *Hypoxic preconditioning enhances the therapeutic potential of the secretome from cultured human mesenchymal stem cells in experimental traumatic brain injury.* Clinical Science, 2013. **124**(3): p. 165-176.

142. Horwitz, E., et al., *Clarification of the nomenclature for MSC: The International Society for Cellular Therapy position statement.* Cytotherapy, 2005. **7**(5): p. 393-395.

143. Salem, H.K. and C. Thiemermann, *Mesenchymal stromal cells: current understanding and clinical status.* Stem cells, 2010. **28**(3): p. 585-596.

144. Gutiérrez-Fernández, M., et al., *Effects of intravenous administration of allogenic bone marrow-and adipose tissue-derived mesenchymal stem cells on functional recovery and brain repair markers in experimental ischemic stroke.* Stem cell research & therapy, 2013. **4**(1): p. 11.

145. Walker, P.A., et al., *Progenitor cell therapies for traumatic brain injury: barriers and opportunities in translation.* Disease models & mechanisms, 2009. **2**(1-2): p. 23-38.

146. Zeng, X., et al., *Dopaminergic differentiation of human embryonic stem cells.* Stem cells, 2004. **22**(6): p. 925-940.

147. Ma, L., Y. Liu, and S.-C. Zhang, *Directed differentiation of dopamine neurons from human pluripotent stem cells.* Human Pluripotent Stem Cells: Methods and Protocols, 2011: p. 411-418.

148. Liu, Y., et al., *Directed differentiation of forebrain GABA interneurons from human pluripotent stem cells.* Nature protocols, 2013. **8**(9): p. 1670-1679.

149. Dhara, S.K. and S.L. Stice, *Neural differentiation of human embryonic stem cells.* Journal of cellular biochemistry, 2008. **105**(3): p. 633-640.

150. Ying, Q.-L., et al., *Conversion of embryonic stem cells into neuroectodermal precursors in adherent monoculture.* Nature biotechnology, 2003. **21**(2): p. 183-186.

151. Bain, G., et al., *Embryonic stem cells express neuronal properties in vitro.* Developmental biology, 1995. **168**(2): p. 342-357.

152. Mohamad, O., et al., *Efficient neuronal differentiation of mouse ES and iPS cells using a rotary cell culture protocol.* Differentiation, 2013. **86**(4): p. 149-158.

153. Okabe, S., et al., *Development of neuronal precursor cells and functional postmitotic neurons from embryonic stem cells in vitro.* Mechanisms of development, 1996. **59**(1): p. 89-102.

154. Lee, S.-H., et al., *Efficient generation of midbrain and hindbrain neurons from mouse embryonic stem cells.* Nature biotechnology, 2000. **18**(6): p. 675-679.

155. Hess, D.C. and C.V. Borlongan, *Cell-based therapy in ischemic stroke.* Expert review of neurotherapeutics, 2008. **8**(8): p. 1193-1201.

156. Mahmood, A., D. Lu, and M. Chopp, *Marrow stromal cell transplantation after traumatic brain injury promotes cellular proliferation within the brain.* Neurosurgery, 2004. **55**(5): p. 1185-1193.

157. Gao, J., et al., *The dynamic in vivo distribution of bone marrow-derived mesenchymal stem cells after infusion.* Cells Tissues Organs, 2001. **169**(1): p. 12-20.

158. Allers, C., et al., *Dynamic of distribution of human bone marrow-derived mesenchymal stem cells after transplantation into adult unconditioned mice.* Transplantation, 2004. **78**(4): p. 503-508.

159. Tolar, J., et al., *Host factors that impact the biodistribution and persistence of multipotent adult progenitor cells.* Blood, 2006. **107**(10): p. 4182-4188.

160. Bliss, T.M., R.H. Andres, and G.K. Steinberg, *Optimizing the success of cell transplantation therapy for stroke.* Neurobiology of disease, 2010. **37**(2): p. 275-283.

161. Barbash, I.M., et al., *Systemic delivery of bone marrow–derived mesenchymal stem cells to the infarcted myocardium.* Circulation, 2003. **108**(7): p. 863-868.

162. Li, Y., et al., *Treatment of stroke in rat with intracarotid administration of marrow stromal cells.* Neurology, 2001. **56**(12): p. 1666-1672.

163. Walczak, P., et al., *Dual-modality monitoring of targeted intraarterial delivery of mesenchymal stem cells after transient ischemia.* Stroke, 2008. **39**(5): p. 1569-1574.

164. Hanson, L.R., et al., *Intranasal administration of CNS therapeutics to awake mice.* JoVE (Journal of Visualized Experiments), 2013(74): p. e4440-e4440.

165. Wei, N., et al., *Delayed intranasal delivery of hypoxic-preconditioned bone marrow mesenchymal stem cells enhanced cell homing and therapeutic benefits after ischemic stroke in mice.* Cell transplantation, 2013. **22**(6): p. 977-991.

166. Sun, J., et al., *Intranasal delivery of hypoxia-preconditioned bone marrow-derived mesenchymal stem cells enhanced regenerative effects after intracerebral hemorrhagic stroke in mice.* Experimental neurology, 2015. **272**: p. 78-87.

167. Henkin, R.I., *Intranasal delivery to the brain.* Nature biotechnology, 2011. **29**(6): p. 480-480.

168. Danielyan, L., et al., *Intranasal delivery of cells to the brain.* European journal of cell biology, 2009. **88**(6): p. 315-324.

169. Donega, V., et al., *Intranasal mesenchymal stem cell treatment for neonatal brain damage: long-term cognitive and sensorimotor improvement.* PloS one, 2013. **8**(1): p. e51253.

170. Danielyan, L., et al., *Therapeutic efficacy of intranasally delivered mesenchymal stem cells in a rat model of Parkinson disease.* Rejuvenation research, 2011. **14**(1): p. 3-16.

171. Kabadi, S.V. and A.I. Faden, *Neuroprotective strategies for traumatic brain injury: improving clinical translation.* International journal of molecular sciences, 2014. **15**(1): p. 1216-1236.

172. Tajiri, N., et al., *Intravenous transplants of human adipose-derived stem cell protect the brain from traumatic brain injury-induced neurodegeneration and motor and cognitive impairments: cell graft biodistribution and soluble factors in young and aged rats.* Journal of Neuroscience, 2014. **34**(1): p. 313-326.

173. Lozano, D., et al., *Neuroinflammatory responses to traumatic brain injury: etiology, clinical consequences, and therapeutic opportunities.* Neuropsychiatr Dis Treat, 2015. **11**(97): p. 106.

174. Yu, S., et al., *Severity of controlled cortical impact traumatic brain injury in rats and mice dictates degree of behavioral deficits.* Brain research, 2009. **1287**: p. 157-163.

175. Acosta, S.A., et al., *Influence of post-traumatic stress disorder on neuroinflammation and cell proliferation in a rat model of traumatic brain injury.* PloS one, 2013. **8**(12): p. e81585.

176. Acosta, S.A., et al., *Long-term upregulation of inflammation and suppression of cell proliferation in the brain of adult rats exposed to traumatic brain injury using the controlled cortical impact model.* PloS one, 2013. **8**(1): p. e53376.

177. Molcanyi, M., et al., *Trauma-associated inflammatory response impairs embryonic stem cell survival and integration after implantation into injured rat brain.* Journal of neurotrauma, 2007. **24**(4): p. 625-637.

178. Zhao, B., et al., *Changes of BDNF expression in neurons in traumatic brain injury rats.* Sichuan da xue xue bao. Yi xue ban= Journal of Sichuan University. Medical science edition, 2012. **43**(2): p. 236-9, 249.

179. Kim, H.-J., J.-H. Lee, and S.-H. Kim, *Therapeutic effects of human mesenchymal stem cells on traumatic brain injury in rats: secretion of neurotrophic factors and inhibition of apoptosis.* Journal of neurotrauma, 2010. **27**(1): p. 131-138.

180. van Velthoven, C.T., et al., *Mesenchymal stem cell transplantation attenuates brain injury after neonatal stroke.* Stroke, 2013. **44**(5): p. 1426-1432.

181. Kurozumi, K., et al., *Mesenchymal stem cells that produce neurotrophic factors reduce ischemic damage in the rat middle cerebral artery occlusion model.* Molecular Therapy, 2005. **11**(1): p. 96-104.

182. Kurozumi, K., et al., *BDNF gene-modified mesenchymal stem cells promote functional recovery and reduce infarct size in the rat middle cerebral artery occlusion model.* Molecular Therapy, 2004. **9**(2): p. 189-197.

183. Xiong, L.-L., et al., *Neural Stem Cell Transplantation Promotes Functional Recovery from Traumatic Brain Injury via Brain Derived Neurotrophic Factor-Mediated Neuroplasticity.* Molecular Neurobiology, 2017: p. 1-16.

184. Horie, N., et al., *Transplanted Stem Cell-Secreted VEGF Effects Post-Stroke Recovery*. Inflammation, and Vascular Repair. Stem Cells, 2011. **29**: p. 584.

185. Li, Y., et al., *VEGF-B inhibits apoptosis via VEGFR-1-mediated suppression of the expression of BH3-only protein genes in mice and rats.* Journal of Clinical Investigation, 2008. **118**(3): p. 913-923.

186. Wang, L., et al., *Neural progenitor cells treated with EPO induce angiogenesis through the production of VEGF.* Journal of Cerebral Blood Flow and Metabolism, 2008. **28**(7): p. 1361-1368.

187. Zigova, T., et al., *Intraventricular administration of BDNF increases the number of newly generated neurons in the adult olfactory bulb.* Molecular and cellular neurosciences, 1998. **11**(4): p. 234-45.

188. Pencea, V., et al., *Infusion of brain-derived neurotrophic factor into the lateral ventricle of the adult rat leads to new neurons in the parenchyma of the striatum, septum, thalamus, and hypothalamus.* The Journal of neuroscience : the official journal of the Society for Neuroscience, 2001. **21**(17): p. 6706-17.

189. Nonomura, T., et al., *Signaling pathways and survival effects of BDNF and NT-3 on cultured cerebellar granule cells.* Developmental Brain Research, 1996. **97**(1): p. 42-50.

190. Hasan, A., et al., *Mesenchymal Stem Cells in the Treatment of Traumatic Brain Injury.* Frontiers in Neurology, 2017. **8**.

191. Galindo, L.T., et al., *Mesenchymal stem cell therapy modulates the inflammatory response in experimental traumatic brain injury.* Neurology research international, 2011. **2011**.

192. Augello, A., et al., *Bone marrow mesenchymal progenitor cells inhibit lymphocyte proliferation by activation of the programmed death 1 pathway.* European journal of immunology, 2005. **35**(5): p. 1482-1490.

193. Di Nicola, M., et al., *Human bone marrow stromal cells suppress T-lymphocyte proliferation induced by cellular or nonspecific mitogenic stimuli.* Blood, 2002. **99**(10): p. 3838-3843.

194. Zappia, E., et al., *Mesenchymal stem cells ameliorate experimental autoimmune encephalomyelitis inducing T-cell anergy.* Blood, 2005. **106**(5): p. 1755-1761.

195. Corcione, A., et al., *Human mesenchymal stem cells modulate B-cell functions.* Blood, 2006. **107**(1): p. 367-372.

196. Aggarwal, S. and M.F. Pittenger, *Human mesenchymal stem cells modulate allogeneic immune cell responses.* Blood, 2005. **105**(4): p. 1815-1822.

197. Honmou, O., et al., *Intravenous administration of auto serum-expanded autologous mesenchymal stem cells in stroke.* Brain, 2011: p. awr063.

198. Whitney, N.P., et al., *Inflammation mediates varying effects in neurogenesis: relevance to the pathogenesis of brain injury and neurodegenerative disorders.* Journal of neurochemistry, 2009. **108**(6): p. 1343-1359.

199. Bishop, E.T., et al., *An in vitro model of angiogenesis: basic features.* Angiogenesis, 1999. **3**(4): p. 335-44.

200. Horie, N., et al., *Transplanted Stem Cell-Secreted VEGF Effects Post-Stroke Recovery, Inflammation, and Vascular Repair.* Stem Cells, 2011.

201. Oki, K., et al., *Human-induced pluripotent stem cells form functional neurons and improve recovery after grafting in stroke-damaged brain.* Stem Cells, 2012. **30**(6): p. 1120-33.

202. Wang, Y.M., et al., *VEGF overexpression induces post-ischaemic neuroprotection, but facilitates haemodynamic steal phenomena.* Brain, 2005. **128**: p. 52-63.

203. Li, Y., et al., *Erythropoietin-induced neurovascular protection, angiogenesis, and cerebral blood flow restoration after focal ischemia in mice.* J Cereb Blood Flow Metab, 2007. **27**(5): p. 1043-54.

204. Duncan, K., et al., *Stem cell-paved biobridges facilitate stem transplant and host brain cell interactions for stroke therapy.* brain research, 2015. **1623**: p. 160-165.

205. Kim, J., et al., *Functional integration of dopaminergic neurons directly converted from mouse fibroblasts.* Cell stem cell, 2011. **9**(5): p. 413-419.

206. Tønnesen, J., et al., *Functional integration of grafted neural stem cell-derived dopaminergic neurons monitored by optogenetics in an in vitro Parkinson model.* PloS one, 2011. **6**(3): p. e17560.

207. Kim, J.-H., et al., *Dopamine neurons derived from embryonic stem cells function in an animal model of Parkinson's disease.* Nature, 2002. **418**(6893): p. 50-56.

208. Wernig, M., et al., *Neurons derived from reprogrammed fibroblasts functionally integrate into the fetal brain and improve symptoms of rats with Parkinson's disease.* Proceedings of the National Academy of Sciences, 2008. **105**(15): p. 5856-5861.

209. Steinbeck, J.A., et al., *Optogenetics enables functional analysis of human embryonic stem cell-derived grafts in a Parkinson's disease model.* Nature biotechnology, 2015. **33**(2): p. 204-209.

210. Park, K.I., et al., *Global gene and cell replacement strategies via stem cells*, in *Neural Stem Cells for Brain and Spinal Cord Repair*. 2003, Springer. p. 289-332.

211. Bellenchi, G.C., et al., *Adult neural stem cells: an endogenous tool to repair brain injury?* Journal of neurochemistry, 2013. **124**(2): p. 159-167.

212. Sun, D., *The potential of endogenous neurogenesis for brain repair and regeneration following traumatic brain injury.* Neural regeneration research, 2014. **9**(7): p. 688.

213. Riess, P., et al., *Embryonic stem cell transplantation after experimental traumatic brain injury dramatically improves neurological outcome, but may cause tumors.* Journal of neurotrauma, 2007. **24**(1): p. 216-225.

214. Ronne-Engstrom, E. and T. Winkler, *Continuous EEG monitoring in patients with traumatic brain injury reveals a high incidence of epileptiform activity.* Acta Neurologica Scandinavica, 2006. **114**(1): p. 47-53.

215. Hunt, R.F., S.W. Scheff, and B.N. Smith, *Posttraumatic epilepsy after controlled cortical impact injury in mice.* Experimental neurology, 2009. **215**(2): p. 243-252.

216. Mahmood, A., et al., *Long-term recovery after bone marrow stromal cell treatment of traumatic brain injury in rats.* Journal of neurosurgery, 2006. **104**(2): p. 272-277.

217. Mahmood, A., D. Lu, and M. Chopp, *Intravenous administration of marrow stromal cells (MSCs) increases the expression of growth factors in rat brain after traumatic brain injury.* Journal of neurotrauma, 2004. **21**(1): p. 33-39.

218. Mahmood, A., et al., *Treatment of traumatic brain injury in adult rats with intravenous administration of human bone marrow stromal cells.* Neurosurgery, 2003. **53**(3): p. 697-703.

219. Mahmood, A., et al., *Long-lasting benefits after treatment of traumatic brain injury (TBI) in rats with combination therapy of marrow stromal cells (MSCs) and simvastatin.* Journal of neurotrauma, 2008. **25**(12): p. 1441-1447.

220. Li, L., et al., *Transplantation of marrow stromal cells restores cerebral blood flow and reduces cerebral atrophy in rats with traumatic brain injury: in vivo MRI study.* Journal of neurotrauma, 2011. **28**(4): p. 535-545.

221. Harting, M.T., et al., *Intravenous mesenchymal stem cell therapy for traumatic brain injury: Laboratory investigation.* Journal of neurosurgery, 2009. **110**(6): p. 1189-1197.

222. Park, B.-N., et al., *Early distribution of intravenously injected mesenchymal stem cells in rats with acute brain trauma evaluated by 99m Tc-HMPAO labeling.* Nuclear medicine and biology, 2011. **38**(8): p. 1175-1182.

223. Yoon, J.-K., et al., *In vivo tracking of 111 In-labeled bone marrow mesenchymal stem cells in acute brain trauma model.* Nuclear medicine and biology, 2010. **37**(3): p. 381-388.

224. Mahmood, A., et al., *Human marrow stromal cell treatment provides long-lasting benefit after traumatic brain injury in rats.* Neurosurgery, 2005. **57**(5): p. 1026.

225. Qu, C., et al., *Treatment of traumatic brain injury in mice with marrow stromal cells.* Brain research, 2008. **1208**: p. 234-239.

226. Sanchez-Ramos, J., et al., *Adult bone marrow stromal cells differentiate into neural cells in vitro.* Experimental neurology, 2000. **164**(2): p. 247-256.

227. Haus, D.L., et al., *Transplantation of human neural stem cells restores cognition in an immunodeficient rodent model of traumatic brain injury.* Experimental neurology, 2016. **281**: p. 1-16.

228. Mahmood, A., et al., *Intracranial bone marrow transplantation after traumatic brain injury improving functional outcome in adult rats.* Journal of neurosurgery, 2001. **94**(4): p. 589-595.

229. Lu, D., et al., *Intraarterial administration of marrow stromal cells in a rat model of traumatic brain injury.* Journal of neurotrauma, 2001. **18**(8): p. 813-819.

230. Gao, J., et al., *Transplantation of primed human fetal neural stem cells improves cognitive function in rats after traumatic brain injury.* Experimental neurology, 2006. **201**(2): p. 281-292.

231. Kota, D.J., et al., *Propranolol and mesenchymal stromal cells combine to treat traumatic brain injury.* Stem cells translational medicine, 2016. **5**(1): p. 33-44.

232. Skardelly, M., et al., *Long-term benefit of human fetal neuronal progenitor cell transplantation in a clinically adapted model after traumatic brain injury.* Journal of neurotrauma, 2011. **28**(3): p. 401-414.

233. Hoane, M.R., et al., *Transplantation of neuronal and glial precursors dramatically improves sensorimotor function but not cognitive function in the traumatically injured brain.* Journal of neurotrauma, 2004. **21**(2): p. 163-174.

234. Wei, L., et al., *Stem Cell Transplantation Therapy for Multifaceted Therapeutic Benefits after Stroke.* Progress in Neurobiology, 2017.

235. Chau, M., et al., *Regeneration after stroke: Stem cell transplantation and trophic factors.* Brain Circulation, 2016. **2**(2): p. 86.

236. Vawda, R., J. Wilcox, and M. Fehlings, *Current stem cell treatments for spinal cord injury.* Indian journal of orthopaedics, 2012. **46**(1): p. 10.

237. Savitz, S.I., et al., *Neurotransplantation of fetal porcine cells in patients with basal ganglia infarcts: a preliminary safety and feasibility study.* Cerebrovascular diseases, 2005. **20**(2): p. 101-107.

238. Cox Jr, C.S., et al., *Autologous bone marrow mononuclear cell therapy for severe traumatic brain injury in children.* Neurosurgery, 2011. **68**(3): p. 588-600.

239. Tian, C., et al., *Autologous bone marrow mesenchymal stem cell therapy in the subacute stage of traumatic brain injury by lumbar puncture.* Exp Clin Transplant, 2013. **11**(2): p. 176-81.

240. Wang, S., et al., *Umbilical cord mesenchymal stem cell transplantation significantly improves neurological function in patients with sequelae of traumatic brain injury.* Brain research, 2013. **1532**: p. 76-84.

241. Park, H. and M.-m. Poo, *Neurotrophin regulation of neural circuit development and function.* Nature Reviews Neuroscience, 2013. **14**(1): p. 7-23.

242. Poo, M.-m., *Neurotrophins as synaptic modulators.* Nature Reviews Neuroscience, 2001. **2**(1): p. 24-32.

243. Lohof, A.M., N.Y. Ip, and M.-m. Poo, *Potentiation of developing neuromuscular synapses by the neurotrophins NT-3 and BDNF.* Nature, 1993. **363**(6427): p. 350.

244. Kang, H. and E.M. Schuman, *Long-lasting neurotrophin-induced enhancement of synaptic transmission in the adult hippocampus.* Science, 1995. **267**(5204): p. 1658.

245. Taliaz, D., et al., *Knockdown of brain-derived neurotrophic factor in specific brain sites precipitates behaviors associated with depression and reduces neurogenesis.* Molecular psychiatry, 2010. **15**(1): p. 80-92.

246. Yamashita, K., et al., *Post-occlusion treatment with BDNF reduces infarct size in a model of permanent occlusion of the middle cerebral artery in rat.* Metabolic brain disease, 1997. **12**(4): p. 271-280.

247. Schäbitz, W.-R., et al., *Intravenous brain-derived neurotrophic factor enhances poststroke sensorimotor recovery and stimulates neurogenesis.* Stroke, 2007. **38**(7): p. 2165-2172.

248. Yu, S.-J., et al., *Local administration of AAV-BDNF to subventricular zone induces functional recovery in stroke rats.* PloS one, 2013. **8**(12): p. e81750.

249. Lee, H.J., et al., *Human neural stem cells genetically modified to overexpress brain-derived neurotrophic factor promote functional recovery and neuroprotection in a mouse stroke model.* Journal of neuroscience research, 2010. **88**(15): p. 3282-3294.

250. Chen, B., et al., *Neuroprotective effect of grafting GDNF gene-modified neural stem cells on cerebral ischemia in rats.* Brain research, 2009. **1284**: p. 1-11.

251. Lee, H., et al., *Human neural stem cells overexpressing glial cell line-derived neurotrophic factor in experimental cerebral hemorrhage.* Gene therapy, 2009. **16**(9): p. 1066-1076.

252. Levi-Montalcini, R., *The nerve growth factor: thirty-five years later.* Bioscience reports, 1987. **7**(9): p. 681-699.

253. Zhao, Y., et al., *Neural stem cell transplantation and nerve growth factor promote neurological recovery in rats with ischemic stroke.* Nan fang yi ke da xue xue bao= Journal of Southern Medical University, 2008. **28**(7): p. 1123-1126.

254. Zhu, W., Y. Mao, and L. Zhou, *Reduction of neural and vascular damage by transplantation of VEGF-secreting neural stem cells after cerebral ischemia*, in *Intracranial Pressure and Brain Monitoring XII*. 2005, Springer. p. 393-397.

255. Lee, H.J., et al., *Human neural stem cells over-expressing VEGF provide neuroprotection, angiogenesis and functional recovery in mouse stroke model.* PloS one, 2007. **2**(1): p. e156.

256. Doeppner, T.R., et al., *Transplantation of TAT-Bcl-x L-transduced neural precursor cells: Long-term neuroprotection after stroke.* Neurobiology of disease, 2010. **40**(1): p. 265-276.

257. Wei, L., et al., *Transplantation of embryonic stem cells overexpressing Bcl-2 promotes functional recovery after transient cerebral ischemia.* Neurobiology of disease, 2005. **19**(1): p. 183-193.

258. Wei, L., et al., *Angiogenesis and stem cell transplantation as potential treatments of cerebral ischemic stroke.* Pathophysiology, 2005. **12**(1): p. 47-62.

259. Liu, N., et al., *Effects of transplantation with bone marrow-derived mesenchymal stem cells modified by Survivin on experimental stroke in rats.* Journal of translational medicine, 2011. **9**(1): p. 105.

260. Theus, M.H., et al., *In vitro hypoxic preconditioning of embryonic stem cells as a strategy of promoting cell survival and functional benefits after transplantation into the ischemic rat brain.* Experimental neurology, 2008. **210**(2): p. 656-670.

261. Wei, L., et al., *Transplantation of hypoxia preconditioned bone marrow mesenchymal stem cells enhances angiogenesis and neurogenesis after cerebral ischemia in rats.* Neurobiology of disease, 2012. **46**(3): p. 635-645.

262. Sart, S., T. Ma, and Y. Li, *Preconditioning stem cells for in vivo delivery.* BioResearch open access, 2014. **3**(4): p. 137-149.

263. Hu, X., et al., *Hypoxic preconditioning enhances bone marrow mesenchymal stem cell migration via Kv2. 1 channel and FAK activation.* American Journal of Physiology-Cell Physiology, 2011. **301**(2): p. C362-C372.

264. Afzal, M.R., et al., *Preconditioning promotes survival and angiomyogenic potential of mesenchymal stem cells in the infarcted heart via NF-κ B signaling.* Antioxidants & redox signaling, 2010. **12**(6): p. 693-702.

265. Sakata, H., et al., *Minocycline-preconditioned neural stem cells enhance neuroprotection after ischemic stroke in rats.* Journal of Neuroscience, 2012. **32**(10): p. 3462-3473.

266. Pasha, Z., et al., *Preconditioning enhances cell survival and differentiation of stem cells during transplantation in infarcted myocardium.* Cardiovascular research, 2008. **77**(1): p. 134-142.

267. Mohamad, O., et al., *Vector-free and transgene-free human iPS cells differentiate into functional neurons and enhance functional recovery after ischemic stroke in mice.* PLoS One, 2013. **8**(5): p. e64160.

268. Song, M., et al., *Restoration of intracortical and thalamocortical circuits after transplantation of bone marrow mesenchymal stem cells into the ischemic brain of mice.* Cell transplantation, 2013. **22**(11): p. 2001-2015.

269. Liu, X., et al., *Cell based therapies for ischemic stroke: from basic science to bedside.* Progress in neurobiology, 2014. **115**: p. 92-115.

270. Burdick, J.A., R.L. Mauck, and S. Gerecht, *To serve and protect: hydrogels to improve stem cell-based therapies.* Cell stem cell, 2016. **18**(1): p. 13-15.

271. Park, K.I., Y.D. Teng, and E.Y. Snyder, *The injured brain interacts reciprocally with neural stem cells supported by scaffolds to reconstitute lost tissue.* Nature biotechnology, 2002. **20**(11): p. 1111-1117.

272. Prasanphanich, A., et al., *Influence of shear stress on transcatheter stem cell delivery quality.* Journal of Vascular and Interventional Radiology, 2017. **2**(28): p. S12.

273. Aguado, B.A., et al., *Improving viability of stem cells during syringe needle flow through the design of hydrogel cell carriers.* Tissue Engineering Part A, 2011. **18**(7-8): p. 806-815.

274. Uemura, M., et al., *Matrigel supports survival and neuronal differentiation of grafted embryonic stem cell-derived neural precursor cells.* Journal of neuroscience research, 2010. **88**(3): p. 542-551.

275. Jin, K., et al., *Transplantation of human neural precursor cells in Matrigel scaffolding improves outcome from focal cerebral ischemia after delayed postischemic treatment in rats.* Journal of Cerebral Blood Flow & Metabolism, 2010. **30**(3): p. 534-544.

276. Yan, Z.-J., et al., *Neural stem-like cells derived from human amnion tissue are effective in treating traumatic brain injury in rat.* Neurochemical research, 2013. **38**(5): p. 1022-1033.

277. Zhang, H., et al., *Combining Injectable Plasma Scaffold with Mesenchymal Stem/Stromal Cells for Repairing Infarct Cavity after Ischemic Stroke.* Aging and Disease, 2017. **8**(2): p. 203.

278. Chen, C., et al., *Collagen/heparin sulfate scaffolds fabricated by a 3D bioprinter improved mechanical properties and neurological function after spinal cord injury in rats.* Journal of Biomedical Materials Research Part A, 2017. **105**(5): p. 1324-1332.

279. Zeng, Q. and W. Chen, *The functional behavior of a macrophage/fibroblast co-culture model derived from normal and diabetic mice with a marine gelatin–oxidized alginate hydrogel.* Biomaterials, 2010. **31**(22): p. 5772-5781.

280. Xue, S., et al., *Transplantation of adipocyte-derived stem cells in a hydrogel scaffold for the repair of cortical contusion injury in rats.* Journal of neurotrauma, 2015. **32**(7): p. 506-515.

281. Heile, A. and T. Brinker, *Clinical translation of stem cell therapy in traumatic brain injury: the potential of encapsulated mesenchymal cell biodelivery of glucagon-like peptide-1.* Dialogues Clin Neurosci, 2011. **13**(3): p. 279-286.

282. Wu, G.-Y., K. Deisseroth, and R.W. Tsien, *Spaced stimuli stabilize MAPK pathway activation and its effects on dendritic morphology.* Nature neuroscience, 2001. **4**(2): p. 151-158.

283. Lendvai, B., et al., *Experience-dependent plasticity of dendritic spines in the developing rat barrel cortex in vivo.* Nature, 2000. **404**(6780): p. 876-881.

284. Zhang, L.I. and M.-m. Poo, *Electrical activity and development of neural circuits.* Nature Neuroscience, 2001. **4**: p. 1207-1214.

285. Hanson, M.G. and L.T. Landmesser, *Normal patterns of spontaneous activity are required for correct motor axon guidance and the expression of specific guidance molecules.* Neuron, 2004. **43**(5): p. 687-701.

286. Carmichael, S.T., *Plasticity of cortical projections after stroke.* The Neuroscientist, 2003. **9**(1): p. 64-75.

287. Carmichael, S.T. and M.-F. Chesselet, *Synchronous neuronal activity is a signal for axonal sprouting after cortical lesions in the adult.* Journal of Neuroscience, 2002. **22**(14): p. 6062-6070.

288. Jones, T.A. and T. Schallert, *Use-dependent growth of pyramidal neurons after neocortical damage.* Journal of Neuroscience, 1994. **14**(4): p. 2140-2152.

289. Vicario-Abejón, C., et al., *Role of neurotrophins in central synapse formation and stabilization.* Nature Reviews Neuroscience, 2002. **3**(12): p. 965-974.

290. Narisawa-Saito, M., et al., *Brain-derived neurotrophic factor regulates the expression of AMPA receptor proteins in neocortical neurons.* Neuroscience, 1999. **88**(4): p. 1009-1014.

291. Goldberg, J.L., et al., *Retinal ganglion cells do not extend axons by default: promotion by neurotrophic signaling and electrical activity.* Neuron, 2002. **33**(5): p. 689-702.

292. Zhou, F.-Q., et al., *Neurotrophins support regenerative axon assembly over CSPGs by an ECM-integrin-independent mechanism.* Journal of cell science, 2006. **119**(13): p. 2787-2796.

293. Liu, Y., R.M. Grumbles, and C.K. Thomas, *Electrical stimulation of embryonic neurons for 1 hour improves axon regeneration and the number of reinnervated muscles that function.* Journal of Neuropathology & Experimental Neurology, 2013. **72**(7): p. 697-707.

294. Al-Majed, A.A., et al., *Brief electrical stimulation promotes the speed and accuracy of motor axonal regeneration.* Journal of Neuroscience, 2000. **20**(7): p. 2602-2608.

295. Kobelt, L.J., et al., *Short duration electrical stimulation to enhance neurite outgrowth and maturation of adult neural stem progenitor cells.* Annals of biomedical engineering, 2014. **42**(10): p. 2164-2176.

296. Miyamoto, E., *Molecular mechanism of neuronal plasticity: induction and maintenance of long-term potentiation in the hippocampus.* Journal of pharmacological sciences, 2006. **100**(5): p. 433-442.

297. West, A.E., et al., *Calcium regulation of neuronal gene expression.* Proceedings of the National Academy of Sciences, 2001. **98**(20): p. 11024-11031.

298. Kolarow, R., T. Brigadski, and V. Lessmann, *Postsynaptic secretion of BDNF and NT-3 from hippocampal neurons depends on calcium–calmodulin kinase II signaling and proceeds via delayed fusion pore opening.* Journal of Neuroscience, 2007. **27**(39): p. 10350-10364.

299. Matsuda, N., et al., *Differential activity-dependent secretion of brain-derived neurotrophic factor from axon and dendrite.* Journal of Neuroscience, 2009. **29**(45): p. 14185-14198.

300. Holtzheimer, P.E., et al., *Subcallosal cingulate deep brain stimulation for treatment-resistant unipolar and bipolar depression.* Archives of general psychiatry, 2012. **69**(2): p. 150-158.

301. Benabid, A.L., et al., *Deep brain stimulation of the subthalamic nucleus for the treatment of Parkinson's disease.* The Lancet Neurology, 2009. **8**(1): p. 67-81.

302. Gross, R.E., *Deep brain stimulation in the treatment of neurological and psychiatric disease.* Expert review of neurotherapeutics, 2004. **4**(3): p. 465-478.

303. Laxpati, N.G., W.S. Kasoff, and R.E. Gross, *Deep brain stimulation for the treatment of epilepsy: circuits, targets, and trials.* Neurotherapeutics, 2014. **11**(3): p. 508-526.

304. Lin, J.Y., et al., *ReaChR: a red-shifted variant of channelrhodopsin enables deep transcranial optogenetic excitation.* Nature neuroscience, 2013. **16**(10): p. 1499-1508.

305. Johnstone, D.M., et al., *Turning on lights to stop neurodegeneration: the potential of near infrared light therapy in Alzheimer's and Parkinson's disease.* Frontiers in neuroscience, 2015. **9**.

306. Whitaker, V.R., et al., *Whisker stimulation enhances angiogenesis in the barrel cortex following focal ischemia in mice.* Journal of Cerebral Blood Flow & Metabolism, 2007. **27**(1): p. 57-68.

307. Li, W.-L., et al., *Enhanced neurogenesis and cell migration following focal ischemia and peripheral stimulation in mice.* Developmental neurobiology, 2008. **68**(13): p. 1474.

308. Pascual-Leone, A., et al., *Rapid-rate transcranial magnetic stimulation of left dorsolateral prefrontal cortex in drug-resistant depression.* The Lancet, 1996. **348**(9022): p. 233-237.

309. Ferrucci, R., et al., *Transcranial direct current stimulation in severe, drug-resistant major depression.* Journal of affective disorders, 2009. **118**(1): p. 215-219.

310. Paz, J.T., et al., *Closed-loop optogenetic control of thalamus as a tool for interrupting seizures after cortical injury.* Nature neuroscience, 2013. **16**(1): p. 64-70.

311. Bestmann, S., et al., *Functional MRI of the immediate impact of transcranial magnetic stimulation on cortical and subcortical motor circuits.* European Journal of Neuroscience, 2004. **19**(7): p. 1950-1962.

312. Datta, A., et al., *Gyri-precise head model of transcranial direct current stimulation: improved spatial focality using a ring electrode versus conventional rectangular pad.* Brain stimulation, 2009. **2**(4): p. 201-207. e1.

313. Aravanis, A.M., et al., *An optical neural interface: in vivo control of rodent motor cortex with integrated fiberoptic and optogenetic technology.* Journal of neural engineering, 2007. **4**(3): p. S143.

314. Etoc, F., et al., *Subcellular control of Rac-GTPase signalling by magnetogenetic manipulation inside living cells.* Nature nanotechnology, 2013. **8**(3): p. 193-198.

315. Leibiger, I.B. and P.-O. Berggren, *Regulation of glucose homeostasis using radiogenetics and magnetogenetics in mice.* Nature medicine, 2015. **21**(1): p. 14.

316. Long, X., et al., *Magnetogenetics: remote non-invasive magnetic activation of neuronal activity with a magnetoreceptor.* Science bulletin, 2015. **60**(24): p. 2107-2119.

317. Mancuso, J.J., et al., *Optogenetic probing of functional brain circuitry.* Experimental physiology, 2011. **96**(1): p. 26-33.

318. Tye, K.M. and K. Deisseroth, *Optogenetic investigation of neural circuits underlying brain disease in animal models.* Nature reviews. Neuroscience, 2012. **13**(4): p. 251.

319. Armbruster, B.N., et al., *Evolving the lock to fit the key to create a family of G protein-coupled receptors potently activated by an inert ligand.* Proceedings of the National Academy of Sciences, 2007. **104**(12): p. 5163-5168.

320. Chen, Y., et al., *Chemical control of grafted human PSC-derived neurons in a mouse model of Parkinson's disease.* Cell stem cell, 2016. **18**(6): p. 817-826.

321. Jann, M., Y. Lam, and W. Chang, *Rapid formation of clozapine in guinea-pigs and man following clozapine-N-oxide administration.* Archives internationales de pharmacodynamie et de therapie, 1993. **328**(2): p. 243-250.

322. Stroh, A., et al., *Tracking stem cell differentiation in the setting of automated optogenetic stimulation.* Stem cells, 2011. **29**(1): p. 78-88.

323. Weick, J.P., et al., *Functional Control of Transplantable Human ESC-Derived Neurons Via Optogenetic Targeting.* Stem cells, 2010. **28**(11): p. 2008-2016.

324. Boyden, E.S., et al., *Millisecond-timescale, genetically targeted optical control of neural activity.* Nature neuroscience, 2005. **8**(9): p. 1263-1268.

325. Deisseroth, K., et al., *Next-generation optical technologies for illuminating genetically targeted brain circuits*. 2006, Soc Neuroscience.

326. Nagel, G., et al., *Channelrhodopsin-2, a directly light-gated cation-selective membrane channel.* Proceedings of the National Academy of Sciences, 2003. **100**(24): p. 13940-13945.

327. Airan, R.D., et al., *Temporally precise in vivo control of intracellular signalling.* Nature, 2009. **458**(7241): p. 1025-1029.

328. Oh, E., et al., *Substitution of 5-HT1A receptor signaling by a light-activated G protein-coupled receptor.* Journal of Biological Chemistry, 2010. **285**(40): p. 30825-30836.

329. Yizhar, O., et al., *Optogenetics in neural systems.* Neuron, 2011. **71**(1): p. 9-34.

330. Wang, H., et al., *Molecular determinants differentiating photocurrent properties of two channelrhodopsins from chlamydomonas.* Journal of Biological Chemistry, 2009. **284**(9): p. 5685-5696.

331. Berndt, A., et al., *High-efficiency channelrhodopsins for fast neuronal stimulation at low light levels.* Proceedings of the National Academy of Sciences, 2011. **108**(18): p. 7595-7600.

332. Berndt, A., et al., *Bi-stable neural state switches.* Nature neuroscience, 2009. **12**(2): p. 229-234.

333. Gunaydin, L.A., et al., *Ultrafast optogenetic control.* Nature neuroscience, 2010. **13**(3): p. 387-392.

334. Lin, J.Y., et al., *Characterization of engineered channelrhodopsin variants with improved properties and kinetics.* Biophysical journal, 2009. **96**(5): p. 1803-1814.

335. Bamann, C., et al., *Structural guidance of the photocycle of channelrhodopsin-2 by an interhelical hydrogen bond.* Biochemistry, 2009. **49**(2): p. 267-278.

336. Kleinlogel, S., et al., *Ultra light-sensitive and fast neuronal activation with the Ca2+-permeable channelrhodopsin CatCh.* Nature neuroscience, 2011. **14**(4): p. 513-518.

337. Lanyi, J. and D. Oesterhelt, *Identification of the retinal-binding protein in halorhodopsin.* Journal of Biological Chemistry, 1982. **257**(5): p. 2674-2677.

338. Gradinaru, V., et al., *Molecular and cellular approaches for diversifying and extending optogenetics.* Cell, 2010. **141**(1): p. 154-165.

339. Gradinaru, V., K.R. Thompson, and K. Deisseroth, *eNpHR: a Natronomonas halorhodopsin enhanced for optogenetic applications.* Brain cell biology, 2008. **36**(1-4): p. 129-139.

340. Zhao, S., et al., *Improved expression of halorhodopsin for light-induced silencing of neuronal activity.* Brain cell biology, 2008. **36**(1-4): p. 141-154.

341. Chow, B.Y., et al., *High-performance genetically targetable optical neural silencing by light-driven proton pumps.* Nature, 2010. **463**(7277): p. 98-102.

342. Flytzanis, N.C., et al., *Archaerhodopsin Variants with Enhanced Voltage Sensitive Fluorescence in Mammalian and Caenorhabditis elegans Neurons.* Nature communications, 2014. **5**: p. 4894.

343. Sohal, V.S., et al., *Parvalbumin neurons and gamma rhythms enhance cortical circuit performance.* Nature, 2009. **459**(7247): p. 698-702.

344. Carter, M.E., et al., *Tuning arousal with optogenetic modulation of locus coeruleus neurons.* Nature neuroscience, 2010. **13**(12): p. 1526-1533.

345. Adamantidis, A.R., et al., *Neural substrates of awakening probed with optogenetic control of hypocretin neurons.* Nature, 2007. **450**(7168): p. 420-424.

346. Han, X., et al., *Millisecond-timescale optical control of neural dynamics in the nonhuman primate brain.* Neuron, 2009. **62**(2): p. 191-198.

347. Lobo, M.K., et al., *Cell type–specific loss of BDNF signaling mimics optogenetic control of cocaine reward.* Science, 2010. **330**(6002): p. 385-390.

348. Covington, H.E., et al., *Antidepressant effect of optogenetic stimulation of the medial prefrontal cortex.* Journal of Neuroscience, 2010. **30**(48): p. 16082-16090.

349. Gao, G., L.H. Vandenberghe, and J.M. Wilson, *New recombinant serotypes of AAV vectors.* Current gene therapy, 2005. **5**(3): p. 285-297.

350. Aschauer, D.F., S. Kreuz, and S. Rumpel, *Analysis of transduction efficiency, tropism and axonal transport of AAV serotypes 1, 2, 5, 6, 8 and 9 in the mouse brain.* PloS one, 2013. **8**(9): p. e76310.

351. Nathanson, J.L., et al., *Preferential labeling of inhibitory and excitatory cortical neurons by endogenous tropism of adeno-associated virus and lentivirus vectors.* Neuroscience, 2009. **161**(2): p. 441-450.

352. Nathanson, J.L., et al., *Short promoters in viral vectors drive selective expression in mammalian inhibitory neurons, but do not restrict activity to specific inhibitory cell-types.* Frontiers in neural circuits, 2009. **3**: p. 19.

353. Dong, B., H. Nakai, and W. Xiao, *Characterization of genome integrity for oversized recombinant AAV vector.* Molecular therapy, 2010. **18**(1): p. 87-92.

354. Xu, Z.-L., et al., *Optimization of transcriptional regulatory elements for constructing plasmid vectors.* Gene, 2001. **272**(1): p. 149-156.

355. Kügler, S., E. Kilic, and M. Bähr, *Human synapsin 1 gene promoter confers highly neuron-specific long-term transgene expression from an adenoviral vector in the adult rat brain depending on the transduced area.* Gene therapy, 2003. **10**(4): p. 337-347.

356. Campsall, K.D., et al., *Characterization of transgene expression and Cre recombinase activity in a panel of Thy-1 promoter-Cre transgenic mice.* Developmental dynamics, 2002. **224**(2): p. 135-143.

357. Wang, X., et al., *Distribution of CaMKIIα expression in the brain in vivo, studied by CaMKIIα-GFP mice.* Brain research, 2013. **1518**: p. 9-25.

358. Campagnola, L., H. Wang, and M.J. Zylka, *Fiber-coupled light-emitting diode for localized photostimulation of neurons expressing channelrhodopsin-2.* Journal of neuroscience methods, 2008. **169**(1): p. 27-33.

359. Montgomery, K.L., et al., *Wirelessly powered, fully internal optogenetics for brain, spinal and peripheral circuits in mice.* nAture methods, 2015.

360. Park, S.I., et al., *Soft, stretchable, fully implantable miniaturized optoelectronic systems for wireless optogenetics.* Nature biotechnology, 2015. **33**(12): p. 1280-1286.

361. Kim, T.-i., et al., *Injectable, cellular-scale optoelectronics with applications for wireless optogenetics.* Science, 2013. **340**(6129): p. 211-216.

362. Montgomery, K.L., et al., *Beyond the brain: Optogenetic control in the spinal cord and peripheral nervous system.* Science translational medicine, 2016. **8**(337): p. 337rv5-337rv5.

363. Tannous, B.A., et al., *Codon-optimized Gaussia luciferase cDNA for mammalian gene expression in culture and in vivo.* Molecular Therapy, 2005. **11**(3): p. 435-443.

364. Berglund, K., et al., *Combined optogenetic and chemogenetic control of neurons.* Optogenetics: Methods and Protocols, 2016: p. 207-225.

365. Tung, J.K., C.-A. Gutekunst, and R.E. Gross, *Inhibitory luminopsins: Genetically-encoded bioluminescent opsins for versatile, scalable, and hardware-independent optogenetic inhibition.* Scientific reports, 2015. **5**: p. 14366.

366. Berglund, K., et al., *Light-emitting channelrhodopsins for combined optogenetic and chemical-genetic control of neurons.* PLoS One, 2013. **8**(3): p. e59759.

367. Berglund, K., et al., *Luminopsins integrate opto-and chemogenetics by using physical and biological light sources for opsin activation.* Proceedings of the National Academy of Sciences, 2016. **113**(3): p. E358-E367.

368. Weick, J.P., Y. Liu, and S.-C. Zhang, *Human embryonic stem cell-derived neurons adopt and regulate the activity of an established neural network.* Proceedings of the National Academy of Sciences, 2011. **108**(50): p. 20189-20194.

369. Cheng, M.Y., et al., *Optogenetic neuronal stimulation promotes functional recovery after stroke.* Proceedings of the National Academy of Sciences, 2014. **111**(35): p. 12913-12918.

370. Shah, A.M., et al., *Optogenetic neuronal stimulation of the lateral cerebellar nucleus promotes persistent functional recovery after stroke.* Scientific Reports, 2017. **7**: p. 46612.

371. Song, M., et al., *Optogenetic stimulation of glutamatergic neuronal activity in the striatum enhances neurogenesis in the subventricular zone of normal and stroke mice.* Neurobiology of Disease, 2017. **98**: p. 9-24.

372. Park, S., et al., *Optogenetic control of nerve growth.* Scientific reports, 2015. **5**: p. 9669.

373. Daadi, M.M., et al., *Optogenetic stimulation of neural grafts enhances neurotransmission and downregulates the inflammatory response in experimental stroke model.* Cell transplantation, 2016. **25**(7): p. 1371-1380.

374. McDonald, J.W., et al., *Transplanted embryonic stem cells survive, differentiate and promote recovery in injured rat spinal cord.* Nature medicine, 1999. **5**(12): p. 1410-1412.

375. Bliss, T., et al., *Cell transplantation therapy for stroke.* Stroke, 2007. **38**(2): p. 817-826.

376. Kelly, S., et al., *Transplanted human fetal neural stem cells survive, migrate, and differentiate in ischemic rat cerebral cortex.* Proceedings of the National Academy of Sciences of the United States of America, 2004. **101**(32): p. 11839-11844.

377. Englund, U., et al., *Grafted neural stem cells develop into functional pyramidal neurons and integrate into host cortical circuitry.* Proceedings of the National Academy of Sciences, 2002. **99**(26): p. 17089-17094.

378. Espuny-Camacho, I., et al., *Pyramidal neurons derived from human pluripotent stem cells integrate efficiently into mouse brain circuits in vivo.* Neuron, 2013. **77**(3): p. 440-456.

379. Ideguchi, M., et al., *Murine embryonic stem cell-derived pyramidal neurons integrate into the cerebral cortex and appropriately project axons to subcortical targets.* Journal of Neuroscience, 2010. **30**(3): p. 894-904.

380. Tornero, D., et al., *Human induced pluripotent stem cell-derived cortical neurons integrate in stroke-injured cortex and improve functional recovery.* Brain, 2013. **136**(12): p. 3561-3577.

381. Wu, H.-M., et al., *Redefining the pericontusional penumbra following traumatic brain injury: evidence of deteriorating metabolic derangements based on positron emission tomography.* Journal of neurotrauma, 2013. **30**(5): p. 352-360.

382. Mohamad, O., et al., *Efficient neuronal differentiation of mouse ES and iPS cells using a rotary cell culture protocol.* Differentiation, 2013. **86**(4-5): p. 149-58.

383. Bain, G., et al., *Embryonic stem cells express neuronal properties in vitro.* Dev Biol, 1995. **168**(2): p. 342-57.

384. Bottenstein, J.E. and G.H. Sato, *Growth of a rat neuroblastoma cell line in serum-free supplemented medium.* Proc Natl Acad Sci U S A, 1979. **76**(1): p. 514-7.

385. Ogle, M.E., et al., *Inhibition of prolyl hydroxylases by dimethyloxaloylglycine after stroke reduces ischemic brain injury and requires hypoxia inducible factor-1alpha.* Neurobiol Dis, 2012. **45**(2): p. 733-42.

386. Hitoshi, N., Y. Ken-ichi, and M. Jun-ichi, *Efficient selection for high-expression transfectants with a novel eukaryotic vector.* Gene, 1991. **108**(2): p. 193-199.

387. Mitsui, K., et al., *The homeoprotein Nanog is required for maintenance of pluripotency in mouse epiblast and ES cells.* cell, 2003. **113**(5): p. 631-642.

388. Berndt, A., et al., *Structure-guided transformation of channelrhodopsin into a light-activated chloride channel.* Science, 2014. **344**(6182): p. 420-424.

389. Bain, G., et al., *Retinoic acid promotes neural and represses mesodermal gene expression in mouse embryonic stem cells in culture.* Biochem Biophys Res Commun, 1996. **223**(3): p. 691-4.

390. Lee, J.H., et al., *Regulation of therapeutic hypothermia on inflammatory cytokines, microglia polarization, migration and functional recovery after ischemic stroke in mice.* Neurobiology of Disease, 2016. **96**: p. 248-260.

391. Silver, D.J., et al., *Chondroitin sulfate proteoglycans potently inhibit invasion and serve as a central organizer of the brain tumor microenvironment.* Journal of Neuroscience, 2013. **33**(39): p. 15603-15617.

392. Lee, J.H., et al., *Therapeutic effects of pharmacologically induced hypothermia against traumatic brain injury in mice.* Journal of neurotrauma, 2014. **31**(16): p. 1417-1430.

393. Theus, M.H., et al., *In vitro hypoxic preconditioning of embryonic stem cells as a strategy of promoting cell survival and functional benefits after transplantation into the ischemic rat brain.* Exp Neurol, 2008. **210**(2): p. 656-70.

394. Yu, S.P., Z. Wei, and L. Wei, *Preconditioning strategy in stem cell transplantation therapy.* Transl Stroke Res, 2013. **4**(1): p. 76-88.

395. Chen, D., et al., *Intranasal Delivery of Apelin-13 Is Neuroprotective and Promotes Angiogenesis After Ischemic Stroke in Mice.* ASN Neuro, 2015. **7**(5).

396. Choi, K.-E., et al., *A novel stroke therapy of pharmacologically induced hypothermia after focal cerebral ischemia in mice.* The FASEB Journal, 2012. **26**(7): p. 2799-2810.

397. Li, Y., et al., *Erythropoietin-induced neurovascular protection, angiogenesis, and cerebral blood flow restoration after focal ischemia in mice.* Journal of Cerebral Blood Flow & Metabolism, 2007. **27**(5): p. 1043-1054.

398. Wang, L.-L., et al., *Mobilization of endogenous bone marrow derived endothelial progenitor cells and therapeutic potential of parathyroid hormone after ischemic stroke in mice.* PloS one, 2014. **9**(2): p. e87284.

399. Coggeshall, R.E., *A consideration of neural counting methods.* Trends in neurosciences, 1992. **15**(1): p. 9-13.

400. Bouet, V., et al., *The adhesive removal test: a sensitive method to assess sensorimotor deficits in mice.* Nature protocols, 2009. **4**(10): p. 1560-1564.

401. Zhang, L., et al., *A test for detecting long-term sensorimotor dysfunction in the mouse after focal cerebral ischemia.* Journal of neuroscience methods, 2002. **117**(2): p. 207-214.

402. Bouët, V., et al., *Sensorimotor and cognitive deficits after transient middle cerebral artery occlusion in the mouse.* Experimental neurology, 2007. **203**(2): p. 555-567.

403. Hamm, R.J., et al., *The rotarod test: an evaluation of its effectiveness in assessing motor deficits following traumatic brain injury.* Journal of neurotrauma, 1994. **11**(2): p. 187-196.

404. Sarkar, C., et al., *Impaired autophagy flux is associated with neuronal cell death after traumatic brain injury.* Autophagy, 2014. **10**(12): p. 2208-2222.

405. Kang, R., et al., *The Beclin 1 network regulates autophagy and apoptosis.* Cell Death & Differentiation, 2011. **18**(4): p. 571-580.

406. Baehrecke, E.H., *Autophagy: dual roles in life and death?* Nature reviews Molecular cell biology, 2005. **6**(6): p. 505-510.

407. Luo, C.-L., et al., *Autophagy is involved in traumatic brain injury-induced cell death and contributes to functional outcome deficits in mice.* Neuroscience, 2011. **184**: p. 54-63.

408. Zhang, J.H., et al., *The vascular neural network—a new paradigm in stroke pathophysiology.* Nature Reviews Neurology, 2012. **8**(12): p. 711-716.

409. Chen, S., J. Pickard, and N. Harris, *Time course of cellular pathology after controlled cortical impact injury.* Experimental neurology, 2003. **182**(1): p. 87-102.

410. Silver, J. and J.H. Miller, *Regeneration beyond the glial scar.* Nature Reviews Neuroscience, 2004. **5**(2): p. 146-156.

411. Oudega, M. and T. Hagg, *Neurotrophins promote regeneration of sensory axons in the adult rat spinal cord.* Brain research, 1999. **818**(2): p. 431-438.

412. Wan, L., R. Xia, and W. Ding, *Low-frequency electrical stimulation improves neurite outgrowth of dorsal root ganglion neurons in vitro via upregulating Ca2+-mediated brain-derived neurotrophic factor expression.* Neural Regen. Res, 2010. **5**(16): p. 1256-1260.

413. Wood, M. and R.K. Willits, *Short-duration, DC electrical stimulation increases chick embryo DRG neurite outgrowth.* Bioelectromagnetics, 2006. **27**(4): p. 328-331.

414. Koppes, A.N., A.M. Seggio, and D.M. Thompson, *Neurite outgrowth is significantly increased by the simultaneous presentation of Schwann cells and moderate exogenous electric fields.* Journal of neural engineering, 2011. **8**(4): p. 046023.

415. Schmidt, C.E., et al., *Stimulation of neurite outgrowth using an electrically conducting polymer.* Proceedings of the National Academy of Sciences, 1997. **94**(17): p. 8948-8953.

416. Chang, K.-A., et al., *Biphasic electrical currents stimulation promotes both proliferation and differentiation of fetal neural stem cells.* PLoS One, 2011. **6**(4): p. e18738.

417. Moody, W.J. and M.M. Bosma, *Ion channel development, spontaneous activity, and activity-dependent development in nerve and muscle cells.* Physiological reviews, 2005. **85**(3): p. 883-941.

418. Chen, D., S.P. Yu, and L. Wei, *Ion channels in regulation of neuronal regenerative activities.* Translational stroke research, 2014. **5**(1): p. 156-162.

419. Tao, X., et al., *Ca 2+ influx regulates BDNF transcription by a CREB family transcription factor-dependent mechanism.* Neuron, 1998. **20**(4): p. 709-726.

420. Carmel, J.B., et al., *Chronic electrical stimulation of the intact corticospinal system after unilateral injury restores skilled locomotor control and promotes spinal axon outgrowth.* Journal of Neuroscience, 2010. **30**(32): p. 10918-10926.

421. Yoon, Y.-S., et al., *The effect of electric cortical stimulation after focal traumatic brain injury in rats.* Annals of rehabilitation medicine, 2012. **36**(5): p. 596-608.

422. Xue, L., et al., *The effect of stromal cell-derived factor 1 in the migration of neural stem cells.* Cell biochemistry and biophysics, 2014. **70**(3): p. 1609-1616.

423. Berglund, K., et al., *Light-Emitting Channelrhodopsins for Combined Optogenetic and Chemical-Genetic Control of Neurons.* PLoS ONE, 2013. **8**: p. e59759.

424. Tung, J.K., C.-A. Gutekunst, and R.E. Gross, *Inhibitory luminopsins: genetically-encoded bioluminescent opsins for versatile, scalable, and hardware-independent optogenetic inhibition.* Sci. Reports, 2015. **5**(14366).

425. Hofherr, A., B. Fakler, and N. Klöcker, *Selective Golgi export of Kir2. 1 controls the stoichiometry of functional Kir2. x channel heteromers.* Journal of cell science, 2005. **118**(9): p. 1935-1943.

426. Gong, Y., J.Z. Li, and M.J. Schnitzer, *Enhanced archaerhodopsin fluorescent protein voltage indicators.* PLoS One, 2013. **8**(6): p. e66959.

427. Hanson, L.R. and W.H. Frey, *Intranasal delivery bypasses the blood-brain barrier to target therapeutic agents to the central nervous system and treat neurodegenerative disease.* BMC neuroscience, 2008. **9**(3): p. S5.

428. Chauhan, M.B. and N.B. Chauhan, *Brain Uptake of Neurotherapeutics after Intranasal versus Intraperitoneal Delivery in Mice.* Journal of neurology and neurosurgery, 2015. **2**(1).

429. Simon, S.M. and G. Blobel, *Mechanisms of translocation of proteins across membranes,* in *Endoplasmic Reticulum*. 1993, Springer. p. 1-15.

430. Yang, J., et al., *Coupling optogenetic stimulation with NanoLuc-based luminescence (BRET) Ca++ sensing.* Nature Communications, 2016. **7**: p. 13268.

431. Suzuki, K., et al., *Five colour variants of bright luminescent protein for real-time multicolour bioimaging.* Nature Communications, 2016. **7**.